

MAJOR ELEMENT GEOCHEMISTRY OF THE
AMAZON RIVER SYSTEM

by

ROBERT FORSTER STALLARD

B.S., Massachusetts Institute of Technology
(1974)

SUBMITTED IN PARTIAL FULFILLMENT OF THE
REQUIREMENTS FOR THE DEGREE OF
DOCTOR OF PHILOSOPHY

at the

MASSACHUSETTS INSTITUTE OF TECHNOLOGY

and the

WOODS HOLE OCEANOGRAPHIC INSTITUTION

January 1980

(c) Massachusetts Institute of Technology 1980

Signature of Author

Richard P. Von Herzen
Joint Program in Oceanography, Massachusetts Institute of
Technology - Woods Hole Oceanographic Institution, and the
Department of Earth and Planetary Sciences, Massachusetts
Institute of Technology, January 1980

Certified by

U

John M. Edmond
Thesis Supervisor

Accepted by

Richard P. Von Herzen, Chairman, Joint Oceanographic
Committee for Earth Sciences, Massachusetts Institute
of Technology-Woods Hole Oceanographic Institution

Lindgren
MASSACHUSETTS INSTITUTE
OF TECHNOLOGY

JUN 10 1980

MAJOR ELEMENT GEOCHEMISTRY OF THE
AMAZON RIVER SYSTEM

by

ROBERT FORSTER STALLARD

Submitted to the Massachusetts Institute of Technology
Woods Hole Oceanographic Institution Joint Program
in Chemical Oceanography on 10 January 1980 in
partial fulfillment of the Degree of Doctor
of Philosophy in Chemical Oceanography

ABSTRACT

Samples of surface waters and precipitation were collected on the Amazon main channel, its major tributaries, and headwater rivers in the Peruvian and Bolivian Andes. Collection was done between 1976 and 1978. The bulk of the samples were obtained during traverses of the Amazon Basin, on the main channel, in the May-July peak discharge period of 1976 and 1977. The intent of the sampling was to identify the dominant processes controlling the chemistry of rivers within the Amazon River system and to quantify the relative importance of these processes.

Analyses of precipitation and surface water are used to estimate the fluxes of marine cyclic salts through that part of the Amazon Basin draining past Obidos (80% of the basin). Amazon precipitation chemistry can be divided into two principal components, marine and terrestrial. The marine component (determined from analyses of marine rain) consists of Na, K, Mg, Ca, and Cl in approximately seasalt proportions, while S is doubly enriched relative to seasalt. The excess sulfur is probably derived from gas-phase inputs. The terrestrial component makes an important contribution of K, Ca, S, and N, and is in part related to biological emissions. The chloride content of lowland rivers, which drain regions lacking significant geological contributions of chloride, shows a systematic decrease with increasing distance from the Atlantic Ocean. This trend is used to define the cyclic salt background for Amazonian surface waters. Cyclic salts, in general, make only a minor contribution, relative to terrestrial inputs, to the chemistry of Amazon Basin rivers, even those draining intensely weathered terrains. An estimated 19.0%-Cl, 7.9%-Na, 1.4%-Mg, 3.8%-S, 0.5%-K, and 0.1%-Ca of the dissolved load at Obidos during peak discharge is cyclic.

Within the Amazon Basin, the regional geology of highland and lowland areas contrasts markedly. Major exposures of marine and brackish water sedimentary rocks are concentrated in the Andes and the southwest lowlands. The Peruvian and south Ecuadorian Andes exhibit abundant exposures of carbonates and evaporites. The latter are expressed as numerous salt springs, salt extrusions, and intercalations in red beds. The Bolivian Andes contain a thick section of Paleozoic grey-green to black shales. Carbonates and evaporites (CaSO_4) are found in the southwest lowlands. The remainder of the lowlands are covered by purely siliceous rock types, excepting narrow strips of Paleozoic carbonates

and evaporites (CaSO_4), exposed along the lower Amazon Valley.

The contrast between the highlands and the lowlands is also reflected in differing denudation regimes. In flatlands, denudation rates are controlled largely by the capacity of transport processes to remove dissolved and solid materials (the latter generally accumulate as soils). In the highlands and hilly areas, denudation rates are limited by the rates at which weathering processes can mobilize materials.

Samples can be separated into four principal groupings based on relationships between total cation charge (TZ+) and geology: (1) Rivers with $0 < \text{TZ}^+ < 200 \mu\text{Eq/l}$ drain the most intensely weathered materials (Upper Tertiary sediments, soils of the Negro Basin and similarly weathered regions). (2) Rivers with $200 < \text{TZ}^+ < 450 \mu\text{Eq/l}$ drain siliceous terrains. (3) Rivers with $450 < \text{TZ}^+ < 3000 \mu\text{Eq/l}$ drain marine sediments with high cation concentrations (resulting from the presence of carbonates and minor evaporites in the Peruvian Andes, and reduced shales and minor carbonates in the Bolivian Andes). (4) Rivers with $\text{TZ}^+ > 3000 \mu\text{Eq/l}$ drain evaporites. Rivers in categories (1) and (2) exhibit an approximately 2:1 (mole) relationship between Si and (Na+K) (corrected for cyclic salt inputs), which characterizes the weathering of many major primary silicate minerals to kaolinite. In categories (3) and (4), rivers tend to have 1:1 (equivalent) ratios of Na:Cl and $(\text{Ca}+\text{Mg}):(\text{alkalinity}+\text{SO}_4)$, caused primarily by the weathering of carbonates and evaporites.

A mass conservation model is used to predict discharges along the main channel and on its tributaries. The predicted discharges agree with measured values, showing that the transport of major dissolved species down the main channel is conservative with respect to chemical removal.

The calculated discharges are used to estimate preliminary denudation rates for various parts of the Amazon Basin. For Na, Mg, Ca, alkalinity, SO_4 and Cl, great contrasts in denudation rates are observed between areas which drain cation-rich lithologies, such as carbonates, marine shales, and evaporites (e.g., the Andes and the southwest lowlands), and areas which drain only siliceous rock types. The Peruvian Andes contribute 50-60% of the terrestrially derived Na, Mg, Ca, alkalinity, and SO_4 and 90% of the Cl in the Amazon dissolved load. Denudation rates for these species are 10-20 times greater in the Peruvian Andes than in lowland areas having exclusively siliceous lithologies. In contrast, Si and K show only small variations in denudation rates over the basin., reflecting the widespread distribution of their siliceous parent phases. This information is used to calculate the contributions that various lithological groupings (silicates carbonates, evaporites) make to the dissolved load for different species.

Thesis Supervisor: Dr. John M. Edmond

Title: Associate Professor of Earth and Planetary Sciences

Dedicated to
the people of the Amazon
Isabel
Ginna
and
my parents, Burrell and Loula May

Acknowledgements

I greatly appreciate John M. Edmond for extending me this marvelous research opportunity and providing the quality laboratory and academic environments in which one can learn and work.

Members of my thesis committee, Carl Nordin, Fred Sayles, and Karl Turekian deserve thanks for their attention and help in the preparation of this volume. The same gratitude must be extended to Russ McDuff, who persevered through a number of drafts and provided valuable criticism.

In addition, discussions with various people proved particularly important in the development of this thesis: Chapter I - Maryanne Carroll, Reginald Newell, and Carlos Nobre, Chapter III - Carlos Brockmann, Peter Goreau, Victor Holm, and Paulo Lamdim, Chapter IV - Ed Boyle and Harald Sioli, Chapter V - Bob Meade, and Appendices II and III - Bob Collier and Barry Grant. Barbara Grant, and Linda Menke provided computer advice. Darlene Ketten, Barbara Mangum, Isabel Morales, Carlos Nobre, and Roger Shrimpton provided important linguistic aid.

This work would never have been possible without the help of numerous people in the field, both on the R.V. Alpha Helix and on the ground in Bolivia, Brazil, Columbia, and Peru.

The crew and scientific party of the R.V. Alpha Helix worked well together and the ship provided an excellent research environment, where most goals were efficiently accomplished. Barry Grant played an essential role in the organization of the laboratory and shipboard analyses and handling of samples. Ginny Conger helped develop the rain sampler.

Several people collected essential samples which could not be obtained during field work. These samples were crucial in the interpretation of the chemical data. Eng. Walter Fernández Dávila Kaupil and Eng. Uladislao Sánchez collected dry season samples from the Nanay and Amazon. Jerry

Leenheer and Roger Shrimpton obtained samples from the upper Negro and Branco. Jerry also obtained samples from the Solimoes and lower Negro.

Four separate explorations of Andean rivers provided samples essential to this study. On the last three trips I was accompanied by John Edmond, Isabel Morales, and Russ McDuff, respectively. Samples could not have been collected without the help of many people. Unfortunately, there is no way to recall them all and the places in which they lent assistance: Huánuco - Sr. Néstor Armas Wenzel; Iquitos - Engineers Dávila and Sánchez, Jorge Portocapero F., the staff of Linea Amazonica; La Paz - Dr. Carlos E. Arze L., Eng. Mario Canedo Puza, Eng. Guillermo DaSilva; Leticia - Mr. Peters; Lima - Dr. Arturo Alcalde Mongrut, Admiral Guillermo Faura Guig and Sra. Faura; Puilluana Salt Dome - Pedro Vasquez, Donarío Piche Guerro and his two sons; Riberalta - Maryknoll fathers (Padre Pedro Chabot) and their medical boat pilot; Tingo María - Pablo Cezal; Tocache - Mario Bazán, his brother and the boat pilot named Arturo; Pto. Villarroel - Gloria and Silvio Bastos; and Yurimaguas - Sr. Pina and Sr. Cesar G. Young Rios.

The staff of INPA under Director, Dr. Warwick Kerr, provided invaluable support, and served as a reservoir of expertise and as a forum for ideas during the several stop-overs in Manaus, during the expedition. I hope that INPA keeps up the good work. Special thanks to Roger and Regina Shrimpton for their hospitality, assistance, and enlightening discussions.

Althea Wright and Loretta Toccio were immensely helpful in the final assembly and production of this volume.

I thank Isabel Morales who was a great partner in this work.

This study was supported by a N.S.F. three-year graduate fellowship and N.S.F. grant #OCE77-27148. Work on the R.V. Alpha Helix proceeded under the auspices of the Conselho Nacional de Desenvolvimento Científico e Tecnológico of Brazil and the Consejo Nacional de Investigación of Peru.

CONTENTS

2	Abstract
5	Acknowledgements
7	Contents
12	Chapter I, Introduction
17	Chapter II, Amazon precipitation chemistry and the marine contribution to the dissolved load
18	II.1.....Introduction
22	II.2:1...Collection and analysis
26	II.2:2...Analytical methods
32	II.2:3...Discussion of sampling
33	II.3.....Background
33	II.3:1...Amazon Basin meteorology
34	II.3:2...Previous studies of Amazon precipitation chemistry
35	II.4:1...Sources of materials in Amazon precipitation
35	II.4:2...Anthropogenic inputs
37	II.4:3...Marine components in Amazon precipitation
38	II.4:4...Processes transferring materials from the oceans to the atmosphere
43	II.4:5...The chemistry of the marine component in Amazon precipitation
50	II.4:6...Terrestrial inputs
56	II.4:7...Composition versus altitude of aerosols
56	II.4:8...Relationship between terrestrial inputs and precipitation chemistry
58	II,4:9...Gaseous inputs and the acidity of rain
61	II.5.....Cyclic salt corrections (observations)
70	II.6.....Cyclic salt corrections (results), summary for the basin
74	Chapter III, Environmental setting of the Amazon Basin, with emphasis on geology and soils
75	III.1....Global setting of the Amazon Basin
76	III.2....Major features of the basin
79	III.3:1..The distribution of rock types in the Amazon Basin
79	III.3:2..Igneous and metamorphic rocks
79	III.3:3..Sedimentary rocks
91	III.4:1..Topography and denudation processes
92	III.4:2..Denudation, soils, and vegetation in the lowlands
96	III.4:3..Mineral stability and element mobility in Amazon soils
100	III.4:4..Laterites and podzols in the Amazon region
102	III.4:5..Ground water circulation
102	III.4:6..Significance of the three weathering environments (savanna, forest, caatinga/campina)
104	III.4:7..Slope processes
105	III.4:8..Andean slopes
107	III.5....Biological processes in Amazonian geochemistry
110	Chapter IV, Examination of the processes controlling the chemistry of the dissolved load of the Amazon River
111	IV.1.....Sampling
112	IV.2.....Previous observations of Amazon regional water chemistry
116	IV.3:1...Introduction to the chemical data

116	IV.3:2...Chemistry of the Amazon main channel in relation to world averages (dissolved, suspended, and bed load)
118	IV.3:3...Ion dominance
124	IV.3:4...Multivariate analyses
129	IV.3:5...Concentrations versus total cations
156	IV.4:1...River chemistry and rock types
156	IV.4:2...Main channel (1)
156	IV.4:3...Maranon drainage (2)
177	IV.4:4...Ucayali drainage (3)
177	IV.4:5...Madera drainage (4)
179	IV.4:6...Andean magnesium and calcium inputs
180	IV.4:7...Other Andean headwater rivers: Napo, Ica, and Japurá (5)
181	IV.4:8...Negro drainage (6)
182	IV.4:9...Other shield rivers: Xingu, Tapajós, and Trombetas (7)
187	IV.4:10...Lowland rivers draining marine sediments: Javari, Juruá, and Purus (8)
187	IV.4:11...Rivers draining Upper Tertiary and later sediments (9)
188	IV.4:12...Várzea (flood plain) waters (10)
189	IV.4:13...Terrestrial biological effects
190	IV.5.....Geological control of high TZ+ rivers
201	IV.6:1...Weathering reactions
202	IV.6:2...Applicability of thermodynamic models to river data
202	IV.6:3...Carbon dioxide and pH
203	IV.6:4...Carbonate rock weathering
216	IV.6:5...Silicate weathering
220	IV.6:6...Recapitulation of silicate occurrences in the Amazon Basin
220	IV.6:7...Amazon data and activity-activity diagrams
230	IV.6:8...Montmorillonite stability
234	IV.6:9...Reaction mass-balance relationships
246	IV.7.....Cation ratios and silicate weathering
251	IV.8:1...Iron and aluminum
252	IV.8:2...Properties of Amazon iron and aluminum phases
254	IV.8:3...Relationship of iron and aluminum with other species
275	IV.9.....Summation
279	Chapter V, Model of discharges for the Amazon and its tributaries based on chemical data
280	V.1.....Discharge model, introduction
282	V.2.....Theory
286	V.3:1...Application of discharge model to Amazon data
289	V.3:2...Selection of stations
295	V.3:3...Time variations of discharge
297	V.4.....Results of the flux model
309	V.5.....Summation
310	Chapter VI, General conclusion (with estimated denudation rates)
319	Appendix I, Tabulation of sample locations
324	Appendix II, Collection procedures
327	Appendix III, Analytical methods
339	Bibliography
366	Biographic sketch

FIGURES

- 23 II.1.....Precipitation sample location maps
29 II.2.....Charge balance of analyses of precipitation
39 II.3.....Reference line used for calculating distances from the
Atlantic coast
41 II.4.....Average value of Cl in precipitation as a function of
distance from the Atlantic coast
45 II.5.....Na, K, Mg, and Ca versus Cl in precipitation
47 II.6.....SO₄, H⁺, NO₃, and NH₄ versus Cl in precipitation
51 II.7.....Na and K versus Cl in 1977 precipitation
59 II.8.....Hydrogen ion versus sulfate in precipitation
63 II.9.....Chloride in surface waters versus distance from the
Atlantic coast
65 II.10....Sodium and potassium in surface waters versus distance
from the Atlantic coast
67 II.11....Sulfate in surface waters versus distance from the
Atlantic coast
77 III.1....Map of morphostructural regions
81 III.2....Lithologic map
85 III.3....Map of the distribution of formations which contain
evaporite minerals in the Amazon Basin
87 III.4....Photograph of a salt cliff in the Pilluana Salt Dome and
photograph of a block of rock salt from the Pilluana Dome
93 III.5....Photograph: Andean front near the Peru-Bolivia border
97 III.6....Histogram of Si/Al in forest and savanna soils

113 IV.1.....Location map of surface water samples
121 IV.2.....Graphs of Amazon surface water data (after Gibbs 1970)
showing the effect of cyclic salt corrections
125 IV.3.....Graphs of Amazon data according to Hill (1942) and Piper
(1944)
131 IV.4.....Na and Cl versus total cations (TZ+)
134 IV.5.....Ca, Mg, and SO₄ versus TZ+
138 IV.6.....Alk(C), NO₃, and PO₄ versus TZ+
142 IV.7.....Si and K versus TZ+
146 IV.8.....H⁺, Fe, Al, and color versus TZ+
152 IV.9.....Normalized inorganic charge balances (NICB) versus TZ+
171 IV.10....Photograph of the headwaters of the Huallaga and the
Maranon rivers
173 IV.11....Photograph of the lower courses of the Huallaga and
Ucayali rivers
183 IV.12....Photograph of the upper Negro River Basin
185 IV.13....Photograph of the upper Branco River Basin
193 IV.14....(Na+K) versus Cl in Amazon surface waters
195 IV.15....(Ca+Mg) versus (Alk(C)+SO₄)
197 IV.16....(Ca+Mg) versus Alk(C)
199 IV.17....Ternary diagram of (Mg+Ca), Alk(C), and SO₄
205 IV.18....Histograms of carbon dioxide vapor pressures in Amazon
surface waters
207 IV.19....Saturation index of dolomite versus the saturation
index of calcite for Amazon surface waters
211 IV.20....Alk(C) versus the saturation index of calcite in Amazon
surface waters

- 213 IV.21....(Ca+Mg) versus the saturation index of calcite
221 IV.22....Stability diagram of sodium aluminosilicates
223 IV.23....Stability diagram for potassium aluminosilicates
225 IV.24....Stability diagram for calcium aluminosilicates
227 IV.25....Stability diagram for magnesium aluminosilicates
231 IV.26....Stability index for montmorillonite versus TZ+
240 IV.27....Si versus (Na+K-Cl) in surface waters
243 IV.28....Stability index for montmorillonite versus Si/(Na+K-Cl)
248 IV.29....(Na+K-Cl)/TZ+ versus TZ+, and Mg/(Mg+Ca) versus
K/(Na+K-Cl)
255 IV.30....Treated (filtered and acidified) aluminum versus
untreated aluminum in lowland waters
257 IV.31....Treated iron versus untreated iron in lowland waters
259 IV.32....Treated aluminum versus treated iron in lowland rivers
261 IV.33....Ca, Si, Fe, and Al versus Alk(t) in the zone of mixing
of the Negro River with the main channel
263 IV.34....Fe and Al versus TZ+ in lowland rivers
267 IV.35....Fe versus H⁺, color, and NICB in lowland rivers
271 IV.36....Al versus H⁺, color, and NICB in lowland rivers
277 IV.37....Ternary diagram of Si, Alk(C), and (Cl+SO₄) in Amazon
surface waters
- 287 V.1.....Diagram of stations used in the discharge model
291 V.2.....Photograph of the confluence of the Madeira River with
the main channel
293 V.3.....Alk(t) in main channel cross sections
299 V.4.....Results of the model for 1976 without the Aranapu Paraná
301 V.5.....Results of the model for 1977 without the Aranapu Paraná
303 V.6.....Results of the model for 1976 with the Aranapu Paraná
305 V.7.....Results of the model for 1977 with the Aranapu Paraná
307 V.8.....Predicted versus observed concentrations at Obidos for
Na, K, Mg, Ca, Alk(t), Cl, and SO₄
- 331 AIII.1...Total CO₂ predicted from Alk(t) and pH versus
measured total CO₂

TABLES

19	II.1.....	Estimates of the percentage of river borne material that is contributed by atmospheric inputs
25	II.2.....	Precipitation sample descriptions
27	II.3.....	Analytical information for precipitation
28	II.4.....	Analytical results for precipitation
36	II.5.....	Sources of trace constituents (H ⁺ , Na, K, Mg, Ca, Cl, S, N-, P, Si, Al, Fe) in the Amazon atmosphere
54	II.6.....	Measurements of trace constituents in tropical atmospheres
71	II.7.....	Predicted cyclic Cl and measured Cl in Amazon surface waters
81	III.1....	Representative analyses of rocks and soils found in the Amazon Basin
117	IV.1.....	Comparison of the global average and Amazonian compositions of dissolved, suspended, and bed loads
119	IV.2.....	Observed ranges for various parameters
120	IV.3.....	Amazon surface waters classified after Meybeck (1979)
157	IV.4.....	Summaries of the geology of all the river basins that were sampled
161	IV.5.....	Analytical results for Amazon surface water samples
229	IV.6.....	Thermodynamic constants for weathering reactions
237	IV.7.....	Normative mineralogies of average shield and shale
238	IV.8.....	Products of weathering the average shield and shale
290	V.1.....	Discharge model equations
313	VI.1.....	Estimation of the contributions to the dissolved load made by various source regions in the Amazon Basin
316	VI.2.....	Estimation of the contributions to the dissolved load from the weathering of various general lithologies (silicates, carbonates, and evaporites), as well as from cyclic salts

Chapter I

Introduction

I. INTRODUCTION

The earth's surface environment can be viewed as being partitioned into several major geochemical reservoirs: the atmosphere, oceans, sediments, regolith, basement rocks, and biomass. A complex interplay of processes alters material within the reservoirs and transfers material between them. A primary working hypothesis for the study of global geochemical cycles is that the transfers between reservoirs are balanced in terms of their inputs and outputs such that the bulk compositions of the reservoirs change minimally through time.

Continental denudation, the focus of this study, is a major aspect of global geochemical cycling, involving the transport of materials from bedrock and atmospheric reservoirs to the ocean. The transfer is mediated by a wide variety of chemical, biological, and physical weathering processes, often involving intermediate storage in soil, biomass, lake and ground waters, and continental sediment. Due to this complexity, the simple concept of the transfer between reservoirs becomes exceedingly difficult to apply in actuality. Consequently, many investigations of global geochemistry do not extend beyond the most basic compilations of transfer rates between reservoirs.

The great number and diversity of rivers flowing into the ocean necessitates generalization of fluxes and mechanisms using data obtained from larger rivers draining different environments such as the Amazon, Congo, and Mekong in the tropics; the Colorado and Nile through deserts; Mississippi and the Yangtze in temperate regions; and the Mackenzie, Yukon, and the Lena at high latitudes. Adequate data on the chemistry of these rivers in the natural state are often lacking as a consequence of a variety of factors including inaccessibility, human activities, and poor or incomplete analysis.

Much of what is known about the chemistry and material fluxes of rivers on a global scale is based on a few compilations of river data, often from diverse sources, and on models utilizing these data.

Dissolved Solids:

Clarke (1924)
Durum, Heidel, and Tison (1960)
Livingstone (1963)
Meybeck (1976)

Suspended Solids

Fournier (1960, 1968)
Holeman (1968)
Curtis, Culbertson, and Chase (1973)
Martin and Meybeck (1979)

Bed Material:

Potter (1978)

Global Models:

Conway (1942)
Eriksson (1959, 1960)
Gibbs (1970, 1971)
Feth (1971)
Garrels and Mackenzie (1971)
Holland (1978)
Meybeck (1976, 1977, 1979)
Martin and Meybeck (1979)
Potter (1978)

The original data on which these studies are based are inadequate.

Livingstone (1963) notes some of the problems:

- (1) Insufficient spatial and temporal coverage: Many rivers show wide variations in flow and composition, yet are represented by only a few samples. Data for some of the largest rivers in the world have not been reported at all.

(2) Inaccurate or incomplete analyses: Much of the data in the compilations was not collected for geochemical purposes and is of poor quality. Even when samples are collected for geochemical studies, samples are treated and analyzed in different manners. Varying operational definitions are used to define dissolved, colloidal, suspended, and adsorbed phases. Finally, samples may become contaminated by the handling procedure, for example the storing samples to be analyzed for silica in glass.

The second point must be emphasized, as many of the measurements were made prior to the advent of modern analytical instrumentation and techniques having greatly increased sensitivity and precision (e.g. atomic absorption).

In contrast to global modelling, the study of single large river basins, is far more mechanistically oriented and usually does not suffer from the inconsistencies of gathering data from diverse sources. Of particular interest are the large basin studies, as the present work belongs to this category. Only two river basins have been subject to comprehensive geochemical investigations: the Amazon (Sioli 1954a, b, 1955, 1957a, b, 1963, 1964, 1968, Gibbs 1965, 1967a, b, 1972) and the Mackenzie (Hitchon et al. 1969, Hitchon and Krouse 1972, Reeder et al. 1972, Peake et al. 1972). Studies of large river basins have the advantage of being comparative, due to the diversity of terrains within a large basin, and internally consistent since the analyses for a particular property are done in one laboratory.

The Mackenzie River study is the only examination of a large river system utilizing modern instrumentation. Like the current Amazon project the bulk of the data is derived from one part of the year. The work on the Amazon also includes samples of precipitation, lacking in the

Mackenzie work. Having precipitation measurements permits estimates of atmospheric inputs, and allows for prior correction for these inputs before examination of terrestrial controls of surface water chemistry.

This study will be presented in four parts:

- (1) Atmospheric Inputs - The chemistry of precipitation will be examined; this information will be used to establish the atmospheric contribution to river water. (Chapter II)
- (2) Environmental Data - The geology and denudation regimes of the Amazon Basin will be summarized. (Chapter III)
- (3) River Chemistry - Chemical relationships based on traditional classification schemes, on thermodynamic considerations, and on hypothesized weathering reaction mass balances will be compared to geological and environmental data for the various rivers sampled, so as to establish a consistent view of weathering processes in the Amazon Basin. (Chapter IV)
- (4) Chemical Transport and Denudation - Detailed examination of discharge and chemical transport will be undertaken for the two river transects. These information will be applied to calculating denudation rates. (Chapters V & VI)

Chapter II

Amazon precipitation chemistry and the marine contribution to the Amazon dissolved load.

II.1 INTRODUCTION, AMAZON PRECIPITATION CHEMISTRY

It is widely agreed that the atmospheric contribution to dissolved materials in surface waters can be substantial, and that corrections for this input are required prior to calculating weathering mass balances. Table (II.1) presents examples of estimates of atmospheric inputs to surface waters. The three global estimates are calculations made on the basis of reviews of available literature. The examples taken from small watershed studies were calculated from coordinated measurements of atmospheric inputs and river outputs. The atmospheric contributions for several elements are quite large and vary considerably between estimates. The disparity between estimates suggests that great uncertainty exists in procedures used to estimate atmospheric contributions to river systems.

There are no direct procedures for measuring the net flux of atmospherically derived materials being transported out of a drainage basin in river water, either in an absolute sense or relative to contributions from weathering. This requires that two distinct aspects of the problem be examined. Firstly, the sources of material in atmospheric inputs to the river basin must be identified, primarily to determine if all the material is to be considered as being derived from outside of the river drainage. Secondly, criteria must be established for calculating the contribution of the atmospheric inputs to the river water.

In the studies of small river basins, long term sampling of precipitation and dry fallout is assumed to provide a good lower bound to the net atmospheric input into the basin. The absence of appreciable sulfur, chlorine, and nitrogen bearing minerals in the bedrock of the basins of the

TABLE II. 1
 PERCENTAGE OF
 RIVER-BORNE DISSOLVED MATERIAL REPRESENTED BY
 ATMOSPHERIC INPUTS

	<u>To the Continents:</u>			<u>To Small River Basins:</u>	
	<u>E</u>	<u>G & M</u>	<u>H</u>	<u>H.B.</u>	<u>P.B.</u>
Na	43 %	35 %	19 %	21%	45%
K	4 %	15 %	14 %	38%	42%
Mg	9 %	7 %	2.9%	18%	48%
Ca	0.4%	0.7%	1.3%	16%	71%
C _{inorg.}	≈0 %	0.2%	60 %*	--	10%
Cl	75 %	55 %	27 %	139%**	100%
S	59 %	6 %	39 %	107%**	100%

E -Eriksson (1960)

G & M -Garrels and Mackenzie (1971)

H -Holland (1978)

H.B. -Hubbard Brook, Likens et al. (1977)

P.B. -Pond Branch, Cleaves et al. (1970)

* includes atmospheric carbon "fixed" by rock weathering

** considered to be 100% within the resolution of the estimates

tabulated examples, means that the net atmospheric input of these elements would equal river output under steady state conditions. The difference between combined precipitation and dry fallout inputs, and river output is assumed to represent material transferred from the atmosphere to the ground or vegetation by impaction, absorption, and surface reaction. The principal weakness in this assumption is the failure to account for the possibility that some of the material in precipitation and dry fallout, perhaps a dominant proportion, is locally derived and is therefore not a component of the net atmospheric flux into the basin. Major locally derived contributions to atmospheric inputs are expected, as the bulk of materials contributed to the atmosphere by surface sources has a short residence time and does not travel long distances (c.f. Bolin et al. 1974).

The estimates of atmospheric contributions to continental runoff used assumptions similar to those utilized in the study of small river basins, however the assumptions are not supported by an adequate body of data. The net loss of material from continents is taken from estimates based on data compilations for large river systems (see Chapter I). Eriksson (1960) computes airborne inputs as the river output less human and rock weathering contributions. The latter contribution is determined on the basis of geology and does not include evaporite inputs, which he dismisses as insignificant. Garrels and Mackenzie (1971) base their calculations on a single, 1937, estimate for average rain composition, uncorrected for terrestrial inputs. They ignore later work. Holland (1978), who fails to state his assumptions, apparently uses winter precipitation chloride data of Junge and Gustafson (1957) and applies a continental average evaporation correc-

tion to the data. Why he did not use the annual data of Junge and Werby (1958) is unclear. He appears to have calculated the marine component of other ions using seasalt ratios. The sulfate input is apparently assumed to be entirely anthropogenic.

The following discussion of the atmospheric contribution to Amazonian surface waters is in two parts. The first focuses on the chemistry of precipitation collected during the period of May to July 1976 and 1977 on transects of the Amazon Basin along the main channel. Chemical, geographic, and time series relationships are used to establish sources of various chemical species in the samples and in particular to distinguish marine and terrestrial components. The second part establishes the relationship between the distance from the Atlantic Ocean and the chloride content of rivers which drain terrains lacking chloride bearing rocks. This relationship is utilized to calculate cyclic salt contributions to Amazon surface waters.

II.2:1 COLLECTION AND ANALYSIS

Precipitation samples were collected off the northeast coast of South America and in Brazil, Peru, Columbia, and Bolivia, (Figure II.1, Table II.2). A majority of the samples were collected utilizing a sequential sampler on board the R.V. Alpha Helix in the period of mid-May to mid-July, which extends from the end of the wet season well into the dry season for much of the Amazon Basin south of the equator. Additional rain samples were collected in Peru, using a small funnel collector placed atop small-town hotel roofs. Snow samples were collected in July and December on Chacaltaya Mountain, Bolivia (5200m).

The shipboard sequential sampler used a large funnel of approximately 0.25m^2 . Storms prior to 2 June 1976 were sampled utilizing a funnel consisting of a polyethylene sheet draped over a frame. After this date an acrylic plastic funnel was used. The 1976 samples were measured and distributed to bottles by a rocker mechanism of acrylic plastic, analogous to that of rocker-type rain gauges. To reduce handling, 1977 samples were collected directly in 500 ml bottles. The funnel was covered with a plastic sheet between storms, and was rinsed three times with distilled water immediately prior to sample collection. Sampling was done at least 100 meters from land, but usually greater than 500 meters. The collector was mounted on the flying bridge (~8 m above the water surface), away from the rigging and the smoke stack, both of which represented potential sources of contamination. A person was present during collection to cover the sampler if rain was passing through the rigging or the exhaust stream, and to record which samples might be so contaminated. The samples were biased towards large storms, as each sample represents an equal amount of precipitation, and it proved difficult to collect uncontaminated samples

Figure II.1

Sample location map for Amazon precipitation

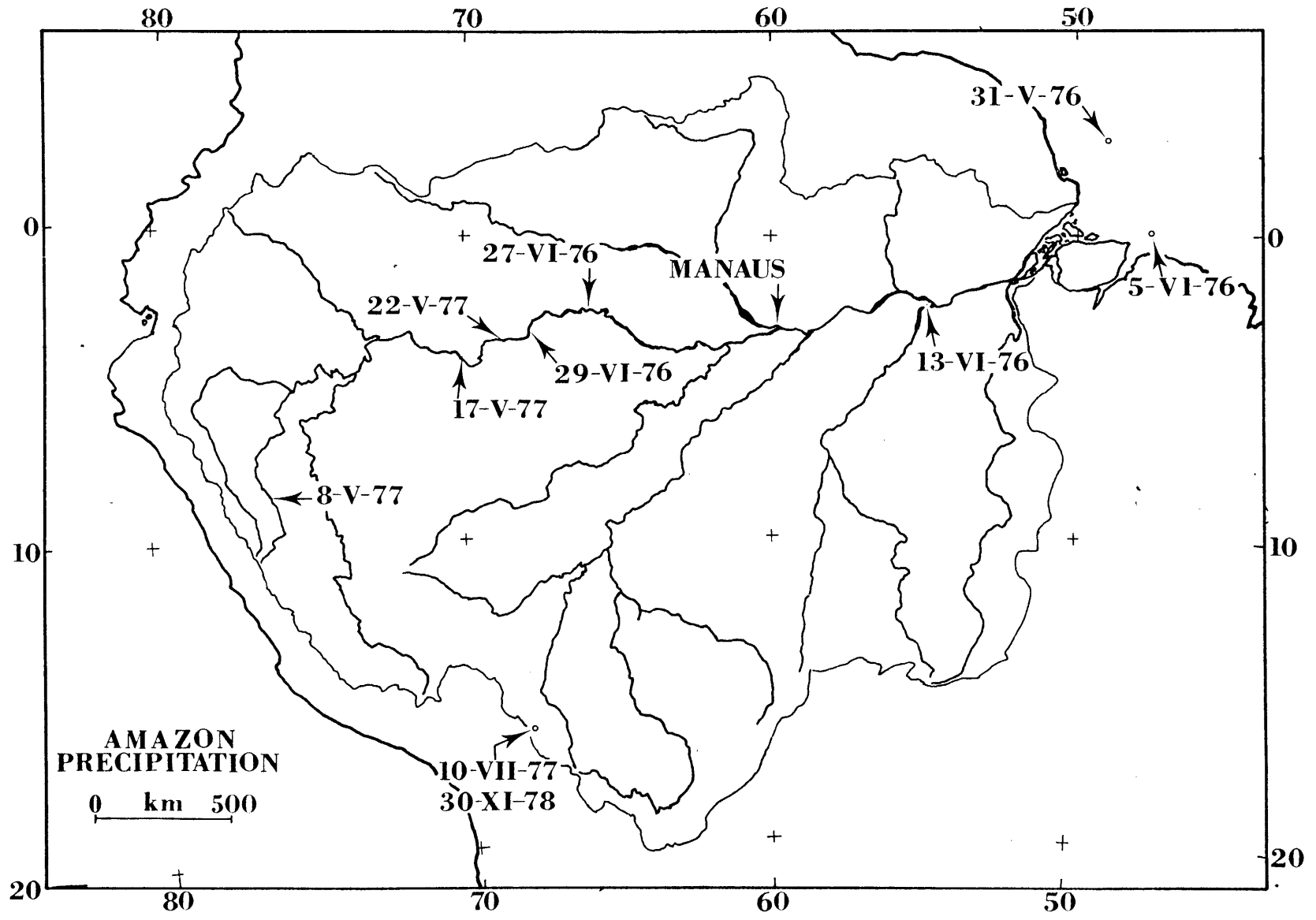


TABLE II. 2
SAMPLE DESCRIPTION

<u>DATE*</u>	<u>DESCRIPTION OF EVENT</u>	<u>DURATION</u>	<u>NUMBER OF SAMPLES</u>	<u>SAMPLE VOLUME</u>
31- V-76	light shower	15 min.	1	100 ml
5-VI-76	light shower	15 min.	1	200 ml
13-VI-76	intense rain ⁼	30 min.	8	all 500 ml
27-VI-76	light shower	30 min.	1	500 ml
29-VI-76	light rain showers	3 hr.	8	all 500 ml
8- V-77	moderate rain	1 hr.	1	300 ml ⁺
17- V-77	intense rain ⁼	30 min.	11	all 500 ml
22- V-77	intense shower ⁼	5-10 min.	2	500+300 ml
10-VII-77	fresh snow	--	4 ^x	2000 ml
30-XI-78	few day old snow	--	4 ^x	2000 ml

* refer to Figure II.1 for locations

= all samples took less than five minutes to collect

+ 20 cm funnel

x acidified + unacidified splits
 snow melted in polyethylene bags,
 hot leached in distilled water

from showers due to wind shifts. During a heavy rain, the ship could be directed into the wind for a sufficient period to collect a large number of samples. Samples suspected of being contaminated usually showed elevated levels of sulfate, chloride, and hydrogen ions, and to a lesser extent other species. Only one Peruvian rain sample was free of insect parts and pieces of vegetation, and was therefore considered uncontaminated.

Additional sampling bias towards large storms was caused by meteorological factors. Anderson et al. (1974) show that clouds, and by inference showers, form preferentially over land in the Amazon Basin. The large rivers frequently stand out sharply as cloud-free areas in satellite photographs. The contrast is due to the greater sensible and latent heating over land. Presumably large storms are not so strongly affected by surface differences, as can be seen in the spreading of very active storms in satellite photos.

II.2:2 Analytical Methods

Analytical methods and precisions are summarized in Table (II.3); a detailed discussion of analytical techniques is found in Appendix (III). Analytical results are found in Table (II.4). Showers sampled at sea yielded small volumes (Table II.2), hence the incomplete analyses and the lower precisions. Figure (II.2) is a plot of analyzed anions against analyzed cations, showing that there are no major omissions for charged species. The failure to analyze for ammonia in 1977 does not have a significant effect on the charge balance. The 1976 samples show poorer charge balances than 1977 samples as a result of more handling steps and lower analytical precisions.

TABLE II. 3
ANALYTICAL INFORMATION

<u>SPECIES</u>	<u>INSTRUMENTATION</u>	<u>PRECONCENTRATION</u>	<u>PRECISION (est. 2σ), the greater of:</u>
pH	electrode	--	0.05 pH units
Na	atomic absorpt.	--	0.2 μmole/l or 2% 1976* 0.1 μmole/l or 1% 1977+
K	" "	--	0.1 μmole/l or 1%*
Mg	" "	--	0.1 μmole/l or 1% 1976* 0.03 μmole/l or 1% 1977+
Ca	" "	--	0.1 μmole/l or 1%*
Cl	titration	<5x 1976 >10x 1977	0.8 μmole/l or 1% 1976* 0.3 μmole/l or 1% 1977
SO ₄	colorimetric	5x 1976 10x 1977	0.8 μmole/l or 4% 1976* 0.4 μmole/l or 4% 1977
NO ₃ ^x	"	--	0.4 μmole/l or 4%
NH ₄ ^x	"	--	0.5 μmole/l or 5%
Silica	"	--	0.3 μmole/l or 2%
Fe	"	--	0.1 μmole/l or 3%
Al	"	--	0.1 μmole/l or 3%
NICB [#]	---	--	E/Z+

x occasional random high blanks

+ multiple analyses

* halve the precisions for the 1976 marine rain analyses,
as half volumes were used in the analyses.

normalized inorganic charge balance (total charge)/(total cations)
its error (E/Z+) is calculated from the analytical precisions

TABLE II.4

AMAZON PRECIPITATION: ANALYTICAL RESULTS

STA.	PARAMETER: -LOCATION-	TZ+ PH	NA	K	MG	CA	CL	SO4	NO3	NH4	NICB	EZ/+
RA01	31- V-76	-- --	232.	4.7	30.6	4.2	289.	29.9	--	--	--	--
RA02	5-VI-76	-- --	130.	4.3	16.2	3.7	141.1	24.8	--	--	--	--
RA03	13-VI-76	126. 4.74	75.	2.7	8.6	4.1	89.2	12.7	4.9	5.3	0.0517	0.026
RA04	13-VI-76	36. 4.94	18.6	1.3	1.4	0.8	25.9	4.1	2.3	0.0	-0.0283	0.068
RA05	13-VI-76	37. 4.87	14.2	1.5	1.5	2.2	14.0	7.8	2.5	0.1	0.1147	0.070
RA06	13-VI-76	37. 4.88	19.5	0.4	1.2	0.7	18.0	5.7	2.3	0.6	0.1442	0.069
RA07	13-VI-76	46. 4.71	21.8	0.5	1.5	0.7	24.4	6.7	3.0	0.1	0.1133	0.067
RA08	13-VI-76	49. 4.71	20.6	1.6	1.4	1.4	22.7	9.3	3.7	1.7	0.0682	0.064
RA09	13-VI-76	37. 4.76	16.2	1.2	0.9	0.3	13.8	9.4	3.0	0.3	0.0433	0.077
RA10	13-VI-76	28. 4.83	9.8	0.4	0.8	0.3	10.5	7.1	2.1	0.3	0.0145	0.097
RA11	27-VI-76	21. 5.32	9.9	1.0	1.0	1.4	8.4	5.7	4.3	0.4	-0.1992	0.098
RA12	29-VI-76	32. 5.03	13.2	2.1	1.8	1.4	14.0	8.3	5.5	0.8	-0.1505	0.072
RA13	29-VI-76	21. 5.04	7.4	1.2	0.9	0.5	5.7	5.9	4.0	0.0	-0.0722	0.110
RA14	29-VI-76	27. 4.97	9.2	0.9	1.4	1.5	11.5	7.3	2.9	0.0	-0.1055	0.089
RA15	29-VI-76	-- 4.85	1.6	0.5	0.2	0.0	1.9	6.5	--	0.2	--	--
RA16	29-VI-76	33. 4.82	12.0	2.0	1.2	0.8	15.8	8.2	1.6	0.3	-0.0194	0.081
RA17	29-VI-76	28. 5.05	11.7	1.1	2.0	0.7	14.9	6.0	3.6	0.8	-0.1111	0.081
RA18	29-VI-76	29. 5.05	9.7	1.5	2.0	1.5	8.4	7.0	3.5	2.0	0.0920	0.077
RA19	29-VI-76	17. 5.07	4.7	1.1	0.7	0.5	5.7	4.2	2.6	0.4	-0.0087	0.130
RA20	8- V-77	-- 5.67	1.7	1.0	0.84	4.6	3.4	1.9	--	--	--	--
RA21	17- V-77	18. 5.08	4.2	1.7	0.47	1.6	5.9	6.3	1.0	--	-0.0938	0.080
RA22	17- V-77	32. 5.34	22.3	0.7	1.71	0.6	23.2	2.8	0.6	--	0.0534	0.039
RA23	17- V-77	21. 5.16	10.0	1.4	0.87	0.4	11.7	2.3	0.2	--	0.1714	0.066
RA24	17- V-77	15. 5.26	7.3	0.4	0.59	0.3	8.9	1.8	0.6	--	0.0740	0.084
RA25	17- V-77	24. 5.20	14.9	0.6	0.94	0.3	14.0	5.4	0.0	--	-0.0484	0.055
RA26	17- V-77	25. 5.33	16.7	0.5	1.00	0.4	16.2	2.4	0.0	--	0.1082	0.050
RA27	17- V-77	17. 5.31	10.1	0.3	0.59	0.2	10.9	2.9	0.9	--	-0.0852	0.072
RA28	17- V-77	22. 5.35	14.4	0.5	0.82	0.5	15.1	2.2	0.2	--	0.0523	0.055
RA29	17- V-77	16. 5.42	10.3	0.4	0.58	0.3	11.8	1.4	0.1	--	0.0264	0.072
RA30	17- V-77	11. 5.32	5.0	0.2	0.28	0.2	6.0	1.6	0.3	--	0.0482	0.111
RA31	17- V-77	12. 5.25	5.4	0.3	0.28	0.1	6.4	2.0	0.1	--	0.0509	0.107
RA32	22- V-77	-- 5.04	5.3	2.4	0.51	1.4	6.7	5.8	--	--	--	--
RA33	22- V-77	-- 5.18	2.7	0.7	0.25	0.5	3.9	3.0	--	--	--	--
M-06	10-VII-77*	14. 5.16	0.3	0.2	0.17	2.9	1.5	3.2	--	--	0.3665	0.100
BPA07	30-XI-78*	12. 5.75	2.3	0.9	0.38	3.1	1.1	2.1	3.4	--	0.0422	0.092

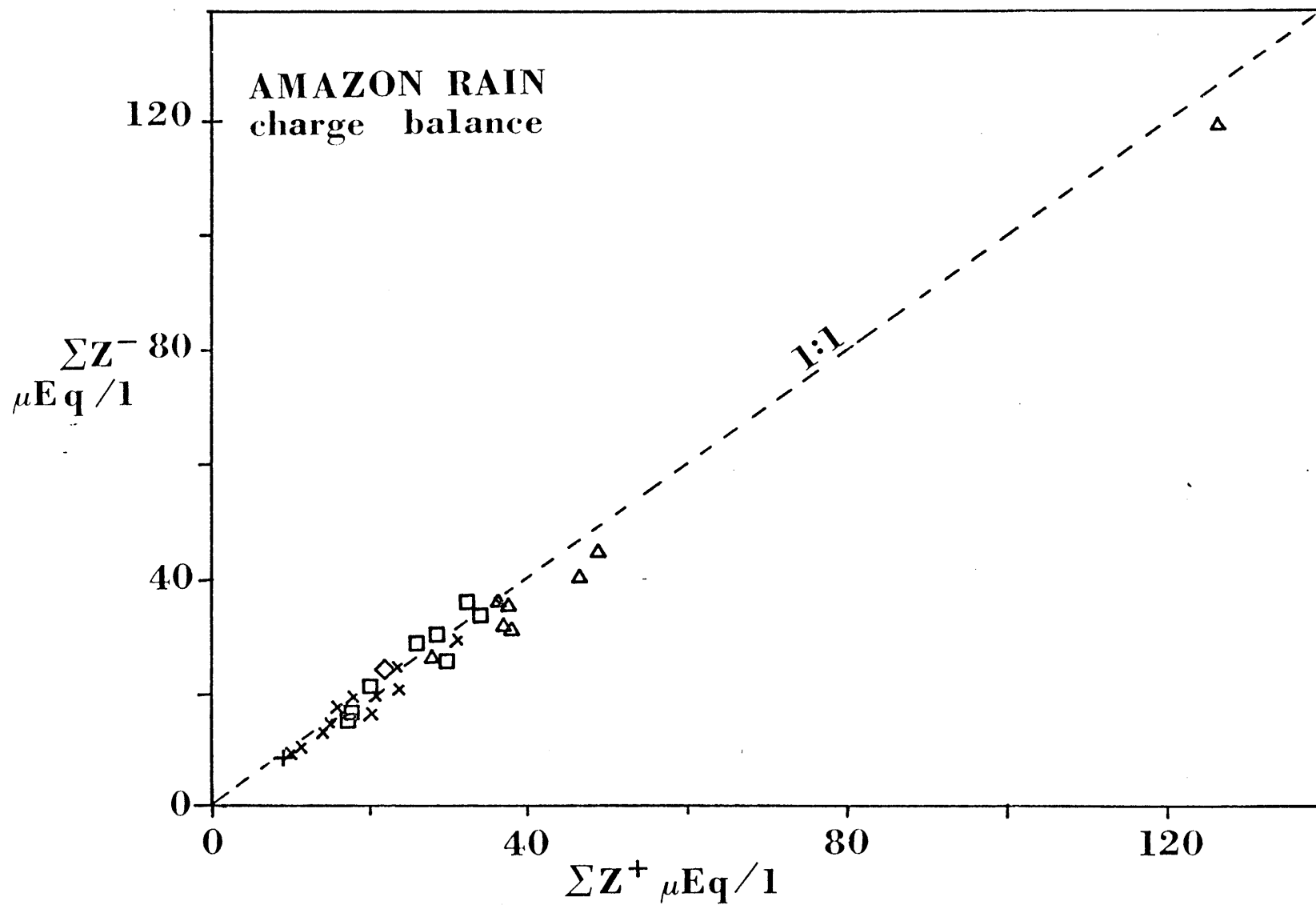
* SNOW SAMPLE

Figure II.2

Charge balance in Amazon precipitation

Symbol key:

13-VI -76 ---Δ
27-VI -76 ---◇
29-VI -76 ---□
8- V -77 ---†
17- V -77 ---×
22- V -77 ---✕
10-VII-77 ---}+
30-XI -78 ---}+



II.2:3 Discussion of Sampling

Since the objective of this study is to identify the sources of material in precipitation based on chemical relationships, sequential sampling is ideally suited. It provides a large number of samples with a wider range of concentrations than would be obtained by bulk sampling. In addition, this technique provides information about time variations within storms, which can be used to infer the part of the atmospheric column from which the chemical constituents are derived.

Time variations of chemistry during storms reflect in general the effects of washout and rainout (Junge 1963). Washout involves scavenging by falling drops and is most effective for particulates of $>1 \mu$ diameter. Rainout involves removal onto condensing droplets and affects particulates of all sizes and gases, though through a variety of mechanisms. The sharp drop in concentration near the beginning of many storms is a washout effect. Washout operates on particulates below the cloud base; the chemistry of showers is dominated by washout, while in heavy rains it is dominated by rainout (Junge 1963). Consequently, the chemistry of washout can be used as a guide to the $>1 \mu$ aerosol composition of the lower atmosphere, and rainout chemistry to the composition of particulates (including $>1 \mu$ particulates) and soluble gases more widely distributed through the air column. From this information, one can make inferences about the residence times and transport histories of the particulates involved. Bolin et al. (1974) demonstrate, using a model of a turbulent boundary layer, that the atmospheric residence time of particulates increases with altitude, and that the increase is especially rapid as one passes through the boundary layer. Materials injected at the

surface would therefore be rapidly recycled within the basin. Much of the material higher in the column would, in general, be derived from a more distant source than material lower in the column.

Finally, sequential sampling procedures limit a major source of error encountered in bulk sampling. Galloway and Likens (1976, 1978) point out that perhaps the largest source of error in bulk sampling is that of leaving the sample in the collector for prolonged periods (they recommend no more than a week), which allows for evaporation, biological activity, and contamination by falling debris. For sequential sampling, the residence time of samples in the collector is short and sources of contamination can be more closely monitored. This procedure could be followed for bulk sampling, but typically is not; presumably the work required for the equivalent quantity of data would be prohibitive.

II.3 BACKGROUND

II.3:1 Amazon Basin Meteorology

The Amazon River Basin lies entirely within the tropics, being situated between 6° north latitude and 20° south latitude. Average temperatures are very uniform over lowland parts of the basin (22 - 26°C) and decrease systematically with altitude. Treeline ranges from 3500-4500 meters, while the perpetual snow line occurs from 4000 - 5000 meters. In excess of 3500 mm/yr precipitation falls in the northwest lowlands. This amount decreases to less than 2000 mm/yr in the extreme northeastern and southern parts of the basin (Hoffmann 1975, Salati et al. 1978, Hjelmfelt 1978). Precipitation amounts increase markedly in the Subandean zone and on the east flanks of the Andes, due to orographic effects; up to 7000 mm/yr precipitation is recorded (Hoffmann 1975). Precipitation amounts drop to less than 1000 mm/yr in the central Andes. Moisture and air transport is in an east to west direction, with moisture taking from 6 days (in July) to 10 days (in the period January to October) to reach the Subandean zone from the Atlantic (Molion 1975).

The annual motions of the inter tropical convergence zone play a significant role in the seasonal distribution of precipitation (Hjelmfelt 1978, Salati et al. 1978) and cloudiness (c.f. Miller 1971). South of the equator there is a distinct dry period from June to August, while to the north of the equator the dry season lasts from January to March. In the part of the basin bracketing the equator, the seasonal drought is less well defined, lasting August to November in the east and being nonexistent in the west. The recycling of water by evapotranspiration increases the amount of precipitation falling during

the dry season in the western part of the basin (Molion 1975, Lettau et al. 1979). It is estimated that 88% of the water in the precipitation which falls in the western part of the basin has fallen at least once before during transit. Much of the eastern flank of the Andes lacks a pronounced dry season, however the seasonal variations in precipitation that occur tend to reflect variations to the east.

Typical storms of the Amazon Basin are of a convective type, driven primarily by local latent and sensible heating. These storms average about one hour in duration (Hjelmfelt 1978). Their intensity varies considerably, from light showers to storms producing several centimeters of rain per hour. All storms sampled during this study were of this category. Precipitation associated with frontal events, "friagem", is comparatively rare, as these occur, on average, five times a year (Ratisbona 1976).

II.3:2 Previous Studies of Amazon Precipitation Chemistry

Several studies have reported analyses of precipitation from the Amazon Basin. Ungemach (Ungemach 1969, Anon. 1972b) presents a two year (1966-1968) time series of plant macronutrient concentrations in precipitation, from near Manaus, Brazil. As sampling from the R.V. Alpha Helix took place during the transition from wet to dry seasons, it is important to note that Ungemach observes that concentrations do not vary markedly within seasons, and that the dry season concentrations are generally higher than wet season concentrations. On this basis, it seem reasonable to say that concentrations in precipitation collected from the R.V. Alpha Helix are higher than the annual average. Concentrations from Ungemach and several studies reporting single analyses (Gibbs 1970, Brinkmann and Santos 1973, Nortcliff and Thornes 1978) are close to those of this study.

II.4:1 SOURCES OF MATERIALS IN AMAZON PRECIPITATION

The elements examined in this study (Na, K, Mg, Ca, Cl, S, P, Al, Si, Fe) have short residence times as particulates or gases, on the order of 1 to 10 days (Junge 1963, Junge 1974, Junge and Werby 1958, Rahn et al. 1976). It is assumed that these elements are derived from sources generating a characteristic mixture of elements, for example the seasalt aerosol. Furthermore, gases and $< 5 \mu$ particulates can be expected to be transported in the same manner in the lower troposphere, (i.e. they have the same diffusivities and are not affected by gravity, c.f. Junge 1963). Hence the chemistry of material being removed from the atmosphere will retain some of the chemical characteristics of its sources. These can be grouped into the general categories of marine, terrestrial, and anthropogenic inputs.

Potential sources of elements and species in precipitation falling in the Amazon Basin are summarized in Table (II.5). Sodium, potassium, magnesium, calcium, silicon, iron, and aluminum are generated exclusively as particulates. Nitrogen in precipitation is derived directly or indirectly from gas phases. Chlorine and sulfur have particulate and gas sources. Primary element associations are marine inputs, Cl-Na-Mg-S; soil inputs, Al-Fe-Si-Ca; biological inputs, N-S-K; burning of vegetation, Ca-K-P-(N); and industrial pollution (of doubtful significance), S-N-Cl. The remainder of this section examines the potential inputs and relates them to the chemistry of precipitation in the basin.

II.4:2 Anthropogenic Inputs

Pollution is unimportant, except on a localized basis. At present, there are few industries in the lowlands that could act as a major source;

TABLE II. 5
SOURCES OF TRACE CONSTITUENTS IN THE AMAZON ATMOSPHERE

<u>SPECIES/ ELEMENT</u>	<u>MARINE INPUTS</u>	<u>TERRESTRIAL INPUTS</u>	<u>POLLUTION INPUTS*+</u>
H	reaction of gas phase inputs	reaction of gas phase inputs	reaction of gas phases in burning
Na	salt spray ^x	minor: burning, soil dust	land clearing ⁺
K	salt spray ^x	vegetation, burning, minor soil dust	land clearing ⁺
Mg	salt spray ^x	minor: burning, dust	land clearing ⁺
Ca	salt spray ^x	soil dust	land clearing ⁺
Cl	salt spray ^x gas phase?	—	—
S	salt spray, gas phase	gas phase from decay processes	fuel burning
N	gas phase?	gas phase from decay, maybe burning	fuel burning
P	—	vegetation, burning	land clearing ⁺
Si	—	soil dust	land clearing ⁺
Al	—	soil dust	land clearing ⁺
Fe	—	soil dust	land clearing ⁺

* Only the burning and dust associated with land clearing is considered to be important.

+ Land clearing is included in this column in that it represents exaggerated inputs of vegetation combustion products and dust over what is the normal background. Inputs from land clearing would not be chemically distinguishable from natural inputs.

x These elements are expected to be found in near seasalt proportions. Sulfate is expected in higher proportions due to gaseous contributions.

furthermore, mean atmospheric motions into the basin (c.f. Molion 1975, Ratisbona 1976) do not pass over significant outside sources. The several lowland mining centers, for example Amapa (Mn) and Rondonia (Sn), process oxide ores (Goodland and Irwin 1975). These would be a minor source of materials compared to the Andean mining centers where sulfide ores are processed. Material from the Andes, however, would tend to be blown to the west, out of the basin. The most important anthropogenic input is the burning of vegetation, which will be treated later as a terrestrial input.

II.4:3 Marine Components in Amazon Precipitation

The importance of the contribution of marine derived materials in atmospheric gases and aerosols has long been recognized (c.f. Eriksson 1952, 1955, 1959, 1960, Junge 1963). Marine materials transported through the atmosphere to the continents and returned to the oceans have come to be known as cyclic salts, a term which originally included evaporite inputs (Conway 1942). Maps of chloride concentrations and fluxes in precipitation over continents show steep gradients near the coast (Junge and Gustafson 1957, Junge and Werby 1958, Eriksson 1959, 1960), evidence of a marine source. Other ions show similar gradients, although the pattern is not so clear, being obscured by terrestrial and anthropogenic inputs. Steepest gradients are seen on the leeward side of continents and against mountain ranges (where inland transport is hindered by orographic precipitation). The concentration of chloride in Amazon precipitation decreases with increasing distance from the Atlantic (Figures II.3, II.4), consistent with an Atlantic Ocean origin.

II.4:4 Processes Transferring Materials from the Oceans to the Atmosphere

Two principal mechanisms transfer material from the oceans to the atmosphere: aerosol formation from bubble bursts and spray, and gas transfer. All substances dissolved in seawater are transferred during the formation of the aerosol. It is not precisely known to what degree fractionation occurs during droplet formation, however evidence suggests that little fractionation occurs for the major ions (Junge 1963, MacIntyre 1974); the more dilute species show greater fractionation.

The release of reduced gaseous sulfur compounds into the marine atmosphere is thought to be a significant additional source of sulfur. Compounds thought to be important are hydrogen sulfide and dimethylsulfide (DMS) (c.f. Graedel 1979). The most probable sources of these compounds are emissions from reduced coastal sediments and low-level releases from open ocean metabolism. Both compounds are produced by the decomposition of amino acids containing thiol groups; however sulfate respiration is a far more important source of H_2S (Schlegel 1974). Observed concentrations in the marine atmosphere are in the range of 0.2 to 4 nmoles S/m^3 air for H_2S (Slatt et al. 1978), DMS (Maroulis and Bandy 1977), and their intermediate oxidation product SO_2 (Lodge et al. 1960, Maroulis et al. 1978). Complete oxidation to SO_3 or H_2SO_4 is thought to take less than a day, and a reduced sulfur flux of about 6×10^{13} g S/yr would be necessary to sustain these concentrations (Graedel 1979). This sulfur flux is about one quarter that estimated by Eriksson (1959) for the transfer of sulfur to the atmosphere by sea spray, as SO_4 . The SO_3 and H_2SO_4 , produced from H_2S and DMS, are thought to react rapidly

Figure II.3

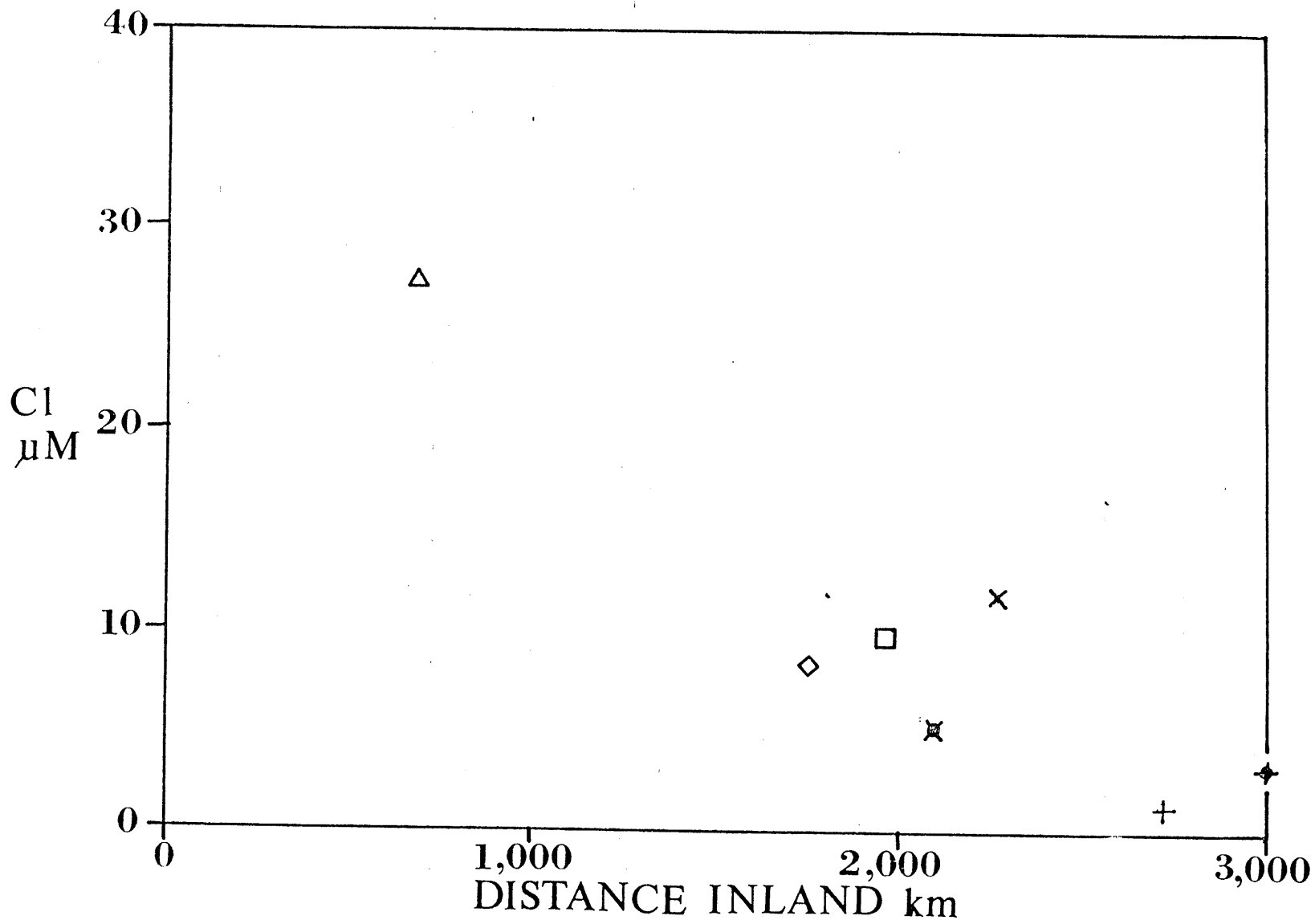
Map of the reference line used in calculating distances from the Atlantic coast. This line is perpendicular to the mean surface wind direction near the coast (c.f. Ratisbona 1976), where the marine aerosol is confined to lower altitudes (Junge and Gustafson 1957). A perpendicular to this line is parallel to the lines of mean air motion farther inland (c.f. Molion 1975), where the marine aerosol is more widely distributed through the air column (Junge and Gustafson 1957). Wind directions do not change appreciably throughout the year.

Figure II.4

Average value of chloride in different precipitation events plotted as a function of distance from the Atlantic Ocean.

Symbol key:

13-VI -77 -- Δ
27-VI -76 -- ◇
29-VI -76 -- □
8- V -77 -- †
17- V -77 -- ×
22- V -77 -- ✕
Chacaltaya - +



with water vapor and ammonia to form droplets (Junge 1963), and with sea spray (Eriksson 1959). Eriksson argues that the second reaction would cause HCl to be released from sea spray, as evaporation would cause the pH to drop and the HCl vapor pressure to rise enough to drive off HCl. Marine aerosol chemical data are consistent with this mechanism. Lodge et al. (1960) observe a five fold enrichment of sulfur compared to its seasalt proportions, and Meinert and Winchester (1977) observe a two to three fold enrichment of sulfur compared to its seasalt ratio to K and Ca (which are in seasalt proportions), while Cl is 25-40% depleted.

II.4:5 The Chemistry of the Marine Component in Amazon Precipitation

The ratios of Na, K, Mg, and Ca to Cl in marine precipitation (samples RA01 and RA02, Table II.4) range about the seasalt ratios:

mole ratios	<u>Seasalt</u>	<u>RA01</u>	<u>RA02</u>
Na/Cl	0.852	0.802	0.921
K/Cl	0.018	0.016	0.030
Mg/Cl	0.101	0.106	0.115
Ca/Cl	0.019	0.015	0.026

This is consistent with a dominantly sea spray origin for these species in precipitation. The deviations from seasalt ratios suggest that some degree of fractionation is involved. This is not unreasonable as these samples are from showers, and their chemistry would tend to be dominated by the washout of only coarse ($> 1 \mu$) particulates and would not represent the bulk composition of the aerosol.

Sulfate is roughly twice its seasalt proportions (SO_4/Cl mole ratios: seasalt-0.052, RA01-0.103, RA02-0.176), an indication that additional sources of sulfur contribute to marine precipitation. Reduced gas inputs would be a reasonable source of the excess. If one assumes

that part of the sulfate is derived from sea spray in seasalt proportions, a roughly equal contribution of sulfur from gas phase inputs is indicated. The relative contributions from these two sources would change depending on wind conditions and the generation of spray.

If chemical alterations and differential removal are slight, the marine component in inland precipitation would retain its chemical identity. Due to turbulent mixing during transport, this marine rain component would have ion proportions similar to average marine rain off the northeast coast of South America. As sampling was inadequate to establish a marine rain average, the assumption is made that the marine component in inland precipitation has seasalt proportions for all species relative to chloride (chloride is assumed to be entirely marine), except for sulfate. For the lack of a better estimate, a $SO_4:Cl$ ratio of $0.127 = (SO_{4RA01} + SO_{4RA02}) / (Cl_{RA01} + Cl_{RA02})$ is assumed to be the best representation of the marine contribution of sulfate in inland rain.

The chemical contribution of the marine rain component can be clearly identified in inland precipitation when the data is plotted against chloride content. This confirms that the composition of the marine component does not undergo major changes during inland transport. All data plot about or above marine rain trends drawn through the data (Figures II.5, II.6). The degree to which data plot above the trend provides an indication of the relative contributions of marine and terrestrial components. Na and Mg show minimal terrestrial contributions. All other species are dominated by terrestrial inputs, and NO_3 and NH_4 show no marine contributions. The plot of hydrogen ion

Figure II.5

Sodium, potassium, magnesium, and calcium versus chloride in Amazon inland precipitation. The lines indicate ratios for the two marine rain samples and seasalt.

Symbol key:

13-VI -76 -- Δ
27-VI -76 -- ◇
29-VI -76 -- □
8- V -77 -- †
17- V -77 -- ×
22- V -77 -- ✕
10-VII-77 -- }
30-XI -78 -- }+

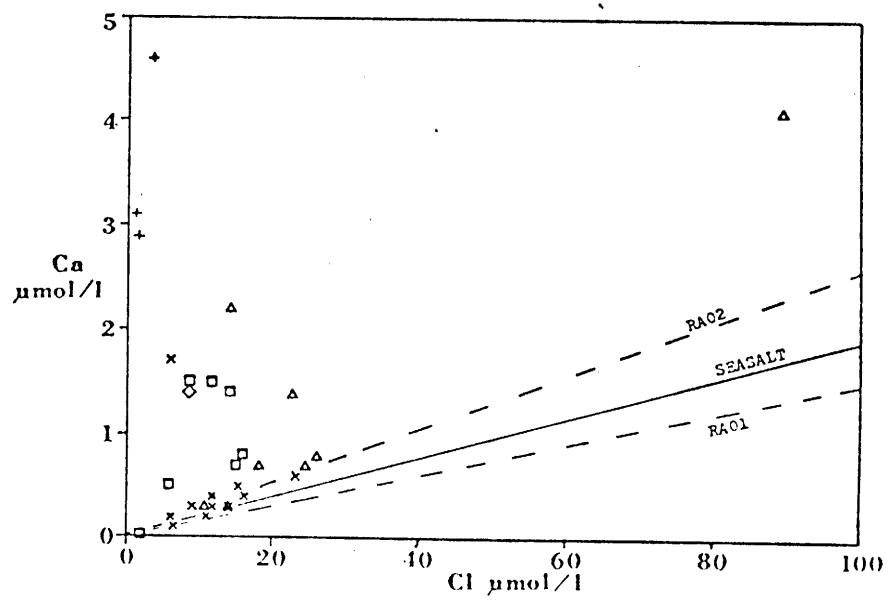
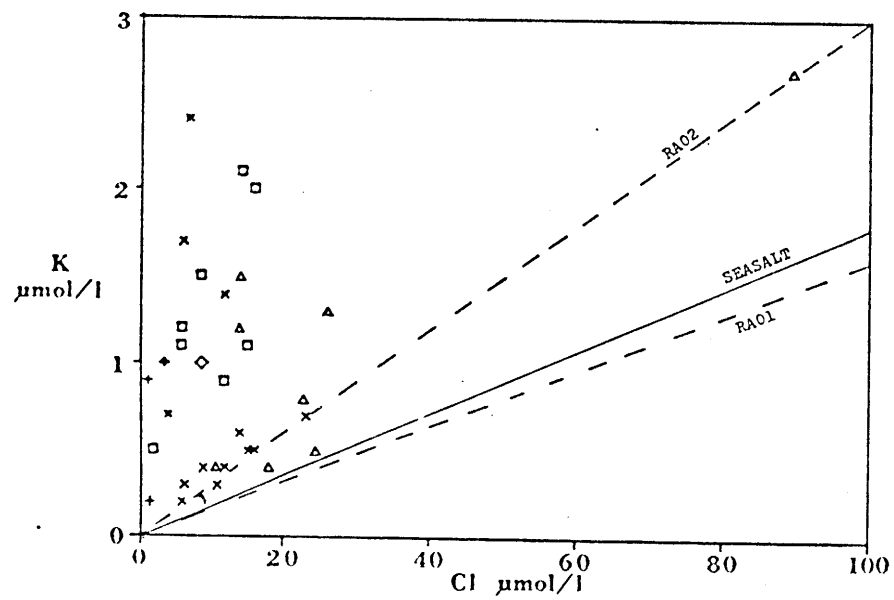
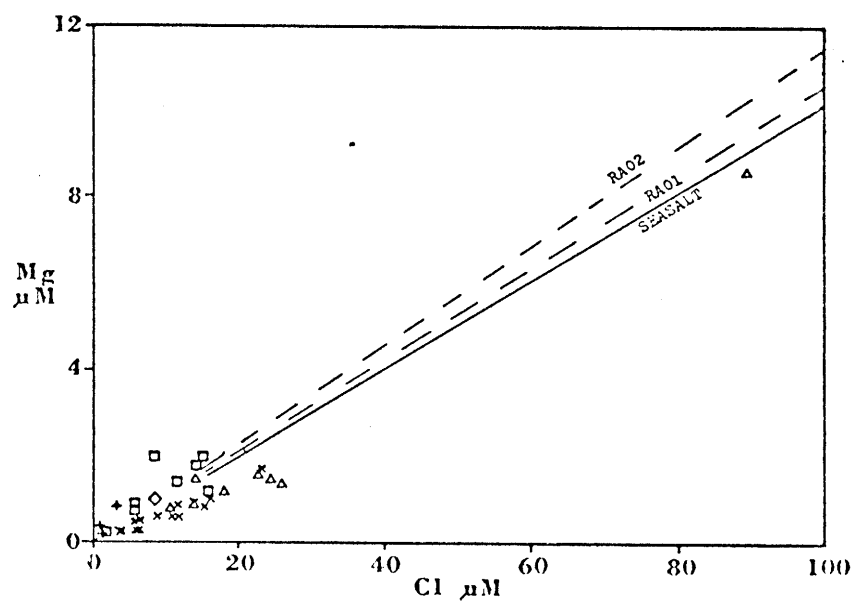
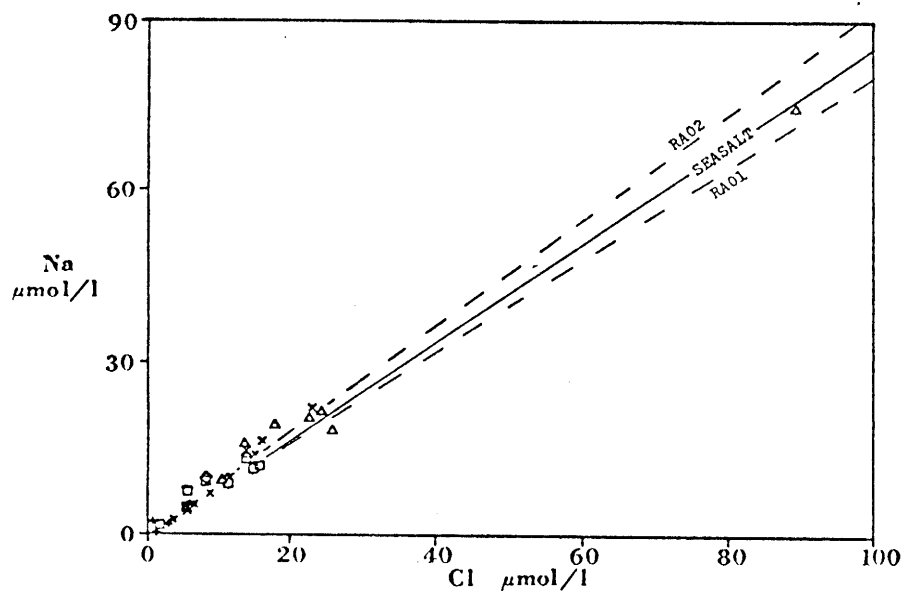
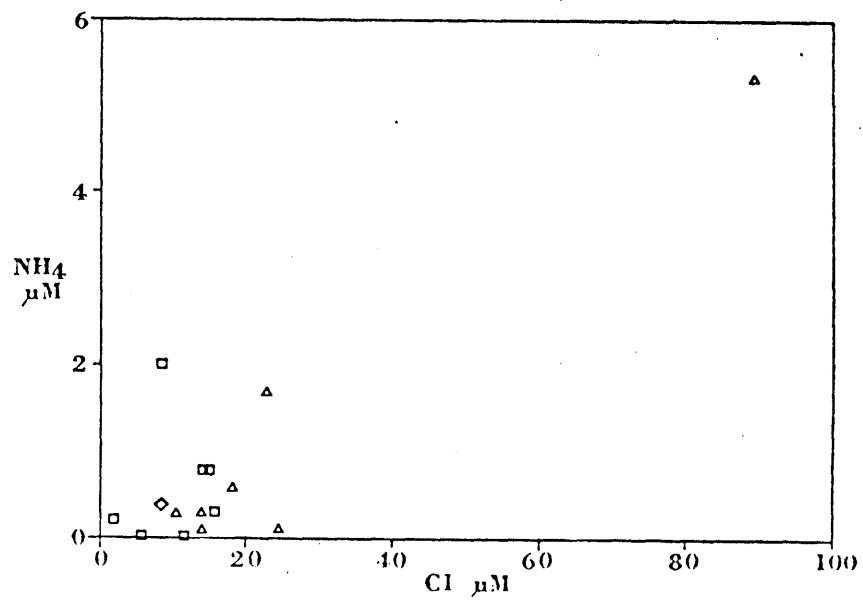
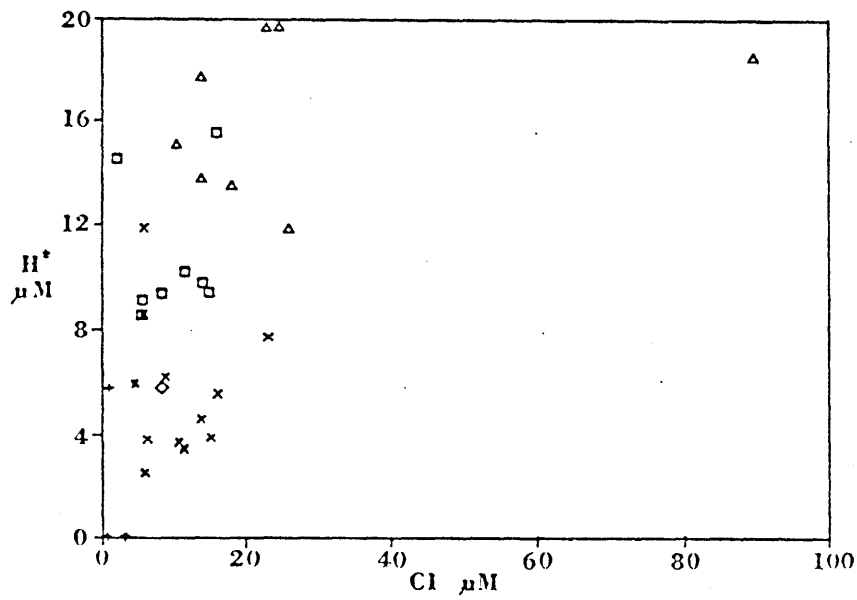
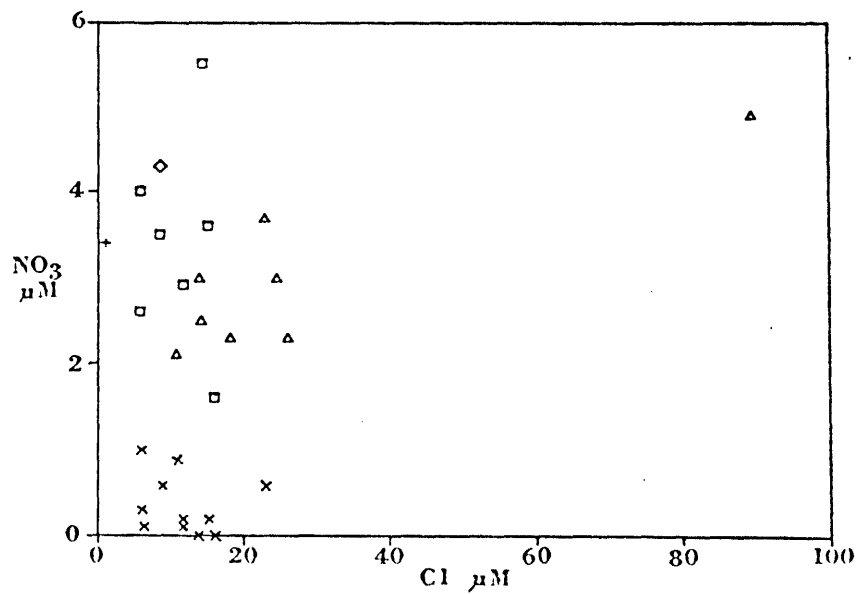
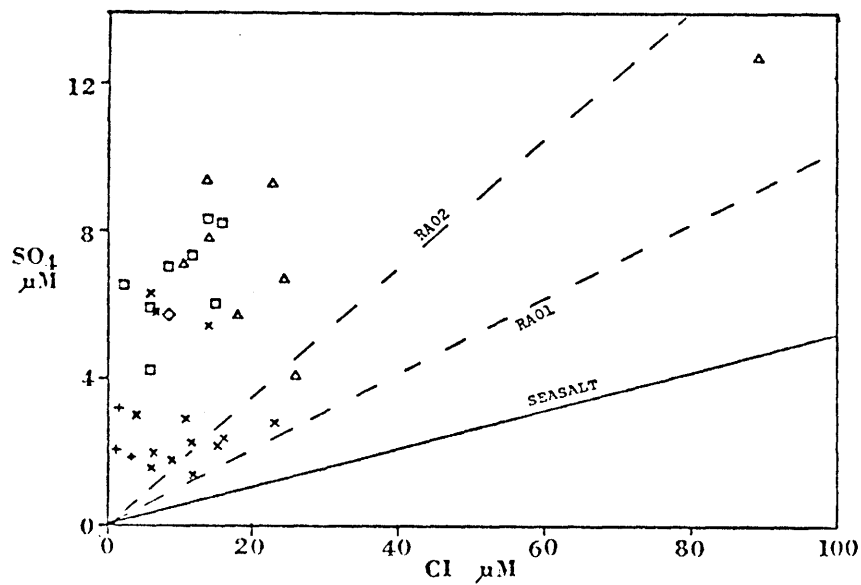


Figure II.6

Sulfate, nitrate, hydrogen ion, and ammonia versus chloride in Amazon inland precipitation. Ratios for the two marine rain samples and seasalt are indicated in the sulfate graph. Note that the seasalt line falls well below the data and the two marine rain ratios. Bicarbonate resulting from the equilibration with atmospheric CO₂ is subtracted from the hydrogen ion data (see Section II.4:9). Note that it is possible to envision a diagonal lower bound for the hydrogen ion data.

Symbol key:

13-VI -76 --- Δ
27-VI -76 --- ◇
29-VI -76 --- □
8- V -77 --- ◆
17- V -77 --- ×
22- V -77 --- ✕
10-VII-77 --- }
30-XI -78 --- }+



against chloride appears to be bounded by a diagonal line, consistent with the presence of sulfuric acid in marine rain.

Minor fractionation and alteration of the marine component is apparent in the inland rain samples. Magnesium ratios to chloride and sodium, in inland rain, show considerable variation relative to the marine rain ratios. The rain Mg:Na ratio (Na is used, as it is analyzed to a greater precision than Cl) tends to be higher than the seasalt Mg:Na ratio in light rain (Table II.2) and lower than the seasalt ratio in intense rain (Table II.2), suggesting that a physical separation process is occurring, involving rain out and wash out. The relationships between Na and Cl in 1977 data (analyzed to greater precision than 1976 data, most samples are from intense rain) show deviations from the seasalt ratio, perhaps due to additions of SO_3 or H_2SO_4 and loss of HCl through the mechanism proposed by Eriksson (1959, see above). Sodium in 1977 data plots near the seasalt Na-Cl trend, while the lowest concentrations of sodium and almost all the magnesium data plot below their respective seasalt trends (Figure II.7). The one high magnesium point is from a shower, and reflects the Mg fractionation just mentioned. Regressions through the data trends are given on the plots.¹ For sodium, the slope is not statistically different from 1.0, but is different from the seasalt slope.

¹All regressions in this study use a reduced axis criterion, chosen because there is no a priori statistical grounds for selecting any particular parameter as an independent variable (c.f. Jones 1979). Briefly, the slope, $A = (\text{linear least squares slope}) / (\text{correlation coefficient})$. The intercept, $B = \bar{Y} - A\bar{X}$, \bar{X} and \bar{Y} being data averages.

The Na-Cl slope of approximately one suggests that chloride in the sea spray aerosol has been lost to the extent that only NaCl remains. The Cl intercepts for the two regressions are close, being 1.52 and 1.03 $\mu\text{moles/l}$ respectively (these values are greater than blanks treated like the samples). This Cl intercept is interpreted as representing a background phase, perhaps HCl displaced from sea spray as the result of the reaction with SO_3 or H_2SO_4 . It should be noted that the changes in the composition of the marine component described here would not necessarily result in significant deviations from marine rain proportions in time averaged bulk precipitation (being a mixture of light and intense rain).

II.4:6 Terrestrial inputs

Within the Amazon Basin and adjacent areas, three principal categories of terrestrial inputs can be identified: biological emissions, soil dust, and combustion products from burning vegetation. The first class of inputs is widely distributed in the basin, while the other two tend to be localized and restricted to drier conditions.

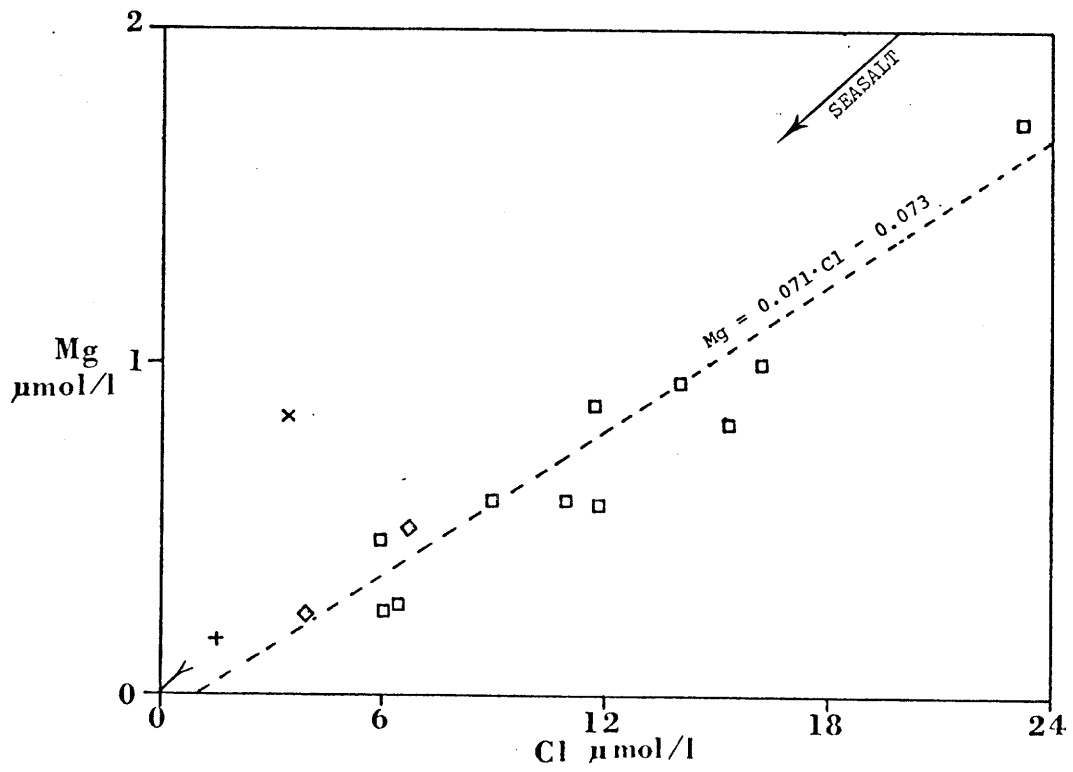
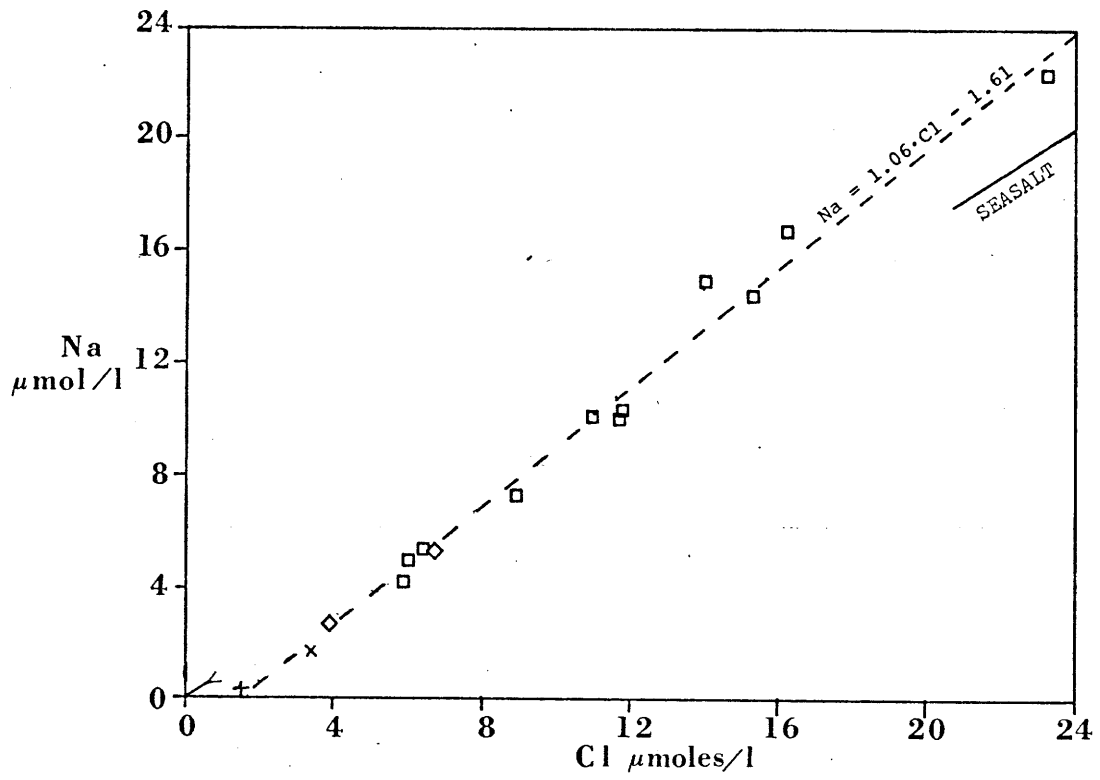
The principal areas where soil dust inputs might be important are in grasslands (particularly in burnt over areas), along river courses (during low water), along dirt roads, and throughout the Andes above the level of dense vegetation. Most soils in the Amazon Basin are highly depleted in soluble cations (c.f. Table IV.4). Principal exceptions are soils from coastal zones, the Andean and Subandean regions, and the flood plains of rivers which receive Andean sediments, such as the main channel and the Madeira River. Lawson and Winchester (1979) attribute Si, Al, Fe, and Ca in aerosols

Figure II. 7

Magnesium and sodium versus chloride in 1977 inland precipitation.

Symbol key:

8- V -77 -- X
17- V -77 -- □
22- V -77 -- ◇
10- V -77 -- +



from forested sites near Manaus, Brazil and Zongo, Bolivia to soil inputs (Table II.6).

Burning occurs primarily at the end of the dry season in the grassland areas located in the northeast, south, and southeast parts of the Amazon Basin, and on the periphery of these areas. The clearing of vegetation for agriculture and hunting has occurred since precolonial times, however the practice has greatly expanded as the result of the recent deforestation of vast tracts of land for the purpose of cattle raising along highways (Jahoda and O'Hearn 1975, Goodland and Irwin 1975, Sioli 1977). Chemically, fire inputs should resemble ashed plant material, with roughly equimolar proportions of Ca, Mg, and K, and about one half as much Na (Stark 1971, Scott 1977, Klinge 1977, Herrera et al. 1978). Significant contributions of P and N are likely, the latter depending on the chemistry of the combustion process.

Tropical vegetation has been demonstrated to be a source of particulates onto which certain elements are concentrated. Lawson and Winchester (1979) have shown that the aerosol concentrations of soil derived elements (Al, Si, Fe, and Ca) are suppressed during rainfall episodes, while other elements (K, P, and S) show this concentration reduction only in fine ($> 1\mu$) phases; they associate these elements with vegetational sources (Table II.6). Crozat (1979) reports that high levels of K, relative to other elements are observed in near-ground-level aerosols from the Ivory Coast, especially during the rainy season and at night. The source is thought to be fluid exudates on leaves (guttational fluids).

Sulfur has been measured on aerosols and both sulfur and nitrogen

TABLE II. 6
 SELECTED TRACE CONSTITUENTS
IN TROPICAL ATMOSPHERES

Manaus, Brazil:

<u>SPECIES/ ELEMENT</u>	<u>ATMOSPHERIC CONCENTRATION</u>	<u>PREDICTED RAIN CONCENTRATION</u>
	<u>umoles/m³</u>	<u>umoles/l*</u>
NH ₃ (g)	1000 (1)	50
SO ₂ (g)	≈13 (1)	0.65
H ₂ S	trace(2)	--
<1 u S	4.3 (4)	0.22
>1 u S	2.0 (3)	0.10
<1 u P	0.21(5)	0.011
>1 u P	2.6 (3)	0.13
<1 u K	2.0 (4)	0.10
>1 u K	4.7 (3)	0.24
<1 u Fe	1.1 (4)	0.055
>1 u Fe	4.9 (3)	0.25
>1 u Al	20. (3)	1.0
>1 u Si	74. (3)	3.7
>1 u Ca	2.7 (3)	0.14

Ivory Coast:

SO ₂ (g)	60. (6)	3.0
S (s)	18. (6)	0.9

- (1) Lodge et al. (1974)
- (2) R. Bradley, I.N.P.A. (personal communication)
- (3) Lawson and Winchester (1979), before rainfall
- (4) from Fig. 1 and 3, Lawson and Winchester (1979), before rainfall
- (5) from Fig. 3, Lawson and Winchester (1979), after rainfall
- (6) Delmas et al. (1978), inland station; coastal station displays higher values

* Predicted assuming complete coprecipitation of water and trace constituent, assumed moisture content 20 g H₂O / m³ air

have been measured on reduced gas phases in tropical forests (Table II.6); biogenic inputs are considered to be the most probable sources. On land, DMS is expected to be produced in soils and other restricted environments, where conditions are slightly aerobic (Lovelock et al. 1972, Rasmussen 1974), while hydrogen sulfide emissions characterize more reducing environments, especially where sufficient sulfate is present to make conditions favorable for sulfate metabolism (Schlegel 1974). Due to the presence of cloud droplets, airborne organic compounds, and bright sunlight, the complete oxidation of DMS and H_2S in a continental tropical atmosphere may be particularly rapid, perhaps a period of several hours to a day (c.f. Graedel 1978, Calvert et al. 1978, Hegg and Hobbs 1978). Soils, particularly more alkaline soils, have been shown to be a significant source of NH_3 and of NO_3 from NH_3 oxidation (Junge 1958).

Weakly reducing environments, offering potential sources of reduced sulfur and nitrogen gases, are widely distributed in the Amazon Basin, however strongly reducing conditions are uncommon and localized. Nutrients in organic litter are processed by rapid decay and assimilation into the biomass (Went and Stark 1968, Herrera et al, 1978), associated with a surface mycorrhizal root mat. Presumably the surface root mat could be the locus of reduced gas generation. There is evidence that acid reducing conditions are utilized in the surface root mat to retain nitrogen in the soil as the ammonium ion (Jordan and Medina 1977). These conditions would facilitate the release of H_2S . The direct input of H_2S into the atmosphere from the occasional overturning of flood plain lakes of the Amazon main channel has been described by Brinkmann and Santos (1974). This combination of strongly reducing conditions and high sulfate levels, found in the lakes, is not described for other

parts of the Amazon Basin. This is probably due to the lack of widespread geologic sources of sulfur.

II.4:7 Composition Versus Altitude of Aerosols

The composition of washout relative to rainout suggests that the seasalt aerosol is concentrated at lower altitudes near the coast and dispersed to higher altitudes farther inland. The storm nearest the coast (13-VI-76) shows a sharp drop in chloride concentration with time, which is a typical washout effect. By inference, the marine phases are localized in the lower atmosphere. The far inland storm (17-V-77) shows a rise in chloride concentration after the first sample, indicative of its dispersion to higher altitudes and depletion at lower altitudes.

Species which are dominantly terrestrial (e.g. Ca, K, NO_3) show a drop with time in both the 13-IV-76 and 17-V-77 storms, suggesting that terrestrially derived components are localized in the lower atmosphere both near the coast and farther inland. Showers, which are probably washout dominated, sampled in 1976, show a high concentration of terrestrial species. The difference in the altitude distribution of marine and terrestrial components reflects the introduction of the latter over the whole basin. Ungemach (Ungemach 1969, anon. 1972b) reports similar washout effects for species which are terrestrially derived, the effect being especially pronounced for phosphorous.

II.4:8 Relationship Between Terrestrial Inputs and Precipitation Chemistry

The precipitation chemistry data from this study, together with data of Ungemach and of Lawson and Winchester (1979), can be combined to show that fine particulates are more important than coarse particulates in contributing terrestrial materials to precipitation. Ungemach (1969) gives the $\bar{\text{N}}:\bar{\text{P}}$ ratio (mole ratios are used throughout) in rain, which with data from this study (values are corrected for marine inputs,

using marine rain proportions relative to chloride), is used to calculate ratios of $\bar{S}:\bar{K}:\bar{P}$ for comparison with the particulate data of Lawson and Winchester (1979) (data are given in Table II.6). Ungemach reports equimolar proportions of nitrate, ammonia, and organic nitrogen in rain near Manaus, with the ratio of total nitrogen to total phosphorous being 63:1. As some of the nitrogen in precipitation is derived from gas phases, the ratio of N:P in rain should be higher than in particulates. The ratio of nitrate to ammonia from this study is 4:1, while Ungemach reports 1:1; the difference may be due to Ungemach's sampling in closer proximity to vegetation and soils. The S:N ratio in rain is 1.3:1, and S:K ratio is 5:1. Combining the above ratios, one gets a S:K:P ratio of 82:16:1. This is quite different from the ratios in $>1 \mu$ particulates (Table II.6) in which the S:K:P ratio is 1:2.4:1.3. However, ratios for the fine particulate data (Table II.6) show a S:K:P ratio of about 20:9.5:1, which is much closer to rain proportions. Clearly the fine particulates must be a major source of these elements in precipitation.

The available atmospheric data for the rain forest suggests that fine particulate and gas sources are reasonable, as is illustrated in the case of sulfur. The concentration of water vapor at ground level in the rain forest is roughly $20 \text{ g H}_2\text{O}/\text{m}^3$ air. The combined sulfur dioxide concentration of Lodge et al. (1974) and fine particulate concentration of Lawson and Winchester (1979) is about $17 \text{ nmoles S}/\text{m}^3$ air (Table II.6). If all the sulfur is condensed with the water vapor, a solution of $0.85 \mu\text{moles S/l}$ would be produced, the right order of magnitude for rain. This would be an underestimate in that reduced gases and marine inputs are not accounted for. Predicted concentrations of other species are summarized in Table (II.6).

II.4:9 Gaseous Inputs and the Acidity of Rain

A significant fraction of sulfur and nitrogen in precipitation is derived from gaseous inputs, the primary charged forms found in rain being sulfate, nitrate, and ammonium ion (Junge 1958, 1963, Junge and Werby 1958). The oxidation reactions that form sulfate and nitrate result in acid precipitation unless these anions are neutralized by basic phases such as the ammonium ion, soil carbonates, or combustion ashes. The four ions related to gaseous inputs (H^+ , NH_4^+ , NO_3^- , SO_4^{--}) approximately charge balance suggesting that major neutralization by Na, K, Mg, and Ca does not occur. Sulfate is corrected (SO_4^*) for seasalt (spray) inputs which charge balance with other species. Two calculations are presented (Figure II.8): one includes sulfate and hydrogen ion which are analyzed in all samples, and the other includes all ions when analyses are available. Regressions through the data are:

$$(H^*) = 1.014(2 SO_4^*) + 0.361 \quad (r=0.805)$$

$$(H^* + NH_4^+) = 0.897(2 SO_4^* + NO_3^-) + 0.165 \quad (r=0.791)$$

Where H^* is the measured hydrogen ion concentration, H, corrected for equilibration with atmospheric carbon dioxide ($H^* = H - 10^{-11.32}/H$).

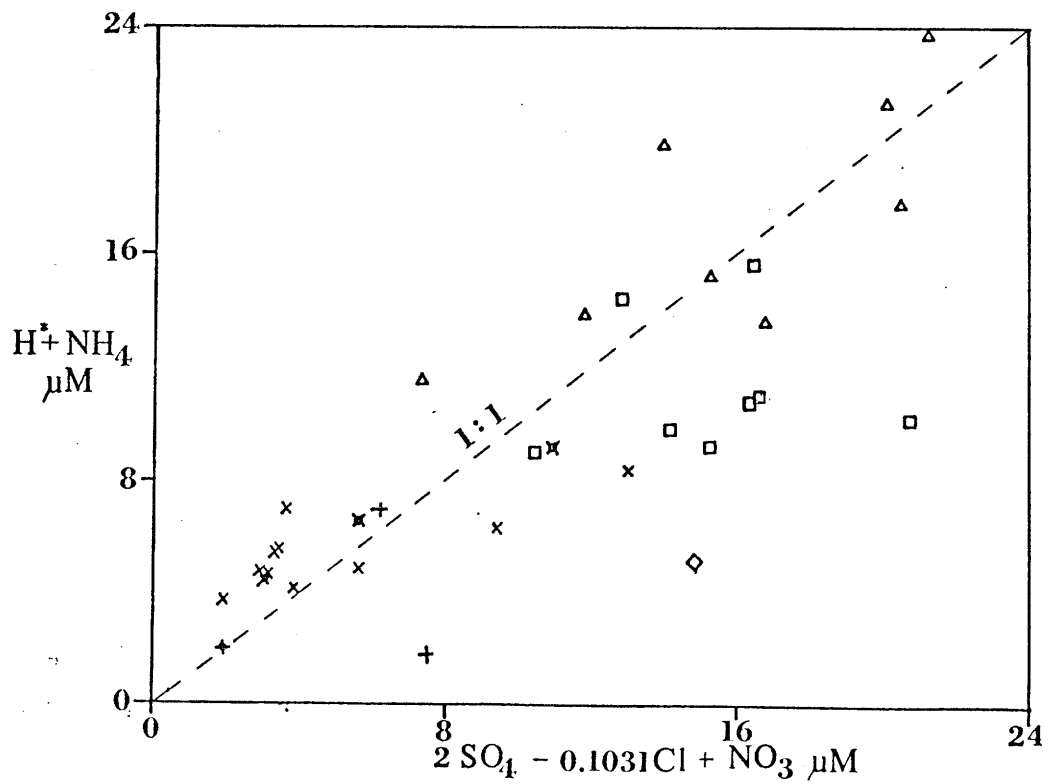
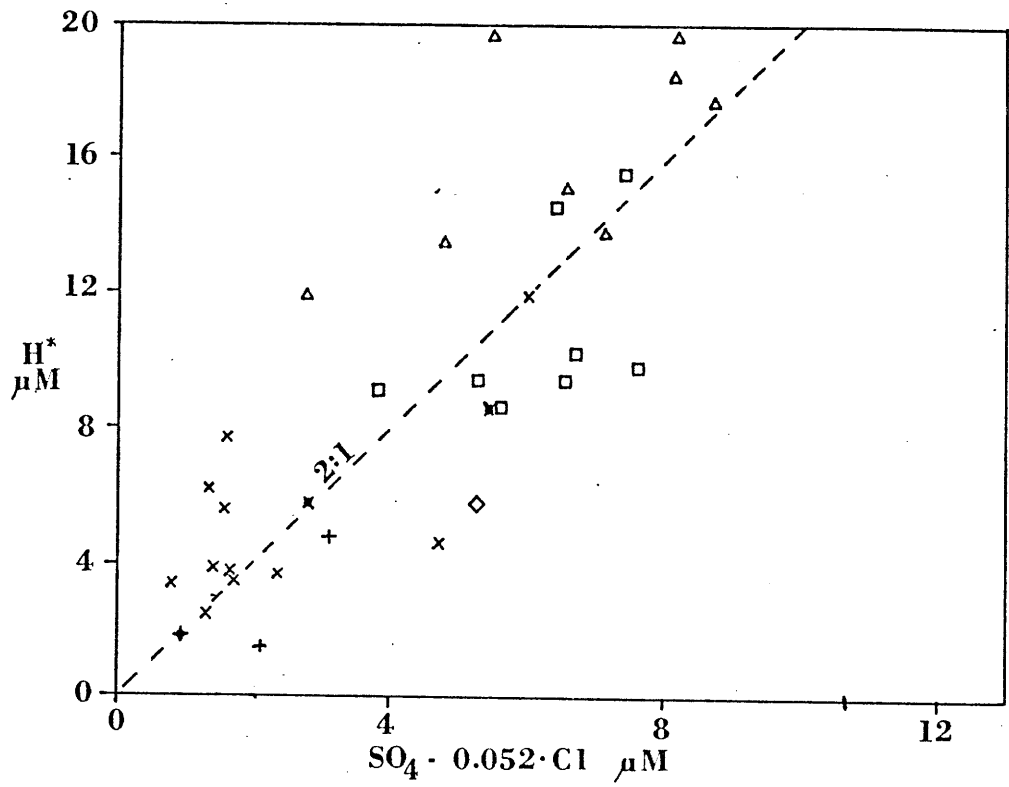
Statistically the slopes are not different from one .

Figure II.8

Hydrogen ion (corrected for equilibration with atmospheric CO₂) plotted against sulfate (corrected for charge balanced seasalt component). In the lower diagram, nitrate and ammonia are included with the 1976 samples, and nitrate with the 8-V-77 and 17-V-77 samples.

Symbol key:

13-VI -76 -- Δ
27-VI -76 -- ◇
29-VI -76 -- □
8- V -77 -- ◆
17- V -77 -- ✕
22- V -77 -- ✖
10-VII-77 -- }+
30-XI -78 -- }



II.5 CYCLIC SALT CORRECTIONS

Several estimates of the net contribution of atmospherically derived materials to Amazon surface waters have been published. Ungemach (Ungemach 1967, 1968, Anon. 1972a,b) has compared atmospheric fluxes into (determined from precipitation measurements at Manaus) and out of the Negro River system. He found rates of input to be similar to rates of output for all elements (N, P, Ca, Mg, K, Na) except Fe. Ungemach does not differentiate between extra basin and recycled inputs. Gibbs (1970) argues that 81% of the Na, K, Mg, and Ca in the dilute lowland rivers of the Amazon Basin are cyclic. Gibbs (1972), assumes that all the chloride in the Amazon River is cyclic (he ignores possible geologic sources) and calculates that 90% of the sodium at high discharge and 55% of the sodium at low discharge is cyclic.

It has long been known that chloride in surface waters, with no terrestrial sources of chloride, declines systematically as a function of distance from the coast (Jackson 1905). This is a reflection of the loss of chloride from marine air masses moving inland (Eriksson 1955, 1959, 1960, Gorham 1961). This observation is used as the foundation of a set of assumptions for calculating the cyclic salt component in surface waters of the Amazon River system:

- (1) The chloride in lowland rivers having little or no marine rock formations (see Table IV.4 for a detailed summary of their geology) was assumed to be ocean derived via the atmosphere. There are two important exceptions:
 - (a) The Tapajós and Trombetas rivers cross narrow surface exposures of CaSO_4 along the flanks of the Amazon Trough. Steams in these strips are sulfate but not chloride rich (Sioli 1963).
 - (b) The Purus, Juruá, and Javari rivers are rapidly eroding marine formations in their headwaters. Only the lowest concentrations of chloride observed in these rivers is assumed to be entirely cyclic (1977 Purus and Juruá), being close to values in adjacent rivers not eroding these sediments.

(2) Marine contributions for other components were calculated from chloride using their seasalt proportions, except for sulfate where the marine rain proportions were used. To charge balance the marine component, the extra sulfate was assumed to be sulfuric acid.

The concentration of chloride in lowland rivers is plotted as a function of distance from the coast (Figure II.9). The data trend is quite smooth, consisting of a steep drop-off inland to 1200 km followed by a gradual decline. Averaged chloride in precipitation (Figure II.4) bears a close resemblance to the distribution in lowland rivers.

Only the three next most abundant ions in seawater (Na, Mg SO₄) show significant cyclic salt contributions in any of the rivers, with the exception of one near-coastal river (Matari, S337A), draining strongly weathered sediments. In this river about 15% of the calcium and potassium is cyclic; no other river had more than 3% marine contribution of these two elements.

Measured concentrations of sodium and magnesium and their estimated cyclic components are presented in Figure II.10. Only the near-coastal Matari River is dominated by cyclic inputs of both these elements. The upper Rio Negro has a 50% contribution of cyclic sodium. In all other rivers the cyclic input of Na and Mg is minor, compared to inputs from weathering.

Sulfate provides an interesting contrast to sodium and magnesium as its concentration is lower than the predicted cyclic component in the Matari and Xingu rivers (Figure II.11), both of which are near-coastal and lacking in major identifiable terrestrial sources of sulfate. In lowland rivers with identifiable geological sources of sulfur, the

Figure II.9

Concentration of chloride in selected lowland rivers as a function of distance from the Atlantic Coast. Rivers having sulfate containing marine sediments are also plotted. Distances are measured to the geographic center of the respective basin.

Symbol key:

basins without marine sediments -- Δ
basins with marine sediments -- ∇

Rivers

Marari -- MI
Trombetas -- TR
Xingu -- XI
Branco -- BR
Tapajós -- TP
All Negro -- NG
Upper Negro -- UN
Coari -- CO
Tefé -- TF
Jutaí -- JT
Purus -- PU
Jandiatuba -- JN
Juruá -- JR
Nanay -- NY

Precipitation -- ■

see also Fig. II.4

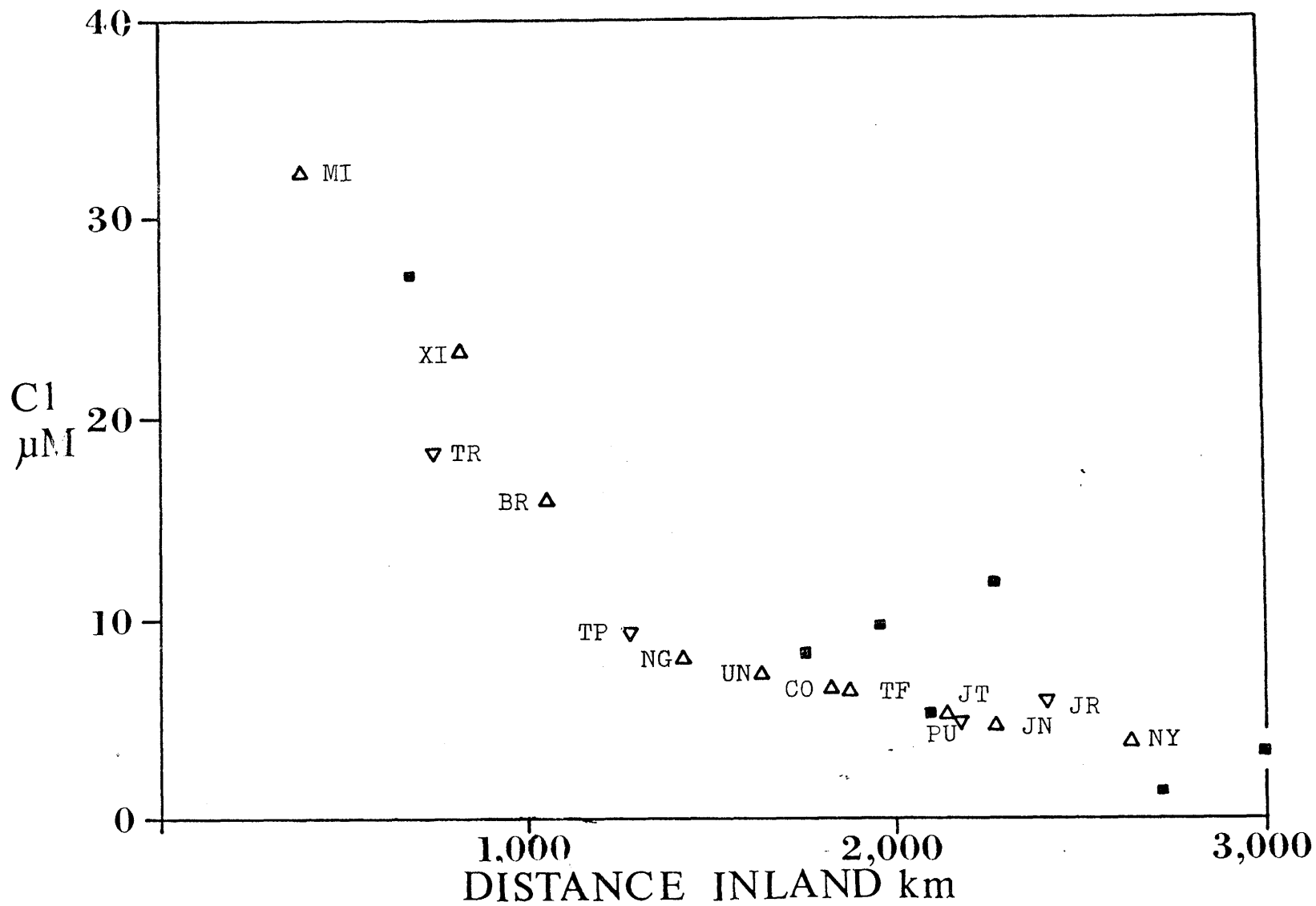


Figure II.10

Concentration of sodium and cyclic sodium (predicted from the Cl data of Figure II.9), and magnesium and cyclic magnesium, plotted as a function of distance from the Atlantic coast.

Symbol key:

basins without marine sediments -- Δ
basins with marine sediments -- ∇
predicted marine component -- +

Rivers

Matari -- MI
Trombetas -- TR
Xingu -- XI
Branco -- BR
Tapajós -- TP
All Negro -- NG
Upper Negro -- UN
Coari -- CO
Tefé -- TF
Jutaí -- JT
Purus -- PU
Jandiatuba -- JN
Juruá -- JR
Nanay -- NY

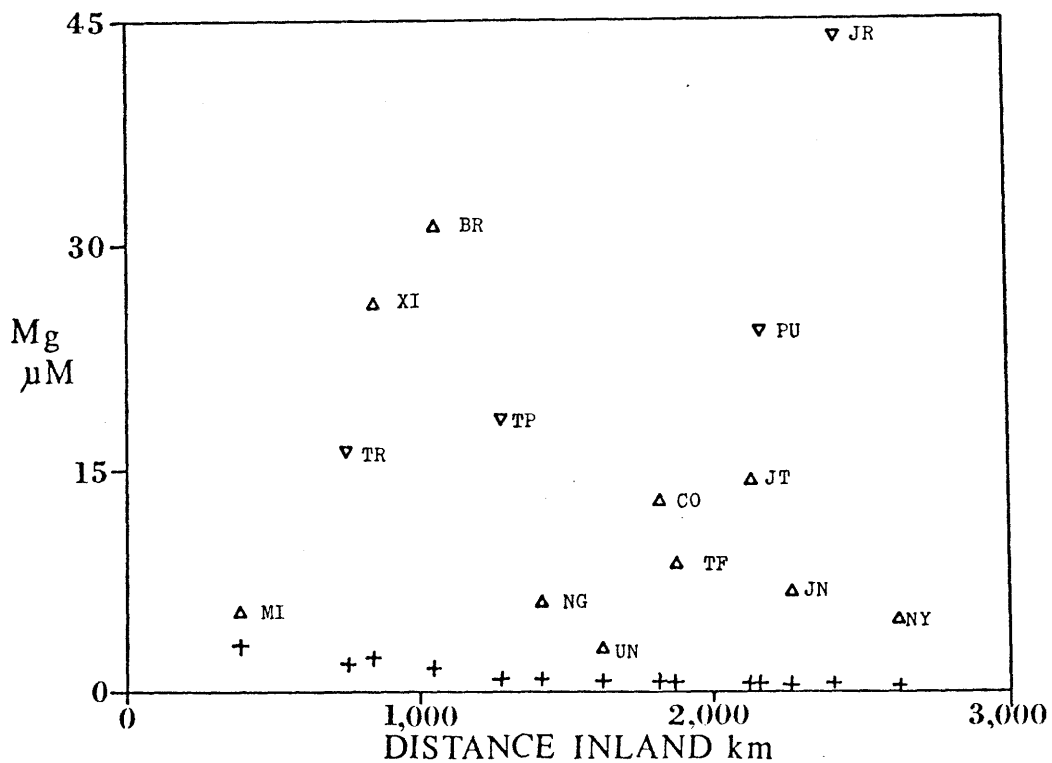
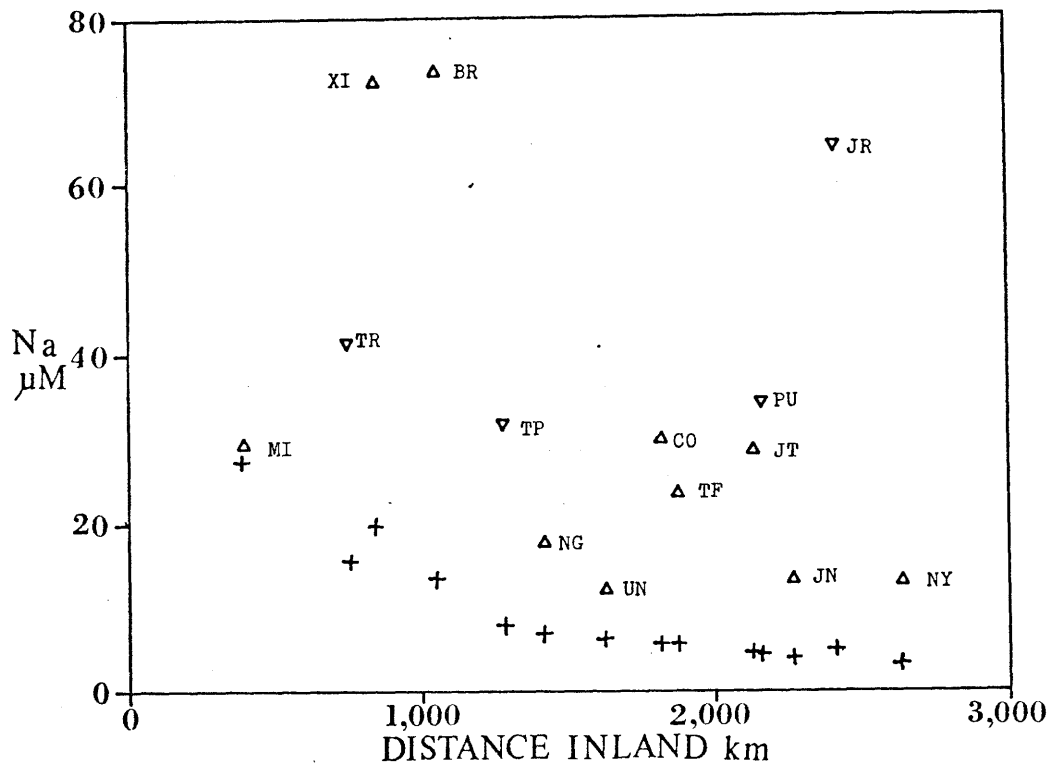


Figure II.11

Upper:

Concentration of sulfate and predicted marine sulfate components in lowland rivers plotted as a function of the distance from the Atlantic coast. Also plotted are mean concentrations of sulfate in precipitation. Note that concentrations of sulfate in precipitation are higher than in many rivers.

Lower:

Ratio of chloride to sulfate in both selected rivers and precipitation, plotted as a function of distance from the Atlantic coast.

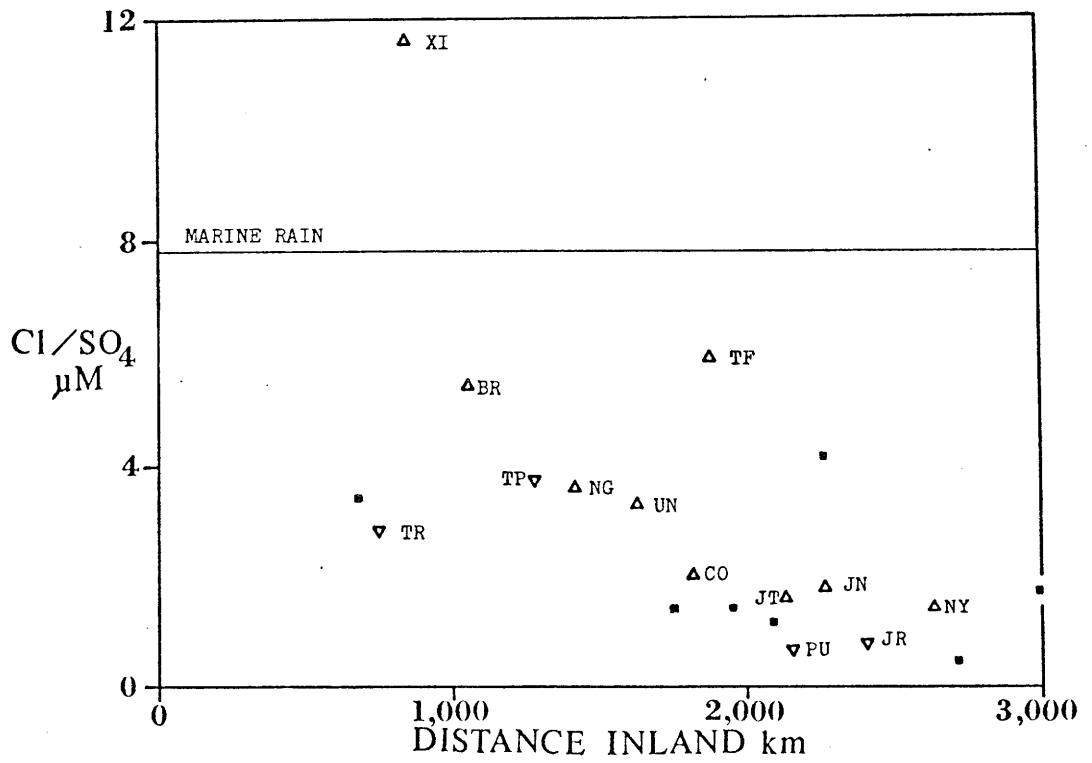
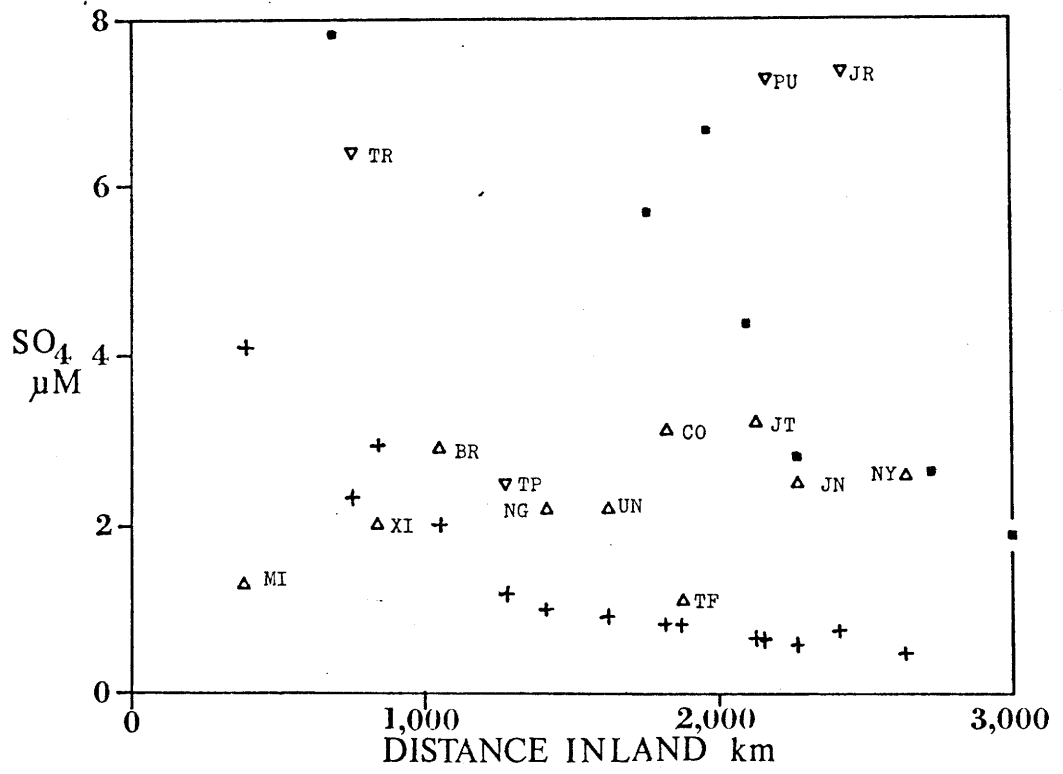
Symbol key:

basins without marine sediments -- Δ
basins with marine sediments -- ∇
predicted marine component -- \dagger

Rivers

Matari -- MI
Trombetas -- TR
Xingu -- XI
Branco -- BR
Tapajós -- TP
All Negro -- NG
Upper Negro -- UN
Coari -- CO
Tefé -- TF
Jutaí -- JT
Purus -- PU
Jandiatuba -- JN
Juruá -- JR
Nanay -- NY

Precipitation -- ■



sulfate concentrations tend to be relatively high. The average sulfate concentrations for the storms sampled in this study are considerably greater than the sulfate concentrations of some inland rivers, suggesting that a sulfate deficit exists in lowland rivers relative to precipitation, a deficit not seen if only the marine rain component is considered. Chloride to sulfate ratios are plotted in Figure II.11 to highlight the sulfate poor character of many lowland rivers, compared to precipitation. It should be emphasized that showers, which show lower levels of chloride and higher levels of sulfate, are under represented in the sampling (c.f. Section II.2:1).

There are several possible explanations for the sulfate-poor nature of lowland rivers. It may reflect seasonal storage of sulfur in the biomass, loss of sulfur to the atmosphere, or a major rise in the $\text{SO}_4:\text{Cl}$ ratio in the marine component. This latter possibility appears unlikely as the sulfate in the Matari is even below the concentration predicted using the seasalt $\text{Cl}:\text{SO}_4$ ratio. It seems very unlikely that the marine aerosol $\text{Cl}:\text{SO}_4$ ratio ever rises above seasalt proportions. It is not possible to test short term biomass storage without a time series extending over at least one year. Loss of sulfur to the atmosphere is consistent with observations of precipitation chemistry, which indicate major terrestrial contributions to sulfate in inland precipitation (Figure II.6). If this is occurring, some sulfate in inland regions must again be recycled, since the sulfate concentration in the most dilute inland rivers is well below values in inland precipitation (see Figure II.11).

II.6 CYCLIC SALTS IN THE ENTIRE BASIN

Cyclic chloride concentrations for all the main channel tributaries not included in Figure II.4. were calculated from curves fitted through the trend in the figure. Inland of the Purus River, curves were fit through the 1976 and 1977 data separately to account for slightly higher values in the 1977 inland data. Coverage in the coastal part of the trend was inadequate for separating the two years (1976 Branco and Matari samples are lacking). The cyclic chloride concentrations for Andean rivers were taken to be the same as that of the Nanay River (most inland lowland sample) for the same time of the year. Main channel values were calculated assuming that cyclic chloride, along with other major ions, is mixed conservatively when a tributary joins the main channel (These calculations are discussed in detail in Chapter V). Cyclic chloride concentrations for all samples are given in Table II.7.

The most down-river samples can be used to calculate the cyclic salt component in the June runoff, using cyclic chloride as a reference. Calculated cyclic salt contributions are:

<u>Element</u>	<u>Cyclic Percentage</u>
Cl	19.0 %
Na	7.9 %
Mg	1.4 %
S	3.8 %
Ca	0.1 %
K	0.5 %
C _{inorg}	-0.3 %*

*negative as a result of hydrogen ions in model precipitation, does not include inputs via weathering reactions.

These values are lower than any estimate given in Table II.1, the closest estimate being that of Holland (1978), which was calculated

Table II.7

Measured chloride concentrations (CL) ($\mu\text{mole/l}$) and predicted cyclic Cl contributions (CYCL) for Amazon surface waters.

MAIN CHANNEL (1)

STA.	PARAMETER: -LOCATION-	CL	CYCL
S250	AM. IQUITOS	183.	3.8
S247	AM. PEVAS	129.8	3.8
S243	AM. LETICIA	100.1	3.8
S241	SO. ASSACA-	104.3	3.8
S240	SO. SAO PA-	106.0	3.8
S237	SO. A. JUTAI	80.9	3.9
S235	SO. BUITAI	76.6	3.9
S234	SO. FONTE B	74.3	4.0
S232	SO. ALVAREZ	74.2	4.1
S228	SO. JUTICA	65.4	4.4
S227	SO. LARANJ-	63.5	4.4
S224	SO. CAMARA	56.0	4.5
S223	SO. ANORI	57.3	4.5
S220	SO. MANACA-	47.4	4.6
S219	SC. A. NEGRO	47.8	4.6
S209	AM. OBIDOS	30.5	5.4
S207	AM. APIXUNA	28.0	6.9
S203	AM. GURUPA	30.4	6.1
S202	AM. UPUTAI	139.2	6.8
S302	AM. IQUITOS	156.	3.8
S303	AM. A. NAPO	156.	3.8
S305	AM. PEVAS	151.	3.8
S306	AM. LETICIA	137.0	3.8
S307	SO. A. SAO P	122.1	3.8
S311	SC. A. ICA	114.8	3.9
S314	SO. A. JUTAI	99.7	3.9
S316	SO. A. JURUA	83.0	4.1
S321	SO. A. COARI	61.0	4.4
S323	SO. A. PURUS	57.4	4.5
S326	SO. A. NEGRO	42.1	4.6
S329	AM. OBIDOS	31.0	5.5
S334	AM. A. TAPA-	33.5	5.7
S336	AM. A. XINGU	31.2	5.9
SOL1	SC. A. NEGRO	54.9	5.4
SOL2	SC. A. NEGRO	59.4	5.4
AMI01	AM. IQUITOS	188.	2.8
BPA09	AM. IQUITOS	158.	3.3

MARANON DRAINAGE (2)

STA.	PARAMETER: -LOCATION-	CL	CYCL
S-2	HU. HUANUCO	403.	3.8
A-02	HU. HUANUCO	145.0	3.8
A-03	HUIGUERAS	32.8	3.8
A-04	HUACHIPA	16.0	3.8
A-07	HU. TINGO M	469.	3.8
A-05	SALT SP.	39200.	3.8
A-06	MONZON R.	54.0	3.8
A-08	ASPASARTA	10.5	3.8
A-09	UCHIZA R.	83.0	3.8
A-10	CACHIYACU	15400.	3.8
A-12	HU. TOCACHE	505.	3.8
A-11	TOCACHE P.	6.4	3.8
A-13	HU. BALSAL Y	392.	3.8
A-14	HUALLABAMB	63.7	3.8
A-15	SAPOSOA R.	724.	3.8
A-16	MAYO R.	323.	3.8
A-17	HU. YURIMA-	943.	3.8
A-18	SHANUSI R.	95.6	3.8
A-19	PARANAPURA	438.	3.8
BPA10	MARANON C-	123.5	3.3
BPA16	CANA S.	71600.	3.3
BPA13	HU. YURMA-H	823.	3.3
BPA14	SHANUSI R.	52.0	3.3
BPA15	PARANAPURA	124.4	3.3

UCAYALI DRAINAGE (3)

STA.	PARAMETER: -LOCATION-	CL	CYCL
S-1	UCAYALI R.	362.	3.8
A-01	MONTARO R.	234.	3.8
M-08	URUBAMBA	5680.	3.8
M-09	STREAM A-C	94.9	3.8
BPA08	URUBAMBA	2440.	3.3
BPA11	UCAYALI C-	191.	3.3

MADEIRA DRAINAGE (4)

STA.	PARAMETER: -LOCATION-	CL	CYCL
S212	MADEIRA R.	13.6	5.9
S328	MADEIRA R.	12.6	5.9
M-05	ICHILO R.	6.4	3.8
M-04	M. DE DIOS	15.9	3.8
M-03	BENI RIVER	52.7	3.8
M-02	MAMORE GU-	21.3	3.8
M-01	MADEIRA PV	22.6	3.8
BPA01	ICHILO R.	5.6	3.3
BPA02	SAN MATEO	92.2	3.3
BPA03	ESPIRITU S	259.	3.3
BPA04	MAMORE TR-	72.5	3.3
BPA05	GUAPAY P.	470.	3.3
BPA06	PIRAY R.	75.2	3.3

OTHER ANDEAN (5)

STA.	PARAMETER: -LOCATION-	CL	CYCL
S249	NAPO RIVER	8.5	3.8
S238	ICA R.	7.1	4.2
S231	JAPURA R.	37.4	5.3
S304	NAPO R.	9.4	3.8
S313	ICA RIVER	8.1	4.2
S318	JAPURA R.	49.5	5.3

NEGRO DRAINAGE (6)

STA.	PARAMETER: -LOCATION-	CL	CYCL
S216	NEGRO R.	6.8	6.8
S327	NEGRO R.	7.6	7.6
UN1	U. NEGRO R.	7.6	7.6
UN2	U. NEGRO R.	7.0	7.0
BR1	BRANCO R.	15.5	15.5
BR2	BRANCO R.	16.0	16.0
LN1	NEGRO R.	15.2	15.2
LN2	NEGRO R.	9.5	9.5

SHIELD DRAINING (7)

STA.	PARAMETER: -LOCATION-	CL	CYCL
S208	TROMBETAS	20.6	20.6
S206	TAPAJOS R.	9.0	9.0
S204	XINGU R.	19.3	19.3
S332	TROMBETAS	15.7	15.7
S335	TAPAJOS R.	9.8	9.8
S337	XINGU R.	27.1	27.1

MARINE DRAINING (8)

STA.	PARAMETER: -LOCATION-	CL	CYCL
S242	JAVARI R.	16.1	4.1
S233	JURUA R.	16.0	5.1
S222	PURUS R.	15.1	5.0
S301	JAVARI R.	22.6	4.1
S317	JURUA R.	5.9	5.8
S324	PURUS R.	5.0	5.0
S331	STREAM OB-	53.1	15.5

U. TERT.+. DRAINING (9)

STA.	PARAMETER: -LOCATION-	CL	CYCL
S236	JUTAI R.	5.1	5.1
S230	TEPE RIVER	5.6	5.6
S225	COARI R.	6.2	6.2
A-21	NANAY R.	3.8	3.8
S309	JANDIATUBA	4.6	4.6
S309A	VARZEA L.	4.6	4.6
S315	JUTAI R.	5.5	5.5
S319	TEPE RIVER	7.5	7.5
S319A	TEPE RIVER	7.4	7.4
S322	COARI R.	6.5	6.5
S337A	MATARI R.	32.1	32.1
NAN01	NANAY R.	2.8	2.8
BPA12	NANAY R.	3.3	3.3

using seasalt ratios relative to chloride (see Section II.1). The reason for these differences include the failure to exclude locally derived materials from balance calculations (a fault of the small basin studies terrestrial sources of chloride (as is the case for Eriksson 1960 and Gibbs 1972), and analytical difficulties. It should be reiterated that the global and analytical difficulties. It should be reiterated that the global estimates given in Table II.1 are based on data from large river systems, and can be compared directly with the Amazon estimates given here. In a sense these global estimates are low in that they do not include much data from small near-coastal rivers which have particularly high cyclic salt inputs. Since Conway (1942), this zone has been largely ignored in cyclic salt calculations.

Chapter III

Environmental setting of the Amazon Basin, with emphasis on
geology and soils

III.1 THE GLOBAL SETTING OF THE AMAZON BASIN

This study is directed at obtaining information on the processes controlling the composition and flux of dissolved materials in the Amazon River System, focussing on the major crustal elements. Garrels and Mackenzie (1971) present a global model of sedimentary rock evolution, in part using available river chemical flux data. They treated riverine chemical fluxes as time invariant. Yet continents have aggregated and broken up; mountains have uplifted and eroded; continental area has diminished and expanded with sea level changes. Many oceanic and atmospheric cycles are characterized by timescales shorter than these events and could be controlled by them. More recent modeling of geochemical evolution has tried to take some of these features into account (c.f. Holland 1978).

The Amazon Basin is a particularly interesting area to study. Within the Basin there is the broadest range of continental geology, with active orogenic zones, areas of epirogenic uplift, geologically stable areas, and active sedimentary basins. In addition, human activities, which have so thoroughly altered the environments of many large river basins, have yet to have major impact in the Amazon, a feature now rapidly changing. The Amazon is the largest river in the world, having an average discharge of 1.75×10^5 m³/sec (Oltman 1968), about one fifth of the global river output to the oceans. Recent studies of Meade et al. (1979) rank the Amazon third in sediment output to the ocean at $8-9 \times 10^8$ tonnes/year, less than the Yellow River (20×10^8 tonnes/year) and the Ganges-Brahmaputra (22×10^8 tonnes/year) (data from Holeman, 1968). The Amazon ranks first in output of dissolved material, transporting at least 2.9×10^8 tonnes/year versus 1.5×10^8 tonnes/year for the Ganges-Brahmaputra and 1.3×10^8 tonnes/year for the Mississippi (Meybeck, 1976).

III.2 MAJOR FEATURES OF THE AMAZON BASIN

The Amazon Basin occupies much of the South American continent between 5° north latitude and 20° south latitude. At the present time the basin conforms to the classical picture of a large river catchment, being a large smooth plain, bordered by highlands. To the west is the Andean Cordillera ranging from 3000 to 7000 meters; to the north lies the highlands of the Guiana Shield (500-3000 m); and to the south rises the Brazilian Shield (1000-2000 m). To the east of the Andes there exists a trough in which the Amazon drainage is separated, by poorly defined divides, from the Orinoco Basin to the north and the Paraguay Basin to the south.

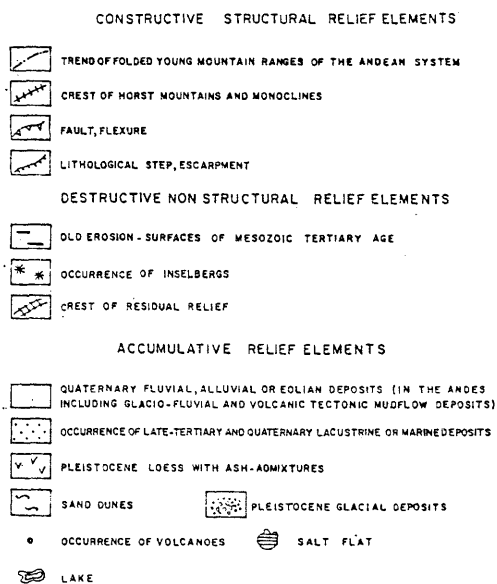
Four major morphostructural zones can be distinguished within the Amazon Basin, these being the Precambrian shields, the Andean Cordillera, the Amazon Trough or Basin, and the Subandean Trough or Depression (Figure III.1). These four zones characterize regions of distinctive geology, soils, landscape, and to some degree climate and vegetation. Since the Phanerozoic the shields have been topographic highs; the Cordillera has been a locus of intermittent orogenic activity; the Amazon Trough has been an area of subsidence; the Subandean Trough has had a complex history, most recently acting as a zone of subsidence. The Andean Cordillera, within the Amazon Basin, can be further divided into four major subzones: the Western Cordillera, the Intercordilleran Region, the Eastern Cordillera, and the Subandean Uplifts. These four subzones control the river drainage network within the Andes and correspond to areas of distinctive geology.

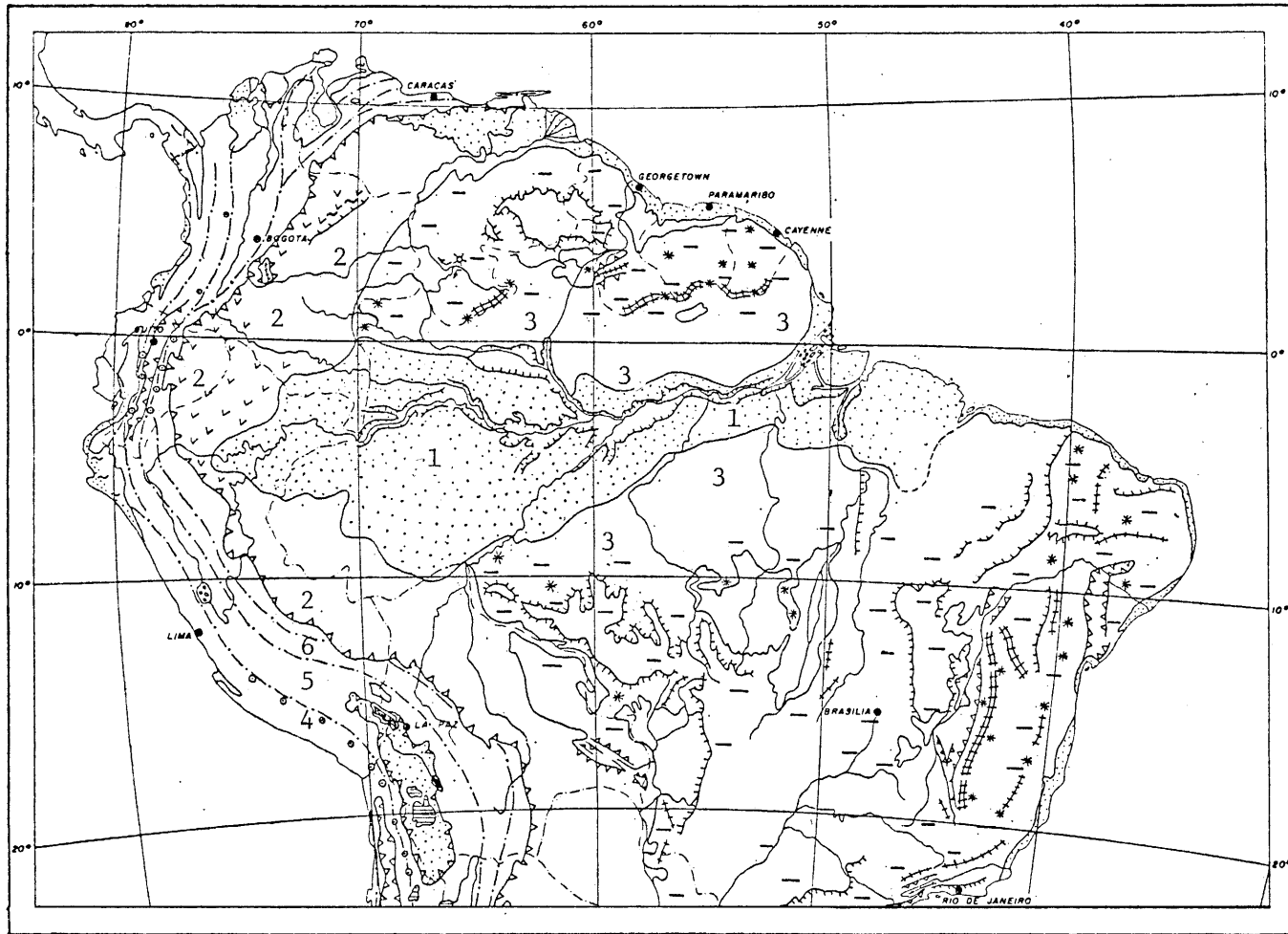
Figure III.1

Morphostructural regions:

1. Amazon Trough
2. Subandean Trough
3. Shields
4. Western Cordillera (Cordillera Occidental)
5. Intercordilleran Zone (includes the altiplano regions)
6. Eastern Cordillera (Cordillera Oriental)
7. Subandean Uplifts

Symbol key:





III.3.1 THE DISTRIBUTION OF ROCK TYPES IN THE AMAZON BASIN

A wide variety of rock types are found in the Amazon Basin (Figure III.2). III.2). Representative chemistries are given in Table III.1; bear in mind that no such data are available for the Amazon region, so the analyses presented are from outside South America. The soil analyses (to be discussed later) are from the Amazon region.

II.3:2 Metamorphic and Igneous Rocks

The bulk of the igneous rocks throughout the Andes (found primarily in the Western Cordillera) and the shields are acid to intermediate in composition. The only poorly lithified volcanics are found in the Western Cordillera in Peru and Eastern Cordillera of Ecuador. The latter occurrence represents the largest exposure of recent volcanics in the Amazon Basin.

In general, metamorphic rocks of the Amazon Basin fall into an acid to intermediate range, except for some Andean Precambrian exposures (found in the Eastern Cordillera of Peru and Ecuador) where unmapped but apparently abundant metabasalt and ultrabasic units are found, and for some small basic intrusions and greenstone complexes in the shield areas.

II.3:3 Sedimentary Rocks

In the Andes and Subandean Trough, the sedimentary lithologies (old to young) are dark shales, limestones and sandstones, red beds, and fluvio-lacustrine sediments. Briefly, the Eastern Cordillera is composed of Precambrian metamorphic rocks and Lower Paleozoic dark shales. The other Andean sub-zones are underlain by younger sedimentary and igneous rocks, with continental units dominating to the east and marine and volcanic units dominating to the west (Gansser 1973, Audebaud et al. 1973).

In the Amazon Trough, the sequence is sandstones and dark shales, limestones and sandstones, evaporites, and shales. This sequence is

Table III.1

EXAMPLES OF THE CHEMISTRY OF VARIOUS
ROCK TYPES AND SOILS
THOUGHT TO BE IMPORTANT
IN THE AMAZON BASIN

All analyses are in mole %

Element	Igneous and Metamorphic							
	Shield (1)	Gabbro (2)	Cont. Basalt (3)	Diorite (2)	Andesite (3)	Grano- diorite (2)	Sodic Granite (3)	Potassic Granite (2)
Na	6.62	4.41	5.21	6.55	6.65	7.46	6.63	5.97
K	3.67	0.79	0.86	1.70	1.46	3.93	4.46	6.96
Mg	2.49	12.11	9.62	9.17	5.75	2.35	0.84	0.78
Ca	4.09	11.95	9.92	9.05	6.76	3.82	2.22	1.43
Si	59.11	48.74	45.92	52.18	53.88	67.02	68.65	72.07
Fe III	1.68	1.93	1.94	2.07	1.65	1.01	0.93	0.65
Fe II	2.28	6.01	5.62	5.28	3.39	1.95	1.27	1.26
Al	18.50	12.76	19.52	12.41	19.71	11.80	14.58	10.42
Ti	0.57	1.00	1.07	1.14	0.56	0.43	0.33	0.28
Mn	0.02	0.15	0.11	0.15	0.08	0.06	0.03	0.05
P	0.17	0.21	0.21	0.30	0.11	0.18	0.03	0.15
C inorg.	0.50	--	--	--	--	--	--	--
Cl	--	--	--	--	--	--	--	--
S ox.	0.10	--	--	--	--	--	--	--
S red.	0.21	--	--	--	--	--	--	--

Element	Sedimentary Rocks							
	Evaporite (1)	Lime- stone (4)	Dolomite (4)	Average Shale (1)	Black Shale (4)	Lithic Arenite (4)	Arkose (4)	Ortho- Quartzit (4)
Na	19.18	0.08	0.35	3.45	1.22	1.73	2.80	0.19
K	0.27	0.35	0.08	3.37	4.13	1.65	3.44	0.25
Mg	6.95	9.68	20.59	3.93	2.96	3.56	0.72	0.14
Ca	22.93	37.52	21.24	6.32	1.61	6.61	2.78	1.70
Si	2.29	4.27	13.30	54.83	63.37	65.76	74.26	94.80
Fe III	0.15	0.11	0.24	2.98	0.28	2.84	1.16	0.30
Fe II	0.08	0.24	0.33	1.44	3.13	1.17	0.56	0.15
Al	0.68	0.79	1.81	16.13	14.31	9.50	9.88	0.82
Ti	0.03	0.04	0.09	0.34	0.49	0.23	0.22	0.15
Mn	0.00	0.03	0.06	0.05	0.04	0.08	0.16	--
P	0.00	0.03	0.32	0.17	0.16	0.08	0.08	--
C inorg.	18.15	46.66	41.37	6.24	2.35	6.79	3.95	1.49
Cl	18.97	0.03	--	0.17	--	--	--	--
S ox.	10.32	0.03	0.00	0.58	--	--	--	--
S red.	--	0.14	0.21	--	6.26	--	--	--

Element	Amazon Soils											
	Weathering Granite (5)	seq., Hard Saprolit	savanna near surface	Soil profile, forest (6) lower upper		(6) old soils, planato	Amazon susp. (7)	Amazon bed sand (8)	Tapajos sand (8)			
Na	6.06	-	0.35	-	0.09	0.10	-	0.01	0.06	2.1	2.3	0.29
K	5.86	-	4.50	-	0.15	0.16	-	0.03	0.87	2.8	2.5	0.21
Mg	0.18	-	0.17	-	0.06	0.02	-	0.03	0.23	2.8	1.3	0.00
Ca	0.86	-	0.02	-	0.03	0.02	-	0.00	0.02	2.4	3.5	0.03
Si	71.80	-	73.82	-	44.14	59.98	-	56.31	40.78	51.2	78.9	97.85
Fe	1.63	-	1.54	-	33.61	10.16	-	12.07	8.95	5.9	1.9	0.33
Al	13.60	-	19.59	-	21.92	28.60	-	30.36	47.19	25.6	7.5	0.22
Ti	--	-	--	-	--	0.69	-	0.96	1.79	0.88	0.31	0.31
Mn	--	-	--	-	--	0.12	-	0.08	0.00	0.11	0.03	0.13
P	--	-	--	-	--	0.08	-	0.08	0.04	0.32	0.05	0.24
C inorg.	--	-	--	-	--	--	-	--	--	--	2.82	0.00
Cl	--	-	--	-	--	0.01	-	0.01	0.06	--	--	--
S	--	-	--	-	--	0.06	-	0.06	0.01	--	0.04	0.03

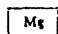
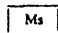
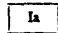

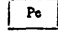
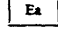
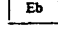
This table is calculated from one or more data tables in the following references:

- (1) Holland (1978)
- (2) Ernst (1969)
- (3) Verhoogen et al. (1970)
- (4) Pettijohn (1975)
- (5) Pasquali et al. (1972)
- (6) Kronberg et al. (1979)
- (7) Martin and Meybeck (1978)
- (8) Potter (1978)

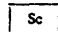
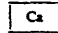
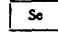
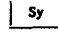
Figure III.2

Lithologic map, symbol key:



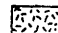

IGNEOUS AND METAMORPHIC ROCKS

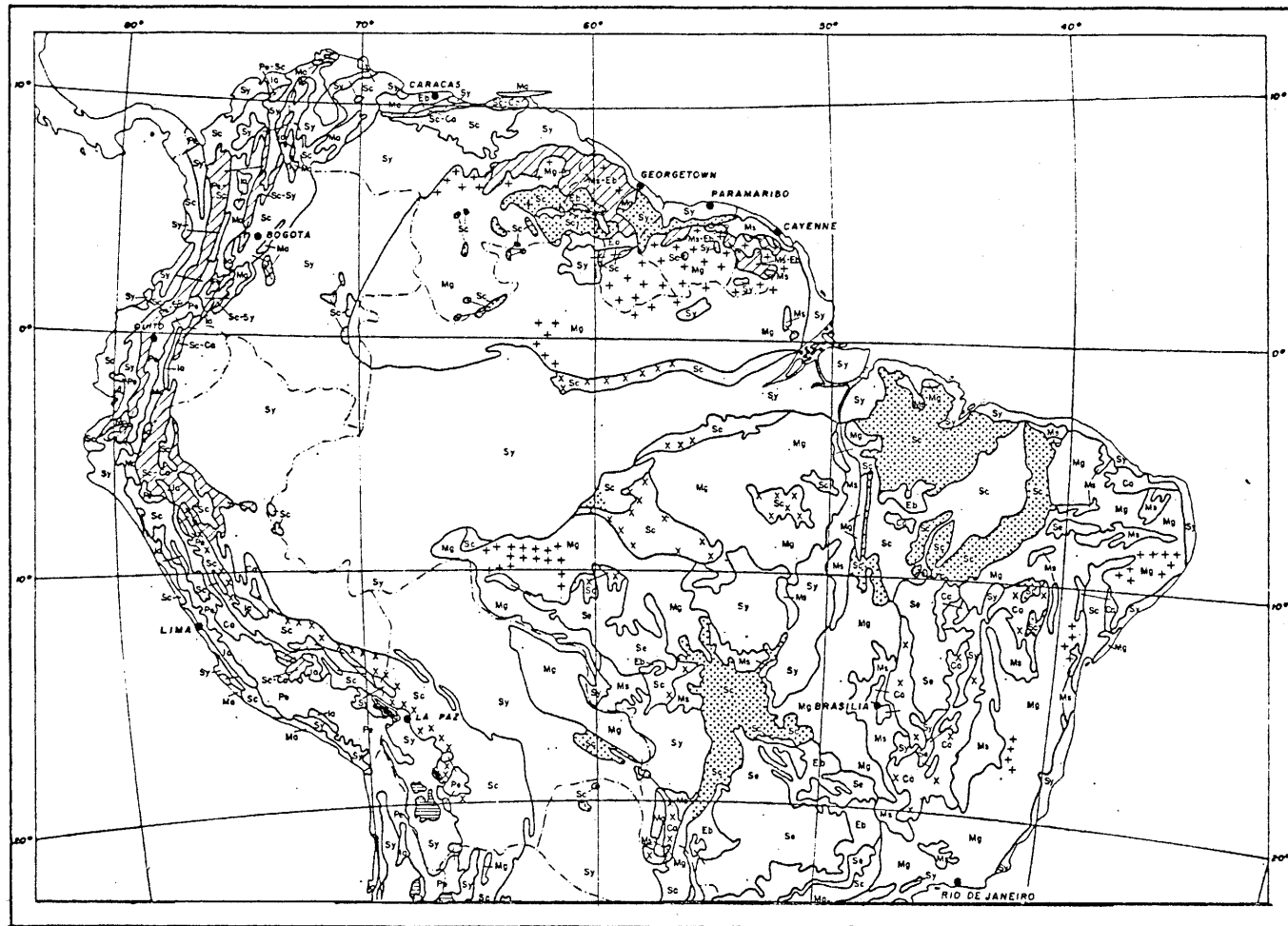
-  Metamorphic Precambrian rocks of the shields and the pampean ranges, mainly consisting of various gneisses and intrusive granites.
-  Metamorphic Precambrian rocks of the shields, mainly consisting of various schists, quartzites, phyllites, slates, and carbonate rocks.
-  Intrusive acid rocks of the Andean system, mainly consisting of granites, granodiorites, diorites.
-  Metamorphic rocks of the Andean system, mainly consisting of gneisses, schists, quartzites, phyllites, with subordinate intrusives.
-  Pyroclastic rocks with interbedded outflows of the Andean system and Patagonia.
-  Effusive acid rocks (rhyolite, quartz, and feldspar porphyries).
-  Effusive basic rocks (basalt, diabase, dolerite, andesite).
- Precambrian granites in the shield areas.
- Metamorphic rocks with old sedimentaries.

SEDIMENTARY ROCKS

-  Clastic consolidated sediments (sandstones, siltstones, shales, conglomerates) with subordinate carbonate sediments.
-  Carbonate sediments (limestone, dolomite) with clastic sediments.
-  Aeolian, fluvial and lacustrine Mesozoic sandstones of the Brazilian shield.
-  Young clastic weakly consolidated and unconsolidated sediments (sands, sandstones, clays, clay-shales, gravels, conglomerates).

The occurrence of loess with ash admixtures is indicated with Vv.

-  Sandy facies of the clastic consolidated and unconsolidated sediments.
-  Salt flats.
-  Land ice.
-  Lakes.



completely covered by Tertiary fluvio-lacustrine sediments, except for two narrow strips bordering the lower Amazon valley. Sandstones and some dark shales cover areas on the shields. (Bigarella 1973, Loczy 1968)

Grey-green to black shales, mixed with sandstones, constitute the major lithology of the Lower Paleozoic sediments in the entire Amazon Basin as well as the upper Precambrian on the shield. The greatest exposures are in the Bolivian Andes, where Ordovician dark shale and sandstones cover an estimated 75% of the area (Ahlfeld 1972). Black shales are particularly rich in reduced sulfur, potassium, and magnesium, having a Mg to Ca mole ratio in excess of one (Pettijohn 1975) (Figure III.1). The Lower Paleozoic section is partially metamorphosed in northern Bolivia and in Peru. On the shield, in the mid-Xingu Basin, Upper Precambrian shales form an area of particularly rich soils (Sombroek 1968, FAO/UNESCO 1971).

Red beds are the predominant post-Permian continental sediments. They are typically red shales and sandstones with a widely varying amount of limestone, evaporites (mostly CaSO_4), reduced shale, volcanic ash, and conglomerate interlayers. The abundance of evaporites appears to diminish forward with time. The source of the sulfate sulfur may be marine, volcanic, or Lower Paleozoic shales (c.f. Benevides 1968, Ruegg and Rosenzweig 1949). The amount of volcanic material in the red beds increases to the west.

The Tertiary fluvial-lacustrine sediments of the Amazon Trough and the soils of the shield are products of intense weathering. The cation depleted nature of these sediments is reflected in a representative analysis (lower forest-soil profile, Table III.1).

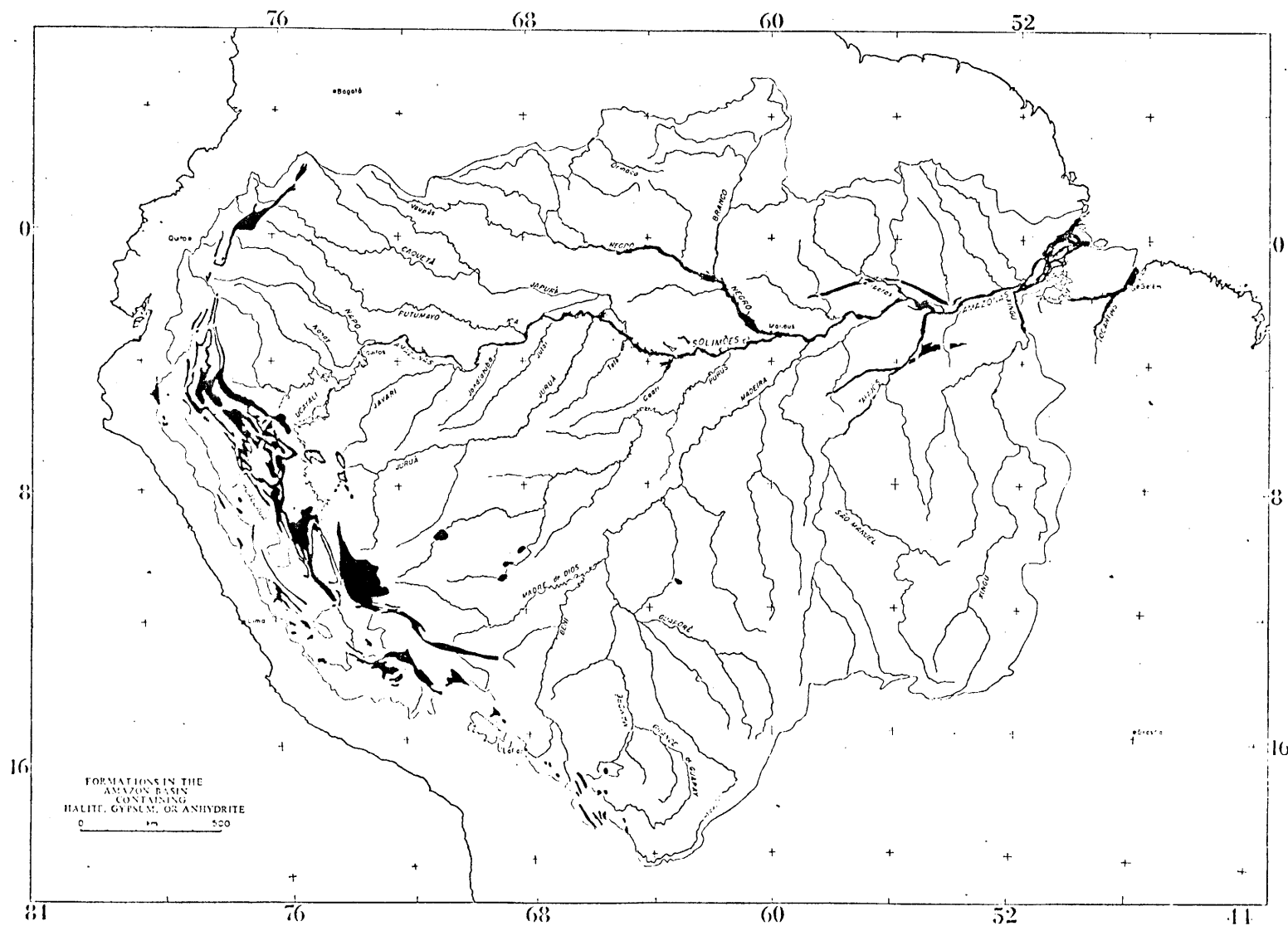
Sedimentary units, characterized as shales, are mineralogically complex and show wide variations in their composition (red beds represent an extreme example of variability). Sodium and potassium are present as aluminosilicate minerals (potassium tends to be concentrated in the clays and micas, and sodium in the feldspars). Magnesium may be present in both carbonate and sheet silicate minerals, while calcium is thought to be present primarily in carbonate minerals (c.f. Holland 1978, p. 114). Note that the inorganic carbon content exceeds the calcium content in all the shales of Table III.1. The inorganic carbon excess is greatest in the black shale suggesting that this shale is more dolomitic than the others (assuming the excess inorganic carbon is balanced by magnesium).

Sandstones in the Andes are typically arenites, while those on the shields are orthoquartzites and arkoses. The arenites are richer than typical shield sandstones (orthoquartzites and arkoses) in weatherable phases (Table III.1).

Carbonate rocks in the Andes are predominantly limestones. In stratigraphic columns where dolomites are designated, they are a subordinate facies (perhaps 5 to 10% of total carbonates). There are no massive Paleozoic dolomite units such as one finds in the North American cordillera. The carbonates with the greatest proportion of dolomites are found in the Pucara Group of lower Jurassic age (c.f. Bellido 1969), outcropping in the Intercordilleran Zone in central and northern Peru. The carbonates of the Amazon Trough also appear to have a higher proportion of dolomites than most of the carbonates in the Andean section.

Figure III.3

Map of the distribution of formations from which evaporite minerals (halite, gypsum, or anhydrite) are reported. This is not a map of evaporite exposures, which are far more limited in area and extent than regions indicated on this map.



FORMATIONS IN THE
 AMAZON BASIN
 CONTAINING
 HALITE, GYPSUM, OR ANHYDRITE

0 500
 km

Formations in which evaporite minerals are reported are concentrated in the Andes (Figure III.3), and those which contain halite tend to be localized to the Andes of central and northern Peru and southern Ecuador (c.f. Benevides 1968). Some of the evaporite minerals (particularly gypsum and anhydrite) are dispersed in red beds, and outcrop in the formations in which they were deposited. In north and central Peru (notably in the Huallaga River Basin) buried evaporites are brought to the surface as salt plugs or domes and expressed as salt springs (Benevides 1968). The larger of the domes have diameters in the order of 5 to 10 km; their aggregate area probably is in the range of 100-200km². Their extrusion rate is such that they are pronounced topographical highs, even though the precipitation is on the order of 1.5 meters/year (Figure III.4). The domes are primarily gypsum and halite. Salt springs have also been reported in Ecuador (Benavides 1968, Tschopp 1953). The springs are thought to be caused by the migration of formation waters up fault planes (c.f. Rigo de Righi and Bloomer 1975, Mabire et al. 1975). The great input of salt to surface waters can be seen by the numerous "Cachiyacu" (salt water) designated on maps of north-central Peru.

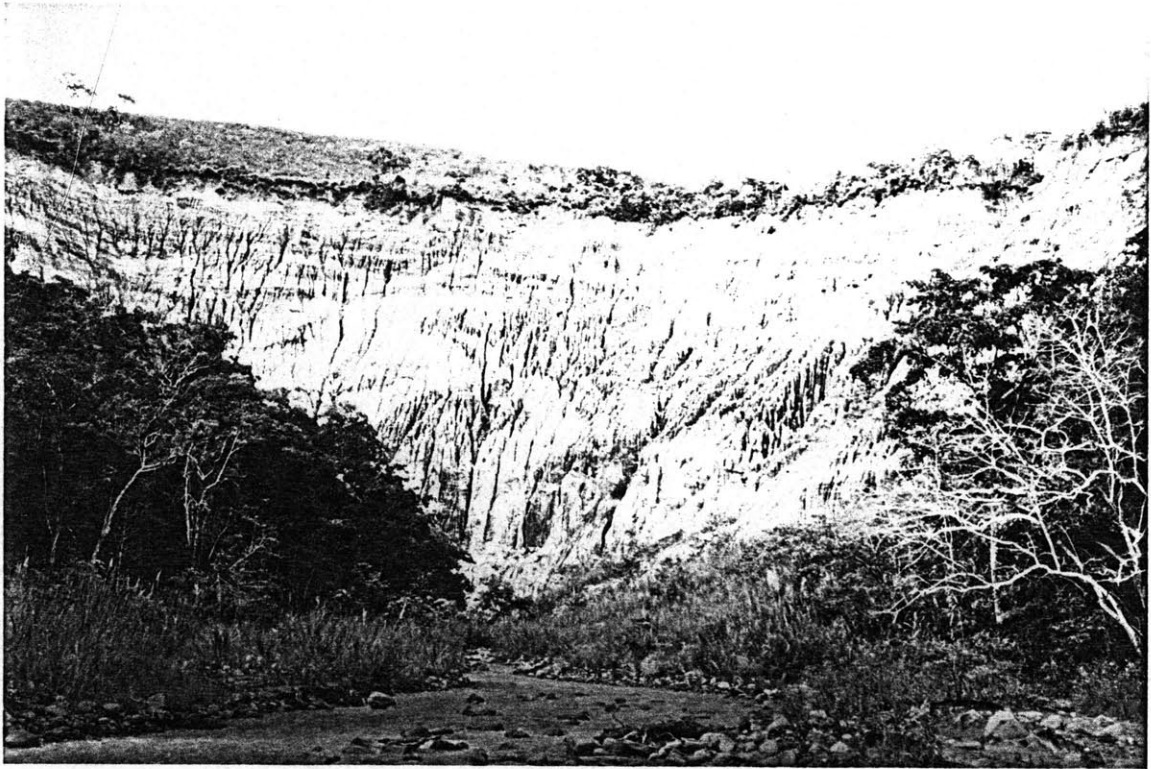
Figure III.4
(two pages)

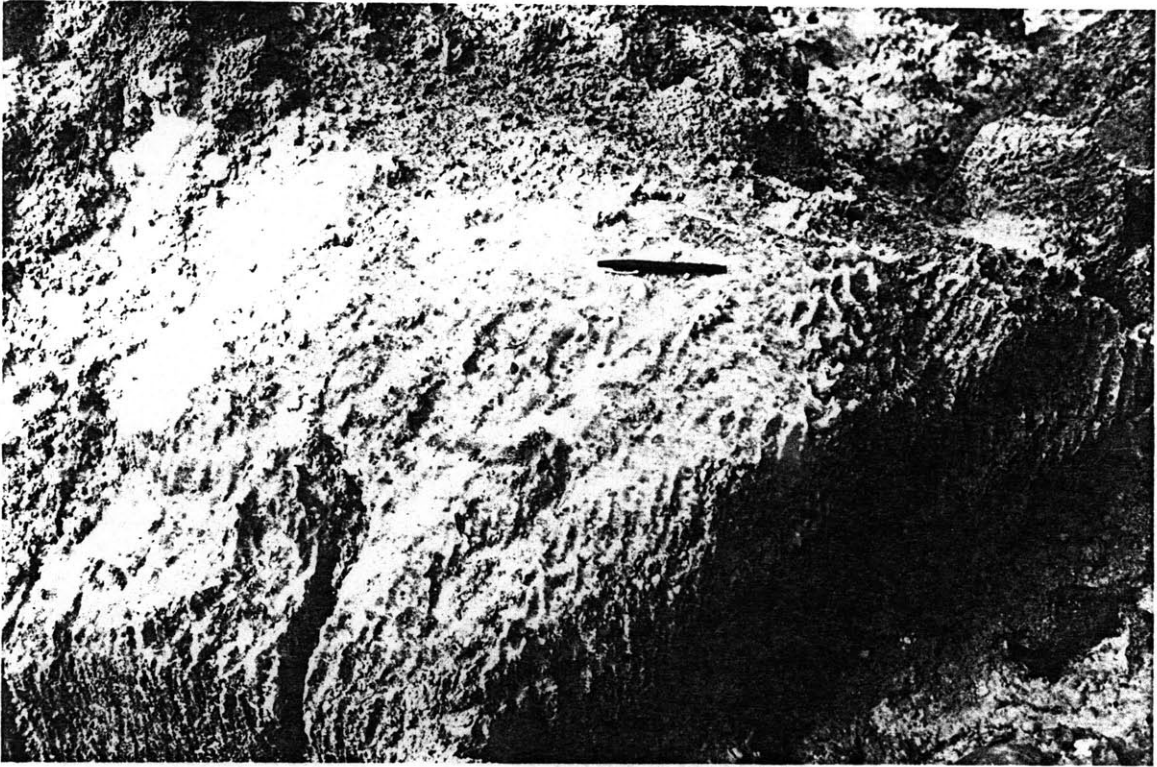
first photograph:

Photograph of a salt cliff (about 100 m high) in the interior of the Pilluana salt diapir. Much of the dark material in the cliff is shale, while the light material tends to be halite and gypsum. Rock salt is mined from the cliff, being exposed during storms. The extremely salty runoff during heavy rains causes fish kills downstream. The stream, Quebrada Caña (BPA16), has a salinity of 4560 ppm. Note the thick soil developed on the top of the cliff; this soil contains abundant gypsum fragments but no halite.

second photograph:

Photograph of a small block of rock salt. This salt block is exposed on the bank of the stream opposite the cliff in the previous photograph, and has therefore been exposed to precipitation for a long time. The salt has a faint pink color.





III. 4.1 Topography and Denudation Processes

The Amazon lowlands are typically a smoothly undulating terrain. Some areas are quite flat, however slight hilliness is typical, and abrupt topographical changes (30° slopes) are found throughout the Tertiary terrains and the shields, marking boundaries between erosion surfaces. Steep slopes are also associated with Subandean uplifts (c.f. photos in Kummel 1948). The Andean front is dramatic and sharp as seen in Figures III.5 and IV.11.

If slopes are sufficiently steep, the products of physical and chemical weathering will be removed as fast as they are produced (barring complications caused by tectonic and climatic change) and soils will be thin. Such a situation is said to be weathering limited as opposed to transport limited, where solid weathering products accumulate (e.g. soil development on the lowlands) (Carson and Kirby 1972). On weathering limited terrains a pronounced dependence on the properties of the substrate is indicated, with the denudation of chemically unstable and physically unstable material being most rapid. A greatly reduced dependence on substrate characterizes transport limited terrains.

Relief provides a logical basis for the separation of the discussion of denudation processes in the Amazon Basin. The discussion of denudation in the flat lowland areas focuses on both weathering products and their transport. For steep terrains, the discussion centers on the importance of lithology, as the transport of materials away from the site of weathering can be assumed to be effective (note that valley-fill accumulation and similar short-range transport does occur).

III. 4:2 Denudation, Soils, and Vegetation in the Lowlands

A clear relationship exists between vegetation and denudation processes. Three principal regimes are identified corresponding to savanna (including all dry grasslands), terra firme forest (or Hylaea) and campina and Amazonian Caatinga (which is a special class of terra firme forest).

The savanna environment is characterized by the abundance of grass, the lack of much shading vegetation, and a climate marked by pronounced wet and dry seasons, the seasonal drought being sufficient to allow for the parching of all but deeply rooted vegetation. Currently savanna is found in the Rio Branco Basin in the north, and through much of the upper Xingu, Tapajos, and non-Andean Madeira Basins (FAO/UNESCO 1971, Hueck & Seibert 1972, Walter 1972, Sarmiento and Monasterio 1975, Prance 1978). Understanding of factors controlling the distribution of savannas has been gained from comparative studies of savannas and forest near the boundary (often sharp) between the two environments (Pasquali et al. 1972, Goldsmith 1974, Zonneveld 1975, Scott 1975, 1977, Sarmiento and Monasterio 1975, Lopez E. and Bisque 1975). Two factors appear to be of primary importance, the desiccation of soils and ground cover during the dry season, and burning either from natural or human causes. Comparative studies of landforms, soils, and stream transport suggest that both surface runoff and accompanying physical denudation (splash erosion, sheet wash, and gully formation) are more pronounced in the savanna than the forest, with savanna soils being both denser and less permeable (Pasquali et al 1972, Zonneveld 1975, Scott 1975, and Sarmiento and Monasterio 1975). Ferruginous crusts and conglomerates (to be referred to as hardened laterite, also known as plinthite and arecife) cover

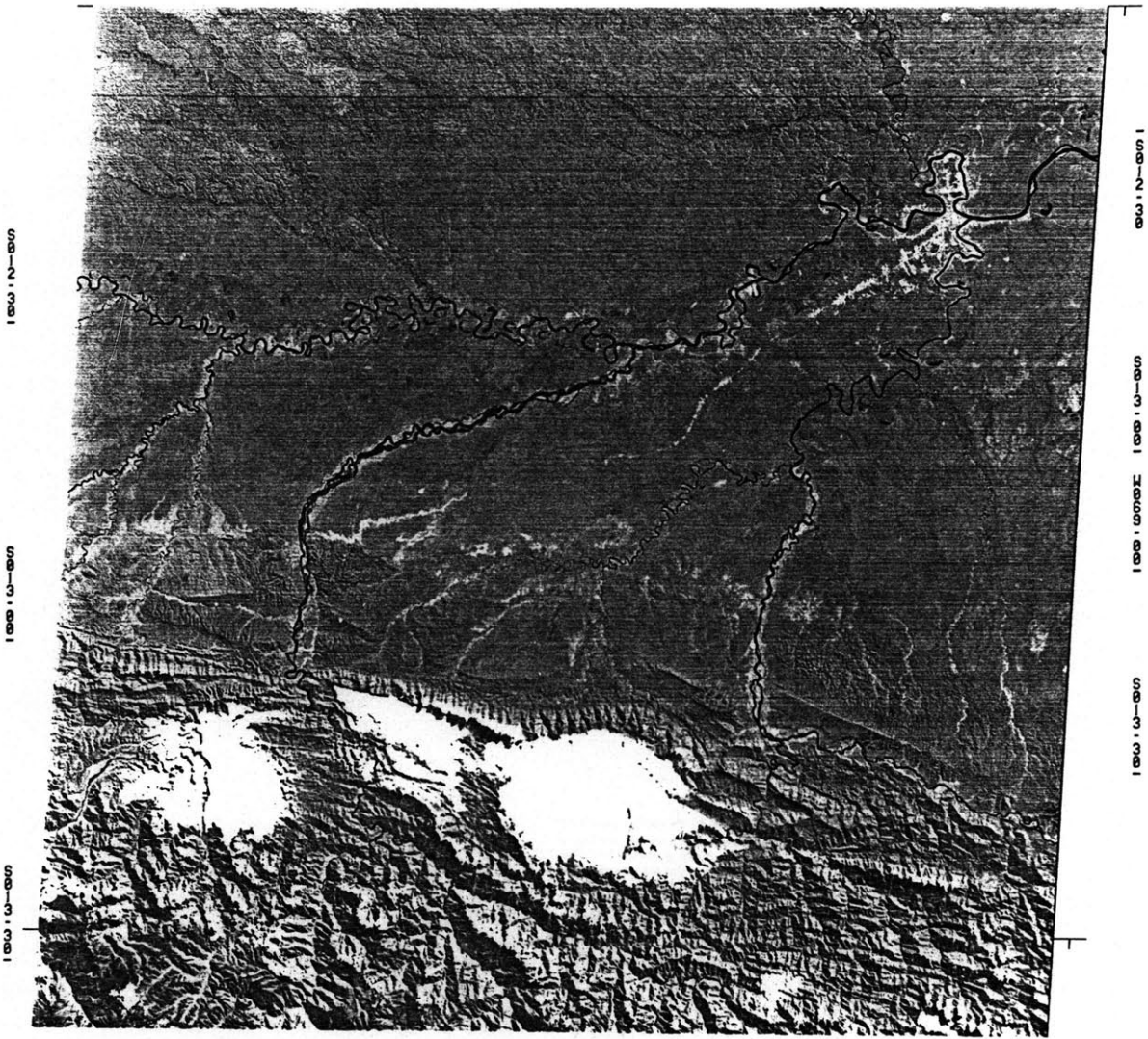
Figure III.5

Photograph of the Andean Front near the Peru-Bolivia border, illustrating the abrupt transition from lowlands to steeply sloping terrain. The east-west flowing river is the Madre de Dios. The white patch in the meander in the upper right of the photo is Puerto Maldonado, Peru.

15812-00

14878-001

14869-301



15812-00

15812-00

15812-00

15812-00

15812-00

15812-00

23JUL75 C S12-57/14869-54 N S12-58/14869-55 MS 6 R SUN EL38 AZ262 189-2619-A-1-N-D-2L NASA ERTS E-2188-14821-6 81

14878-301

14878-001

14869-301

SW

areas of savanna in Venezuela, Colombia, Ecuador, Guiana, and Brazil. In other areas hardened laterite is found some distance beneath the soil surface, where it limits access of roots to the water table (Walter 1972).

Soils of both the forest and the savanna are similar in mineralogy consisting of kaolinite, quartz, and iron and aluminum sesquioxides. Soils found in the savannas are definitely more aluminous than those found in the forests (Figure III.6). This is corroborated by observations of soil mineralogy. Except in areas of unusual substrate, forest soils are dominantly kaolinite, quartz, and iron and aluminum hydroxides. In most analyses quartz and kaolinite are overwhelmingly the dominant phases (Sombroek 1966, Pasquali et al. 1972, Lopez E. and Bisque 1975, Irion 1975, Kronberg et al., 1979, Guerrero 1975), however abundant gibbsite is reported in some soil profiles in savanna areas (Pasquali et al. 1972, Lopez and Bisque 1975 (Venezuela), Kronberg et al. 1979 (near Brasilia)) Pasquali et al. (1972) and Lopez E. and Bisque (1975) observe that the amount of gibbsite relative to kaolinite decreases towards the surface. This is attributed to the reaction of gibbsite with silica migrating to and being concentrated near the surface by evaporation (daytime temperature 60°C).

Soil properties show a definite relationship to topography (Sombroek 1966, Van Wambeke 1978), with cation depleted soils being found on topographic highs and well drained flat terrain, richer (but still cation depleted) soils on slopes, and a wide variation of soils in the low areas, depending on the amount of flooding and the nature of sediments being deposited in the valley. Soils formed on basic rocks and marine sedimentary rocks are often quite varied in composition, ranging from

bauxites to cation rich soils (Sombroek 1966, FAO/UNESCO 1971, Lopez E. and Bisque 1975, Van Wambeke 1978).

The Tertiary sediments of the Amazon Trough (typically kaolinitic to sand facies) are derived from the surrounding shields, and soils developed on them do not differ substantially from the upper horizons of the mature soils of the shield, (Sombroek 1966, FAO/UNESCO 1971).

III.4.3. Mineral Stability and Element Mobility in Amazon Soils

The stability of minerals under tropical weathering has been considered by Pasquali et al (1972) and Lopez E. and Bisque (1975), who have examined the mineralogical changes occurring during the transition from fresh rock to saprolite through the soil profile. The mineral stability sequence is in agreement with the observations of Goldich (1938) and is summarized below:

	<u>Most Stable</u>			<u>Least Stable</u>
Acidic	Quartz	>>	Micas K-Feldspar	>>Na-Feldspar > Ca-Feldspar
Basic	Quartz	>>	Na Feldspar	> Ca-Feldspar > Pyroxenes Amphiboles > Chlorite

The following element mobility is observed in granitic rocks:

Most Mobile

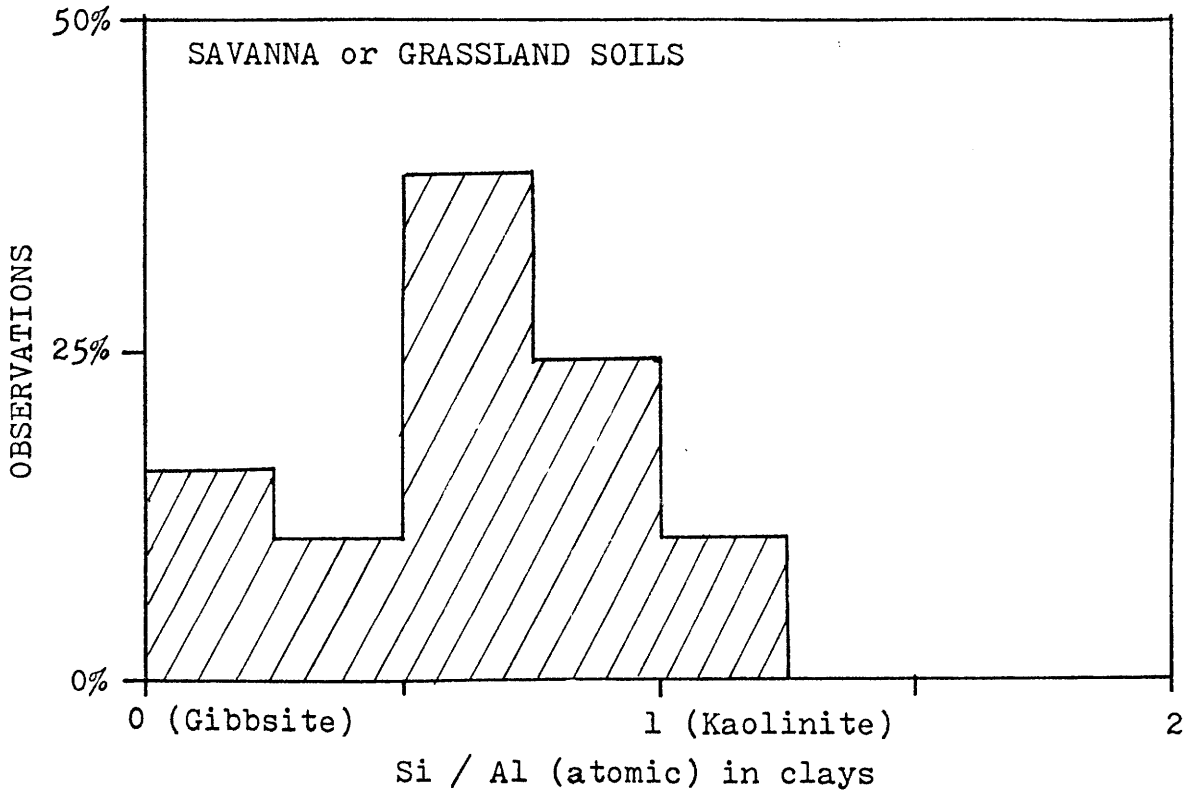
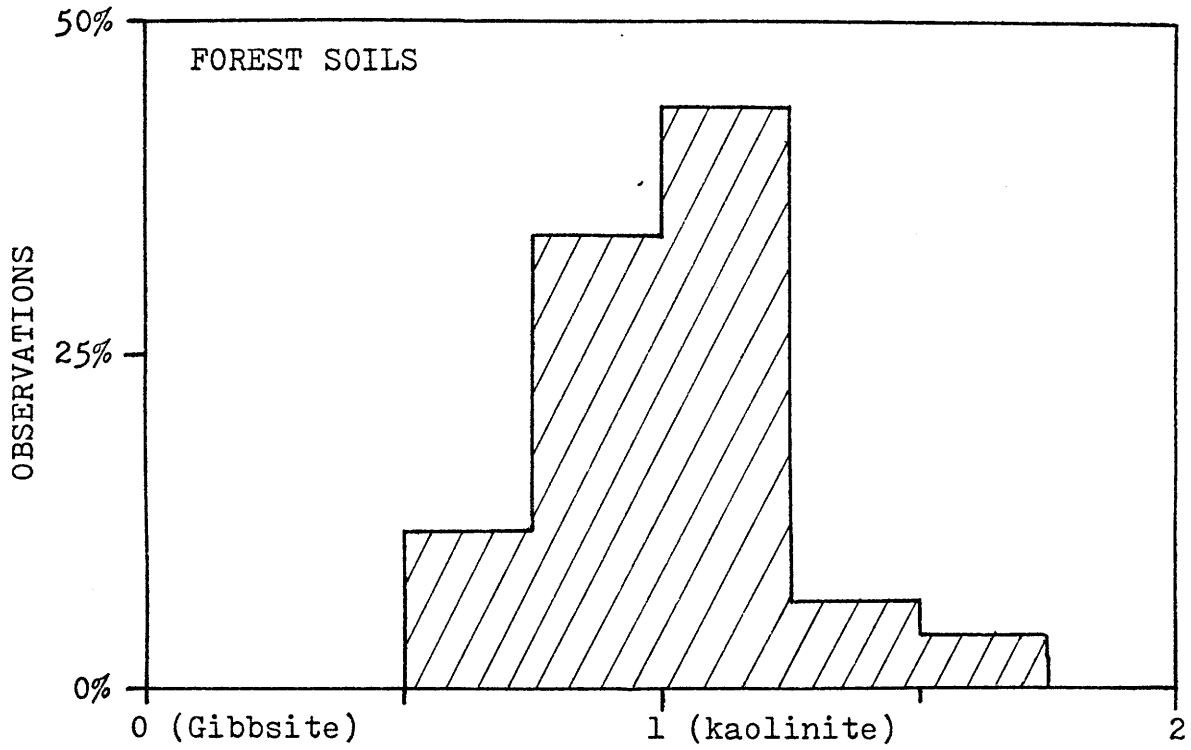
Ca > Na > Mg > K >> Si > Fe* > Al

*variable

The distribution of minerals in profiles developed on acidic and basic rocks show several important features. In the former, plagioclase feldspars are completely weathered (and most of the Ca and Na lost) while the rock is still a hard saprolite (Pasquali et al. 1972). The products of this rapid weathering include kaolinite and gibbsite (gibbsite only in the savanna). Microcline and mica are lost farther up the profile (in the soft saprolite) along with much of the Mg and K. Microcline maintains a fresh appearance

Figure III.6

Graphs illustrating the distribution of Si:Al (clay fraction) ratios in forest and savanna environments in the southern half of the Amazon Basin (Data from Camargo and Falesi 1975).



(along with much of the Mg and K). Microcline maintains a fresh appearance during the weathering process (taken here to mean no obvious weathering rinds form), while biotite bleaches. Quartz persists through the profile. "Floating" spheroids of partially weathered granite are seen in some profiles. In two of the profiles developed on basic rocks reported by Lopez E. and Bisque (1975), unstable primary and secondary minerals (and mobile cations) are found through much of the section, while a third profile is intensely weathered to a bauxite.

It should be noted that these studies were done in areas of relatively young and thin soils where fresh outcrops could be seen. In contrast, soils developed on the older erosion surfaces are thicker, often many tens of meters (FAO/UNESCO 1971, Kronberg et al. 1979). Neither feldspars, micas, nor "floating" less weathered materials are reported in these areas (c.f. Kronberg et al., 1979, Table II).

Unstable minerals have been reported in soils from sedimentary terrains. Sombroek (1966) observes muscovite and chlorite in soils of the lowlands, however no other studies report similar occurrences of chlorite and it is possible that this observation represents a misidentification. Irion (1975, 1976) reports montmorillonite forming from volcanic ash in soils found on Cretaceous to Tertiary rocks in the southwest lowlands.

The final major group of soils are those underlying the campina (sparsely vegetated grassy areas surrounded by forest) and Amazonian Caatinga, found in extensive areas of the Upper Rio Negro Basin and in smaller patches elsewhere (Hueck and Seibert 1972). The soils (giant podzols, tropical podzols, spodzols) are characterized by a surface layer, rich in humus, a thick (up to several meters) bleached quartz A horizon, and an underlying layer (ortstein) rich in aluminous

clays (no iron) and cemented by humic materials (Sioli and Klinge 1961, Klinge 1965,1967, and Sombroek 1966). These soils can occur where the substrate is sandy sediment, however in the Rio Negro Basin the podzols are developed on granites and gneisses. This area is the wettest part of the Amazon lowlands (>2500 mm rain/year, with no dry season) and is fairly flat. Thus there is a substantial sustained flux of water through the environment. Such soils are highly correlated with brown, acidic, cation poor, sediment free surface waters, which are probably responsible for the leaching of Fe and Al from the soil as well as the deposition of humic materials in the soils (Klinge and Ohle 1964, Klinge 1967). Presumably, the persistent wetness allows the organics to endure in the environment, by limiting diffusion of oxygen into soil pores. The exact areal extent of the soils is uncertain. Sioli (1968), Klinge (1967), and Marlier (1973) favor a wide distribution within the upper Rio Negro Basin, as both the brown waters and the Amazonian Caatinga are widely distributed through the region (c.f. Hueck and Seibert 1972).

III.4:4 Laterites and Podzols in the Amazon Region

Contrary to popular belief, near-surface laterites are quite rare, covering about 2% of the basin (Van Wambeke 1978, Sioli and Klinge 1961), and where laterite does occur it often appears to be "fossil" (Sombroek 1966, Mousinho de Meis 1971, Klammer 1971, Grubb 1979). McFarlane (1976) describes two classes of laterites reflecting different modes of evolution, ground water laterites and pedogenetic laterites; in addition some laterites are secondary, being formed by redeposition of laterized material. Ground water laterites are thought to form in the zone of a fluctuating water table, primarily as a result of alternating oxidizing and reducing conditions.

These may become quite thick if the depth to the mean water table increases with time. In actively forming ground water laterites, the concretionary structures (pisoliths) tend to be soft. Pedogenic laterites form in the upper soil horizon, perhaps assisted by working of the soil by organisms. These laterites are thin and form only in a grassland environment, unlike groundwater laterites which also form under forested conditions.

The contemporary laterites in the forested areas of the Amazon region are groundwater laterites (Sombroek 1966). They typically exhibit a sandy horizon over a soft laterite B horizon. In its advanced form the A horizon can become thoroughly bleached (with sparse overlying vegetation). Ground water laterites are invariably observed in:

- (1) Lowlands intermittently covered with rain water
- (2) Lowlands flooded by rivers not carrying a sediment load
- (3) Terrains along rivers, only slightly above river level

The profiles observed by Sombroek showed Si:Al ratios around one (kaolinitic) with profiles developed on crystalline rocks always showing ratios greater than one. No profile could be considered highly leached of silica. These laterites differ from typical laterites described by MacFarlane (1976) in their high silica content and the climatic conditions (neither as dry nor as seasonal in their precipitation) in which they form.

Sombroek (1966) observes that there are great similarities in giant podzol and advanced groundwater laterite profiles. The primary differences between the two are that the former has humic materials in the horizon below the sand and a freer horizontal drainage, capable of transporting materials out of the soil zone. Grubb (1979) suggest that all of these soils should be considered podzols rather than laterites.

The pisoliths found in detailed savanna profiles of Pasquali et al. (1972) and Lopez E. and Bisque (1975) appear to be typical of eroded fossil ground water laterites as per MacFarlane (1976).

III.4.5 Ground water Circulation

The surface soils in the Amazon lowlands are intensely weathered; few primary minerals are found in the surface horizons, yet dissolved products of primary rock weathering are found in all the rivers examined in this study. Ground water circulation is a means of bringing material to the surface.

Ground water circulation has been studied on representative clay-rich forest soils (Nortcliff and Thornes 1978, Nortcliff et al. 1979) and giant podzol soils (Reichardt et al. 1975). Both types of soils are extremely well drained. The fluxes in the forest soil are vertical, even near the soil surface on a hill slope, while fluxes in the podzol are horizontal due to the presence the ortstein layer. Nortcliff et al. (1979) conclude that the free draining nature of the forest soils requires that river water be derived primarily from ground water inputs rather than overland flow

III.4:6 The Significance of the Three Weathering Environments

The three environments: savanna, forest, and Amazon Caatinga when developed on shield terrains, probably correspond to a sequence of increased intensity of chemical weathering and reduced intensity of physical weathering, respectively. The sequence clearly corresponds to one of increasing precipitation and runoff, which has been shown to correspond to increased rates of chemical weathering and more effective dissolution of the original substrate in tropical environments of Kenya (Dunne 1978).

The soil data indicate that the effectiveness of chemical weathering increases with precipitation. For savanna soils, the decreased permeability and increased levels of surface runoff imply that precipitation is much less likely to interact chemically with weatherable materials than is the case with forest soils. However, due to greater overland flow physical weathering is more effective.

The presence of almost pure quartz, the complete loss of iron and the partial loss of aluminum in the giant podzol soils developed on granites suggests very effective and rapid dissolution (referred to the rate of dissolution of quartz) of the original rock. Dissolution or colloid stabilization of aluminum and iron in black water rivers is supported by observations from this study as well as work of Sioli (1954), Sioli and Klinge (1961), Klinge and Olhe (1964), Ungemach (1967), and anon. (1972a). Evidence of the destruction of quartz includes the solution pitting of quartz from tropical sands (c.f. Potter 1978) and the breakdown of quartz grains in savanna soils (c.f. Pasquali et al. 1972). Loughnan and Bayliss (1961) describe a soil developed in a monsoon climate (with a mean annual precipitation about half that of the central Amazon) on sandy shales (similar to the Tertiary fluvio-lacustrine sediments), where quartz is entirely dissolved from the upper profile, leaving an iron and aluminum hydroxide residual. Unlike the Amazon giant podzols, it is apparent that the dissolution rate of Si, from quartz in the soil, has exceeded the dissolution rate of Fe and Al from clay minerals. Assuming that quartz dissolves at an equal rate in laterite and podzol soils, the overall rate of dissolution of minerals in the latter soil must be greater than in the former.

The above weathering sequence for siliceous rocks (seasonally moist = sequioxides/kaolinite, super moist = podzols) differs considerably from that described for basic rocks from Hawaii (Sherman 1949, 1952). Under a climate having similar wet and dry seasons as the Amazon, ferruginous laterites are seen forming on basic rock, while under permanently wet (Negro Basin-like) conditions aluminous laterites develop. Clearly a difference is the role of quartz as a structural element in rapidly weathering granitic soils. Other differences must include the lesser stability of the minerals in basic rock.

III.4:7 Slope Processes.

Slope processes (weathering limited denudation) in the lowlands and the Andes will be considered separately, as the former reflect a more tranquil history of development and are less subject to active tectonic controls.

Two classes of steep relief can be seen in the lowlands. In many areas hills are protected by a laterite or quartzite caps, a clear lithologic control, which reduces erosion rates of underlying material. In contrast other slopes and scarps between erosion surfaces do not exhibit horizontal or vertical lithologic control.

Retreat of slopes is thought to be more rapid under drier, less vegetated conditions (Garner 1968, Holm 1977). Rapid weathering however, is possible under moist conditions. A likely mechanism for rapid slope retreat under wet conditions is the chemical weathering of the parent rocks followed by sliding of the resultant soil (Scott 1975b, Scott and Street 1976, Pain 1972, Garwood et al. 1979) or other forms of solifluction (e.g. soil creep, piping, tree-falls etc.) (Zonneveld 1975). Carson and Kirby (1972) show

that the form of such a slope should be stable through time (parallel retreat).

Holm (1977) describes an erosion scarp, which separates two erosion surfaces in the Branco Basin. Both of the surfaces have been peneplaned and little topographic variation is seen marking contrasting lithologies, implying that transport limited denudation is occurring. The scarp itself (having a 30-35° slope) is not associated with faults or a lithologic break, and is in fact quite sinuous. Ridges on the scarp consist of resistant rocks, while valleys are associated with zones of weakness, implying weathering control. It is therefore suggested that the scarp is the locus of erosion for the region.

III.4:8 Andean Slopes

Weathering in the Andes is extremely complex due to tectonism and wide variations in both climate (spatially and temporally) and rock types. On many of the lithologies in the well watered part of the Andes (below about 4000m on the Amazon flank), chemical weathering of the sort discussed for non-Andean slopes, is thought to be the main process controlling denudation (Garner 1959). Even at glacial altitudes, chemical weathering can still make important contributions to surface waters (Reynolds and Johnson 1971).

Very poorly lithified deposits exist throughout the Andes. Accelerated chemical inputs to stream water during the rapid erosion of such deposits has been demonstrated in the Rocky Mountains (Colby et al. 1956, Hembree and Rainwater 1961). Rapid removal of Andean Pleistocene sediments has been observed (Garner 1959, 1968b, Ballivan et al. 1978) and suggested as a major source of solid materials in rivers. The erosion of continental red beds has not been studied. These

are very soft rocks which consist primarily of shales and sandstones and contain thin limestone, evaporate (sulfate), and volcanic ash interlayers (bentonite beds). The effect of red bed erosion is easily seen. All Andean rivers observed during this study acquired an intense red color only after crossing exposures of red beds.

The presence of unstable and cation-rich minerals in the suspended and bed loads of rivers which drain the Andes suggests that extraordinarily rapid erosion is occurring. This is evidenced by the presence of carbonates in the bed load of the lower Amazon (c.f. Potter 1978), the only source of which could be the Andes. The lower Ucayali and Marañon contain a very large percentage of montmorillonite in their clay load (Gibbs 1965, Irion 1975, 1976), while rivers of the high Andes contain primarily chlorite and illite (Irion 1975, 1976). Rivers in the Madeira Basin, which drains the Bolivian Andes, contain high percentages of illite.

The above distribution of clay minerals in the suspended load reflects the geology of the respective basins. Irion (1975, 1976) shows that much of the montmorillonite is derived from the weathering of volcanic glass. Bentonite beds (paleo-volcanic ash layers) being eroded out of red beds may also be important, hence the contrast between high Andean rivers, which have not yet crossed red beds, and their lower courses. Finally, the Paleozoic sediments, which make up the Bolivian Cordillera Oriental, are very rich in illite and biotite (Brockmann et al. 1975), and are undoubtedly the principal source of illite in the Madeira Basin rivers.

III.5 BIOLOGICAL PROCESSES IN AMAZON GEOCHEMISTRY

Roots and root-fungi symbiotic associations (mycorrhiza) play a significant role in the geochemistry of many biologically important elements which are depleted in lowland soils (e.g. Ca, Mg, and K), by transporting the elements to and maintaining them in the biomass through recycling. In savanna, forest, campina, and Amazonian Caatinga, a dense root mat is typically found near the surface of the soil, except in isolated areas of exposed sand, rock, or laterite. The root mat in savanna (dominantly of drought resistant grasses) is utilized for water acquisition during rains, while trees tend to develop deep feeder roots to access water (Walter 1973). In contrast, the root mat in the other soils is composed of tree roots and mycorrhizal tree roots (Went and Stark 1968). On clay soils, roots are concentrated near the surface, with 25% being found in the surface humus layer (Klinge 1973). The root mat can sometimes be rolled off the soil like a carpet. Roots form about 25% of the living biomass in the forest (Klinge and Rodrigues 1973), although in some instances the figure may be as high as 60% (Herrera et al. 1978a). On giant podzols, 80% of the roots are confined to the surface humus layer, and the root biomass is about one quarter that of the forest (Klinge 1973). Deep feeder roots are only seen in forest soils where unweathered minerals are not found far underground (Went and Stark 1968, Stark 1978, Pasquali et al. 1972).

The geochemical implications of the surface root mat are significant. Organic matter is primarily decomposed by bacteria, decay animals (e.g. ants), and mycorrhiza (Stark and Holley 1975). Mycorrhizal rootlets are observed to cover and attach to forest litter, softening and eventually

assimilating it, leaving only a shell of roots (Went and Stark 1968, Herrera et al. 1978a, b). Leaves tagged with ^{32}P have been used to show that direct transfer from litter to roots occurs (Herrera et al. 1978b). If solutions containing ^{32}P and ^{45}Ca are sprayed onto the root mat, from 99% to 99.9% is assimilated by organic materials in the root mat and eventually transferred to the roots and thence the rest of the biomass. (Stark and Jordon, 1978). The ability of mycorrhizal roots to retain a wide range of elements in a non-labile form has been demonstrated (Stark 1972), an effect clearly seen in the data of Pasquali et al. (1972), who observe that the bulk concentration of Ca and K in the organic rich (root) zones is 2 to 10 times that of the soil below. In addition, they do not see retention in savanna soils. The mass of K, Ca, and Mg in the total biomass is about 3 to 5 times that of the weathered solid below (c.f. Stark 1971a,b, 1972, Herrera et al. 1978a).

The effect of element recycling and storage on river geochemistry for an ecosystem that is in steady state should not be great, however if the cycle is broken large amounts of certain elements could be released. For example, in slash-burn agriculture (Brinkman and Nascimento 1973, Scott 1977, Stark 1978), great quantities of nutrient elements are released into the air (as smoke), surface water, ground water, and soil. The seasonal storage of nutrients in the biomass is important in temperate areas (e.g. Likens et al. 1977), and could possibly be significant in the Amazon Basin, especially in areas where pronounced seasonal variations occur.

The behavior of deep forest root systems has been described by Pasquali et al. (1972). They observe roots penetrating as much as nine meters, clustering along granite surfaces and around granite spheroids

in the profile. Presumably these roots transport nutrients to the surface. The roots are also found oriented with the water table. Mottled bands (Tigrito), sometimes containing an axial root, are observed throughout most soil profiles. The bleaching, which is the result of the loss of iron, is thought to be caused by root exudates and decay.

Evidence suggest that the organic matter, produced by vegetation, has a direct chemical role in soil processes. Sombroek observes that all the ion exchange capacity in Amazon soils can be accounted for by organic matter ($39 \mu\text{Eq/g}$ per %C). Furthermore, when the carbon content of the soil drops below 0.5% the amount of readily dissolved phosphorous in the soil drops dramatically, being tightly bound instead to iron and aluminum. Lopez and Bisque (1975) observe that in surface horizons of savanna and forest soils, amorphous iron oxides will recrystallized into goethite only when the carbon content drops below 0.5%. These observations indicate that iron and aluminum hydroxides in soils are rather effectively bound by soil organics

Laboratory studies have shown that at room temperature and pH's resembling those in the Amazon, recrystallization of iron (Kodama and Schnitzer 1977) and aluminum (Violante and Jackson 1979) is inhibited by organics in solution. However, they assist in the formation of crystalline kaolinite, perhaps by forming an Al-O bond thereby facilitating coordination with silica (Linares and Huertes 1971, Hem and Lind 1974). If organics are not present, amorphous aluminum hydroxide or gibbsite forms. In the Amazon region, savanna soils tend to be lower in organics than forest soils (Lopez and Bisque 1975, Sombroek 1966, Scott 1975), and it is possible that the prevalence of kaolinite in the latter relative to the former may be due to organics.

Chapter IV

Examination of the processes controlling the chemistry of the dissolved load of the Amazon River.

IV.1 SAMPLING

Lowland river sampling centered around two transects of the Amazon Basin, on the main channel, by the R.V. Alpha Helix (June-July 1976 going upriver, May-June 1976 going downriver, Figure IV.1). Boston whalers were used to sample tributaries above the Tefê on the first transect and all but the Iça, Negro, and Madeira rivers during the second. Samples from several lowland sites were obtained for other parts of the year (see Acknowledgements). Sample locations, handling procedures, and analytical methods are given in Appendices I, II and III, respectively.

Samples were collected in Andean rivers, lowland Madeira and Peruvian rivers after transect (1), before and after transect (2) and during November-December 1978 (Figure IV.1). Handling procedures for these are given in Appendix II.

Sampling had three principal objectives:

- (1) to sample the principal tributaries of the main channel
and of the largest main channel tributaries (Marañon, Ucayali,
Madiera, and Branco Rivers)
- (2) to sample rivers draining the extremes of rock type in the
Amazon Basin
- (3) to obtain time series of flows and chemistry from various
main channel sections

The first objective was attained for the main channel, and to a lesser degree for the large tributaries. The large tributary subsampling is adequate to delimit source regions for major water types. The second objective was met satisfactorily, although few one-rock-type rivers were sampled. The last objective was not met satisfactorily due to political and logistical problems. For this reason, the data interpretation focuses on the two transects of the system.

IV.2 PREVIOUS OBSERVATIONS ON REGIONAL WATER CHEMISTRY

The earliest chemical studies of surface waters in the Amazon region recognized the geographical contrasts in chemical properties. Raimondi (1884) observed that the Marañon and Ucayali Rivers were impoverished in dissolved inorganic species and enriched in organics compared to many waters from the Andes. He attributed these observations to biological activity. Katzer (1897, 1903) noted that the lowland tributaries are more dilute than the main channel, which is in turn extraordinarily dilute compared to other rivers.

Waters from the Brazilian Amazon region have long been classified on the basis of their appearance. Three types are observed: white waters, which are rich in dissolved and suspended materials; clear waters, which are poor in dissolved and suspended material; and black waters, which are intensely colored by humic matter, and are typically more dilute than clear waters (c.f. Sioli 1967).

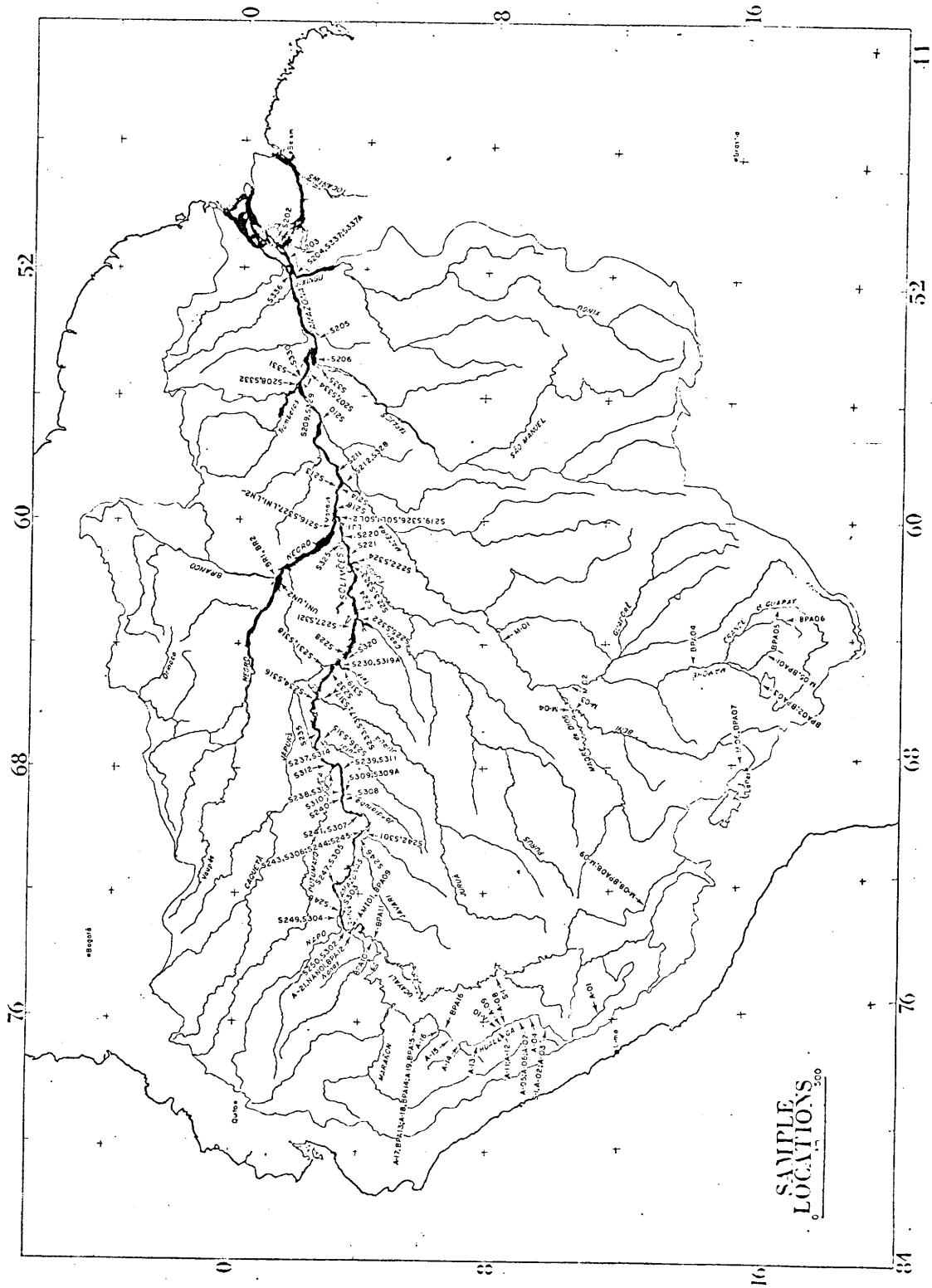
The white water type is characteristic of all rivers that have substantial drainage in the Andes, especially the main channel of the Amazon and the Madeira River (Sioli 1957, 1964, 1968, 1975, Gibbs 1965, 1967, 1972, Schmidt 1972a, Furch 1976). These are much closer compositionally to typical river waters than any of the rivers originating in the lowlands.

Clear waters are the most widely distributed water type in the Amazon Basin. These rivers originate in the shield and raised Tertiary terrain characterized by clay rich soils (Sioli 1954 a,b, 1964, 1968, Klinge and Olhe 1964, Schmidt 1972b, Furch 1976).

The black waters originate in extremely flat areas, and have been linked to distinct vegetation types (Campina-Amazonian Caatinga), and the nutrient poor giant podzol soils. (Sioli 1954a, 1955, 1964, 1968, Sioli and Klinge 1961, Klinge and Olhe 1964, Klinge 1965, 1967, Ungemach 1967,

Figure IV.1

Sample location map. For collection dates and location descriptions refer to Appendix I.



anon. 1972, Schmidt 1972b, Furch 1976).

In previous studies, $\text{Na} > \text{K} > \text{Mg} > \text{Ca}$ is typically reported for black and clear waters ($\text{Mg} > \text{Ca}$ is observed only once in this study for these water types), while $\text{Ca} > \text{Na} > \text{Mg} > \text{K}$ is observed in white waters. The pH of clear and black waters is often less than 5.5. It has been observed that waters originating on Tertiary lake sediments and the quartzites of the shields are depleted in dissolved materials relative to the waters originating on Precambrian igneous and metamorphic terrains (Sioli 1968, Fittkau et al. 1975, Schmidt 1972b, Furch 1976). This is attributed to the weathered nature of the sedimentary substrates. Clear waters with exceptionally high concentrations and near neutral pH drain the isolated bands of carbonates and sulfates of the lowest Amazon Basin (Sioli 1963, 1968).

Studies of Andean and Subandean rivers have been confined to Peru. Patrick (1966) and Swabey (1966) note the wide range of concentration and chemistry. Swabey (1966) suggests that the range of Mg:Ca ratios might be explained by variations in limestone chemistry. Furthermore, salt deposits [e.g. "salt hills" of Herndon (1954) and the "saline waters of the Huallaga" of Spruce (1908)] are suggested to be the principal source of chloride in the Amazon. It is noted that the Amazon at Iquitos is about three times as concentrated as the lower Amazon (due to either seasonal differences in river composition or the incorporation of dilute rivers). Hegewald et al. (1976) observe that lakes in the northern Peruvian Andes are more dilute than those to the south, and that their Mg:Ca ratio increases to the south.

Throughout the Amazon Basin, bicarbonate is the dominant anion in solution. Published analyses for sulfate and chloride show a high degree of inconsistency. Chloride and sulfate concentrations higher than bicarbonate are reported only for some tropical lowland rivers (U.S.G.S. unpublished, Klinge and Olhe 1964, anon. 1972a), and from rivers draining evaporites.

IV.3:1 INTRODUCTION TO CHEMICAL DATA

Various schemes exist for describing and classifying river water chemistry. Chemical classification of river water is of particular value as it provides a means of linking the interpretation of data from watersheds, where environmental factors (vegetation, soils, geology, etc.) affecting water chemistry are poorly understood, with watersheds where such factors are better studied. With this in mind, three types of classificational schemes will be examined using Amazon data:

- (1) Those based on ion dominance. The global geochemical model of Gibbs (1970) and the water types of Meybeck (1979) are essentially of this type. Both consider relative ion abundances as a function of total dissolved material.
- (2) Classification based on methods of multivariate analysis. Examples include the multi-component graph of Hill (1942) and Piper (1944); and factor analyses such as those used in the Mackenzie River study by Reeder et al. (1972).
- (3) Those based on the concentrations of various species as a function of the concentration of dissolved material. Examples of its use (Garrels and Mackenzie 1971, Holland 1978) have not focussed on classification but on description. It is versatile and will serve as the primary introduction to Amazon data.

IV.3:2 Chemistry of the Amazon Main Channel in Relation to World Averages

The Amazon is not a chemically remarkable river. A summary of recent estimates of "world average" compositions of dissolved, suspended and bed materials for world rivers is presented in Table IV.1. The solid phases are given as mole percent of the elements analyzed, and all three phases are tabulated normalized to silicon, the element most evenly distributed between the three components. Average river water could be described as a weak bicarbonate solution in which solid silicate phases are transported. There is a pronounced partitioning of elements between phases relative to silica. Alkalis and alkaline earths are preferentially included in the dissolved material, while aluminum, iron, and manganese are

Table IV.1

COMPARISON OF THE CHEMISTRY
OF DISSOLVED, SUSPENDED, AND
BED MATERIALS FROM THE
AMAZON RIVER
WITH
WORLD AVERAGE VALUES

World Average Values

Element	Diss. μmole/l (1)	Susp. mole % (1)	Bed mole % (2)	Diss. normal. to Si	Susp. normal. to Si	Bed normal. to Si
Na	254.	1.9	0.44	1.47	0.030	0.005
Mg	142.	2.9	1.5	0.82	0.048	0.018
Ca	344.	3.2	1.2	1.99	0.053	0.014
K	34.5	3.1	1.4	0.20	0.050	0.017
Si	173.	61.5	83.4	1.00	1.000	1.000
Cl	185.	--	--	1.07	--	--
S	97.	--	0.02	0.56	--	0.000
Cinorg*	865.	--	0.72	5.00	--	0.009
Fe	0.7	5.2	2.0	0.004	0.085	0.025
Al	1.9	21.1	8.6	0.011	0.343	0.103
Mn	0.2	0.12	0.03	0.001	0.002	0.000
Ti	0.2	0.71	0.58	0.001	0.012	0.007
P	1.3	0.23	0.02	0.008	0.004	0.000
N	16.	--	--	0.092	--	--

Amazon River

Element	Diss. μmole/l S250**	Diss. μmole/l S209***	Susp. mole % (1)****	Bed mole % (2)****	Diss. normal. to Si S250	Diss. normal. to Si S209	Susp. normal. to Si	Bed normal. to Si
Na	278.	63.4	2.1	2.3	1.50	0.53	0.036	0.029
Mg	96.7	39.6	2.8	1.3	0.52	0.33	0.048	0.016
Ca	477.	128.7	2.4	3.5	2.58	1.07	0.042	0.044
K	28.9	20.8	2.8	2.5	0.16	0.17	0.048	0.019
Si	185.	120.	51.2	78.9	1.00	1.00	1.000	1.000
Cl	183.	30.5	--	--	0.99	0.25	--	--
S	73.	17.8	--	0.04	0.39	0.15	--	0.000
Cinorg*	1122.	323.	--	2.82	6.06	2.69	--	0.036
Fe	1.0	1.9	5.9	1.9	0.005	0.016	0.104	0.024
Al	0.8	0.7	25.6	7.5	0.004	0.006	0.448	0.095
Mn	0.1	0.3	0.11	0.03	0.001	0.003	0.002	0.000
Ti	--	--	0.88	0.31	--	--	0.015	0.004
P	0.6	0.3	0.32	0.05	0.003	0.003	0.006	0.001
N	9.4	4.8	--	--	0.051	0.040	--	--

* assumed C_{inorganic} ≈ HCO₃⁻ ≈ titration alkalinity

** Main channel, upper course at Iquitos, Peru

*** Main channel, lower course at Obidos, Brazil

**** Main channel, lower course

(1) Martin and Meybeck (1978)

(2) Potter (1978)

found in the solid matter. An analogous set of analyses from samples taken on the Amazon mainstem is presented in Table IV.1. Water samples from both ends of the main channel are included. A comparison with the global averages demonstrates the typical nature of Amazon mainstem chemistry, being quite close to the world average. Note especially the similarity between world average river chemistry and water from Iquitos. This close similarity belies the great variety of water types found in the Amazon basin. The ranges of concentrations observed during this study for surface waters from the basin are presented in Table IV.2. The range of total dissolved solids (TDS) represented by these samples is roughly 6 ppm to 4000 ppm, comparable to the range of 37 ppm to 8000 ppm for rivers within the United States (Holland 1978).

IV.3:3 Ion Dominance

Meybeck (1979) presents a tabular classification of river waters based on ion dominance (Table IV.3). Meybeck groups surface waters (expressed as the percentage of global river flow to the ocean) into categories based on ion proportions and total dissolved solids (TDS). TDS is parameterized into three classes: (1) rock dominated, (2) precipitation dominated (3) evaporitic.

These classes were originally proposed by Gibbs (1970), who observes that if TDS is plotted against $\text{Na}/(\text{Na}+\text{Ca})$ for waters from throughout the world, a distinctive pattern results. Rivers low in TDS tend to be enriched in Cl and Na relative to HCO_3 and Ca. This Gibbs argues is due to atmospheric inputs dominating the water chemistry. Intermediate levels of TDS are accompanied by enrichment in Ca and HCO_3 , while high levels of TDS correspond to enrichment in Cl and Na. Gibbs asserts that these two groups are dominated, respectively, by rock weathering and evaporation of waters derived from rock weathering with accompanying precipitation of less soluble

Table IV.2
OBSERVED RANGES
FOR VARIOUS PARAMETERS

	<u>precip. minimum</u>	<u>precip. maximum</u>	<u>lowland river minimum</u>	<u>lowland river maximum</u>	<u>Andean river maximum</u>	<u>standard range⁺</u>	<u>units and precision (est. 95%)⁺</u>
pH	4.71	5.75	4.64	7.50	8.5	4.01-10.	0.02 pH units
Sodium	0.3	74.7	8.1	278.	71400	0-100	0.2 umole/l, 2%
Potassium	0.2	2.7	3.8	36.6	178.	0-100	0.1 umole/l, 1%
Magnesium	0.17	8.6	2.6	98.6	2660	0-50	0.1 umole/l, 1%
Calcium	0.0	4.6	3.6	552.	8290	0-200	0.2 umole/l, 1%
Alkalinity	--	--	-16.	1285.	2976.	--	2 uEq/l, 0.2%
Chloride	1.1	89.2	2.6	183.	71600	0-1000	0.3 umole/l, 1%
Sulfate	1.6	12.7	0.0	76.2	9320	0-300	0.3 umole/l, 4%
Nitrate	0.0	4.9	0.0	16.0	61.	0-50	0.4 umole/l, 4%
Silica	--	--	40.5	196.	244.	0-300	0.3 umole/l, 3%
Iron	--	--	0.0	7.3	3.1	0-15	0.1 umole/l, 3%
Aluminum	--	--	0.1	4.4	20.	0-12	0.1 umole/l, 3%
Color @270nm	--	--	65.	627.	19. ⁺⁺		1 cm Abs x 100
Total cations	11.	121.	51.	1570	77200		uEq/l
Tot.diss.sol.	0.5	6.9	4.8	133.	4560		mg/l

+ Analytical parameters, see Appendix III for details

++ Andean minimum

MAJOR CHEMICAL TYPES OF SURFACE WATERS

(Order of dominant ions expressed in eq./l)

(Adapted from Meybeck 1979), along with example of Amazonian river of that type.

Cations	Anions	Percentage #			Amazonian ⁺ Example
		(1)	(2)	(3)	
Ca ⁺⁺ > Na ⁺ > Mg ⁺⁺ > K ⁺	HCO ₃ ⁻ >> Cl ⁻ > SO ₄ ⁻	33.7	--	--	Marañon
	HCO ₃ ⁻ > SO ₄ ⁻ > Cl ⁻	2.3	--	--	Ucayali
	SO ₄ ⁻ > HCO ₃ ⁻ > Cl ⁻	0.3	0.5	--	n/o
	SO ₄ ⁻ > Cl ⁻ > HCO ₃ ⁻	*	*	*	Urubamba
	Cl ⁻ > HCO ₃ ⁻ > SO ₄ ⁻	*	*	*	lower Negro
Ca ⁺⁺ > Mg ⁺⁺ > Na ⁺ > K ⁺	HCO ₃ ⁻ > SO ₄ ⁻ > Cl ⁻	43.4	--	--	Napo
	HCO ₃ ⁻ > Cl ⁻ > SO ₄ ⁻	17.6	--	--	Solimões
	SO ₄ ⁻ > HCO ₃ ⁻ > Cl ⁻	*	*	*	Mamoré
Na ⁺ > Ca ⁺⁺ > Mg ⁺⁺ > K ⁺	HCO ₃ ⁻ > Cl ⁻ > SO ₄ ⁻	--	0.5	1.0	Branco
	SO ₄ ⁻ > Cl ⁻ > HCO ₃ ⁻	--	--	0.1	n/o
	Cl ⁻ > HCO ₃ ⁻ > SO ₄ ⁻	--	--	0.1	lower Negro
	Cl ⁻ > SO ₄ ⁻ > HCO ₃ ⁻	*	*	*	Cachiyacu
Na ⁺ > Mg ⁺⁺ > Ca ⁺⁺ > K ⁺	Cl ⁻ > SO ₄ ⁻ > HCO ₃ ⁻	*	*	*	Matari
Na ⁺ > Ca ⁺⁺ > K ⁺ > Mg ⁺⁺	Cl ⁻ > SO ₄ ⁻ > HCO ₃ ⁻	*	*	*	upper Negro
Na ⁺ > K ⁺ > Ca ⁺⁺ > Mg ⁺⁺	HCO ₃ ⁻ > Cl ⁻ > SO ₄ ⁻	*	*	*	Tefé
Mg ⁺⁺ > Ca ⁺⁺ > Na ⁺ > K ⁺	SO ₄ ⁻ > HCO ₃ ⁻ > Cl ⁻	*	*	*	Guapay

Percentage of global river flow,

(1) Rock-dominated type,

(2) Rain-dominated,

(3) Evaporitic

+ n/o = not observed

* not classified by Meybeck

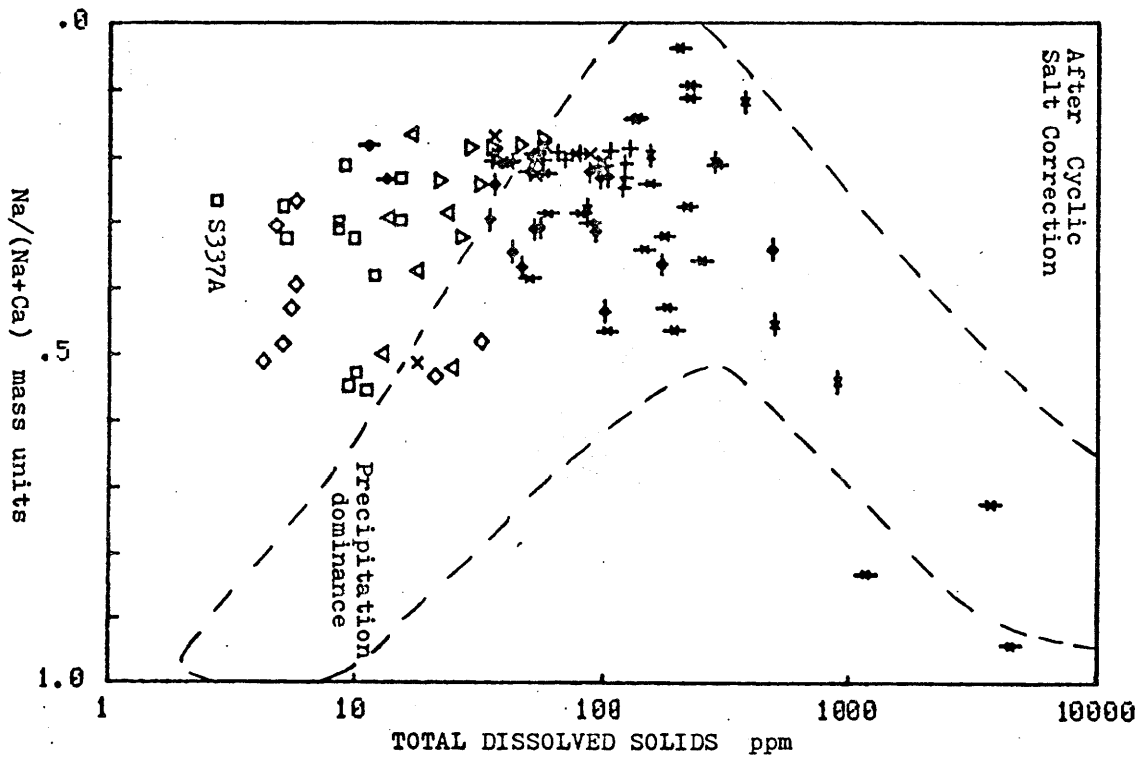
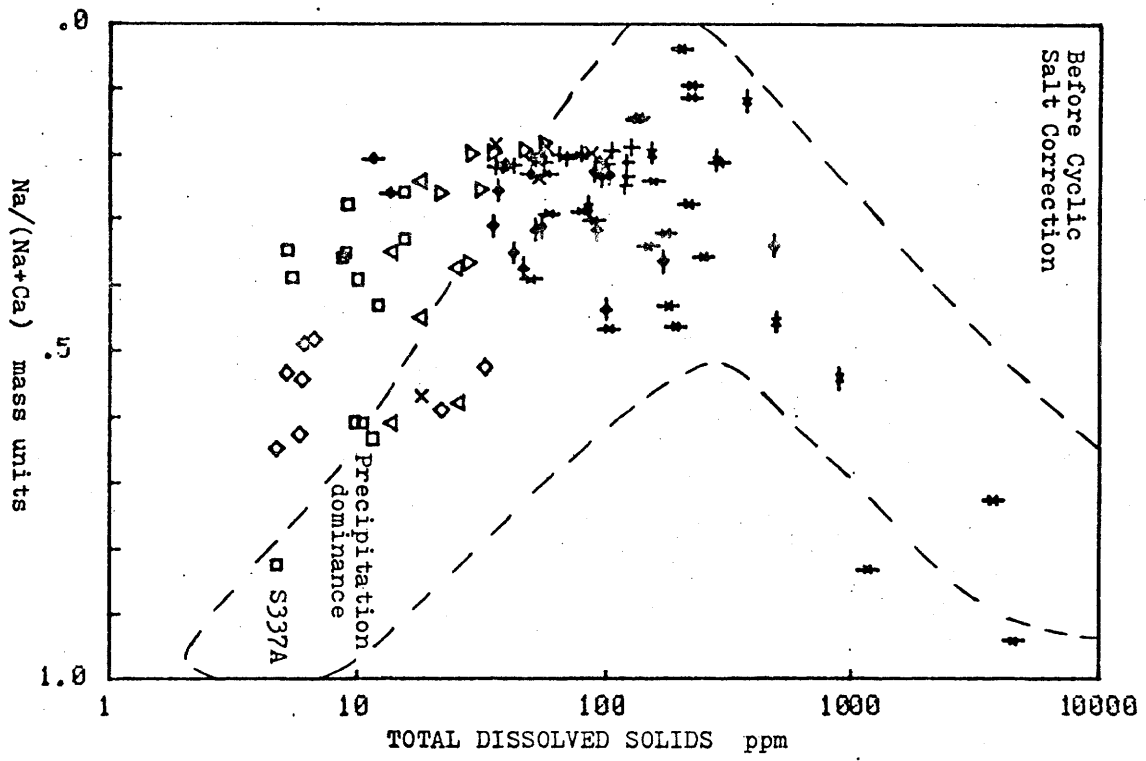
TABLE IV. 3

Figure IV.2

Graphs of Amazon River data, drawn according to Gibbs (1970). The dashed field and designations are taken from Gibb's Figure (3). The graph on the left is of the Amazon Basin data, uncorrected for atmospheric inputs. Note that the data conform adequately to the field defined by Gibbs. The graph on the right is of the same data, corrected for cyclic salt inputs (c.f. Section II.9). If the cyclic salt contribution to the dissolved phases in the sample was large, the points in the precipitation dominance field should shift down and to the left. This occurs for only one sample (S337A), from a near coastal river. Therefore, precipitation inputs do not explain the shape of the field.

Symbol key:

- + - (1) Main Channel
- * - (2) Marañon Drainage
- * - (3) Ucayali Drainage
- * - (4) Madeira Drainage
- ♦ - (5) Other Andean headwater rivers
- ◇ - (6) Negro Drainage
- - (7) Rivers draining shields
- ▽ - (8) Lowland rivers with extensive areas of marine sediments
- △ - (9) Rivers draining only U. Tertiary and Quaternary sediments
- X - (10) Varzêa waters



salts. Feth (1971) points out that the high TDS waters are also influenced by dissolution of evaporites.

Samples from this study conform in a general way to the field defined by Gibbs (Figure IV.2), however at low concentrations the samples are not nearly so sodium enriched. The cyclic salt correction, discussed in Section II.9 provides a test (Figure IV.2) of whether precipitation dominates the chemistry of those rivers which fall into the "precipitation dominance" field. It is clear that correction for precipitation inputs makes only a minor change in the appearance of the graph. A marked shift downward and to the left would be expected if precipitation made a significant contribution to the dissolved solids in a sample. The data, however, show only a slight shift to the left and downward for samples in the "precipitation dominance" field. The greatest TDS drop was 42% in the near-coastal, Matari River (S337A), followed by 16%, 10%, and 8% drops for different Negro River samples. Clearly the vague boomerang shape of the Amazon data field must have other origins.

When Amazon samples are compared to Meybeck's scheme, categories must be added (Table IV.3) to accommodate water types not included by Meybeck. Rivers in the latter category include some very substantial systems such as the Negro (with perhaps 4% of the world's river flow), the Mamoré, the Urubamba, and the Guapay. Sulfate rich water types in the Amazon are apparently different from those found elsewhere, perhaps because of the lack of pollution, a major source of sulfate. Clearly this classification is inadequate, both because it is not comprehensive and because the assumption that low concentration rivers are necessarily precipitation dominated is invalid.

IV.3:4 Multivariate Analyses

The second category of data classification involves identification of characteristic relationships in the data (multivariate analysis) and by so doing effecting the reduction of the complexity of the original data. The relationships are taken to reflect underlying controls, which can be interpreted with auxiliary information (geology, vegetation, soils), and used to construct a description of the system. Two approaches will be examined, graphical and factor analysis. Both forms of multivariate analysis normalize parameters, thus eliminating some information.

The graphical method of Hill (1942) and Piper (1944) utilizes a three field graph (Figure IV.3). The two triangular fields are used to identify relationships among the cations and among the anions, respectively. The diamond field serves to compare cation and anion data; it is simply a skewed version of a graph of (divalent cations)/(total cations) versus (weak acid anions)/(total anions). The diamond shaped field is chosen only to facilitate the appearance and plotting of the graph. Relationships are interpreted as follows: Points plotting along a line through a vertex (e.g., specie Z) represents the situation $Y=aX$ (X,Y being on the opposite vertices); points paralleling a side (e.g. side opposite vertex Z) represent the situation $Z=a(X+Y)$; a straight line, in general, represents the situation $z=aX+bY$ (a plane through the origin in concentration space). A cluster of points is equivalent to both $Z=aX$ and $Z=bY$ being fulfilled. A line in the diamond shaped field represents the situation $(Ca+Mg)=a(HCO_3)+b$. Data from two end member mixing plot as straight lines in these diagrams.

The vertices in the diamond shaped field are chosen so that the data can be interpreted in terms of the chemical parameters of Palmer (1911) (see insert, Figure IV.3), assuming a charge balance. These are:

Figure IV.3

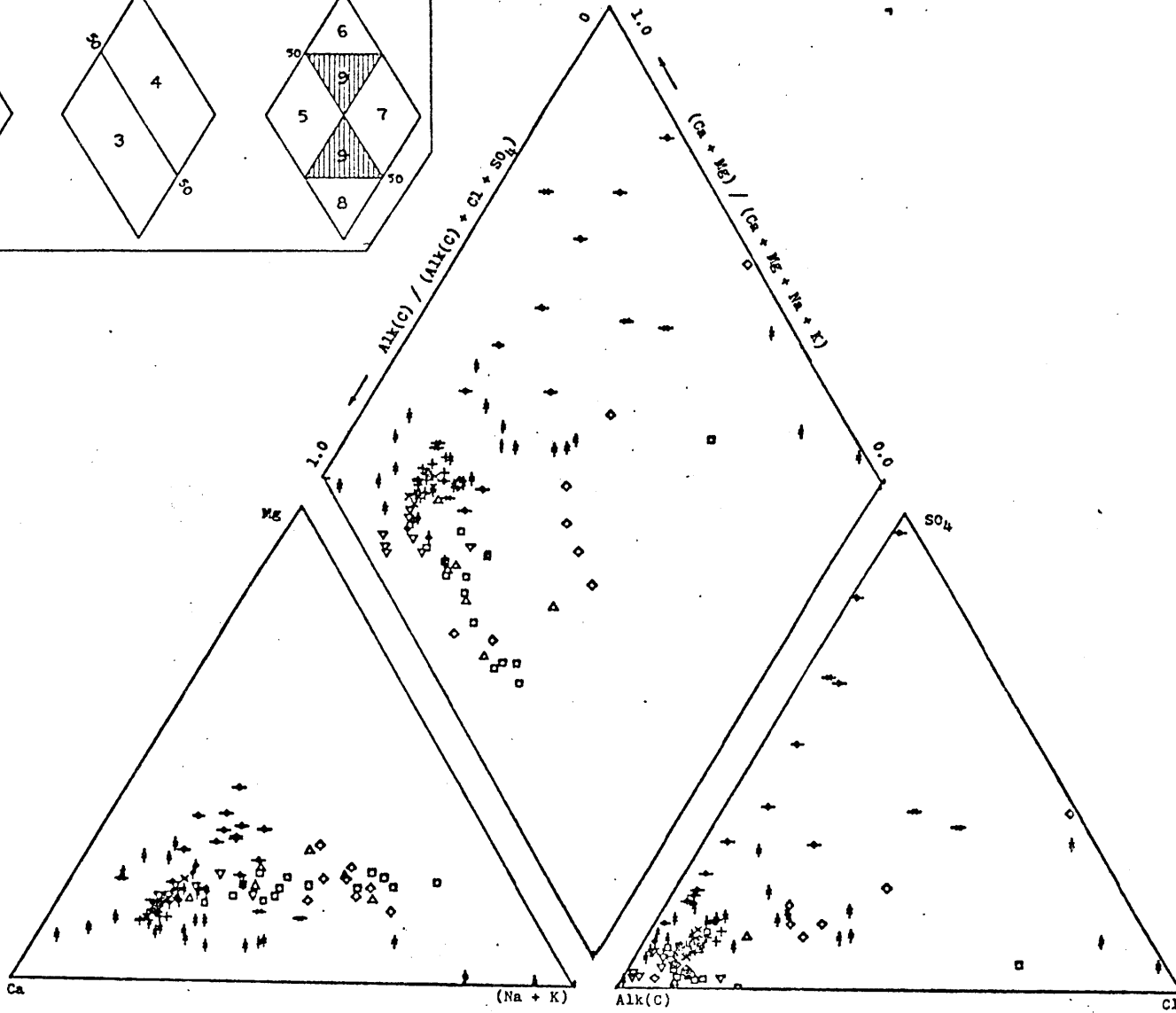
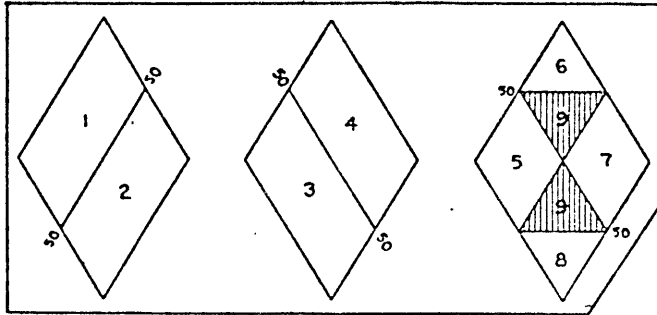
Multivariate graph of major ion data done according to Hill (1942) and Piper (1944). The guide for the classification of water types in the diamond shaped field is given in the insert. The numbers represent:

Differentiation of water-types

Area 1, alkaline earths exceed alkalies; Area 2, alkalies exceed alkaline earths; Area 3, weak acids exceed strong acids; Area 4, strong acids exceed weak acids; Area 5, secondary alkalinity exceeds 50 per cent--that is, chemical properties of the water are dominated by alkaline earths and weak acids; Area 6, secondary salinity exceeds 50 per cent; Area 7, primary salinity exceeds 50 per cent--that is chemical properties are dominated by alkalies and strong acids--ocean water and many brines plot in this area, near its right-hand vertex; Area 8, primary alkalinity exceeds 50 per cent--here plot the waters which are inordinately soft in proportion to their content of dissolved solids; Area 9, no one of the cation-anion pairs in Palmer (1911) exceeds 50 per cent.

Symbol key:

- + - (1) Main Channel
- * - (2) Marañon Drainage
- ✱ - (3) Ucayali Drainage
- ◆ - (4) Madeira Drainage
- † - (5) Other Andean headwater rivers
- ◇ - (6) Negro Drainage
- - (7) Rivers draining shields
- ▽ - (8) Lowland rivers with extensive areas of marine sediments
- △ - (9) Rivers draining only U. Tertiary and Quaternary sediments
- X - (10) Varzēa waters



- (1) Primary salinity (alkali salinity): The fraction of total cations representing monovalent cations balanced by strong acid anions.
- (2) Secondary salinity (permanent hardness): The fraction (if any) of total cations representing divalent cations balanced by strong acid anions (not balanced by monovalent cations).
- (3) Acidity: Strong acids (if any) not balanced by cations other than hydrogen.
- (4) Primary Alkalinity (permanent alkalinity): The fraction of total cations representing monovalent cations (if any) not balanced by strong acids.
- (5) Secondary Alkalinity (temporary alkalinity): The fraction of total cations, representing divalent cations (if any) not balanced by strong acids.

Palmer is an early advocate of transforming analyses into chemical units to facilitate interpretation. The five parameters represent a reduction of the number of degrees of freedom to a manageable few. Palmer justifies the choice of parameters on engineering and geological grounds and in conjunction with silica analyses, observes that:

- (1) Waters from igneous and metamorphic terrains have high primary alkalinities and frequently have high silica concentrations.
- (2) Waters from limestone terrains have high secondary alkalinity and low silica.
- (3) Subtle variations in the proportions of silicate and carbonate rocks are detectable in the relationship between primary and secondary alkalinity.

Amazon data are presented in Figure IV.3. Note the wide variations in properties. Samples exist in which each of HCO_3 , SO_4 , and Cl are overwhelmingly the dominant anion, and Na and Ca are overwhelmingly the dominant cations. Magnesium is the dominant cation in only two samples. The diamond field shows that no clear relationship exists between (Ca+Mg) and HCO_3 in normalized data.

Factor analysis can be viewed as an extension of triangle, ratio, and

polygonal field graphing to higher dimensions for the purpose of exploring more complicated multivariate relationships (Joreskog et al. 1976). The principal example of the application of factor analysis to river data is the Mackenzie River study of Reeder et al. (1972); the techniques used are partially described in Hitchon et al. (1971). Factor analysis as used by Reeder et al. (1972) and many others is purely descriptive, and the mathematical basis for making inferences about other populations (e.g. other rivers) is not well established (Joreskog et al. 1976).

There are two methods (modes) of factor analysis: R-mode and Q-mode. R-mode examines relationships between variables (e.g. chemical species) and identifies a set of factors (less than the number of variables) which if desired can be used to reconstruct the original variables. These factors can be correlated with environmental phenomena. Q-mode examines relationships between samples (e.g. rivers). The number of factors is less than the number of variables, if that is less than the number of samples (as is usually the case). These factors can be related to actual samples through suitable rotations. A classic application (c.f. Imbrie and Van Andel 1964, Joreskog et al. 1976) is to resolve end-members in mixing of sediments. Joreskog et al. (1976) point out that Q-mode analysis is particularly valuable in geologic work, "especially where there is little a priori knowledge of the genetic significance of constituents."

One of the primary weaknesses of factor analysis of river chemistry is that the mathematical manipulation required to transform the data into a "correct" form leads to the creation of parameters not readily interpreted, except qualitatively, in terms of physical reality. In R-mode analysis,

any linear transformation of the data for a given sample will affect the results, while the same is true for Q-mode analysis in the case of a transformation of an analytical variable. All non-linear transformations of variables (e.g. logarithmic transformations) will alter the results. In particular, if non-linear transformations are applied in Q-mode analysis, meaningful end members need not be (and probably are not) generated. In the case of the Mackenzie River, the data are approximately log-normally distributed (Reeder et al. 1972). Data in such a form are not ideally suited, mathematically, for R-mode factor analysis, as high concentration values will essentially drive the results (this is not such a problem with sediment mineralogy where weights total 100%). Reeder et al. (1972) chose to transform the data logarithmically. Consequently their Q-mode results are not interpretable as end members, from which other water types could be formed. An alternative transformation, (for the Q-mode analysis alone) would be to normalize each variable to its range. End members so generated could be used to generate the observed samples.

Reeder et al. (1972) use the principal R-mode factors (derived from the chemical data), geological data, and other sample properties (pH, turbidity etc.) to perform a second R-mode factor analysis. The end result is a qualitative statement that various chemical and geological properties are related, observations which in the case of major species differ little from those of Palmer (1911). The principal value of factor analysis comes in relating constituents for which little a priori knowledge of their genetic significance exists, as is the case with many trace species.

IV.3:5 Concentration Versus Total Cations

The above methods of classification of river chemistry or chemical properties either consider only a few parameters (ion dominance schemes,

multivariate graphs) or manipulate parameters to a degree that information is lost or obscured (factor analysis). As a preliminary to relating river chemistry to basin geology, analyses will be plotted against total cations (TZ+). One geological observation must be made beforehand. Rivers having a TZ+ less than about 450 $\mu\text{Eq/l}$ drain very little marine sedimentary rock while samples with TZ+ greater than about 3000 $\mu\text{Eq/l}$ have major exposures of evaporites or salt springs in their drainage; these lithological contrasts are quite sharp.

Five groupings of data are identified:

- (1) Na and Cl - These elements show a systematic increase in concentration, with the slope becoming steeper (i.e., the Na or Cl ratio to TZ+ becomes greater) at higher concentrations (evaporite inputs) (Figure IV.4).
- (2) Ca, Mg, SO_4 - These species show a systematic (almost linear) increase in concentration, the slope becoming less steep at highest concentrations (showing predominance of NaCl in evaporites (Figure IV.5)).
- (3) $\text{HCO}_3 + 2\text{CO}_3$ (Carbonate Alkalinity - Alk(C)), NO_3 , PO_4 - These species show a wide range of concentrations at low TZ+. (This may reflect biological influence via production of organic acids and production/consumption of nutrients). This is followed by a smooth rise in concentration and a leveling off (likely due to a lack of evaporite inputs) (Figure IV.6).
- (4) Si, K - These two species are grouped together because for most samples they show similar behavior, a TZ+ dependent rise at lower concentrations (note that this is a log-linear plot). There is no subsequent rise with increasing TZ+, for rivers draining marine sediments, except for those rivers with major evaporite inputs, in which K is considerable enriched (Figure IV.7).
- (5) H, Fe, Al, Color - These parameters show a decrease in concentration or intensity with increasing TZ+. The plots of iron and aluminum are complicated by high levels in some Andean rivers. This is thought to be due to passage of fine clays through the .45 μ filters and subsequent dissolution during storage as a result of acidification (see Appendix II) (Figure IV.8).

Charge balance of inorganic species, represents an additional parameter, as it can be taken as an estimate of the abundance of charged organic species (c.f. Cronan et al. 1978). Since the error in the charge balance

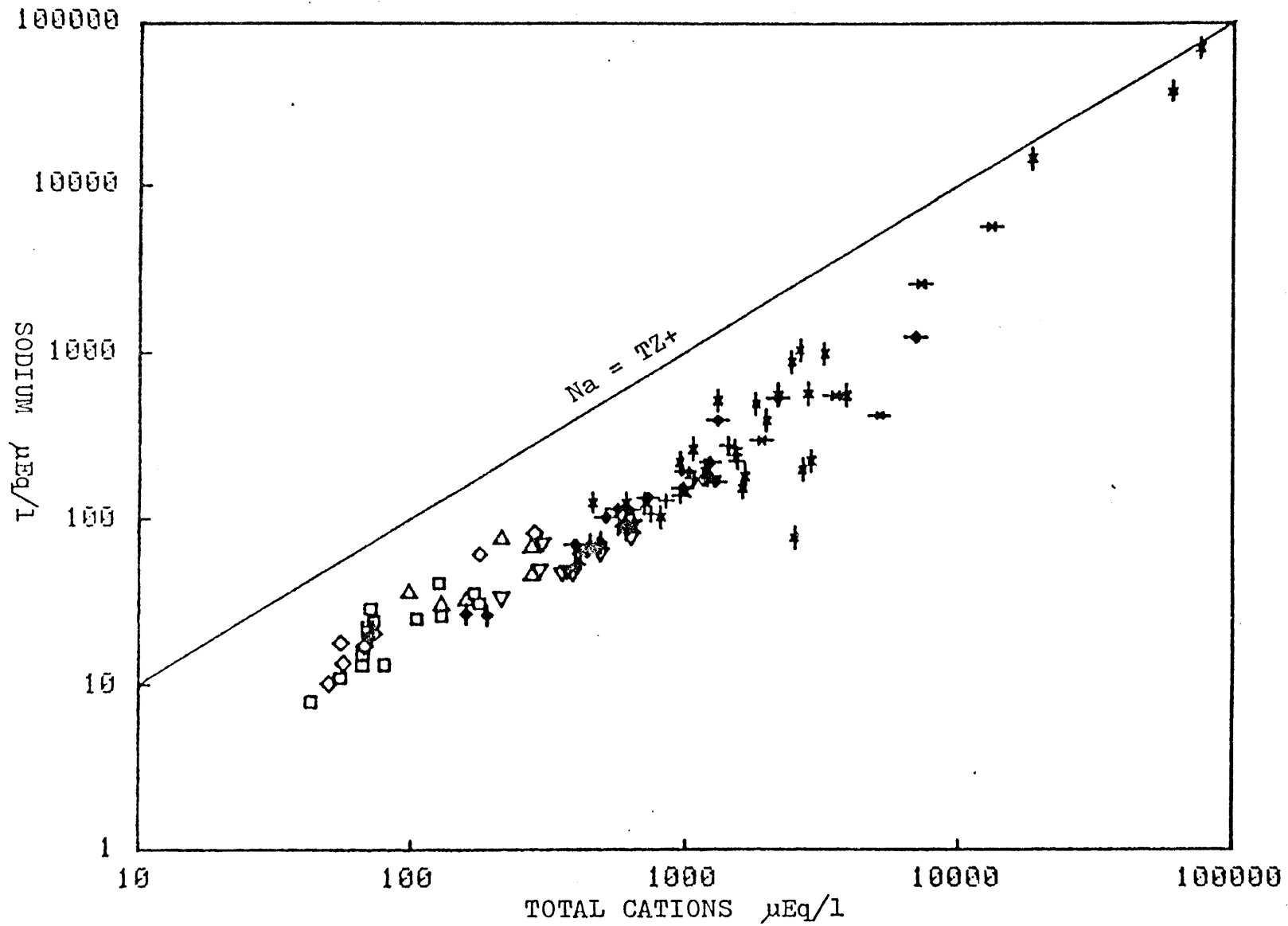
Figure IV.4

Sodium and chloride ($\mu\text{Eq/l}$) versus total cations ($\mu\text{Eq/l}$).

Symbol key:

- + - (1) Main Channel
- * - (2) Marañon Drainage
- * - (3) Ucayali Drainage
- * - (4) Madeira Drainage
- † - (5) Other Andean headwater rivers
- ◇ - (6) Negro Drainage
- - (7) Rivers draining shields
- ▽ - (8) Lowland rivers with extensive areas of marine sediments
- △ - (9) Rivers draining only U. Tertiary and Quaternary sediments
- X - (10) Varzêa waters

Note that main channel points on this and all subsequent graphs are from stations: S209, S219, S234, S240, S250, S302, S311, S316, S326, S329, SOL1, SOL2, AMI01, and BPA09. These samples (see Appendix I for station locations and dates) were chosen to represent the full range of spatial and seasonal coverage.



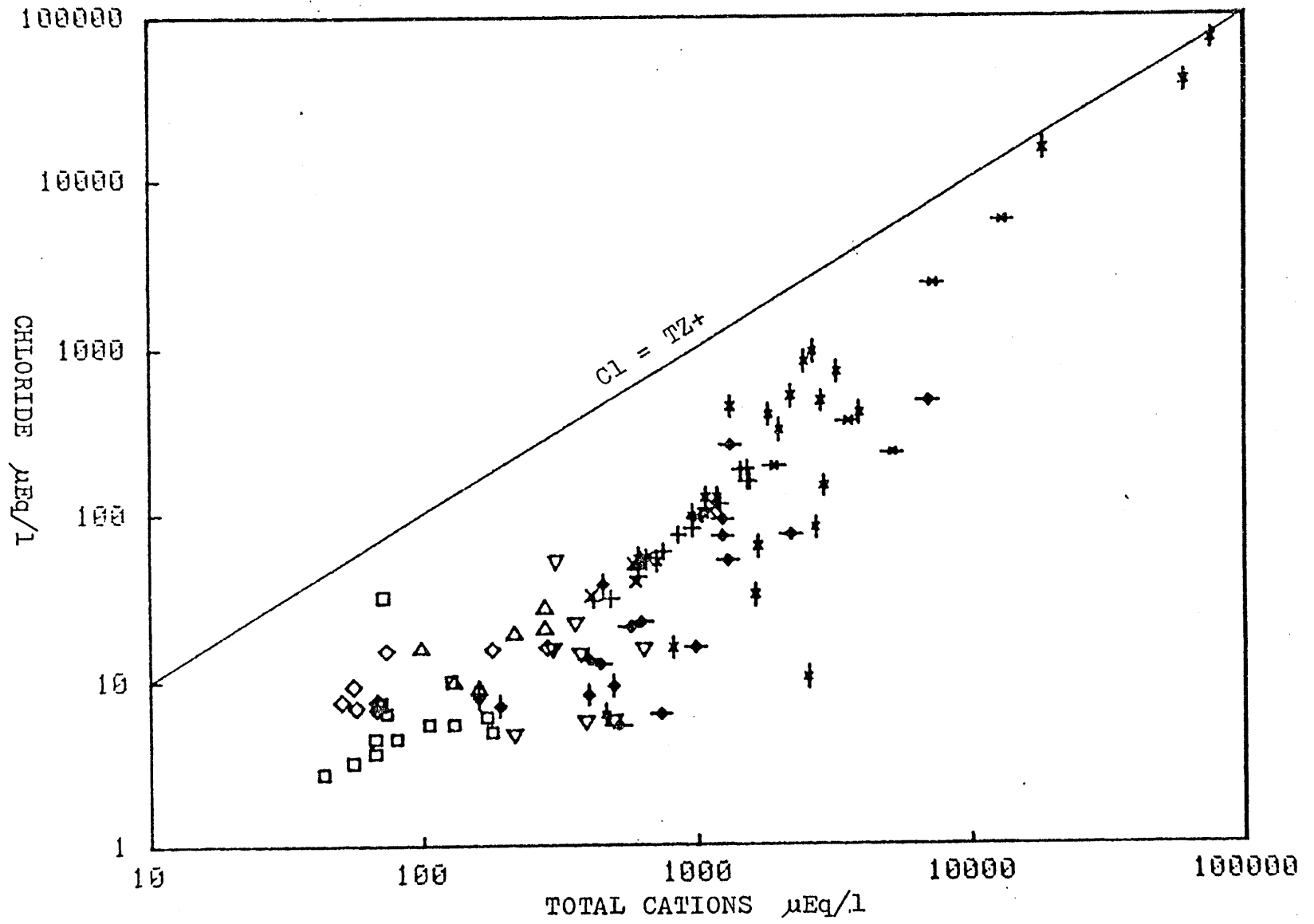
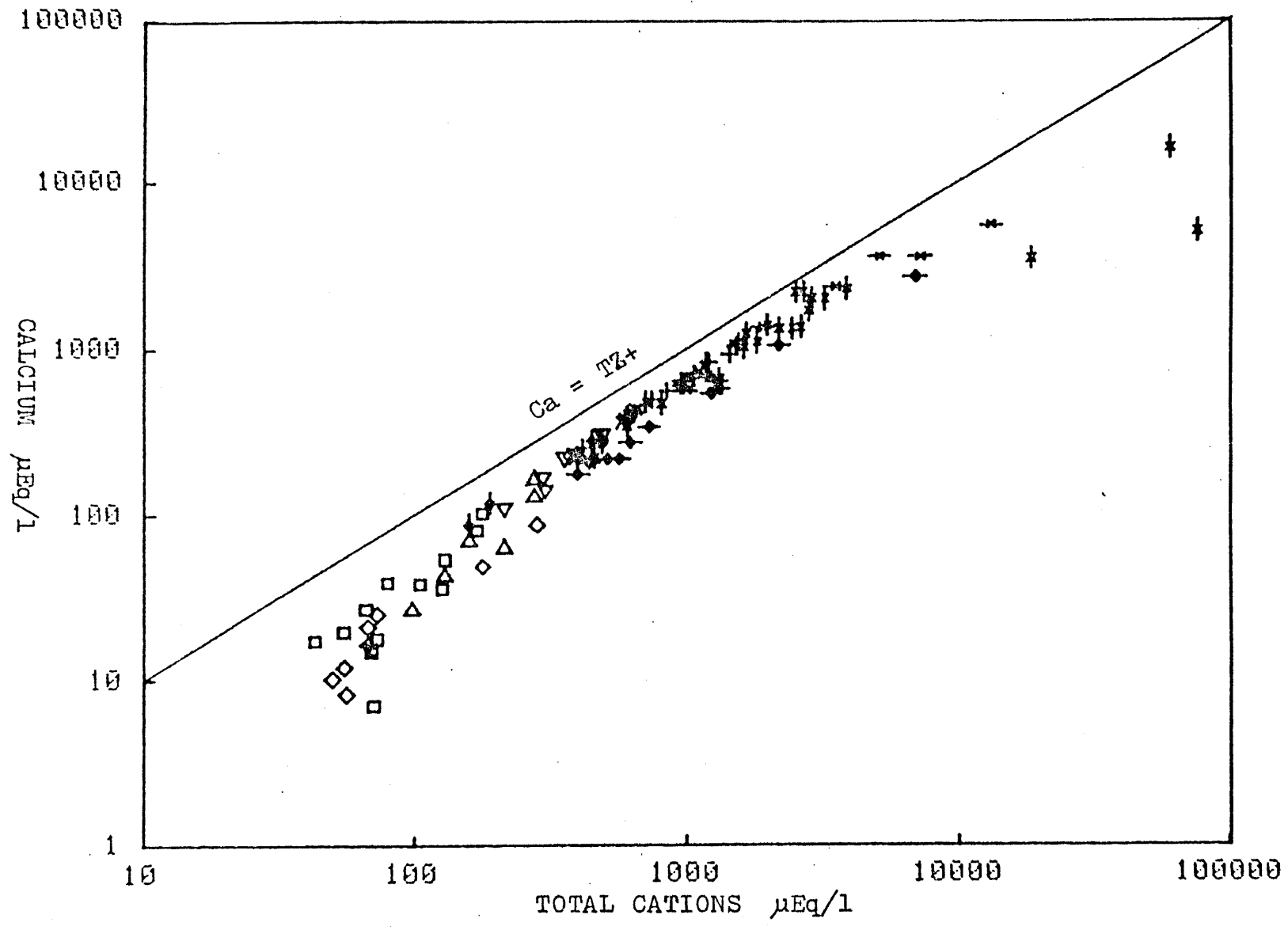


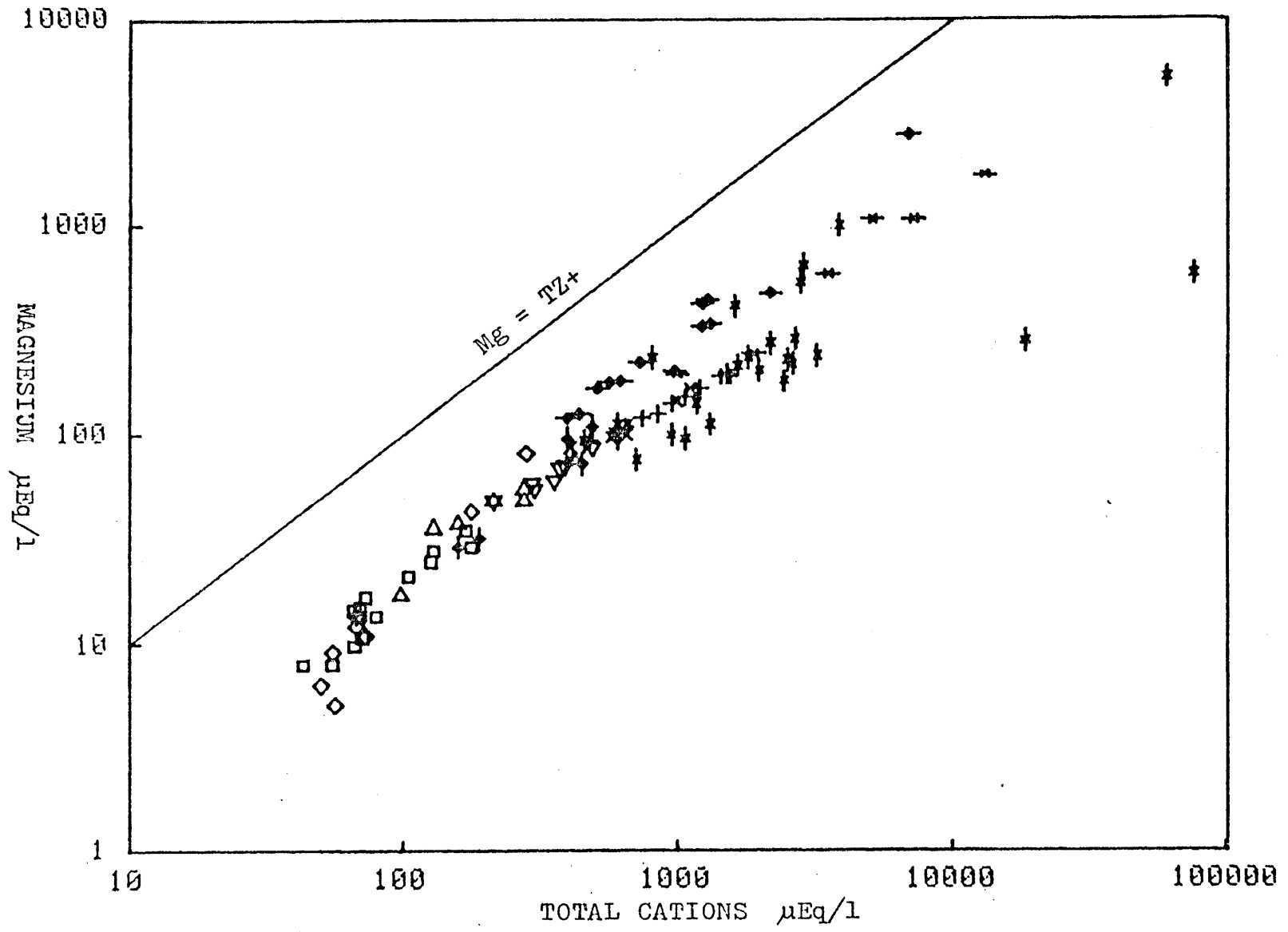
Figure IV.5

Calcium, magnesium, and sulfate ($\mu\text{Eq/l}$) versus total cations ($\mu\text{Eq/l}$).

Symbol key:

- + - (1) Main Channel
- * - (2) Marañon Drainage
- * - (3) Ucayali Drainage
- * - (4) Madeira Drainage
- † - (5) Other Andean headwater rivers
- ◇ - (6) Negro Drainage
- - (7) Rivers draining shields
- ▽ - (8) Lowland rivers with extensive areas of marine sediments
- △ - (9) Rivers draining only U. Tertiary and Quaternary sediments
- X - (10) Varzêa waters





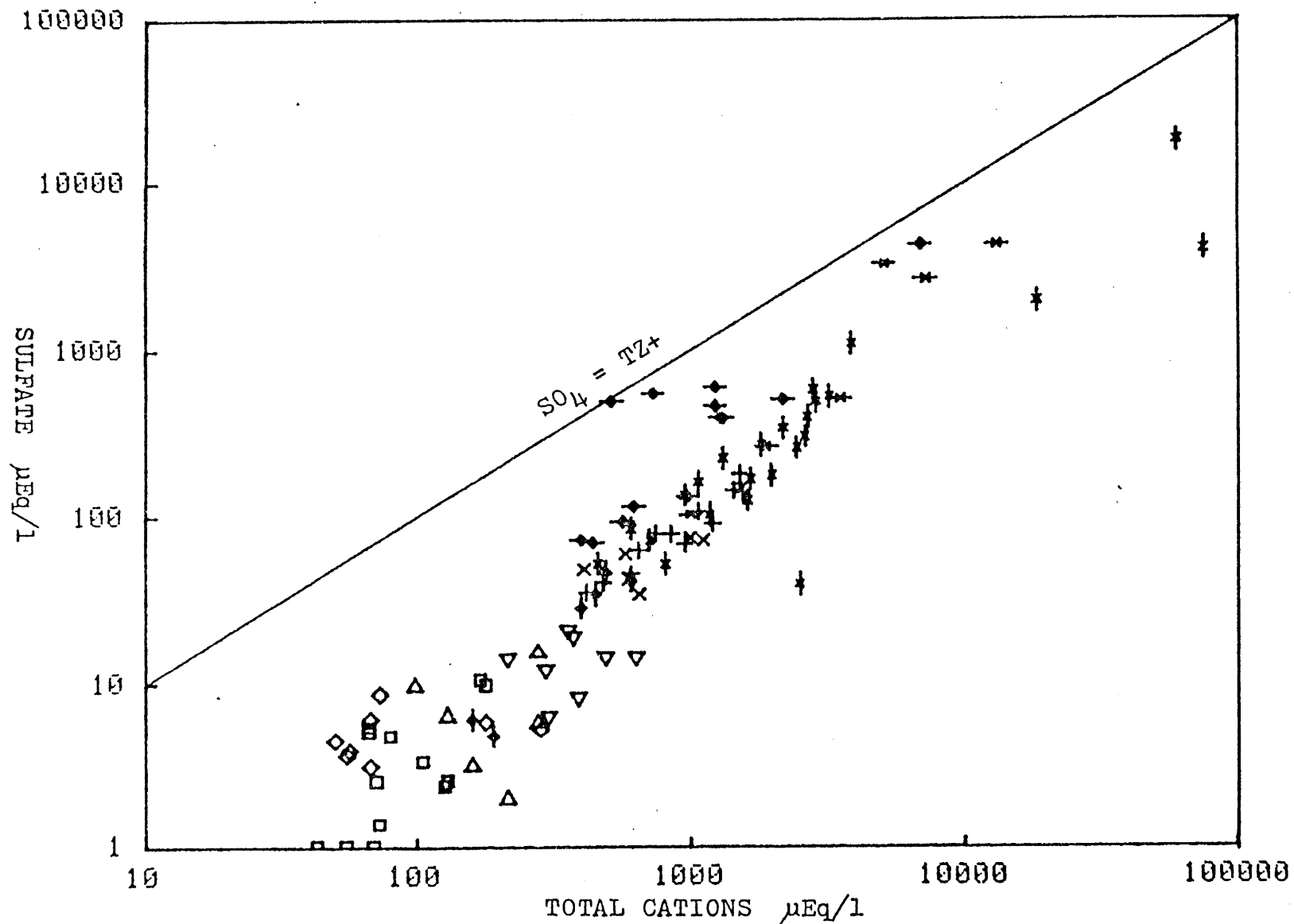
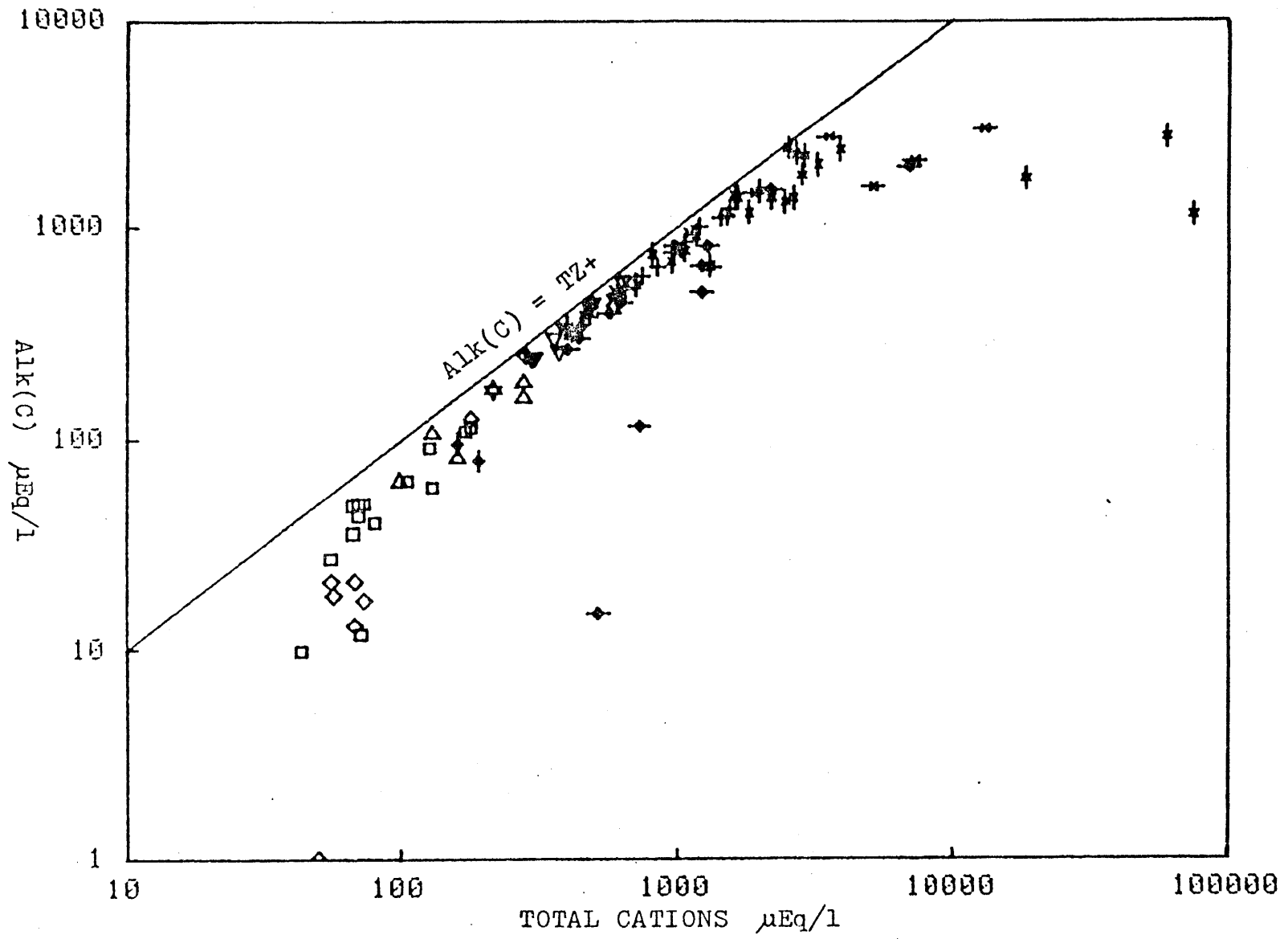


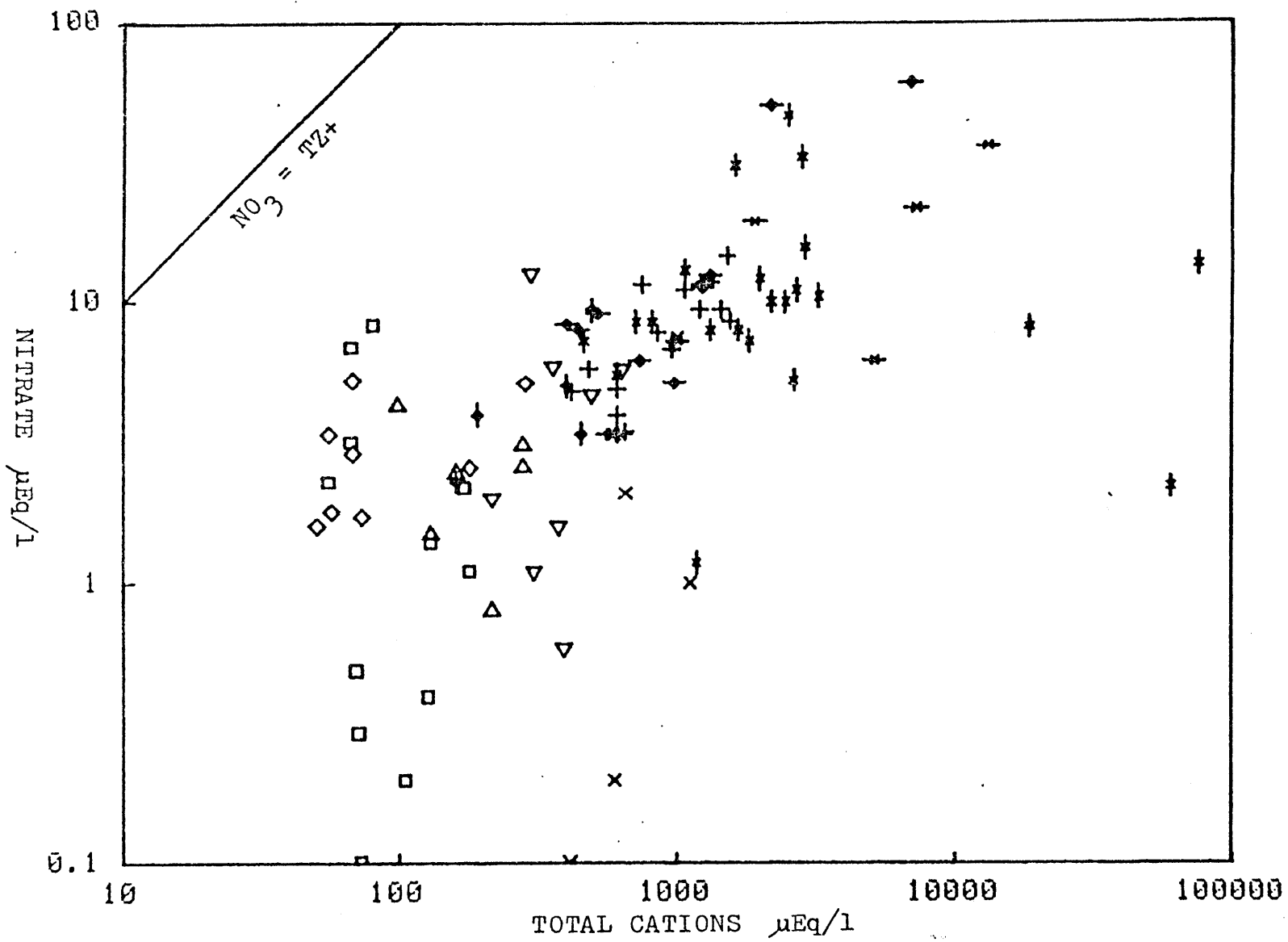
Figure IV.6

Carbonate alkalinity, nitrate ($\mu\text{Eq/l}$), phosphate ($\mu\text{mole/l}$)
versus total cations ($\mu\text{Eq/l}$)

Symbol key:

- + - (1) Main Channel
- * - (2) Marañon Drainage
- * - (3) Ucayali Drainage
- * - (4) Madeira Drainage
- ‡ - (5) Other Andean headwater rivers
- ◇ - (6) Negro Drainage
- - (7) Rivers draining shields
- ▽ - (8) Lowland rivers with extensive areas of marine sediments
- △ - (9) Rivers draining only U. Tertiary and Quaternary sediments
- X - (10) Varzēa waters





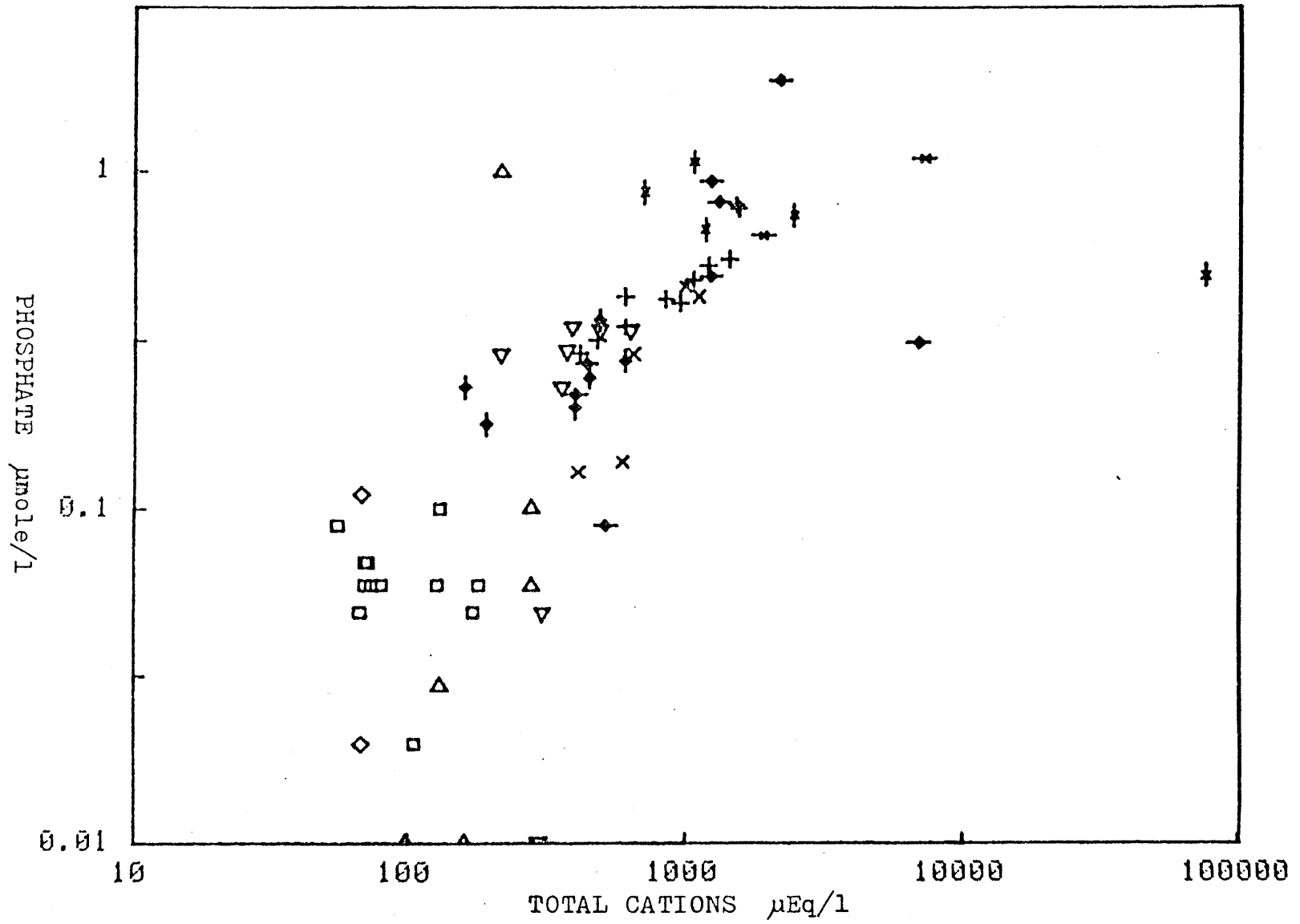
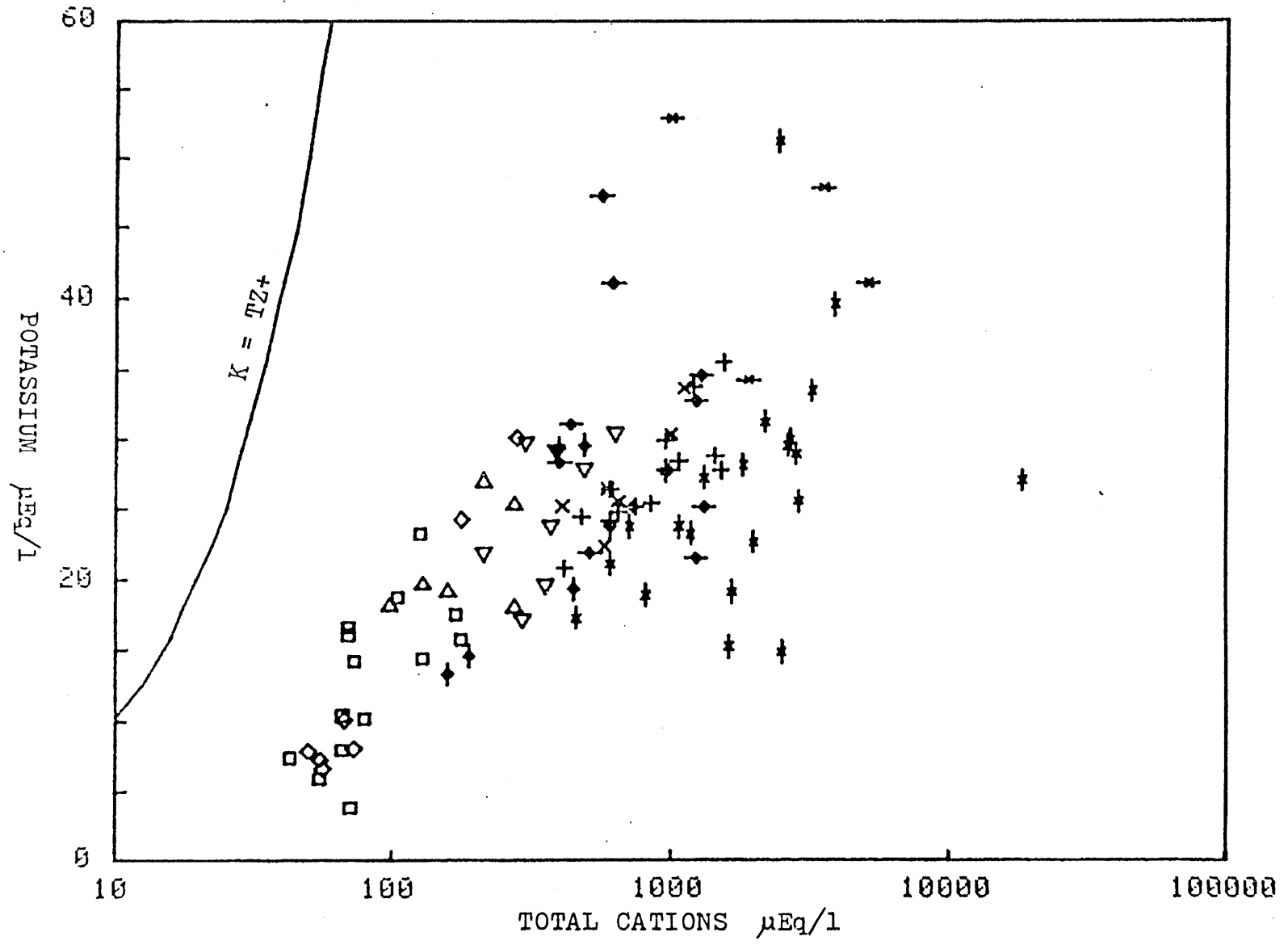


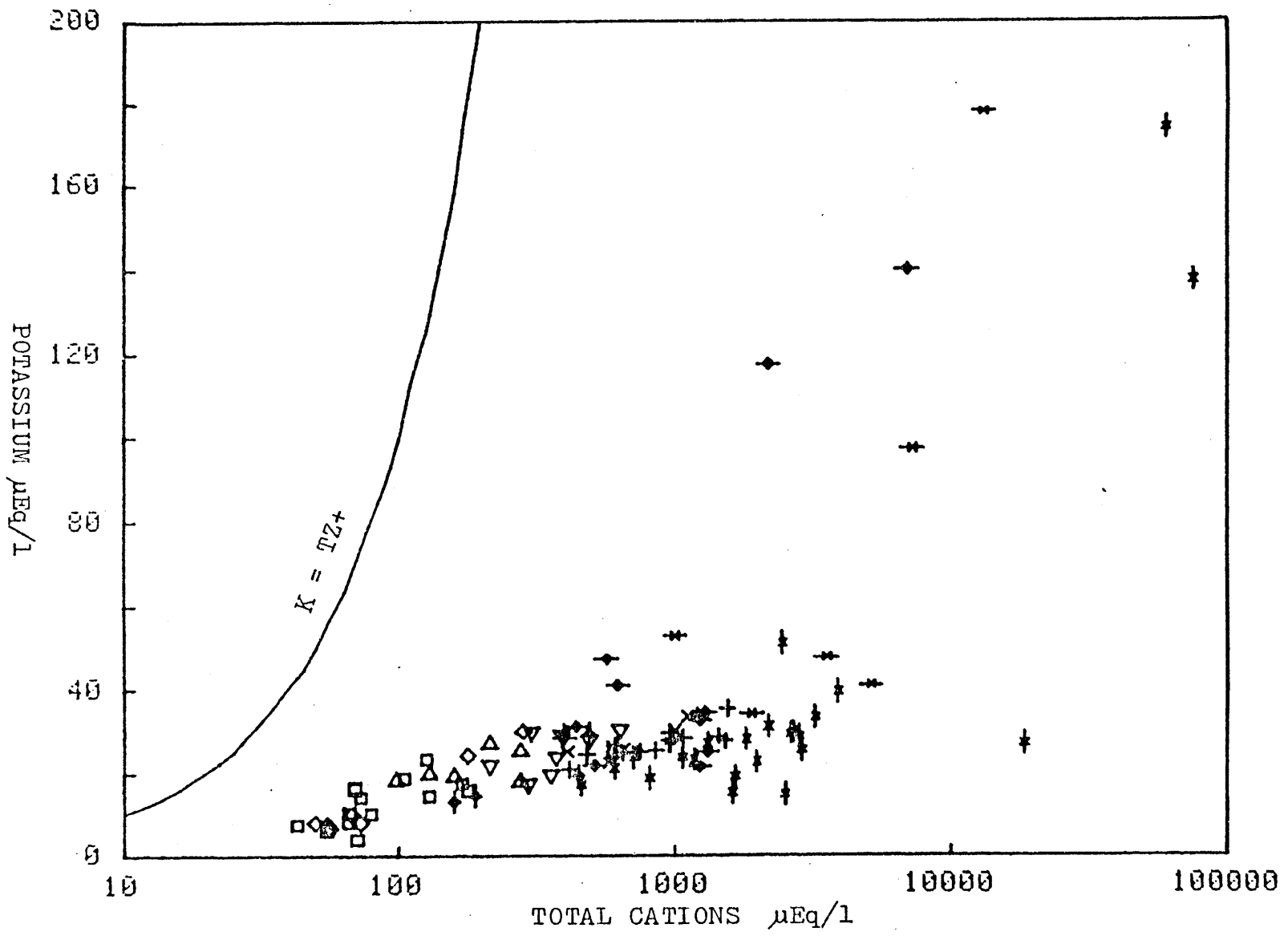
Figure IV.7

Silica and potassium ($\mu\text{mole/l}$) versus total cations ($\mu\text{Eq/l}$). Note that these graphs are log-linear.

Symbol key:

- + - (1) Main Channel
- * - (2) Marañon Drainage
- * - (3) Ucayali Drainage
- * - (4) Madeira Drainage
- ♦ - (5) Other Andean headwater rivers
- ◇ - (6) Negro Drainage
- - (7) Rivers draining shields
- ▽ - (8) Lowland rivers with extensive areas of marine sediments
- △ - (9) Rivers draining only U. Tertiary and Quaternary sediments
- X - (10) Varzēa waters





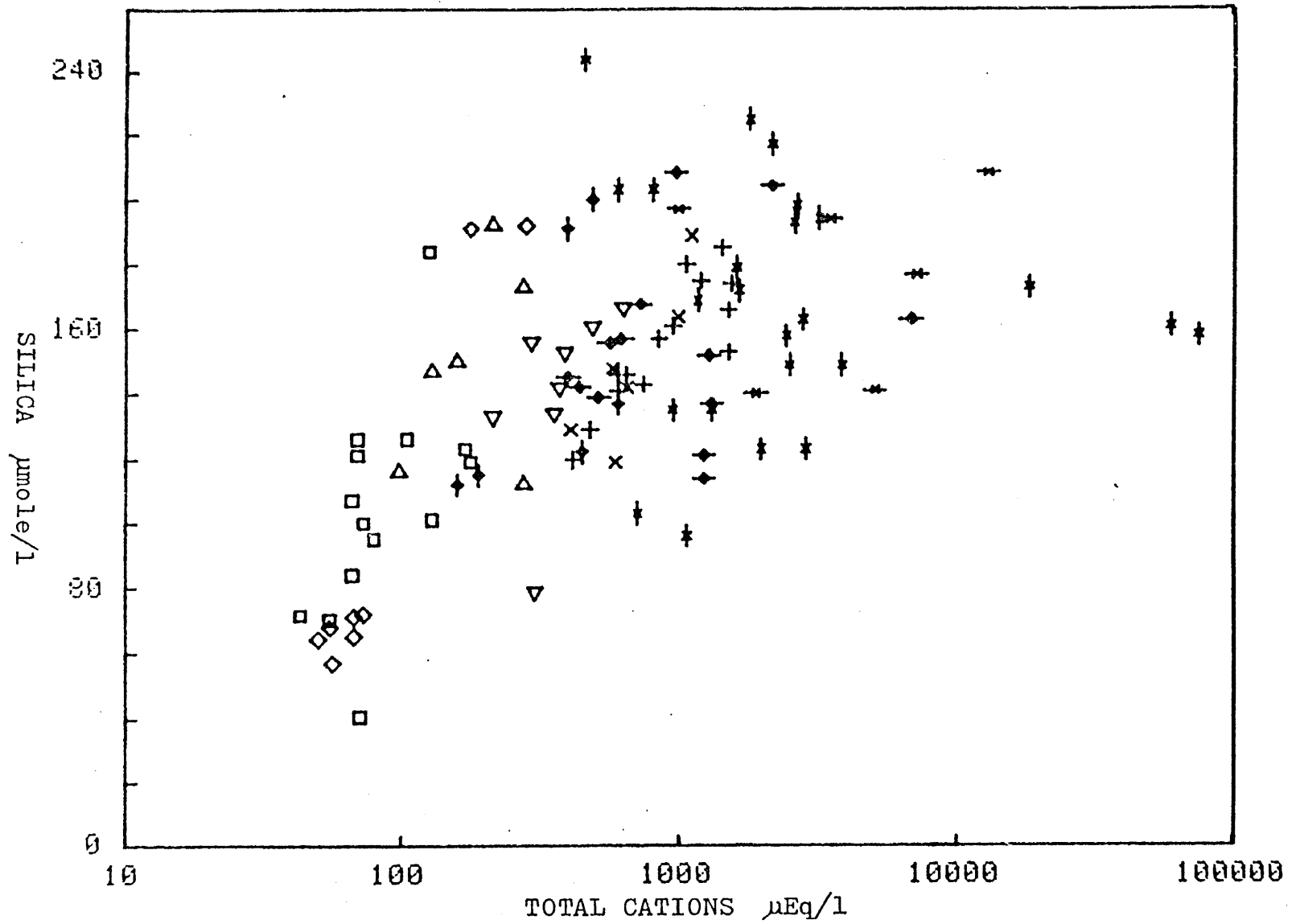
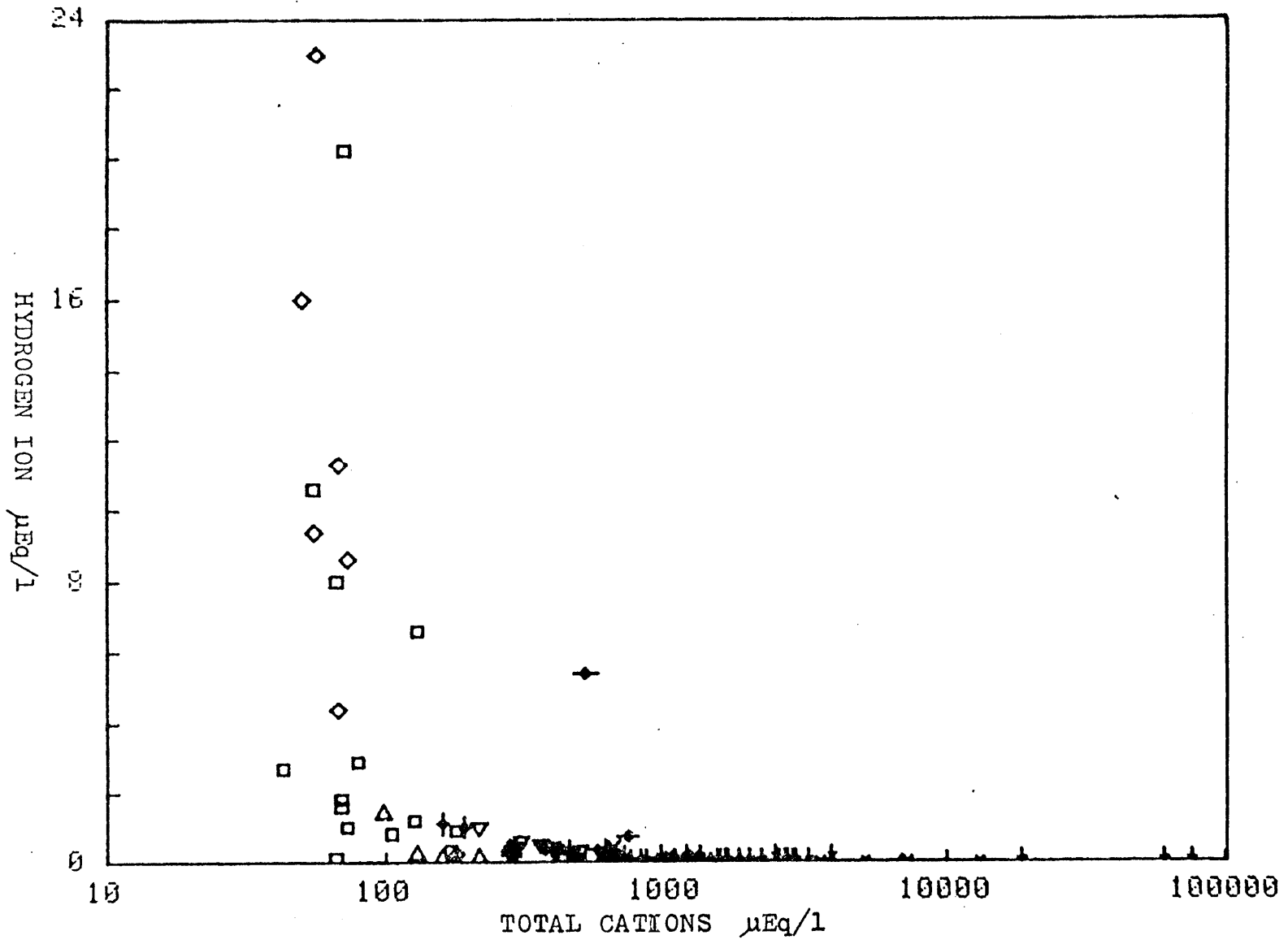


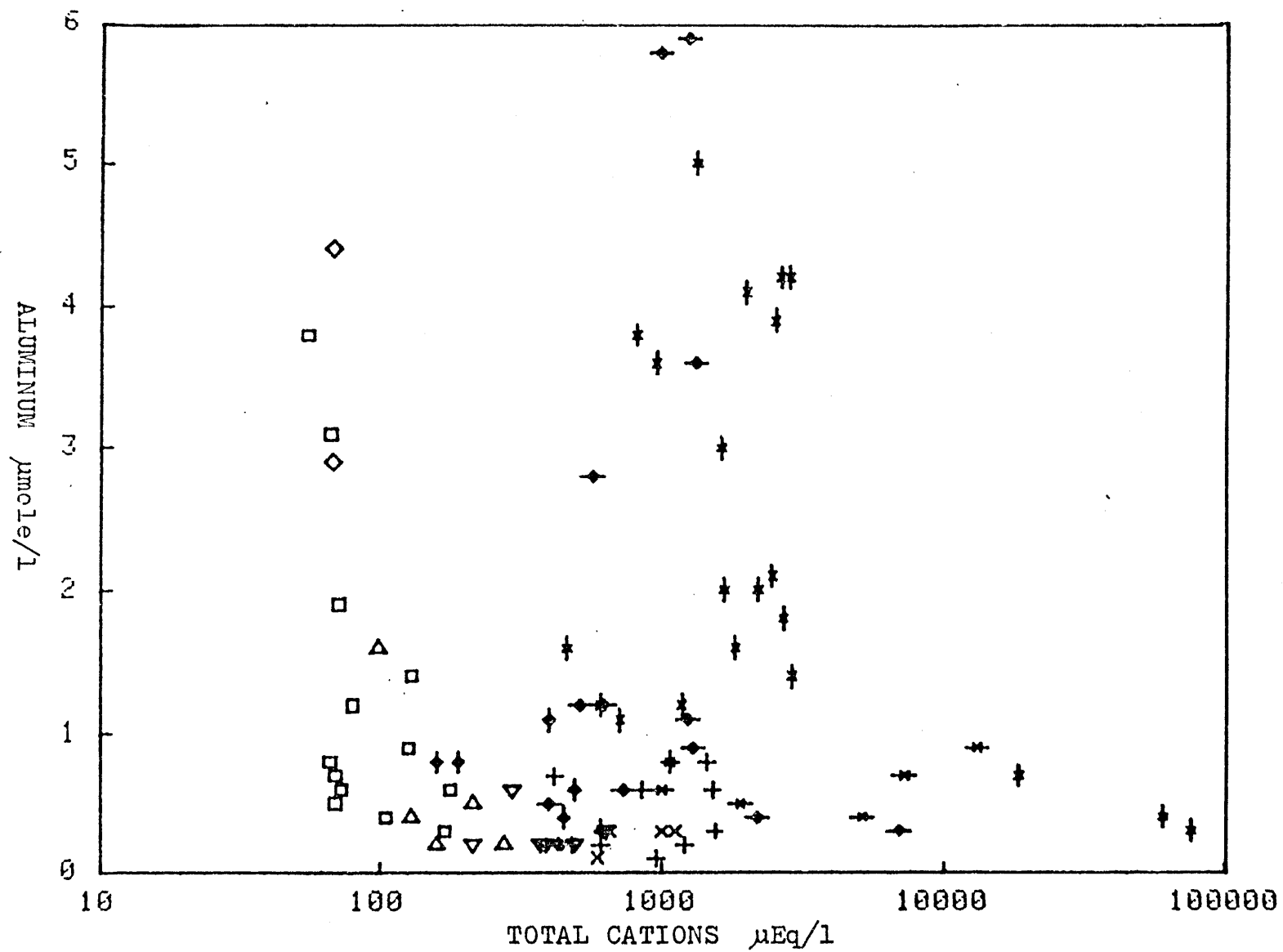
Figure IV.8

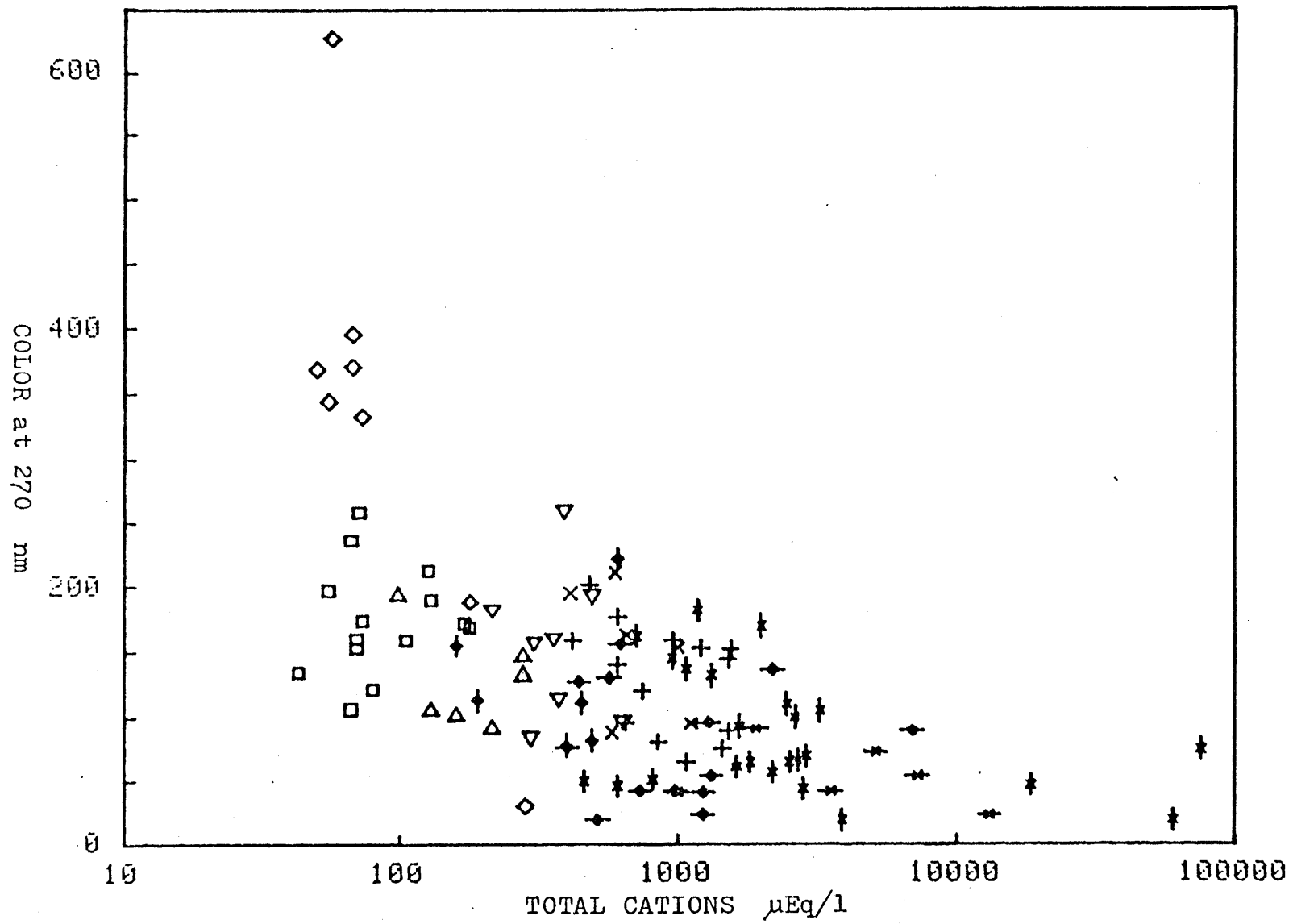
Hydrogen ion, iron, and aluminum ($\mu\text{mole/l}$) and color (absorbance at 270nm, 1 cm cell, units $\times 1000$) versus total cations ($\mu\text{Eq/l}$). Note that the scale is log-linear.

Symbol key:

- + - (1) Main Channel
- * - (2) Marañon Drainage
- * - (3) Ucayali Drainage
- * - (4) Madeira Drainage
- † - (5) Other Andean headwater rivers
- ◇ - (6) Negro Drainage
- - (7) Rivers draining shields
- ▽ - (8) Lowland rivers with extensive areas of marine sediments
- △ - (9) Rivers draining only U. Tertiary and Quaternary sediments
- X - (10) Varzêa waters







is roughly proportional to TZ+, the net inorganic charge will be normalized by TZ+.

Two normalized inorganic charge balances (NICB) will be examined: one assuming that iron and aluminum are not charged species, the other assuming that they are triply charged. This is necessary as the speciation of iron and aluminum is uncertain, and may range between uncharged stabilized colloids and the trivalent form. These two NICB's are plotted in Figure IV.9. Rain samples are included, as they demonstrate that the large imbalances are clearly not an analytical artifact. Errors of the NICB, calculated using estimated analytical errors (Figure IV.9) also support this contention. Like iron, aluminum, hydrogen ion, and color, the NICB show a drop with increasing TZ+. Some of the organic charge represented by the NICB includes ions other than hydrogen, which could be conceivably be derived entirely from organic acids. If the NICB is recalculated (for low TZ+ rivers) without hydrogen ion ($NICB' = NICB - H/TZ+$), the values of NICB' are positive. The ratio of imbalanced charge (20-40 $\mu\text{Eq}/1$) to organic carbon, in low TZ+ rivers, is roughly 0.04-0.08 Eq/mole. The exchange capacity of soil organic carbon at pH 7 is roughly .05 Eq/mole C (see Section III.7).

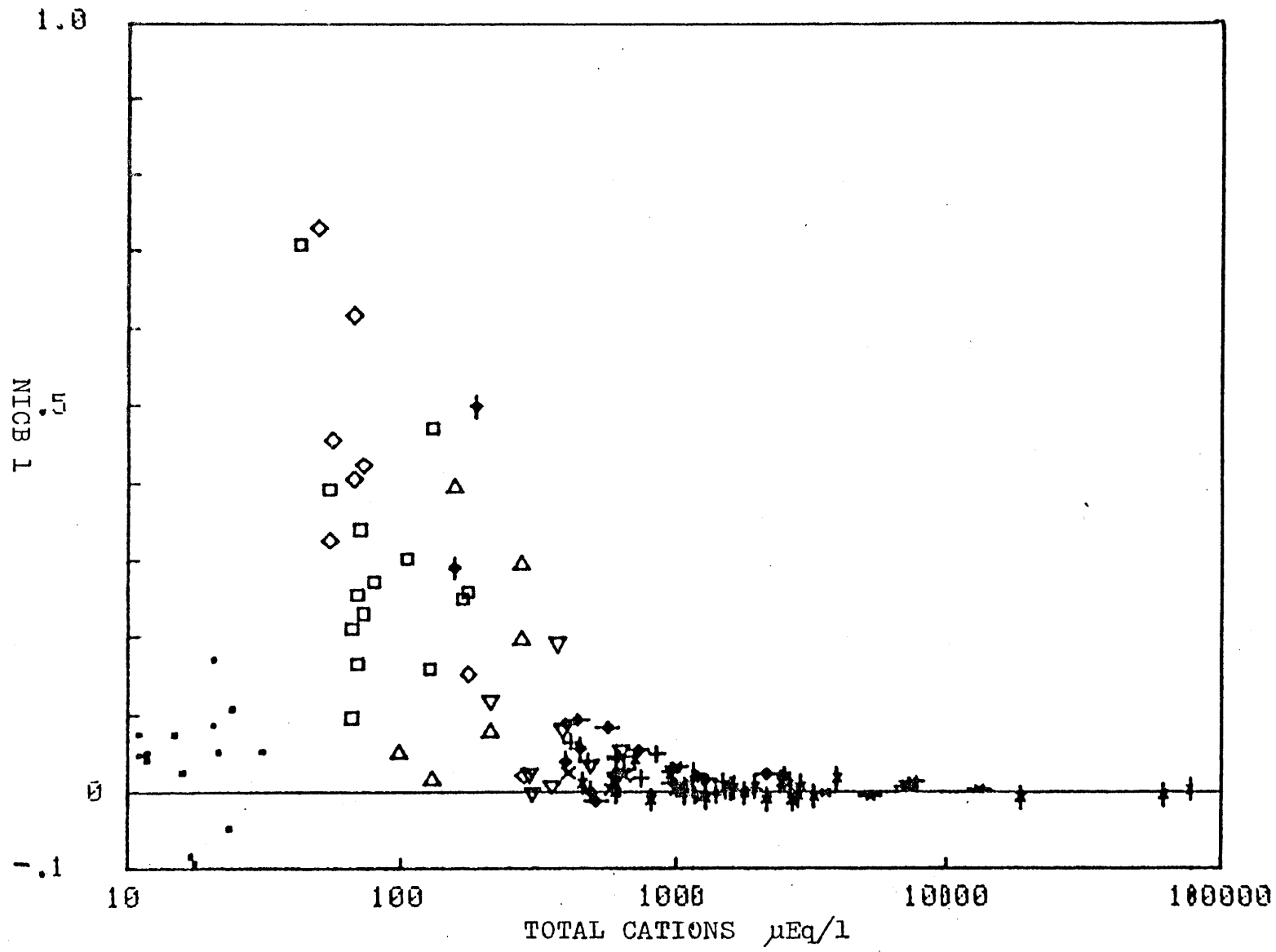
Figure IV.9

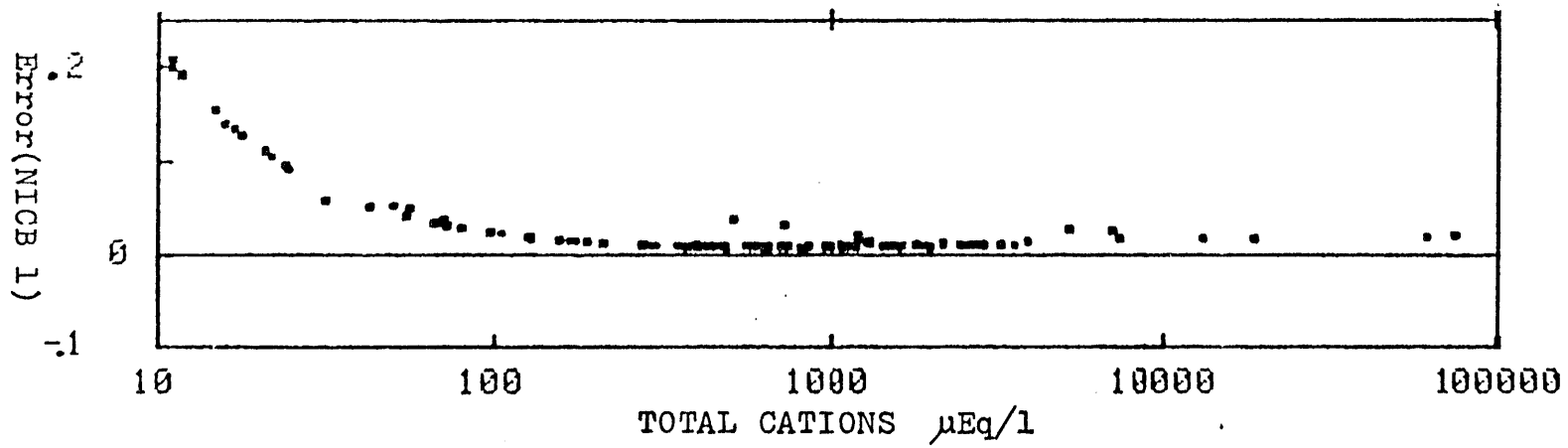
Normalized inorganic charge balances (NICB) versus total cations ($\mu\text{Eq/l}$). The first graph is plotted assuming that iron and aluminum are uncharged species, while the last graph is plotted assuming that they are positive trivalent. 1977 precipitation is included to show that inorganic atmospheric inputs are charge balanced. The estimated error is based on analytical precisions of the individual species.

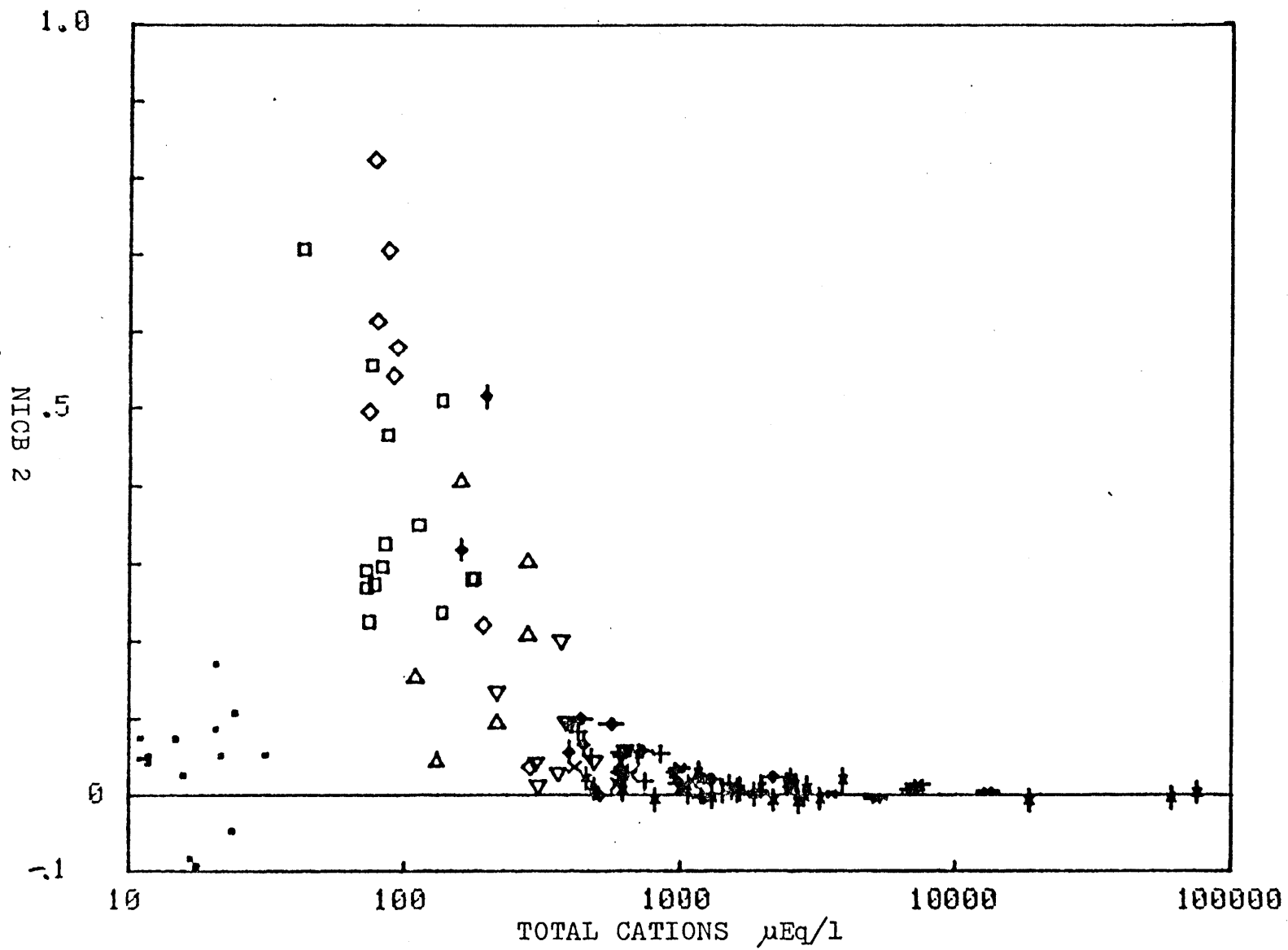
Symbol key:

- + - (1) Main Channel
- ‡ - (2) Marañon Drainage
- * - (3) Ucayali Drainage
- ◆ - (4) Madeira Drainage
- ‡ - (5) Other Andean headwater rivers
- ◇ - (6) Negro Drainage
- - (7) Rivers draining shields
- ▽ - (8) Lowland rivers with extensive areas of marine sediments
- △ - (9) Rivers draining only U. Tertiary and Quaternary sediments
- X - (10) Varzēa waters

- - - Precipitation (first and last graphs)
- - - predicted error (middle graph)







IV.4:1 RIVER CHEMISTRY AND ROCK TYPES

Rock types in the catchments corresponding to each sampling location are summarized in Table IV.4 (analyses are found in Table IV.5). The major features of the relationship between water chemistry and substrate lithologies will be examined focusing on specific geological features that characterize each area and the relation of these to the chemistry of the waters. The following are the main regions or specific water types:

- (1) Main Channel
- (2) Marañon Drainage
- (3) Ucayali Drainage
- (4) Madeira Drainage
- (5) Other Andean Headwater Rivers
- (6) Negro Basin
- (7) Rivers draining shields (other than Negro)
- (8) Lowland rivers with extensive areas of marine sediments
- (9) Rivers draining only Upper Tertiary and Quarternary Sediments
- (10) Várzea lakes.

IV.4:2 Main Channel (1)

The chemistry of the main channel is controlled by mixing of the waters from the various tributaries (c.f. Chapter V). The tributaries with greatest concentrations of dissolved material are the Ucayali, Marañon, Juruá and Madeira, in order of decreasing load. All the tributaries, except the Ucayali, are less concentrated than the main channel at their junction with the main channel; as a result, the concentration decreases going down river.

IV.4:3 Marañon Drainage (2)

Of the two rivers (Marañon and Ucayali) combining to form the main channel, the Marañon is the largest in terms of flow (Raimondi 1879). The Marañon-Pacific divide lies in the western ranges of the Andes. The entire Central Andean geologic column outcrops within its drainage. There are, however, only limited outcrops of Paleozoic; instead Precambrian Rocks form the cores of the Cordillera Oriental in the drainage. Abundant volcanic rocks and extensive marine sections are found in the western part of the

Table IV.4
(4 pages)

GEOLOGIC SUMMARIES OF RIVER BASINS

Major lithologies include the one to five lithologic associations that cover most of the respective basin (>~10%)

Minor lithologies are those that cover small fractions of the basin

Trace lithologies are those that cover sufficiently small fractions of the basin that they are typically not mapped, however they are described in stratigraphic sections. Those lithologies that might be important are tabulated.

Abbreviations:

Rocks

sh	- shales	and.	- andesitic (to rhyolitic)
ss	- sandstones	ryl	- rhyolitic
cg	- conglomerates	volc	- volcanics
ls	- limestones	calc	- calcareous
dol	- dolomite	susp	- suspended
flu	- fluvial	sed	- sediment
lac	- lacustrine		
gla	- glacial		

Colors

gg	- grey-green	yel	- yellow
grn	- green	wht	- white
blk	- black	lgt	- light
brn	- brown	cln	- clean
drk	- dark	clr	- clear

Time

(PC)	- Precambrian	(M)	- Mesozoic
(LP)	- Lower Paleozoic	(MT)	- Mesozoic-Tertiary (orogenic)
(CP)	- Carboniferous-Permian	(PQ)	- Post-Quechua (Plio-Pleistocene to Quaternary)

Mineral stability indicates those minerals that are thermodynamically stable in the water sample from the river in question.

<u>River, Location</u>	<u>Major Lithologies</u>	<u>Minor Lithologies</u>	<u>Trace Lithologies</u>	<u>Special Features</u>	<u>Mineral Stability</u>
MARAÑON DRAINAGE (2), mostly Huallaga subbasin:					
Huallaga, Huánuco : S-2, A-02	metamorph (PC) gg-blk sh/ss (CP, M) drk ls. (CP,M)	-----	evaporites (M) dolomite (M)	grey-brn susp sed	calcite dolomite montmorillonite
Huiguerras, Huánuco : A-03	granite (PM)	drk limest. (CP) gg-blk sh/ss (CP) metamorph (PC)	dolomite (M)	lt grey-brn susp sed	montmorillonite
Huachipa, L.C. A-04	metamorph (PH)	granite (PM)	limestone (M) ultrabasics (PC)	grey-brn susp sed	montmorillonite
Huallaga, Tingo María A-07	metamorph (PC) granite (PM) limest. (CP,M)	gg-blk sh/ss (CP, M)	dolomite (M) red beds (M,MT)	grey-brn susp sed	calcite montmorillonite
Monzón, Tingo María : A-06	metamorph (PC) granite (PM)	-----	red beds (CP) limestone (M)	salt springs grey-red-brn susp sed	montmorillonite
Salt Spring, Tingo María : A-05	evap source? drk limest. (M) drk shales (M) red beds (CP)	-----	-----	faint H2S pebbles w/ carbonate coatings clear shallow	calcite dolomite montmorillonite
Aspasarta, L.C. A-08	limestone (M) red beds (M,MT)	red sandst (MT) flu-lac (PQ)	-----	major fault grey-red susp sed	calcite montmorillonite
Uchiza, L.C. A-09	drk limest (M) red beds (M,MT)	sandst. (M) drk shale (M)	dolomite? (M)	major fault w/ salt spring grey susp sed	calcite dolomite montmorillonite
Cachiyacu, L.C. A-10	drk limest (M) red beds (M,MT)	drk shales (M) evaporites (M)	-----	major fault w/ salt extrusion clear water	calcite dolomite montmorillonite
Huallaga, Tocache : A-11	metamorph (PC) granite (PM)	limest (CP,M) red beds (CP,M, MT)	dolomite (M) evaporites (M)	red-brn susp sed	montmorillonite
Tocache, Tocache A-11	metamorph (PC)	-----	drk shale (M) red beds (CP,M) drk limest (M)	clear water	montmorillonite
Huallaga, Balsayacu : A-13	metamorph (PC)	granite (PM) limest (CP,M) red beds (CP,M, MT)	dolomite (M) evaporites (M)	red-brn susp sed	calcite montmorillonite
Huallabamba, confluence : A-14	metamorph (PC) and. volc (M) limest (CP,M) granite (PM) red beds (M,MT)	cln sandst. (M)	-----	red-brn susp sed	montmorillonite
Saposoá, L.C. A-15	red beds sh/ss (M,MT) limestone (M)	cln sandst (M) gg-blk shale (M)	evaporites (M)	2 salt domes red susp sed	calcite dolomite montmorillonite
Mayo, L.C. A-16	red beds sh/ss (M,MT) limestone (M)	cln sandst (M)	evaporites (M)	salt domes red susp sed	calcite montmorillonite
Caña, Pilluana BPA16	sandst (M) drk shales (M) red beds (M) evaporites (CP)	-----	-----	salt dome clear water	calcite montmorillonite
Huallaga, Yurimaguas : A-17, BPA13	metamorph (PC) red beds (M,MT) limestone (M)	granite (PM) and. volc (M) gg-blk sh/ss (M)	evaporites (CP, M) dolomites (M)	red-brn susp sed salt domes	montmorillonite
Shanusi, Yurimaguas : A-18, BPA14	red beds sh (M, MT)	cln sandst (M) limest (M)	-----	red susp sed major fault	kaolinite/ montmorillonite
Paranapura, Yurimaguas : A-19, BPA15	red beds sh/ss (M,MT)	cln sandst (M) limestn (M)	evaporites (M)	major fault w/ salt springs red susp sed	montmorillonite
Marañon, Nauta BPA10	metamorph (PC) limestones gg-blk sh/ss red beds flu-lac sh/ss/cg	mar volc granites	calc sh/ss dolomites evaporites	red-brn susp sed	montmorillonite

<u>River, Location</u>	<u>Major Lithologies</u>	<u>Minor Lithologies</u>	<u>Trace Lithologies</u>	<u>Special Features</u>	<u>Mineral Stability</u>
UCAYALI DRAINAGE (3)					
Montaro, Chulec : A-01	limestone (M) drk shale (M) red beds (M) and. tuffs (MT,PQ) flu-lac-gla ss/sh (PQ)	-----	coal (M) dolomite (M) sulfide minerlz evaporites (M)	brn susp sed mining-Cu salt extrusion	montmorillonite
Stream, Aguas Calientes : M-09	granite/ granodiorite (M)	-----	-----	hot springs w/ "mineral water" clear stream	montmorillonite
Urubamba, Machu Picchu : M-08, BPA08	red beds (CP,M) and. volc (MT,PQ) limestone (M,MT) meta gg-blk sh (LP)	gg-blk sh (LP) evaporites (bedded) (M) granite/ granodiorite (M)	-----	salt springs, evaporite out- crops red susp sed	calcite dolomite montmorillonite
Ucayali, Pucallpa S-1	meta gg-blk sh (LP) limest (CP,M,MT) red beds (CP,M, MT) and. volc (MT,PQ) flu-lac sh/ss/cg (PQ)	metamorph (PC) shales (CP,M) sandst (CP,M) granite/ granodiorite (M) gg-blk sh (LP,CP, M)	evaporites (M)	red susp sed	calcite dolomite montmorillonite
MADEIRA BASIN (4)					
Espiritu Santo, Villa Tunari : BPA02	gg-blk sh/ss (LP) limest (LP,CP) dolomite (LP)	red beds (MT) flu-lac (PQ)	evaporites w/ NaCl, Na2CO3, MgCO3, CaSO4 (LP)	grey-brn susp sed	montmorillonite
San Mateo, Villa Tunari : BPA02 BPA	gg-blk sh/ss (LP) limest (LP,CP) dolomite (LP)	red beds (MT) flu-lac (PQ)	evaporites w/ NaCl, Na2CO3, MgCO3, CaSO4 (LP)	grey susp sed	montmorillonite
Ichilo, Villarreal : M-05, BPA01	gg-blk sh/ss (LP) flu-lac (PQ)	red beds (MT)	-----	red-brn susp sed	kaolinite
Piray, Santa Cruz : BPA06	gg-blk sh/ss (LP) red-blk mudst (CP) red beds (MT)	flu-lac (PQ) limest (CP)	-----	red susp sed 1st day of rainy season	montmorillonite
Guapay or Grande, Pailas: BPA05	gg-blk sh/ss (LP) red-blk mudst (CP) meta gg-blk sh/ss (LP) red beds (MT) flu-lac (PQ)	marls (M) limest (CP,M)	evaporites (M)	red susp sed 1st day of rainy season salares to south of basin	dolomite montmorillonite
Madre de Dios, Riberalta : M-04	meta gg-blk sh/ss (LP) flu-lac (PQ)	red beds (M,MT) granite/ diorite (M) ryol volc (MT) grn sandst (CP) limest (CP,M)	-----	grey-yel-brn susp sed	montmorillonite
Beni, Riberalta, M-03	gg-blk sh/ss (LP) meta gg-blk sh/ss (LP) mudstone (CP) red beds (M,MT) flu-lac-gla sh/ ss/cg (PQ)	limest (CP,M)	-----	brn susp sed	montmorillonite
Mamoré, Trinidad BPA04	gg-blk sh/ss (LP) flu-lac (PQ) red beds (MT) shield (PC) qtzites (PC,M)	mudstones (CP) limestone (CP)	evaporites (very loc)	grey brn susp sed	kaolinite
Mamoré, Guayaramerin M-02	shield (PC) flu-lac (PQ) red beds (MT) gg-blk sh/ss (LP) qtzites (PC,M)	mudstones (CP) limestones (CP)	evap (loc) (LP,M) ultrabasics (loc) (PC)	grey brn susp sed	kaolinite
Madeira, Porto Velho : M-01	shield (PC) flu-lac (PQ) red beds (MT) gg-blk sh/ss (LP) qtzites (PC,M)	limestones (CP) mudstones (CP)	evap (loc) (LP,M) ultrabasics (loc) (PC)	red-brn susp sed	kaolinite
Madeira, confluence S212, S328	shield (PC) flu-lac (PQ) qtzites (PC,M) arkoses (PC) red beds (MT)	gg-blk ss/sh (LP)	mudstones (CP) limestone (CP) evap (v.loc) ultrabasics (v.loc)	red-brn susp sed	kaolinite

<u>River, Location</u>	<u>Major Lithologies</u>	<u>Minor Lithologies</u>	<u>Trace Lithologies</u>	<u>Special Features</u>	<u>Mineral Stability</u>
OTHER ANDEAN HEADWATER RIVERS (5)					
Napo, confluence S249, S304	red beds (MT) flu-lac (PQ) metamorph (PC) and. volc (MT,PQ)	cln sandst (M)	granites limest (M,MT) gypsum (M)	saline springs (v. loc) brn susp sed	kaolinite/ montmorillonite
Iça, confluence S238, S313	flu-lac (PQ) red beds (M,MT)	shield (PC) qtzites (PC) metamorph (PC)	and. volc (MT,PQ) cln sandst (M) limest (M,MT)	clr-blk water	kaolinite
Japurá, confluence S231, S318	flu-lac (PQ) red beds (M,MT)	shield (PC) qtzites (PC) metamorph (PC)	and. volc (MT,PQ) cln sandst (M) limest (M,MT)	sample contains main channel water, Sec V.3	kaolinite
NEGRO DRAINAGE (6)					
Upper Negro, confluence UN1, UN2	shield (PC)	flu-lac (mostly sands) (PQ)	qtzites (PC)	clr-blk water	kaolinite
Branco, confluence BR1, BR2	shield (PC)	flu-lac (mostly sands) (PQ)	qtzites (PC) argillites (PC) basic intr (PC)	wht susp sed	kaolinite
Lower Negro, Manaus : S216, S327, LN1, LN2	shield (PC) flu-lac (mostly sands) (PQ)	-----	qtzites (PC) argillites (PC) basic intr (PC) shales (LP) sandstones (LP)	clr-blk water	kaolinite
OTHER SHIELD RIVERS (7)					
Trombetas, confluence S208, S332	shield (PC) flu-lac (PQ)	argillites (PC) drk shales (LP)	red ss/sh (CP,MT) limestones (CP) dolomites (CP) gypsum (loc) (CP)	clr water	kaolinite
Tapajós, confluence S206, S335	shield (PC) arenites (PC)	qtzites (PC,M) qrn shales or argillites (PC) red sandst (M)	red ss/sh (CP,MT) limestone (CP) dolomites (CP) gypsum (v.loc) (CP)	clear water	kaolinite
Xingu, confluence S204, S337	shield (PC) flu-lac (PQ)	grn shales or argillites (PC) gg-blk sh/ss (LP) red sandst (M)	red sh/ss (CP,MT) limestones (CP) dolomite (CP)	clear water	kaolinite
RIVERS DRAINING TERTIARY AND PRETERTIARY SEDIMENTS (8)					
Javari, confluence S242, S301	red sh/ss (MT) flu-lac (PQ)	-----	cln sandst (MT) limestones (MT) gypsum (MT) gg-blk sh (MT)	yel-brn susp sed	kaolinite
Juruá, confluence S233, S317	red sh/ss (MT) flu-lac (PQ)	red beds w/ volc ash (MT) limestones (MT) cln sandst (MT)	drk shales (MT) gypsum (economic deposit (MT) shield (PC)	yel-brn susp sed	kaolinite/ montmorillonite
Purus, confluence S222, S324	flu-lac (PQ) red sh/ss (MT)	red beds w/ volc ash (MT) limestones (MT) cln sandst (MT)	drk shales (MT) gypsum (economic deposit (MT) shield (PC)	yel-brn susp sed	kaolinite
Stream, Obidos S331	flu-lac (PQ) over ls-dol-evap (CP)	-----	-----	clear water	kaolinite
RIVERS DRAINING TERTIARY AND LATER SEDIMENTS (9)					
Nanay, Iquitos A-21, NAN1, BPA12	flu-lac (PQ)	-----	-----	clr-blk water	kaolinite
Jandiatuba, confluence S309	flu-lac (PQ)	-----	-----	yel-wht susp sed	kaolinite
Tefé, Tefé S230, S319,a	flu-lac (PQ)	-----	-----	clr-blk water	kaolinite
Coari, Coari S225, S322	flu-lac (PQ)	-----	-----	clr-blk water	kaolinite
Matari, confluence S337A	flu-lac (mostly sands) (PQ)	-----	-----	clr-blk water	kaolinite

Table IV.5

Analytical results for surface water samples collected for this study. Also included are some parameters calculated from the analytical results. This table should be used in conjunction with Table IV.4 and Appendix I.

TZ+	-- Total cations $\mu\text{Eq}/\text{l}$ (Fe and Al are assumed to be not charged)
PH	-- pH
NA	-- Sodium $\mu\text{mole}/\text{l}$
K	-- Potassium $\mu\text{mole}/\text{l}$
MG	-- Magnesium $\mu\text{mole}/\text{l}$
CA	-- Calcium $\mu\text{mole}/\text{l}$
ALK	-- Titration alkalinity $\mu\text{Eq}/\text{l}$
CL	-- Chloride $\mu\text{mole}/\text{l}$
SO4	-- Sulfate $\mu\text{mole}/\text{l}$
SI	-- Silica $\mu\text{mole}/\text{l}$
FE-T	-- Treated iron $\mu\text{mole}/\text{l}$
FE-U	-- Untreated iron $\mu\text{mole}/\text{l}$
AL-T	-- Treated aluminum $\mu\text{mole}/\text{l}$
AL-U	-- Untreated aluminum $\mu\text{mole}/\text{l}$
NICB	-- Net inorganic charge balance
TDS	-- Total dissolved solids ppm
CYCL	-- Cyclic chloride $\mu\text{mole}/\text{l}$
TEMP	-- Temperature $^{\circ}\text{C}$
PO4	-- Phosphate $\mu\text{mole}/\text{l}$
P-T	-- Total phosphate $\mu\text{mole}/\text{l}$
NO3	-- Nitrate $\mu\text{mole}/\text{l}$
NO2	-- Nitrite $\mu\text{mole}/\text{l}$
NH4	-- Ammonia $\mu\text{mole}/\text{l}$
CO2	-- $\frac{P_{\text{CO}_2\text{river}}}{P_{\text{CO}_2\text{atmosphere}}}$
COL	-- Absorbance at 270 nm in 1 cm cell times 1000
TOC	-- Total organic carbon $\mu\text{mole}/\text{l}$
AB.	-- above
AM.	-- Amazon
SO.	-- Solimões
HU.	-- Huallaga

MAIN CHANNEL (1)

STA.	PARAMETER: -LOCATION-	TZ+	PH	NA	K	MG	CA	ALK	CL	SO4	SI	FE-T	FE-U	AL-T	AL-U
S250	AM.IQUITOS	1455.	7.50	278.	28.9	96.7	477.	1122.	183.	73.	185.	1.0	0.1	0.8	1.2
S247	AM.PEVAS	1202.	7.40	201.	28.6	82.3	404.	944.	129.8	57.	184.	1.1	0.0	0.6	0.1
S243	AM.LETICIA	1064.	7.38	173.	28.0	75.5	356.	867.	100.1	51.	179.	1.6	0.0	1.0	0.2
S241	SD.ASSACA-	1076.	7.29	175.	27.9	75.4	361.	855.	104.3	53.	177.	1.1	0.1	0.6	0.1
S240	SD.SAO PA-	1077.	7.40	178.	28.5	76.4	359.	859.	106.0	54.	180.	1.2	0.1	0.8	0.5
S237	SO.A.JUTAI	917.	7.09	137.	25.7	67.6	310.	715.	80.9	41.	159.	1.0	0.0	0.5	0.1
S235	SO.BJUTAI	908.	7.11	133.	26.1	67.6	307.	716.	76.6	40.	160.	1.1	0.0	0.6	0.6
S234	SO.FONTE B	857.	7.03	131.	25.4	63.6	287.	653.	74.3	40.	157.	1.0	0.1	0.6	0.6
S232	SO.ALVAREZ	840.	6.97	131.	26.3	63.0	278.	641.	74.2	36.2	158.	1.3	0.0	0.3	0.2
S228	SO.JUTICA	760.	6.94	117.	25.2	57.2	251.	596.	65.4	29.9	147.	1.1	0.0	0.6	0.2
S227	SO.LARANJ-	703.	6.92	107.	24.3	54.3	231.	552.	63.5	25.8	151.	1.4	0.0	0.9	0.5
S224	SD.CAMARA	650.	6.90	100.	23.4	50.4	213.	511.	56.0	24.2	145.	1.2	0.0	0.1	0.6
S223	SO.ANORI	667.	6.93	101.	23.8	51.9	219.	517.	57.3	25.9	144.	1.3	0.1	0.3	0.3
S220	SO.MANACA-	589.	6.75	88.	23.8	48.5	189.	475.	47.4	22.0	142.	1.7	0.0	0.1	0.3
S219	SO.A.NEGRO	614.	6.74	92.	24.2	49.8	199.	490.	47.8	23.2	141.	1.5	0.1	0.2	0.1
S209	AM.OBIDOS	422.	6.63	63.4	20.8	39.6	128.7	323.	30.5	17.8	120.	1.9	1.2	0.7	0.2
S207	AM.APIXUNA	412.	6.62	62.5	20.7	39.2	124.9	307.	28.0	18.0	121.	1.6	0.4	0.2	0.2
S203	AM.GURUPA	399.	--	62.1	21.1	39.5	118.2	315.	30.4	17.9	123.	0.9	0.2	0.6	0.2
S202	AM.URUTAI	481.	--	129.	22.5	47.3	117.3	308.	139.2	17.0	126.	1.1	1.7	0.4	0.2
S302	AM.IQUITOS	1558.	7.31	225.	35.5	96.7	551.	1252.	156.	70.	174.	1.1	0.1	0.3	0.3
S303	AM.A.NAPO	1567.	7.32	231.	35.6	97.5	552.	1272.	156.	70.	174.	1.2	0.1	0.4	0.4
S305	AM.PEVAS	1421.	7.20	224.	34.6	90.4	491.	1147.	151.	62.	179.	1.5	0.1	0.1	0.4
S306	AM.LETICIA	1383.	7.25	205.	35.8	91.3	480.	1131.	137.0	58.	183.	1.2	0.0	0.5	0.3
S307	SO.A.SAD P	1293.	7.17	198.	34.4	86.4	444.	1058.	122.1	52.	179.	0.9	0.1	0.2	0.3
S311	SO.A.ICA	1225.	7.14	178.	33.8	84.4	422.	1013.	114.8	46.	175.	0.8	0.2	0.2	0.4
S314	SO.A.JUTAI	1105.	7.08	158.	31.7	77.7	380.	894.	99.7	42.	169.	1.1	0.2	0.2	0.6
S316	SO.A.JURUA	960.	6.93	141.	29.9	71.0	324.	774.	83.0	35.3	161.	1.0	0.2	0.1	0.3
S321	SO.A.COARI	778.	6.85	109.	28.0	61.1	260.	644.	61.0	26.1	155.	1.6	0.4	0.2	0.4
S323	SO.A.PURUS	738.	6.83	100.	27.4	59.1	246.	603.	57.4	24.4	151.	1.5	0.7	0.3	0.5
S326	SO.A.NEGRO	609.	6.65	86.	26.5	51.4	197.	501.	42.1	23.0	146.	1.0	0.4	0.2	0.4
S329	AM.OBIDOS	483.	6.66	71.3	24.5	46.9	147.	386.	31.0	20.5	129.	1.7	0.3	0.2	0.3
S334	AM.A.TAPA-	469.	6.66	68.5	23.8	46.2	142.0	377.	33.5	21.3	130.	1.5	0.6	0.2	0.3
S336	AM.A.XINGU	455.	6.80	67.5	23.4	44.4	137.4	359.	31.2	21.9	132.	1.3	0.5	0.1	0.4
SOL1	SO.A.NEGRO	654.	7.20	99.	24.8	55.2	210.	513.	54.9	31.7	146.	--	0.3	--	0.7
SOL2	SO.A.NEGRO	755.	7.20	109.	25.2	60.9	250.	590.	59.4	40.	143.	--	7.3	--	2.9
AMI01	AM.IQUITOS	1527.	--	273.	27.8	101.9	512.	1138.	188.	91.	166.	--	--	--	--
BPA09	AM.IQUITOS	1523.	7.31	248.	27.8	95.6	528.	1172.	158.	80.	153.	1.0	2.3	0.6	2.2

MAIN CHANNEL (1) CONTINUED

STA.	PARAMETER: -LOCATION-	TZ+	NICB	TDS	CYCL	TEMP	PO4	P-T	NO3	NO2	NH4	CO2	COL	TOC
S250	AM.IQUITOS	1455.	-0.0031	122.9	3.8	--	0.56	--	9.4	0.10	0.6	7.28	76.	--
S247	AM.PEVAS	1202.	0.0039	103.0	3.8	--	0.45	--	9.0	0.09	0.4	7.75	69.	--
S243	AM.LETICIA	1064.	-0.0147	94.8	3.8	--	0.44	--	9.5	0.13	0.1	7.47	71.	--
S241	SO.ASSACA-	1076.	0.0001	93.6	3.8	--	0.49	--	10.6	0.02	0.1	9.07	72.	--
S240	SO.SAO PA-	1077.	-0.0062	94.7	3.8	--	0.48	--	11.0	0.02	0.5	7.07	65.	--
S237	SO.A.JUTAI	917.	0.0336	76.8	3.9	--	0.44	--	9.3	0.04	0.2	12.07	71.	444.
S235	SO.BJUTAI	908.	0.0279	76.9	3.9	--	0.44	--	9.3	0.03	0.2	11.54	86.	--
S234	SO.FONTE B	857.	0.0495	70.6	4.0	--	0.42	--	7.8	0.04	0.2	12.68	61.	--
S232	SO.ALVAREZ	840.	0.0532	69.2	4.1	--	0.42	--	7.5	0.04	0.3	14.29	85.	487.
S228	SO.JUTICA	760.	0.0428	63.9	4.4	--	0.04	--	6.2	0.01	0.4	14.27	86.	--
S227	SO.LARANJ-	703.	0.0421	60.0	4.4	--	0.37	--	6.1	0.05	0.5	13.86	99.	--
S224	SO.CAMARA	650.	0.0452	55.7	4.5	--	0.36	--	5.4	0.04	0.6	13.45	101.	399.
S223	SO.ANORI	667.	0.0525	56.2	4.5	--	0.37	--	5.5	0.04	0.1	12.70	103.	--
S220	SO.MANACA-	589.	0.0306	52.2	4.6	--	0.37	--	4.2	0.04	0.6	17.7	107.	380.
S219	SO.A.NEGRO	614.	0.0428	53.1	4.6	--	0.35	--	4.0	--	0.4	18.7	140.	391.
S209	AM.OBIDOS	422.	0.0657	36.7	5.4	--	0.29	--	4.8	0.04	0.6	15.9	159.	--
S207	AM.APIXUNA	412.	0.0866	35.0	6.9	--	0.28	--	5.0	0.07	0.1	15.5	133.	478.
S203	AM.GURUPA	399.	0.0281	37.0	6.1	--	0.29	--	6.1	0.08	--	--	156.	--
S202	AM.URUTAI	481.	-0.0146	43.5	6.8	--	0.29	--	6.3	0.10	--	--	137.	--
S302	AM.IQUITOS	1558.	0.0016	130.4	3.8	--	0.79	0.99	8.6	0.09	1.4	12.57	152.	--
S303	AM.A.NAPO	1567.	-0.0066	132.7	3.8	--	0.78	0.98	8.4	0.09	1.4	12.47	153.	560.
S305	AM.PEVAS	1421.	-0.0065	121.5	3.8	--	0.64	0.80	9.1	0.06	0.4	14.9	151.	--
S306	AM.LETICIA	1383.	-0.0062	119.0	3.8	--	0.63	0.79	8.3	0.04	0.5	13.08	140.	490.
S307	SO.A.SAO P	1293.	-0.0094	111.0	3.8	--	0.59	0.16	9.6	0.02	--	14.7	143.	--
S311	SO.A.ICA	1225.	-0.0033	106.0	3.9	--	0.53	0.54	9.5	0.0	--	15.1	153.	480.
S314	SO.A.JUTAI	1105.	0.0170	93.6	3.9	--	0.45	0.73	8.3	0.05	--	15.4	149.	330.
S316	SO.A.JURUA	960.	0.0265	81.2	4.1	--	0.41	0.62	6.8	0.05	--	18.9	159.	--
S321	SO.A.COARI	778.	0.0193	68.2	4.4	--	0.40	0.44	6.2	0.05	--	19.0	177.	--
S323	SO.A.PURUS	738.	0.0316	63.9	4.5	28.	0.43	1.10	5.8	0.04	--	18.8	179.	830.
S326	SO.A.NEGRO	609.	0.0243	54.6	4.6	--	0.43	0.71	5.0	0.05	--	23.5	177.	--
S329	AM.OBIDOS	483.	0.0402	43.2	5.5	--	0.32	0.37	5.8	0.01	--	17.8	202.	--
S334	AM.A.TAPA-	469.	0.0213	43.1	5.7	--	0.31	0.35	5.8	0.02	--	17.3	189.	580.
S336	AM.A.XINGU	455.	0.0310	41.6	5.9	--	0.33	0.36	6.5	0.05	--	11.97	181.	--
SOL1	SO.A.NEGRO	654.	0.0299	57.1	5.4	--	--	--	3.5	--	--	6.76	96.	--
SOL2	SO.A.NEGRO	755.	0.0190	65.3	5.4	--	--	--	11.6	--	--	7.76	120.	--
AM101	AM.IQUITOS	1527.	0.0130	124.0	2.8	--	--	--	--	--	--	--	89.	--
BPA09	AM.IQUITOS	1523.	0.0126	124.0	3.3	27.	0.81	--	14.7	--	--	11.85	144.	--

MARANON DRAINAGE (2)

STA.	PARAMETER: -LOCATION-	TZ+	PH	NA	K	MG	CA	ALK	CL	SO4	SI	FE-T	FE-U	AL-T	AL-U
S-2	HU.HUANUCO	3940.	--	555.	39.6	504.	1171.	2347.	403.	560.	149.	--	0.2	--	1.1
A-02	HU.HUANUCO	2894.	8.40	224.	25.6	323.	999.	2222.	145.0	246.	123.	0.4	0.1	1.4	0.5
A-03	HUIGUERAS	1633.	8.00	157.	15.3	212.	519.	1438.	32.8	63.	179.	0.5	0.1	3.0	0.7
A-04	HUACHIPA	825.	8.20	103.	18.9	117.6	234.	758.	16.0	26.5	203.	2.5	0.0	3.8	0.5
A-07	HU.TINGO M	2852.	8.10	572.	29.0	272.	854.	1786.	469.	289.	163.	1.3	0.1	4.2	1.3
A-05	SALT SP.	60300.	7.50	38300.	174.	2660.	8290.	2728.	39200.	9300.	161.	0.2	0.0	0.4	0.8
A-06	MONZON R.	613.	7.20	127.	21.1	56.4	176.	469.	54.0	43.	203.	1.1	0.2	1.2	0.4
A-08	ASPASARTA	2557.	7.80	79.	14.9	115.3	1116.	2416.	10.5	20.2	149.	1.4	0.1	3.9	0.6
A-09	UCHIZA R.	2737.	8.30	204.	30.0	147.	1105.	2270.	83.0	202.	198.	0.8	0.1	1.8	0.2
A-10	CACHIYACU	18950.	8.50	15100.	27.1	144.0	1760.	1713.	15400.	1000.	173.	0.1	0.0	0.7	0.4
A-12	HU.TOCACHE	2221.	7.80	561.	31.3	140.6	674.	1382.	505.	173.	217.	0.8	0.1	2.0	0.9
A-11	TOCACHE R.	462.	7.30	126.	17.3	47.3	112.1	390.	6.4	26.6	244.	1.5	0.2	1.6	0.7
A-13	HU.BALSA Y	1862.	8.30	499.	28.2	118.7	549.	1196.	392.	136.	225.	0.9	0.1	1.6	0.5
A-14	HUALLABAMB	1663.	8.00	183.	19.1	108.5	622.	1412.	63.7	86.	172.	0.7	0.0	2.0	0.4
A-15	SAPOSOA R.	3290.	8.30	990.	33.5	121.4	1012.	2040.	724.	268.	194.	4.8	0.1	19.9	0.3
A-16	MAYO R.	2019.	8.40	392.	22.7	102.6	699.	1494.	323.	89.	123.	2.0	0.2	4.1	0.9
A-17	HU.YURIMA-	2673.	7.50	1040.	29.6	110.8	690.	1393.	943.	151.	193.	2.0	0.1	4.2	0.7
A-18	SHANUSI R.	965.	7.20	219.	27.8	50.2	309.	703.	95.6	69.	135.	2.0	0.5	3.6	0.3
A-19	PARANAPURA	1333.	7.20	517.	27.3	57.2	337.	673.	438.	112.	135.	2.5	0.4	5.0	0.5
BPA10	MARANON C-	1183.	7.20	197.	23.3	70.9	411.	926.	123.5	52.	169.	1.4	3.1	1.2	1.6
BPA16	CANA S.	77200.	8.14	71400.	137.3	298.	2540.	1156.	71600.	2080.	158.	0.0	0.0	0.3	0.6
BPA13	HU.YURMA-H	2461.	7.13	890.	51.2	92.2	669.	1335.	823.	130.	158.	0.4	0.2	2.1	0.6
BPA14	SHANUSI R.	710.	6.97	126.	23.8	38.7	242.	545.	52.0	37.	103.	1.6	1.4	1.1	1.2
BPA15	PARANAPURA	1088.	7.57	266.	23.8	47.8	352.	788.	124.4	82.	96.	1.2	3.8	0.8	4.7

STA.	PARAMETER: -LOCATION-	TZ+	NICB	TDS	CYCL	TEMP	PO4	P-T	NO3	NO2	NH4	CO2	COL	TOC
S-2	HU.HUANUCO	3940.	0.0184	289.4	3.8	--	--	--	--	--	--	--	19.	--
A-02	HU.HUANUCO	2894.	0.0076	225.2	3.8	17.	--	--	15.6	--	--	1.49	70.	--
A-03	HUIGUERAS	1633.	0.0036	137.4	3.8	19.	--	--	30.7	--	--	2.57	61.	--
A-04	HUACHIPA	825.	-0.0106	77.8	3.8	21.	--	--	8.7	--	--	0.89	51.	--
A-07	HU.TINGO M	2852.	-0.0044	221.0	3.8	20.	--	--	32.8	--	--	2.54	44.	--
A-05	SALT SP.	60300.	-0.0043	3760.	3.8	24.	--	--	2.2	--	--	13.39	19.	--
A-06	MONZON R.	613.	-0.0004	59.3	3.8	21.	--	--	5.6	--	--	5.65	46.	--
A-08	ASPASARTA	2557.	0.0177	208.6	3.8	23.	--	--	46.	--	--	7.25	65.	--
A-09	UCHIZA R.	2737.	-0.0108	228.8	3.8	28.	--	--	11.2	--	--	2.28	66.	--
A-10	CACHIYACU	18950.	-0.0072	1187.	3.8	25.	--	--	8.3	--	--	0.93	47.	--
A-12	HU.TOCACHE	2221.	-0.0094	178.3	3.8	24.	--	--	10.1	--	--	4.22	57.	--
A-11	TOCACHE R.	462.	0.0114	50.6	3.8	21.	--	--	7.4	--	--	3.75	50.	--
A-13	HU.BALSA Y	1862.	-0.0017	151.5	3.8	24.	--	--	7.4	--	--	1.14	65.	--
A-14	HUALLABAMB	1663.	0.0052	139.4	3.8	21.	--	--	8.1	--	--	2.61	93.	--
A-15	SAPOSOA R.	3290.	-0.0061	256.8	3.8	24.	--	--	10.7	--	--	1.91	105.	--
A-16	MAYO R.	2019.	0.0074	158.6	3.8	23.	--	--	12.1	--	--	1.11	170.	--
A-17	HU.YURIMA-	2673.	0.0110	198.5	3.8	25.	--	--	5.3	--	--	8.62	100.	--
A-18	SHANUSI R.	965.	0.0231	79.8	3.8	26.	--	--	7.0	--	--	8.99	145.	--
A-19	PARANAPURA	1333.	-0.0075	104.4	3.8	25.	--	--	8.1	--	--	8.48	132.	--
BPA10	MARANON C-	1183.	0.0235	98.0	3.3	27.	0.68	--	1.2	--	--	12.06	182.	--
BPA16	CANA S.	77200.	0.0031	4560.	3.3	27.	0.50	--	13.5	--	--	1.34	75.	--
BPA13	HU.YURMA-H	2461.	0.0130	182.8	3.3	26.	0.75	--	10.1	--	--	19.7	110.	--
BPA14	SHANUSI R.	710.	0.0428	58.0	3.3	26.	0.88	--	8.6	--	--	11.96	162.	--
BPA15	PARANAPURA	1088.	-0.0013	89.3	3.3	25.	1.09	--	12.9	--	--	4.22	137.	--

UCAYALI DRAINAGE (3)

STA.	PARAMETER: -LOCATION-	TZ+	PH	NA	K	MG	CA	ALK	CL	SO4	SI	FE-T	FE-U	AL-T	AL-U
S-1	UCAYALI R.	3590.	7.82	552.	47.8	299.	1197.	2711.	362.	262.	194.	--	0.2	--	0.8
A-01	MONTARO R.	5150.	7.40	423.	41.1	544.	1800.	1557.	234.	1690.	141.	0.1	0.0	0.4	0.5
M-08	URUBAMBA	13200.	8.20	5720.	178.	884.	2770.	2976.	5690.	2230.	208.	0.6	0.0	0.9	0.2
M-09	STREAM A-C	1011.	7.50	195.	52.9	98.1	284.	770.	94.9	52.	197.	0.1	0.0	0.6	0.3
BPA08	URUBAMBA	7360.	8.31	2610.	97.4	545.	1780.	2103.	2440.	1350.	177.	0.1	0.0	0.7	0.6
BPA11	UCAYALI C-	1940.	7.37	296.	34.3	123.6	682.	1459.	191.	133.	140.	0.4	0.4	0.5	0.3

STA.	PARAMETER: -LOCATION-	TZ+	NICB	TDS	CYCL	TEMP	PO4	P-T	NO3	NO2	NH4	CO2	COL	TOC
S-1	UCAYALI R.	3590.	-0.0012	285.1	3.8	--	--	--	--	--	--	8.13	42.	--
A-01	MONTARO R.	5150.	-0.0054	373.	3.8	13.	--	--	6.3	--	--	9.76	73.	--
M-08	URUBAMBA	13200.	0.0034	890.	3.8	16.	--	--	35.6	--	--	2.92	23.	--
M-09	STREAM A-C	1011.	0.0340	85.9	3.8	12.	--	--	7.4	--	--	4.05	41.	--
BPA08	URUBAMBA	7360.	0.0135	498.	3.3	17.	1.12	--	21.4	--	--	1.68	54.	--
BPA11	UCAYALI C-	1940.	0.0029	156.2	3.3	28.	0.65	--	19.1	--	--	12.83	91.	--

MADEIRA DRAINAGE (4)

STA.	PARAMETER: -LOCATION-	TZ+	PH	NA	K	MG	CA	ALK	CL	SO4	SI	FE-T	FE-U	AL-T	AL-U
S212	MADEIRA R.	405.	6.70	71.5	28.4	61.2	90.9	272.	13.6	37.	145.	1.1	0.1	0.5	0.1
S328	MADEIRA R.	437.	6.71	64.5	31.1	63.6	106.8	304.	12.6	35.5	142.	0.8	0.4	0.2	0.4
M-05	ICHILO R.	728.	6.20	135.	25.2	114.1	170.	116.	6.4	279.	168.	1.0	0.3	0.6	0.1
M-04	M. DE DIOS	998.	7.20	156.	27.8	102.5	305.	831.	15.9	67.	208.	5.0	0.0	5.8	0.2
M-03	BENI RIVER	1303.	7.00	172.	34.6	224.	324.	828.	52.7	195.	152.	1.8	0.5	0.9	0.2
M-02	MAMORE GU-	569.	6.50	117.	47.2	90.3	111.7	403.	21.3	47.	156.	3.5	1.2	2.8	0.1
M-01	MADEIRA PV	620.	6.50	114.	41.1	91.7	140.9	450.	22.6	58.	157.	2.2	1.6	1.2	0.2
BPA01	ICHILO R.	517.	5.28	104.	21.9	83.0	110.0	10.	5.6	247.	139.	0.9	0.3	1.2	3.1
BPA02	SAN MATEO	1231.	8.04	185.	21.5	168.	344.	669.	92.2	233.	114.	0.3	0.3	5.9	0.4
BPA03	ESPIRITU S	1339.	7.81	393.	25.2	170.	290.	652.	259.	197.	137.	1.1	0.2	3.6	0.4
BPA04	MAMORE TR-	1231.	6.91	221.	32.8	216.	273.	511.	72.5	306.	121.	0.1	0.5	1.1	0.4
BPA05	GUAPAY R.	6920.	7.70	1240.	139.9	1400.	1371.	1970.	470.	2190.	163.	0.1	0.0	0.3	0.5
BPA06	PIRAY R.	2211.	7.71	537.	117.5	244.	534.	1527.	75.2	254.	204.	0.5	2.9	0.4	7.5

STA.	PARAMETER: -LOCATION-	TZ+	NICB	TDS	CYCL	TEMP	PO4	P-T	NO3	NO2	NH4	CO2	COL	TOC
S212	MADEIRA R.	405.	0.0892	35.6	5.9	--	0.22	--	8.4	--	0.4	11.43	77.	--
S328	MADEIRA R.	437.	0.0935	37.5	5.9	27.	0.27	0.51	8.1	0.07	--	12.47	127.	--
M-05	ICHILO R.	728.	0.0545	55.8	3.8	21.	--	--	6.3	--	--	14.08	42.	--
M-04	M. DE DIOS	998.	0.0119	89.2	3.8	27.	--	--	5.2	--	--	10.86	42.	--
M-03	BENI RIVER	1303.	0.0158	103.5	3.8	27.	--	--	11.8	--	--	17.0	96.	--
M-02	MAMORE GU-	569.	0.0834	47.7	3.8	27.	--	--	3.4	--	--	26.6	130.	--
M-01	MADEIRA PV	620.	0.0469	53.7	3.8	28.	--	--	3.4	--	--	30.2	156.	--
BPA01	ICHILO R.	517.	-0.0126	43.5	3.3	23.	0.09	--	9.2	--	--	15.7	19.	--
BPA02	SAN MATEO	1231.	-0.0060	97.4	3.3	22.	0.95	--	11.4	--	--	1.16	23.	--
BPA03	ESPIRITU S	1339.	0.0167	101.2	3.3	22.	0.82	--	12.5	--	--	1.91	54.	--
BPA04	MAMORE TR-	1231.	0.0201	92.1	3.3	27.	0.50	--	11.6	--	--	12.94	41.	--
BPA05	GUAPAY R.	6920.	0.0071	480.	3.3	27.	0.31	--	61.	--	--	7.49	89.	--
BPA06	PIRAY R.	2211.	0.0225	176.9	3.3	26.	1.92	--	51.	--	--	5.95	136.	--

OTHER ANDEAN HEADWATER RIVERS: NAPO, ICA, JAPURA (5)

STA.	PARAMETER: -LOCATION-	TZ+	PH	NA	K	MG	CA	ALK	CL	SO4	SI	FE-T	FE-U	AL-T	AL-U
S249	NAPO RIVER	400.	6.70	53.6	29.4	48.0	110.3	341.	8.5	14.7	191.	1.4	0.2	1.1	0.3
S238	ICA R.	194.	5.99	26.7	14.6	16.1	59.1	80.	7.1	2.5	115.	1.4	2.4	0.8	0.3
S231	JAPURA R.	453.	6.52	71.3	19.3	36.8	143.8	351.	37.4	17.5	122.	1.2	0.1	0.4	0.1
S304	NAPO R.	493.	6.94	73.	29.6	55.3	139.5	427.	9.4	23.7	200.	0.8	0.1	0.6	0.3
S313	ICA RIVER	159.	5.95	27.0	13.3	14.7	44.0	95.	8.1	3.1	112.	1.4	0.5	0.8	0.7
S318	JAPURA R.	605.	6.59	89.	23.8	48.2	198.	494.	49.5	21.3	137.	1.8	0.3	0.3	0.3

STA.	PARAMETER: -LOCATION-	TZ+	NICB	TDS	CYCL	TEMP	PO4	P-T	NO3	NO2	NH4	CO2	COL	TOC
S249	NAPO RIVER	400.	0.0396	41.3	3.8	--	0.20	--	5.1	0.06	0.1	14.34	78.	--
S238	ICA R.	194.	0.4986	11.6	4.2	--	0.18	--	4.0	0.04	1.1	17.6	113.	--
S231	JAPURA R.	453.	0.0568	39.4	5.3	--	0.25	--	3.4	0.05	0.5	22.3	111.	585.
S304	NAPO R.	493.	-0.0002	51.0	3.8	27.	0.37	0.47	9.5	0.05	0.6	10.22	82.	--
S313	ICA RIVER	159.	0.2899	13.7	4.2	--	0.23	0.26	2.3	0.03	--	23.0	155.	--
S318	JAPURA R.	605.	0.0250	53.5	5.3	27.	0.28	0.49	3.5	0.05	--	26.6	221.	--

NEGRO DRAINAGE (6)

STA.	PARAMETER: -LOCATION-	TZ+	PH	NA	K	MG	CA	ALK	CL	SO4	SI	FE-T	FE-U	AL-T	AL-U
S216	NEGRO R.	68.	5.36	17.6	10.1	6.8	10.5	9.	6.8	1.6	70.9	3.9	3.8	2.9	2.4
S327	NEGRO R.	68.	4.95	17.3	10.1	6.1	8.3	9.	7.6	3.1	65.3	4.9	3.4	4.4	4.0
UN1	U.NEGRO R.	51.	4.80	10.4	7.9	3.2	5.2	-16.	7.6	2.3	64.3	--	4.4	--	3.7
UN2	U.NEGRO R.	57.	4.64	13.5	6.6	2.6	4.2	-5.	7.0	2.0	56.9	--	2.4	--	4.3
BR1	BRANCO R.	179.	6.61	62.0	24.3	21.7	24.7	128.	15.5	3.0	191.	--	4.1	--	0.5
BR2	BRANCO R.	285.	6.66	85.	30.1	40.8	44.2	252.	16.0	2.7	192.	--	0.2	--	0.4
LN1	NEGRO R.	74.	5.07	20.8	8.1	5.6	12.7	8.	15.2	4.4	72.0	--	2.4	--	3.1
LN2	NEGRO R.	56.	5.03	17.8	7.3	4.6	6.1	12.	9.5	1.9	67.7	--	1.9	--	3.4

STA.	PARAMETER: -LOCATION-	TZ+	NICB	TDS	CYCL	TEMP	PO4	P-T	NO3	NO2	NH4	CO2	COL	TOC
S216	NEGRO R.	68.	0.6172	6.3	6.8	--	0.02	--	2.9	--	1.0	12.21	371.	763.
S327	NEGRO R.	68.	0.4049	6.1	7.6	29.	0.11	0.22	5.3	0.12	--	52.5	396.	--
UN1	U.NEGRO R.	51.	0.7290	5.3	7.6	--	--	--	1.6	--	--	0.50	369.	--
UN2	U.NEGRO R.	57.	0.4559	4.8	7.0	--	--	--	1.8	--	--	89.6	627.	--
BR1	BRANCO R.	179.	0.1519	22.5	15.5	--	--	--	2.6	--	--	6.69	188.	--
BR2	BRANCO R.	285.	0.0218	33.5	16.0	--	--	--	5.2	--	--	11.68	30.	--
LN1	NEGRO R.	74.	0.4231	6.9	15.2	--	--	--	1.7	--	--	31.2	332.	--
LN2	NEGRO R.	56.	0.3256	5.9	9.5	--	--	--	3.4	--	--	42.2	344.	--

OTHER SHIELD RIVERS: XINGU, TAPAJOS, TROMBETAS (7)

STA.	PARAMETER: -LOCATION-	TZ+	PH	NA	K	MG	CA	ALK	CL	SO4	SI	FE-T	FE-U	AL-T	AL-U
S208	TROMBETAS	281.	6.50	46.6	18.0	24.1	83.7	159.	20.6	7.9	112.	1.0	0.3	0.2	0.2
S206	TAPAJOS R.	160.	6.91	32.7	19.1	18.9	34.9	82.	9.0	1.6	150.	0.8	0.3	0.2	0.2
S204	XINGU R.	215.	7.09	76.	27.0	24.0	31.8	176.	19.3	1.0	192.	0.9	0.1	0.5	0.4
S332	TROMBETAS	99.	5.87	35.9	18.1	8.6	13.2	63.	15.7	4.9	116.	2.4	1.2	1.6	1.6
S335	TAPAJOS R.	129.	6.72	30.6	19.6	17.8	21.5	109.	9.8	3.3	147.	0.9	0.2	0.4	0.3
S337	XINGU R.	281.	6.44	68.3	25.3	28.0	65.4	190.	27.1	3.0	173.	1.3	0.6	0.2	0.3

STA.	PARAMETER: -LOCATION-	TZ+	NICB	TDS	CYCL	TEMP	PO4	P-T	NO3	NO2	NH4	CO2	COL	TOC
S208	TROMBETAS	281.	0.2930	18.8	20.6	--	0.10	--	3.1	--	0.2	10.65	132.	940.
S206	TAPAJOS R.	160.	0.3945	14.1	9.0	--	0.01	--	2.5	0.08	0.3	2.15	101.	--
S204	XINGU R.	215.	0.0767	26.7	19.3	--	0.0	--	0.8	0.11	--	3.04	91.	--
S332	TROMBETAS	99.	0.0504	14.1	15.7	--	0.01	0.03	4.3	0.02	--	18.5	193.	--
S335	TAPAJOS R.	129.	0.0154	18.9	9.8	--	0.03	0.06	1.5	0.03	--	4.43	105.	--
S337	XINGU R.	281.	0.1960	25.9	27.1	30.	0.06	0.14	2.6	0.03	--	15.2	146.	--

LOWLAND RIVERS DRAINING MARINE SEDIMENTS: JAVARI, JURUA, PURUS (8)

STA.	PARAMETER: -LOCATION-	TZ+	PH	NA	K	MG	CA	ALK	CL	SO4	SI	FE-T	FE-U	AL-T	AL-U
S242	JAVARI R.	298.	6.45	51.0	17.2	29.6	85.2	250.	16.1	6.2	156.	1.4	0.1	0.6	0.2
S233	JURUA R.	642.	6.80	81.	30.5	57.1	208.	570.	16.0	7.5	167.	0.7	0.1	0.3	0.2
S222	PURUS R.	374.	6.39	49.8	23.9	34.7	114.7	265.	15.1	9.9	142.	1.3	0.3	0.2	0.1
S301	JAVARI R.	357.	6.34	48.5	19.6	30.3	113.1	304.	22.6	10.7	134.	--	1.3	--	0.5
S317	JURUA R.	490.	6.51	64.5	28.0	44.2	155.	447.	5.9	7.4	161.	1.2	0.4	0.2	0.3
S324	PURUS R.	217.	5.99	34.3	21.9	24.3	55.7	169.	5.0	7.3	133.	1.3	0.7	0.2	0.3
S331	STREAM OB-	307.	6.26	74.	29.8	27.8	73.4	245.	53.1	3.3	79.	--	0.3	--	0.2

STA.	PARAMETER: -LOCATION-	TZ+	NICB	TDS	CYCL	TEMP	PO4	P-T	NO3	NO2	NH4	CO2	COL	TOC
S242	JAVARI R.	298.	0.0237	32.1	4.1	--	0.01	--	12.6	0.14	0.2	18.8	85.	--
S233	JURUA R.	642.	0.0550	57.1	5.1	--	0.34	--	5.8	0.06	0.3	18.9	97.	--
S222	PURUS R.	374.	0.1928	29.4	5.0	--	0.30	--	1.6	0.06	0.7	22.8	115.	--
S301	JAVARI R.	357.	0.0084	35.8	4.1	--	0.23	0.42	5.9	0.07	1.6	29.3	161.	--
S317	JURUA R.	490.	0.0360	46.9	5.8	27.	0.34	0.93	4.7	0.06	--	28.9	194.	--
S324	PURUS R.	217.	0.1178	22.2	5.0	28.	0.29	0.83	2.0	0.04	--	37.5	183.	--
S331	STREAM OB-	307.	-0.0005	28.5	15.5	--	0.05	0.16	1.1	0.0	--	28.6	158.	--

RIVERS DRAINING UPPER TERTIARY SEDIMENTS (9)

STA.	PARAMETER: -LOCATION-	TZ+	PH	NA	K	MG	CA	ALK	CL	SO4	SI	FE-T	FE-U	AL-T	AL-U
S236	JUTAI R.	180.	6.07	31.3	15.8	14.6	51.2	116.	5.1	5.1	119.	1.4	2.3	0.6	1.1
S230	TEFE RIVER	105.	6.08	25.3	18.7	10.5	19.2	63.	5.6	1.7	126.	2.2	6.5	0.4	0.7
S225	COARI R.	172.	6.48	35.7	17.5	17.4	41.5	110.	6.2	5.4	123.	2.2	6.3	0.3	0.6
A-21	NANAY R.	67.	5.10	13.3	8.0	5.0	13.6	40.	3.8	2.6	84.	3.2	6.4	3.1	3.1
S309	JANDIATUBA	80.	5.54	13.3	10.2	6.9	19.8	37.	4.6	2.5	95.	1.0	0.7	1.2	1.0
S309A	VARZEA L.	67.	--	15.2	10.4	7.3	13.5	36.	4.6	2.8	107.	1.0	0.4	0.8	0.7
S315	JUTAI R.	130.	5.19	26.0	14.4	14.0	27.4	53.	5.5	1.3	101.	2.0	1.7	1.4	1.0
S319	TEFE RIVER	70.	5.75	22.5	16.6	6.8	7.5	47.	7.5	0.5	126.	1.1	0.9	0.7	0.8
S319A	TEFE RIVER	70.	5.80	21.3	16.1	7.5	7.8	41.	7.4	0.5	121.	0.7	0.5	0.5	0.6
S322	COARI R.	74.	6.01	24.1	14.2	8.4	8.9	48.	6.5	0.7	100.	0.9	0.8	0.6	0.4
S337A	MATARI R.	71.	4.70	29.3	3.8	5.4	3.6	-8.	32.1	1.3	40.5	3.7	1.9	1.9	1.9
NAN01	NANAY R.	43.	5.57	8.1	7.4	4.0	8.7	7.	2.8	0.0	71.4	--	--	--	--
BPA12	NANAY R.	55.	4.98	11.0	5.9	4.0	9.9	17.	3.3	0.5	70.1	3.0	3.2	3.8	3.6

STA.	PARAMETER: -LOCATION-	TZ+	NICB	TDS	CYCL	TEMP	PO4	P-T	NO3	NO2	NH4	CO2	COL	TOC
S236	JUTAI R.	180.	0.2577	15.9	5.1	--	0.06	--	1.1	0.03	0.2	21.2	169.	--
S230	TEFE RIVER	105.	0.3013	12.2	5.6	--	0.02	--	0.2	0.02	0.7	11.38	159.	--
S225	COARI R.	172.	0.2493	15.9	6.2	--	0.05	--	2.2	0.04	0.9	7.76	172.	--
A-21	NANAY R.	67.	0.0963	8.9	3.8	26.	--	--	3.2	--	--	80.6	236.	--
S309	JANDIATUBA	80.	0.2705	9.3	4.6	--	0.06	0.05	8.5	0.02	--	24.7	121.	--
S309A	VARZEA L.	67.	0.2113	10.1	4.6	--	0.05	0.07	7.0	0.02	--	--	106.	--
S315	JUTAI R.	130.	0.4713	9.1	5.5	27.	0.10	0.22	1.4	0.04	--	80.8	190.	--
S319	TEFE RIVER	70.	0.1653	11.7	7.5	30.	0.07	0.25	0.5	0.02	--	19.5	160.	--
S319A	TEFE RIVER	70.	0.2545	10.7	7.4	34.	0.06	0.11	0.5	0.02	--	16.3	153.	--
S322	COARI R.	74.	0.2302	9.8	6.5	30.	0.06	0.32	0.1	0.04	--	10.68	174.	--
S337A	MATARI R.	71.	0.3391	4.8	32.1	29.	0.07	0.09	0.3	0.0	--	53.9	258.	--
NAN01	NANAY R.	43.	0.7068	5.3	2.8	--	--	--	--	--	--	5.80	134.	--
BPA12	NANAY R.	55.	0.3918	5.5	3.3	26.	0.09	--	2.3	--	--	60.2	197.	--

VARZEA WATERS (10)

STA.	PARAMETER: -LOCATION-	TZ+	PH	NA	K	MG	CA	ALK	CL	SO4	SI	FE-T	FE-U	AL-T	AL-U
S246	CAYARU R.	--	6.60	173.	36.6	87.2	401.	1015.	--	31.6	183.	1.8	--	0.1	--
S245	VARZEA L.	1135.	6.90	175.	33.7	84.9	378.	946.	103.5	37.	189.	2.1	0.0	0.3	0.1
S244	VARZEA L.	--	6.79	--	--	--	--	898.	--	--	196.	2.3	--	0.5	--
S308	VARZEA L.	657.	6.44	90.	25.6	51.0	220.	553.	54.0	17.4	142.	1.1	0.3	0.3	0.3
S312	VARZEA L.	1009.	6.87	148.	30.4	72.3	343.	826.	96.8	38.	164.	1.0	0.2	0.3	0.3
S317A	MINERUA P.	391.	6.41	48.2	29.3	35.4	121.3	345.	5.8	4.2	153.	2.0	0.9	0.2	0.3
S320	CAIAMBE L.	126.	5.91	41.0	23.3	12.4	17.8	92.	10.1	1.2	184.	3.4	3.4	0.9	0.9
S325	CABOLIANA	600.	6.56	89.	26.5	51.4	191.	509.	39.7	21.5	119.	1.4	0.7	0.1	0.4
S330	MAMAURU L.	413.	6.58	58.0	25.2	43.7	121.3	320.	33.0	24.9	129.	1.3	0.7	0.2	0.3
LJ1	JANAURY L	584.	7.10	99.	22.4	49.1	182.	467.	50.3	30.5	148.	--	1.2	--	0.2

STA.	PARAMETER: -LOCATION-	TZ+	NICB	TDS	CYCL	TEMP	P04	P-T	NO3	NO2	NH4	CO2	COL	TOC
S246	CAYARU R.	--	--	--	3.8	--	0.40	--	0.1	0.02	0.4	55.2	109.	--
S245	VARZEA L.	1135.	0.0109	98.0	3.8	--	0.43	--	0.0	0.0	0.2	24.6	95.	--
S244	VARZEA L.	--	--	--	3.8	--	0.40	--	0.0	0.0	0.0	31.5	--	--
S308	VARZEA L.	657.	0.0204	58.3	4.3	--	0.29	0.36	2.1	0.03	--	42.0	163.	--
S312	VARZEA L.	1009.	0.0029	87.6	3.9	27.	0.46	0.47	7.5	0.03	--	22.9	153.	--
S317A	MINERUA P.	391.	0.0808	36.9	5.8	28.	0.35	0.46	0.6	0.02	--	28.5	260.	--
S320	CAIAMBE L.	126.	0.1590	18.8	10.1	--	0.06	0.25	0.4	0.04	--	24.4	213.	--
S325	CABOLIANA	600.	0.0138	53.2	4.6	30.	0.14	0.46	0.2	0.0	--	30.8	211.	--
S330	MAMAURU L.	413.	0.0255	38.4	7.6	--	0.13	0.24	0.1	0.0	--	17.7	195.	--
LJ1	JANAURY L	584.	0.0036	53.8	5.4	--	--	--	3.4	--	--	7.77	88.	--

MAIN CHANNEL (1*): SAMPLES FROM TRIBUTARY MIXING ZONES

STA.	PARAMETER: -LOCATION-	TZ+	PH	NA	K	MG	CA	ALK	CL	SO4	SI	FE-T	FE-U	AL-T	AL-U
S248	AM.B.NAPO	976.	--	174.	28.4	74.1	313.	766.	102.2	48.	187.	1.2	0.0	0.1	0.2
S239	SO.AMATAU	1041.	7.27	163.	28.2	74.7	350.	828.	92.8	51.	176.	1.0	0.0	0.6	0.4
S221	SO.IUARA	444.	6.59	66.4	24.2	41.0	135.2	364.	25.8	15.6	141.	1.3	0.0	0.1	0.3
S218	AM.CONFL.	441.	6.61	66.1	19.0	35.5	142.2	344.	33.5	15.0	118.	2.3	0.2	0.9	0.2
S214	AM.AMATARI	554.	6.68	81.	23.1	44.9	179.	443.	41.5	18.9	137.	1.4	0.1	0.5	0.1
S213	AM.AMATARI	246.	6.18	39.9	14.0	20.3	74.8	155.	18.2	7.4	93.	3.4	2.3	2.1	0.7
S211	AM.ITACOA-	488.	6.65	73.	24.9	51.8	142.8	344.	28.8	25.9	136.	1.3	0.1	0.2	0.1
S210	AM.PARANT-	397.	--	61.4	20.5	38.3	118.8	283.	34.9	16.7	119.	2.1	0.1	0.4	0.1
S205	AM.ITUQUI	404.	6.64	58.0	20.7	37.9	124.4	295.	21.3	15.1	124.	1.3	0.5	0.3	0.2
S310	SO.SAO PA-	1210.	7.04	178.	33.4	82.4	417.	971.	110.9	47.	175.	0.8	0.3	0.1	0.4

STA.	PARAMETER: -LOCATION-	TZ+	NICB	TDS	CYCL	TEMP	P04	P-T	NO3	NO2	NH4	CO2	COL	TOC
S248	AM.B.NAPO	976.	0.0037	85.9	3.8	--	0.40	--	7.8	0.10	0.3	--	71.	--
S239	SO.AMATAU	1041.	0.0080	90.1	3.8	--	0.46	--	9.8	0.04	1.3	9.20	67.	--
S221	SO.IUARA	444.	0.0469	40.8	4.8	--	0.32	--	2.1	0.05	0.7	19.7	109.	449.
S218	AM.CONFL.	441.	0.0690	37.9	5.2	--	0.23	--	3.4	--	0.6	17.8	185.	--
S214	AM.AMATARI	554.	0.0491	48.2	4.8	--	0.36	--	4.2	--	0.8	19.4	110.	--
S213	AM.AMATARI	246.	0.2167	18.3	6.1	--	0.20	--	3.5	--	1.0	21.9	284.	--
S211	AM.ITACOA-	488.	0.1181	39.1	5.2	--	0.30	--	5.7	--	0.6	16.2	99.	753.
S210	AM.PARANT-	397.	0.1043	32.9	5.8	--	0.29	--	4.4	--	1.0	--	133.	--
S205	AM.ITUQUI	404.	0.1299	32.8	5.8	--	0.28	--	4.6	0.09	0.1	14.24	124.	257.
S310	SO.SAO PA-	1210.	0.0194	101.5	3.9	--	0.52	0.57	9.6	0.02	--	18.3	141.	--

basin: limestones, red beds, and igneous and metamorphic rocks are concentrated in its center, while in the east the river flows across the fluvial-lacustrine sediments of the lowlands. Tributaries from the north drain large areas of igneous, metamorphic and recent volcanic rocks.

Most of the sampling was in the Huallaga Basin. The Huallaga rises on the north end of the Peruvian altiplano (Figure IV.10) (Intercordilleran Zone) in a region of complex geology, featuring carbonates (Jurassic), lithified red beds (Permian), dark shales (Paleozoic), Precambrian basement, and extensive sulfide mineralization. The river crosses the Cordillera Oriental and flows into the Subandean Trough, with Precambrian and Paleozoic of the Cordillera on the left and the post-Paleozoic, Subandean, on the right. The river turns to the northeast, and crosses a thick section of red beds and carbonates before flowing over the fluvio-lacustrine cover of the lowlands (Figure IV.11).

The influence of evaporites primarily of Permian and Jurassic age are seen throughout the basin. All rivers with high chlorides have either outcrops of Permian and Jurassic red beds, faults from which salt springs can issue, or salt diapirs. A salt spring (A-05) and two streams draining salt (A-10, BPA16) were sampled. Water draining the diapirs is very chloride rich with a $\text{Cl}:\text{SO}_4$ mole ratio of about 15:1 (A-10) and 34:1 (BPA16) (sea water is 19:1), suggesting rapid dissolution of NaCl versus CaSO_4 . Water from the spring had a $\text{Cl}:\text{SO}_4$ ratio of 4:1, a $\text{SO}_4:\text{Ca}$ ratio of 1.1:1, and smelled faintly of H_2S , suggesting that an additional contribution of sulfur, perhaps reduced, was present. In the stretch of river that passes through the main area of salt domes, A-13 ($\text{Cl}=392 \mu\text{moles/l}$) to A-17 ($\text{Cl}=940 \mu\text{mole/l}$), the chloride concentration increases 2.4 times, suggesting that salt extrusions and springs are a major chloride source in the Huallaga Basin. In contrast, sulfate concentrations increased only slightly (136 to

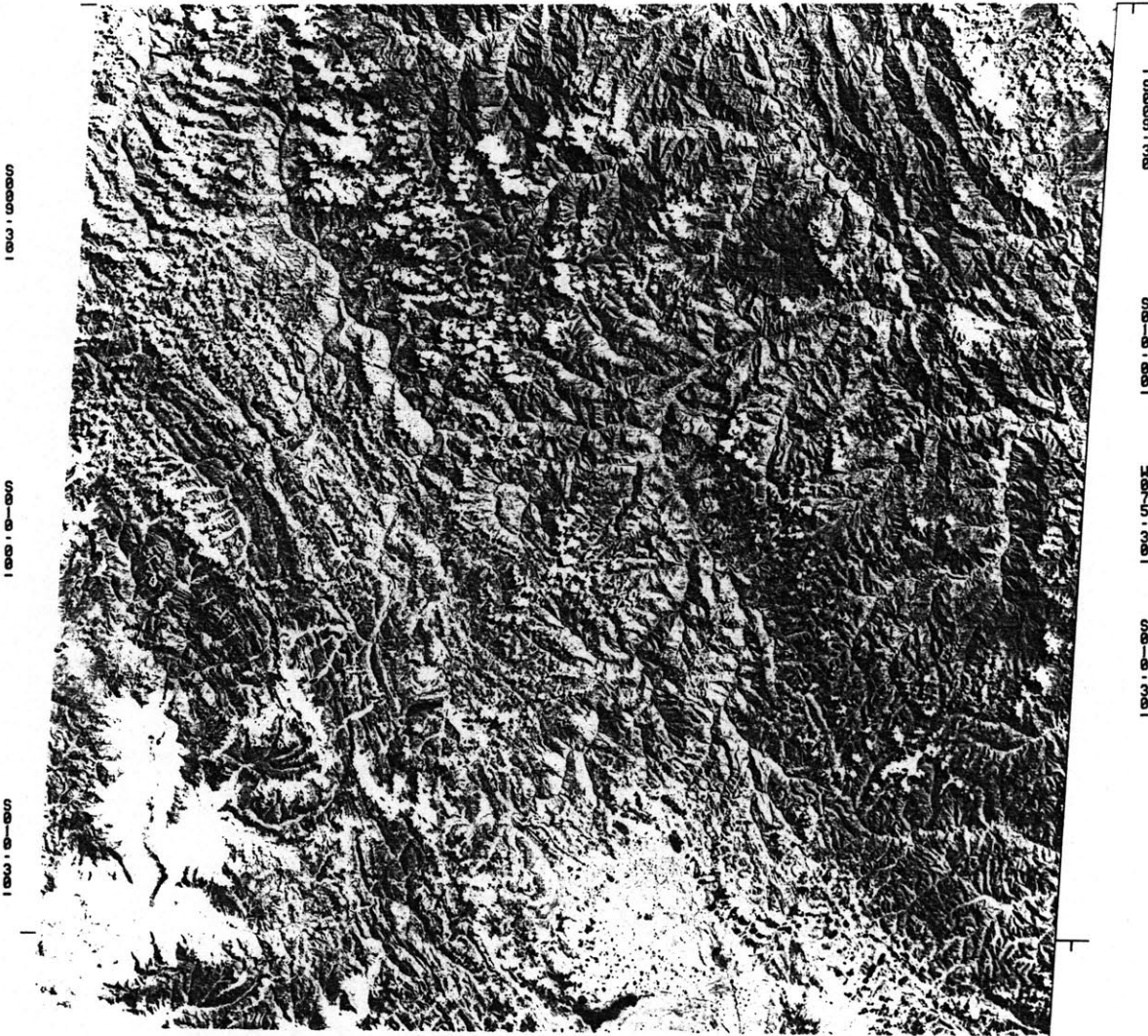
Figure IV.10

Photograph of the headwaters of the Huallaga and Marañon Rivers. The canyon, with the sharp bend to the right of the center of the picture is the valley of the Huallaga River. The bend to the east is followed by a sharp turn to the north. The bright valley in the upper left of the photograph is the canyon of the Marañon. Both rivers rise near the north end of the altiplano, which is the white area in the lower right.

14877-00

14876-301

14876-001



1 0 0 0 1 0 0 0 0 0 0 0

1 0 0 0 1 0 0 0 0 0 0 0

1 0 0 0 1 0 0 0 0 0 0 0

1 0 0 0 1 0 0 0 0 0 0 0

1 0 0 0 1 0 0 0 0 0 0 0

1 0 0 0 1 0 0 0 0 0 0 0

1 0 0 0 1 0 0 0 0 0 0 0

11APR76 C S10-03/14876-24 N S10-03/14876-23 MSS 6 R SUN EL 45 AZ066 189-6203-A-1-N-P-2L NRSA EXTS E-2445-14254-6 01

14877-001

14876-301

14876-001

S011-001

016

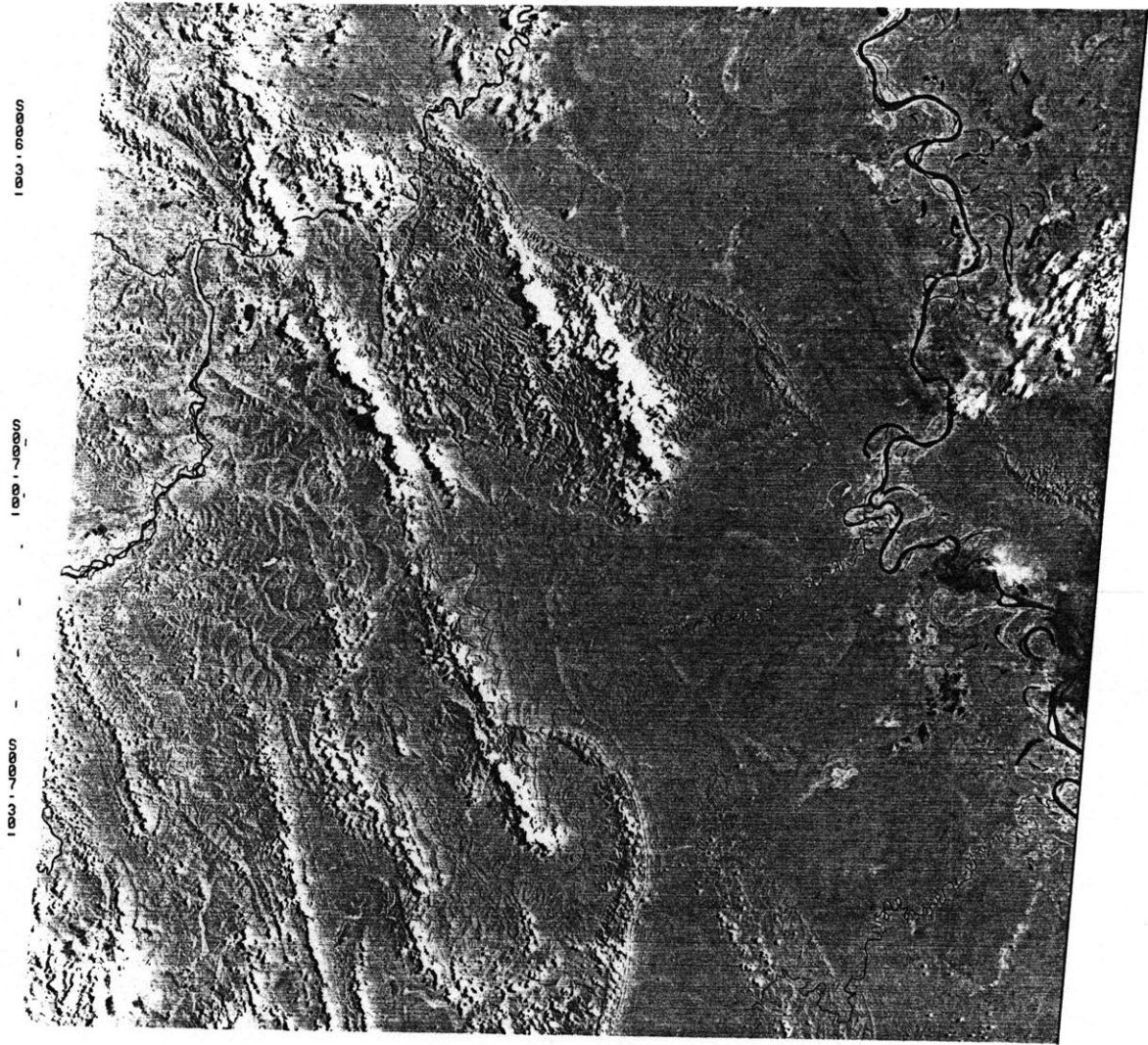
Figure IV.11

Photograph of the lower course of the Huallaga and Ucayali Rivers. The Huallaga is the river crossing the upper left. The other large river is the Ucayali. The hills in the picture represent the edge of the Andean uplift. The uplift of the Pilluana salt dome, sampled in this study (see Figure III.4), has resulted in the formation of the lake (black patch) down and to the right of the large sharp bend in the Huallaga River.

W076-001

W075-301

W075-001



W076-001

W076-001

W076-001

W075-001

W075-001



W076-30 020CT72 C S07-00/W075-45 N S07-06/W075-38 W076-001 R55 6 R SUN EL57 A2085 S008-001 W075-30 188-0388-A-I-N-D-2L NASA ERTS E-1071-14405-6 02



151 $\mu\text{mole/l}$). Sulfur is widely distributed through many rock types in the basin, and salt extrusions are apparently of lesser importance as a sulfate input.

The importance of salt springs or minor extrusions can best be seen by comparing the Aspasarta (A-08) with the Uchiza (A-09) and the Shanusi (A-18,BPA14) with the Paranapura (A-19,BPA15). Each of these pairs has similar geology and a major fault running through the basins, however the Uchiza has higher chloride concentrations than the Aspasarta, and the Paranapura has higher concentrations than the Shanusi. This contrast is thought to be due to minor salt springs and perhaps salt extrusions on the faults in the Uchiza and Paranapura basins. Much of the salt input in the latter basin is localized on the Cachiyacu (salt water) tributary.

Carbonate rocks are found in most of the rivers sampled in the Huallaga Basin. The chemistry of only two of the sampled rivers, the Aspasarta (A-08) and the Uchiza (A-09), appear to be dominated by carbonate weathering. Both basins drain primarily carbonates (Jurassic and Cretaceous respectively) and red beds (Cretaceous). (Ca+Mg) constitute greater than 90% of the cations and HCO_3 greater than 80% of the anions in the samples. The Aspasarta has a Ca:Mg mole ratio of 9.7:1 and the Uchiza has 7.5:1; equivalent ratios of (Ca+Mg):(Na+K) are 26.2:1 and 10.7:1 respectively.

Red beds are such a conglomeration of lithologies that it is hard to characterize their contribution to the dissolved load. Red beds apparently contribute little to the Aspasarta and the Uchiza. The Shanusi and Paranapura drain mostly red beds. They have low silica concentrations, 96-135 $\mu\text{mole/l}$, compared with Huallaga tributaries draining other rock types. If NaCl and CaSO_4 are subtracted from the data, their TZ+ average values are 725 $\mu\text{Eq/l}$ and 658 $\mu\text{Eq/l}$ respectively, still much higher than lowland tributaries.

Precambrian sediments and igneous rocks are the primary lithologies in the Chapira (A-04), Monzón (A-06), and Tocache (A-11) Basins. All have low levels of Ca and Mg compared to Na and K [(Ca+Mg):(Na+K) equivalent ratios are 5.8:1, 3.1:1, and 2.2:1 respectively], low TZ+ (852, 613, 462 $\mu\text{Eq/l}$) and high silica (203, 203, 244 $\mu\text{mole/l}$). All of these rivers have minor sedimentary outcrops in their lower courses (Chapira-limestones; Monzón-limestones, Paleozoic red beds and salt springs; Tocache-Paleozoic red beds); the Tocache Basin has negligible carbonates. The sulfate and chloride present in these rivers may be due to the weathering of the sedimentary rocks and locally mineralized zones in the Precambrian, along with minor precipitation inputs. The substantial increase in the silica between Huallaga samples A-02 (123 $\mu\text{mole/l}$) and A-13 (225 $\mu\text{mole/l}$) and drop in TZ+ (2894 to 1862 $\mu\text{Eq/l}$) is probably due to inputs from rivers draining igneous and metamorphic terrains.

All other samples taken in the Huallaga Basin come from geologically complex catchments. The chemistry of these rivers and the Huallaga itself is consistent with the observations that high silica and low (Ca+Mg):(Na+K) ratios, chloride, sulfate, and TZ+ values characterize rivers draining siliceous terrains, that high alkalinities, calcium, magnesium, and TZ+ characterizes rivers draining carbonate terrains, and that high sodium, chloride, TZ+, and sometimes calcium and sulfate characterizes rivers with even small salt deposits. The steep topography maximizes the exposure of all rock types, as a consequence relatively small areas of carbonate or evaporite rocks make a large contribution to the dissolved load of the rivers.

The Marañon is more dilute than its tributary, the Huallaga, especially with respect to Na and Cl, consistent with observations that extensive evaporite exposures are not characteristic of the geology of the Marañon Basin as a whole.

IV.4:4 Ucayali Drainage (3)

The principal differences between the Ucayali Basin and the Marañon Basin are the increased abundance of Lower Paleozoic sediments (slightly metamorphosed), red beds, Upper Tertiary to recent volcanic sediments, bedded evaporites, and the reduced area of lowland fluvio-lacustrine sediments. The major element solution composition of the Ucayali and the Huallaga are similar except for sodium and chloride, which are more concentrated in the latter river. The geologic layouts of the Ucayali and Huallaga rivers are quite similar, draining from the Intercordilleran Zone, across the Cordillera Oriental into the Subandean Trough. The only tributaries sampled were from the Intercordilleran Zone. Samples from the Urubamba River (M-08, BPA08) show the effects of the great Mesozoic evaporite deposits near Cuzco. These evaporites are either bedded or brought to the surface as large springs (c.f. Benevides 1968, and Section III.3:3). This drainage has very extensive exposures of recent (andesitic) volcanics and lesser exposures of Lower Paleozoic shales, limestones, and granite-granodiorites. The high silica and alkalinity suggest that rapid weathering of both carbonate and silicate rocks is occurring.

IV.4:5 Madeira Drainage (4)

Lower Paleozoic sediment dominates the entire Andean drainage of the Madeira Basin. Samples were taken (M-04, M-03, BPA04) representing a north-south transect of large rivers draining the southern Peruvian and Bolivian Andes. These samples cover a transition from moderately metamorphosed Lower Paleozoic, in southern Peru, to unmetamorphosed Lower Paleozoic in central Bolivia, and a corresponding thickening of the Lower Paleozoic section. These geologic trends are paralleled by changes in river chemistry, notably a drop in the Ca:Mg ratio (3.0, 1.4, and 1.3, respectively) and the Alk:SO₄

ratio (12.4, 4.2, 1.7). Several of the rivers in the Madeira basin (M-03, M-05, BPA01, BPA02, BPA03, BPA04, BPA06) stand out above the SO_4 -TZ+, MG-TZ+ and K-TZ+ trends and below the Cl-TZ+ and the alkalinity-TZ+ trends in Figures IV.4, IV.5, IV.6, and IV.7. In view of the geology (i.e. no evaporites, few limestones and dolomites), the only reasonable explanation for these separate Madeira Basin trends is the weathering of sulfur-containing Lower Paleozoic shales. The weathering of reduced sulfur-containing rocks has been described by Holland (1978 p. 46), who suggests that sulfuric acid generated by the weathering of pyrite should react with silicate minerals in a manner analogous to H_2CO_3 . This is best seen in sample (BPA01 - the Ichilo, draining Devonian shales, see also M-05) where the sulfate is present in excess of the amount needed to balance calcium and magnesium. The high potassium and magnesium trends are a reflection of their greater abundance in black shales than is typical for other rock types (Table III.1). The waters from the Madre de Dios River (M04) are the least sulfur enriched, an indication that metamorphism of the Lower Paleozoic may have lowered the concentration of reduced sulfur in the rocks, or may have made them less prone to weathering; alternatively there may be a significant sedimentary facies change going north, although no change is described in the literature.

The inputs of chloride from Cambrian evaporites is evident in samples from the San Mateo (BPA02) and Espiritu Santo (BPA03) rivers. The Guapay or Grande River (BPA05) and Piray River (BPA06) are compositionally unusual. If sodium is corrected for its NaCl component, a large sodium residual remains (770 and 462 $\mu\text{mole/l}$, respectively), greater than twice the residual for any other sample. Furthermore, the samples have very high potassium, however the silica concentrations are not exceptionally high. These samples include flash flood runoff from the first day of the rainy season. A downstream sample (BPA04), taken the day before, shows none of the sodium bicar-

bonate enrichment of these samples. It is thought this chemistry is due to partial re-resolution of soil salts during rains in a semi-arid climate, as described by Drever and Smith (1978), who demonstrate that resolution results in a preferential release of rapidly soluble salts. Silica is the species most slowly redissolved. Salares (salt pans) are observed in the lowlands immediately to the south of the Guapay Basin, showing that conditions for concentrating soil salts exist in the area. The Guapay has some evaporites in the highland part of its basin.

IV.4:6 Andean Magnesium and Calcium Inputs

Inspection of the Mg-TZ+ plot shows that for rivers draining Andean sedimentary terrains, two distinct Mg-TZ+ trends exist. All the samples from the upper trend are either from the Intercordilleran Zone in Peru (Marañon: S-2,A-02,A-03,A-04,A-07,Ucayali: A-01,M-08,BPA08) or the Madeira Basin (listed above). The samples in the lower trend are from rivers rising in the Subandean Trough, and from main channel and the lower courses of the Marañon, Huallaga, and Ucayali. This latter observation suggests that foreland weathering inputs dominate the chemistry of Andean contributions to the Amazon River. The apparently overwhelming contributions of dissolved materials from the foreland areas undoubtedly reflects the combination of high precipitation (c.f. Hoffman 1975) and runoff on steep slopes developed on easily weathered lithologies (c.f. Section III.4:8). The foreland contribution is well illustrated by the Huallaga samples A-02, A-07, A-12, corresponding to the Cordillera Oriental, and first and second Subandean samples, respectively. The corresponding sequence of Mg:TZ+ ratios is observed: 1:4.5, 1:5.2, and 1:7.9. The high proportions of Mg in the Madeira compared to the main channel, at their confluence, reflects the presence of high magnesium rivers rising in the foreland.

There does not appear to be a single cause for the high magnesium trend. In the north and central Intercordilleran Zone of Peru, the high magnesium may be derived from the Lower Jurassic, Pucara Group, (sequence of limestones with dolomites, and dolomitic limestones) and perhaps outcrops of Lower Paleozoic, in the regions to the south, the Lower Paleozoic shales appear to be the only likely source; these may have dolomitic matrices.

IV.4:7 Other Andean Headwater Rivers: Napo, Iça, Japurá (5)

These rivers begin in the Northern Andes, in a region with much less exposed marine sediment than in the Peruvian and south Ecuadorian Andes.

The Napo River has the most extensive mountain drainage of the three rivers. The Andean drainage rises in the Precambrian-cored Cordillera Central, an area of much recent volcanic activity; ash forms a ubiquitous cover. The rivers cross a thinned Paleozoic and Mesozoic section, with little evaporitic material, and then flow over young fluvial-lacustrine sediments. Chemically the Napo at its confluence with the mainstem resembles the rivers draining the Precambrian in the Huallaga Basin.

The Iça River has a very small Andean drainage compared to its lowland drainage. The Andean part of its drainage is similar to that of the Napo. The dilute nature of the Iça indicates that lowland inputs dominate its chemistry.

The Japurá River has a geology very similar to the Iça, and on this basis would be expected to have a similar chemistry, however this is not the case, as the Japurá is richer in dissolved materials. In Chapter V, it is shown that, at the time of sampling, a 50:50 mixture of Iça-like and main channel water (supplied to the Japurá through the Aranapu Paraná), provides a better fit to water and chemical discharge data, than does an assumption of no main channel contribution. This contribution undoubtedly varies in magnitude during the year. Tastivin (1929) observes that upriver

of the confluence between the Japurá and the Aranapu, the waters of the Japurá are clear (like those of the Iça).

IV.4:8 Negro Drainage (6)

The Negro River drains primarily Precambrian Shield. Tertiary fluvial-lacustrine sediments are found on the south side of its lower course. The basin can be divided into two parts: (1) The upper and lower Negro Basin, and (2) the Branco Basin. The former region is essentially a peneplain, bordered on the north by the highest elevations in Brazil (Figure IV.12). The soils are the most intensely weathered in the Amazon Basin (c.f. Section III.4:2). The upper Negro Basin has no dry season, and the Negro Basin as a whole has the greatest runoff of any lowland region. The Branco Basin (Figure IV.13) has moderately developed topography, with several erosion surfaces separated by scarps. The basin is far drier than the rest of the Negro Basin, having a large area of savanna, a pronounced dry season, and rather low runoff. The Branco carries an appreciable sediment load (kaolinite, Irion 1976), while the Negro has very little suspended sediment; this sediment has a very low Si:Al ratio (Price and Sholkovitz 1978). The Negro River waters are sufficiently acid that they facilitate the flocculation of Branco sediment, having a pH near the zero point of charge for kaolinite (Leenheer and Santos 1979).

The Negro River is the most dilute of all large Amazon tributaries, and is completely unlike any other river draining the shields. The Branco Basin contributes significantly to the dissolved load of the Negro as can be seen by comparing samples from UN2, BR2, and LN2, taken from the upper Negro, Branco, and lower Negro near Manaus, respectively, within the period of a few days. When normalized to silicon, the major element compositions of upper Negro River water and "average shield" rocks are quite similar:

	<u>(UN1 UN2)/2</u>	<u>Shield</u>
Na	0.095	0.112
K	0.119	0.062
Mg	0.035	0.042
Ca	0.073	0.069
Si	1.000	1.000
Fe	0.057	0.067
Al	0.067	0.313

This is indicative of very efficient weathering of rocks in the Negro Basin, including significant dissolution of iron and aluminum from the parent rock. The quartz residual (giant podzol) soil (described in Section III.4:5) is probably the principal solid residue of this intense weathering. A source for the high potassium in the Negro samples may be the degradation of residual potassium-bearing minerals in more clay-rich soils, which are also found in the basin. If this is the case, present weathering in the Negro Basin must be more intense than were the conditions under which the clay-rich soils accumulated.

IV.4:9 Other Shield Rivers: Xingu, Tapajós, Trombetas (7)

These rivers are geologically and climatologically similar to the Branco Basin. All start in elevated shield terrains. The Xingu and Tapajós also have savanna in their headwaters, and all have pronounced wet and dry seasons. The Xingu is in the driest basin. The Trombetas and Tapajós cross the Paleozoic sediments of the Amazon Trough, and both have some exposed gypsum (c.f. Sioli 1963). Higher sulfate is seen in the analyses of the water from the Trombetas (S208, S332) than from the Tapajós (S206, S335). Presumably this difference is because Paleozoic sediments cover a larger fraction of the Trombetas Basin. The Xingu is much more cation rich than the Tapajós, which is adjacent to it. This may be due to the drier climate in its basin or to the extensive area of Precambrian sediments found in its basin (Sombroek 1966, FAO/UNESCO 1971), associated with catio-rich soils.

Figure IV.12

Photograph illustrating the flatlands of the Upper Negro River Basin. The river crossing the middle of the photograph and turning north is the Upper Negro, and the large river coming in from the center left is the Uaupes River. Erosion escarpments can be seen in the upper right of the picture.

14067-30

14067-001

14066-301

14067-301

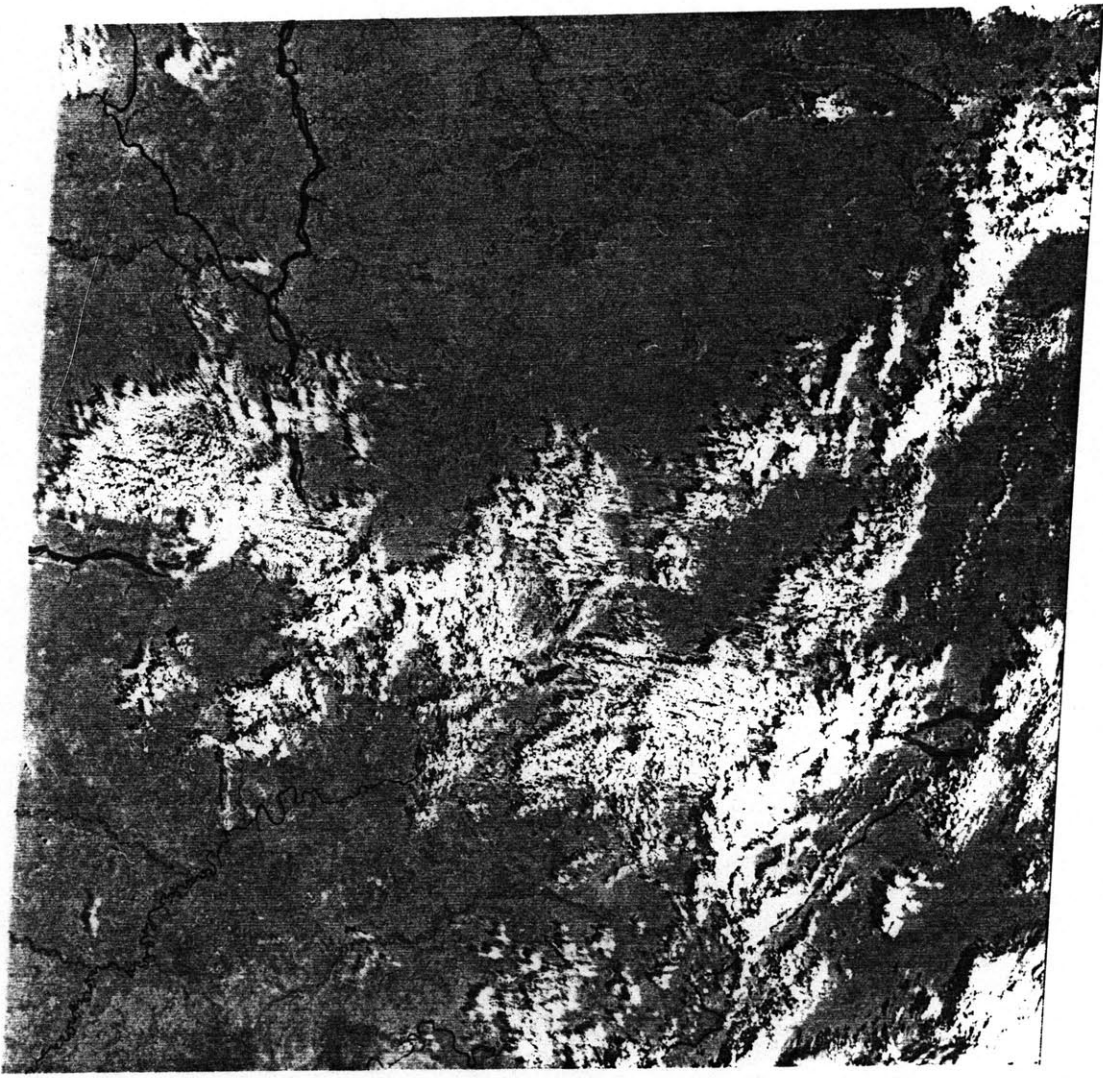
14067-001

14066-301

14067-301

14067-001

14066-301

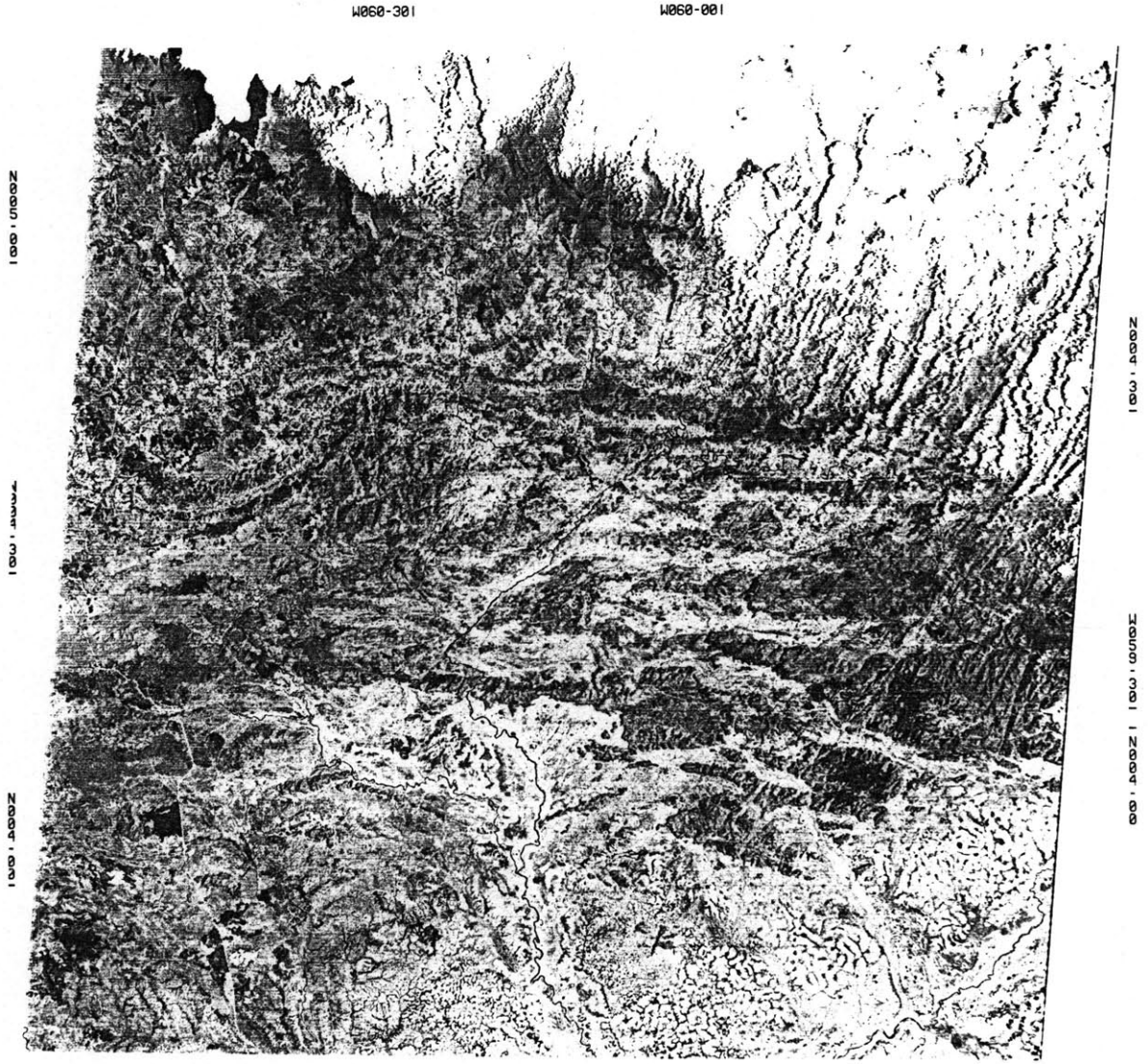


26DEC72 C N00-02/14066-58 N S00-00/14066-52 MSS 6 R SUN EL49 AZ127 188-2173-A-1-N-D-2L NRSA ERTS E-1156-14104-6 01



Figure IV.13

Photograph of the upper Branco Basin. This photograph should be compared to the previous picture. Savanna areas (bright) can be seen in the southern half of the photograph. Several erosional steps can be seen, marked by changes in color and the courses of roads and rivers. A very high escarpment can be seen in the upper left part of the photograph, as the border of a smooth black patch.



041PR73 C N04-24/W060-22 N N04-23/W060-15 MSS 6 R SUN EL52 AZ106 188-3121-N-1-N-D-2L NASA ERTS E-1224-13465-6 01



IV.4:10 Lowland Rivers Draining Marine Sediments: Javari, Juruá, Purus (8)

The headwaters of these rivers drain marine and continental sediment, deposited in the Subandean Trough (separated topographically by uplift), as well as large expanses of Tertiary fluvial-lacustrine sediment. Present headwater topography reaches 1000 meters. The three rivers have the highest dissolved solid levels of rivers not originating in the Andes. The Juruá, which drains the center of the uplifted area, has the highest level of dissolved solids, and except for lower levels of Na, Cl, and SO₄, and higher levels of Si, it resembles the Shanusi (A-18,BPA14), a river draining similar sediments in the Huallaga Basin. Both the Juruá and Purus have economic gypsum deposits in their basins, and all three rivers have considerable montmorillonite in their suspended load (c.f. Gibbs 1965, Irion 1976). When compared to rivers from the shield, the most notable characteristic of these three rivers is the higher concentrations of Ca, Mg and alkalinity, an indication of the importance of carbonate rocks in their basins.

A small stream near Obidos (S331) has been included in this group. This stream rises in Tertiary sediments overlying evaporites. The high chloride in this sample may indicate leaching from the evaporites.

IV.5:11 Rivers Draining Upper Tertiary Sediments (9)

All of these rivers are extremely dilute and are comparable to the Negro in composition. There is considerable variation in their major element composition. As Tertiary sediments are unmapped, however, it is not possible to relate these variations to any specific geological features. When compared to the Negro River, after cyclic salt corrections, the ratio of (Ca+Mg):(Na+K) is higher in the rivers draining Tertiary sediments. The Tefé (S230,S319,S319A) and the Matari (S337A), like the Negro, have K:Na ratios close to one. After cyclic salt corrections, the (near coastal) Matari

River has the lowest concentration of Na, K, Ca, and Si of all rivers sampled. The Nanay River (A-21, NAN01, BPA12), which drains Upper Tertiary sediments deposited near the rising Andes, shows low concentrations of all species, indicating that the sediments which it drains are weathered to a degree comparable to sediments in the Amazon Trough.

IV.4:12 Várzea Waters (10)

The highly productive nature of várzea (floodplain) soils and lakes is well known, being a consequence of the supply of nutrients from water and sediment of the main channel. Much of the water transferred to the floodplain during rising water eventually returns to the river, and biological processing in the várzea may affect chemical budgets in the basin.

Compositions of these lakes range from mainstem water composition to the composition of streams draining the adjacent (usually Tertiary) high ground (Terra firme) (Sioli 1951).

Samples collected during this work can be compared to the chemistry of water from the adjacent main channel:

Similar to main channel:
S244, S245, S246, S325, S330, LJ1

Intermediate:
S308, S312, S317A

Similar to Tertiary Rivers:
S320, S309A

The samples from várzea lakes similar in chemistry to the waters of the main channel provide a means of evaluating the potential effects of biological activity on the composition of surface waters. The nitrate concentration in these samples is greatly reduced, while phosphate, sulfate, and silicate are low in only some samples. This is thought to indicate clear biological effects for nitrate and possible effects for the other three species.

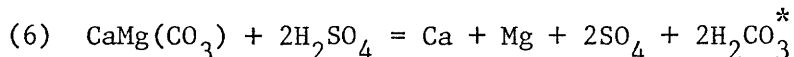
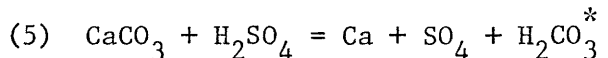
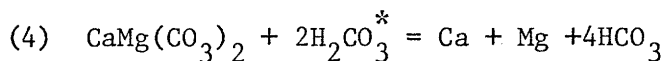
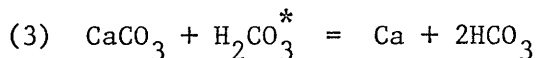
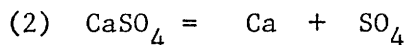
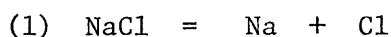
IV.4:13 Terrestrial Biological Effects

There is no direct way to identify the effects of terrestrial biological reservoirs (c.f. Section III.5) on the chemical budgets in the Amazon Basin without a detailed time series from lowland rivers. If biogeochemical budgets were constant and balanced, there would be no sensible effect on geochemical fluxes, however if there are seasonal gains and losses of elements in the biomass, one-time sampling of the type used in this study would not detect the effects. Elements for which a large proportion is found in the biomass, compared to soils, are Ca, Mg, K, N, and perhaps S (c.f. Section II.5). Nitrate and sulfate show substantial variations in lowland rivers between 1976 and 1977 samples. All rivers which were sampled twice and which do not have marine sediments in their catchments (Negro, Tefé, Coari, Jutai, Nanay) show factor of two variations in calcium (the Coari also show a factor of two variation in magnesium). Other species do not show such great variation in these rivers. The variability in sulfate, nitrate, calcium, and magnesium may reflect changes in biological reservoirs.

IV.5 GEOLOGICAL CONTROLS OF HIGH TZ+ RIVERS

Only a few readily weathered minerals are commonly found in marine sedimentary rocks and marine and continental evaporites in the Amazon Basin. These minerals are calcite (CaCO_3 , with some Mg), dolomite ($\text{CaMg}(\text{CO}_3)_2$), gypsum or anhydrite ($\text{CaSO}_4 \cdot 2\text{H}_2\text{O}$, CaSO_4), and Halite. Some evaporite in the Amazon may contain potassium and magnesium salts at low concentrations (most of the high K points in Figure IV.7 are from rivers draining evaporites).

All of these minerals weather congruently (have no solid weathering products):



A source of protons is necessary for rapid weathering of the carbonates. This is typically carbonic acid (Eq. 3 and 4), however sulfuric acid (Eq. 5 and 6, found in precipitation and in the products of the weathering of reduced sulfur minerals, e.g. from black shales) nitric acid (oxidation of ammonia and organic nitrogen), and organic acids (evidenced by NICB) are also probable proton sources. Only HCO_3 and SO_4 are abundant anions in high TZ+ waters. Note that without additional geologic information it would not be possible to differentiate situations where combinations of Reactions (2) to (6) are occurring, there being only three conservative dissolved phases (Ca, Mg, and $\text{HCO}_3 = \text{Alk}$).

The analyzed inorganic species are charge balanced at high TZ+ (Figure

IV.9). If the above reactions are the sources of inorganic ions in these samples, then stoichiometric balances would be expected between (Na+K) and Cl (assuming evaporitic potassium is in a chloride salt), and between $2(\text{Ca}+\text{Mg})$ and $(\text{Alkalinity} + 2\text{SO}_4)$. A stoichiometric balance might be expected between $2(\text{Ca}+\text{Mg})$ and Alkalinity in terrains where sulfur containing minerals are not common, as is the case in many of the carbonate areas in the Andes.

The graph of (Na+K) versus Cl (Figure IV.14) demonstrates that at high concentrations, the data distribution approaches the 1:1 trend characterizing a pure evaporite source. The dispersion of samples above this trend, at lower chloride concentrations, undoubtedly reflect inputs from the weathering of sodium and potassium aluminosilicates which, like carbonate weathering, need a source of protons to proceed efficiently (Section IV.6:5).

The plot of $2(\text{Ca}+\text{Mg})$ versus $(\text{Alkalinity} + 2\text{SO}_4)$ (Figure IV.15) shows a high correlation throughout the entire data range, becoming particularly tight and approaching the theoretical 1:1 limit at higher concentrations. The tendency for data to fall below the 1:1 trend reflects the requirement that a portion of the anions balance Na and K produced by silicate rock weathering. Silicate rock weathering is a minor contribution in high TZ+ waters, hence the convergence to the 1:1 trends in Figures IV.14 and IV.15. The greater scatter of the data at low concentrations in Figure IV.14 reflects the opposing effects of an increased contribution of Na and K relative to Ca and Mg, causing a downward shift in the data, and an increased contribution of NO_3 and organic anions relative to Alk and SO_4 , causing an upward shift.

It is not possible to distinguish inputs of calcium and magnesium from silicate rocks from products of reactions (3-6) on the basis of chemistry

alone (c.f. Garrels 1967, Garrels and Mackenzie 1971, Holland 1978). However, inputs from the weathering of calcium and magnesium silicates should be similar in spatial distribution and magnitude to inputs from the weathering from sodium and potassium silicates, as there are no terrains dominated by silicates that are extremely rich in either alkalis or alkaline earths.

There is apparently an upper limit of alkalinity input from the weathering of carbonates, clearly seen in a plot of (Ca+Mg) versus alkalinity (Figure IV.16). The concentration of (Ca+Mg) varies independently of alkalinity, at high concentrations. In these samples, sulfate replaces alkalinity as the principal species in the charge balance. This is illustrated in a ternary plot of (Ca+Mg), Alkalinity, and SO_4 (Figure IV.17). Note that the samples tend to be confined to a field defined by charge balance trends for $(\text{Ca,Mg})(\text{HCO}_3)_2$ and $(\text{Ca,Mg})\text{SO}_4$ expected from reactions (3-6). The weathering of calcium and magnesium silicates would be expected to also fall in this field, however only rivers draining marine sediments are identified with large symbols on this graph, and silicate contributions are expected to be minimized in these rivers.

Figure IV.14

Sodium plus potassium versus chloride ($\mu\text{Eq/l}$). Note that all the samples fall on or above the one to one trend. The low concentration sample falling on the trend is from the Matari River, a river dominated by cyclic salt inputs.

Symbol key:

- + - (1) Main Channel
- * - (2) Marañon Drainage
- * - (3) Ucayali Drainage
- * - (4) Madeira Drainage
- ↓ - (5) Other Andean headwater rivers
- ◇ - (6) Negro Drainage
- - (7) Rivers draining shields
- ▽ - (8) Lowland rivers with extensive areas of marine sediments
- △ - (9) Rivers draining only U. Tertiary and Quaternary sediments
- X - (10) Varzēa waters

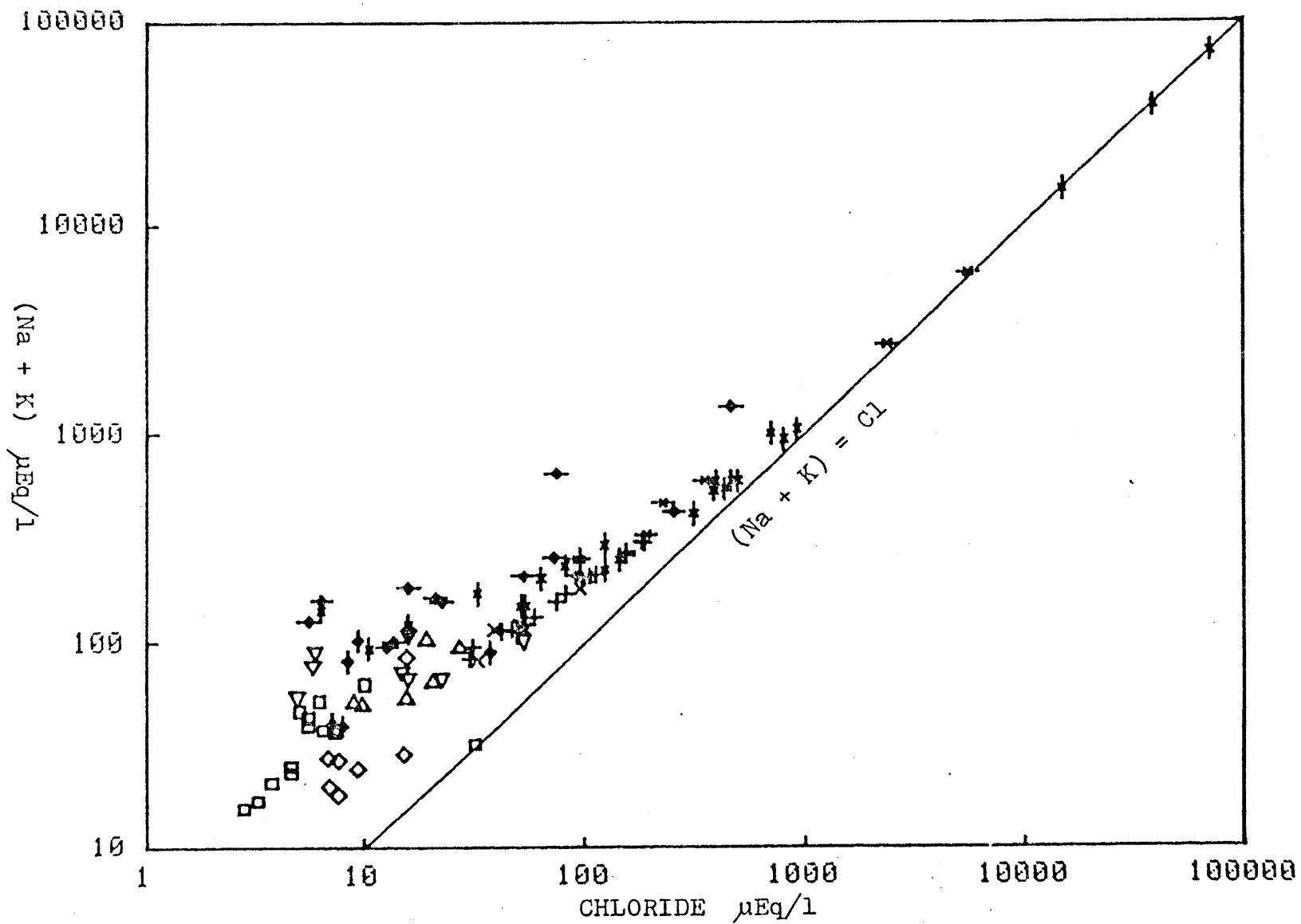


Figure IV.15

Calcium plus magnesium versus carbonate alkalinity plus sulfate ($\mu\text{Eq/l}$). This graph illustrates the charge balance between these parameters for rivers draining marine sediments, as is seen by the dense clustering of points along the one to one trend.

Symbol key:

- + - (1) Main Channel
- * - (2) Marañon Drainage
- * - (3) Ucayali Drainage
- * - (4) Madeira Drainage
- ♦ - (5) Other Andean headwater rivers
- ◇ - (6) Negro Drainage
- - (7) Rivers draining shields
- ▽ - (8) Lowland rivers with extensive areas of marine sediments
- △ - (9) Rivers draining only U. Tertiary and Quaternary sediments
- X - (10) Varzêa waters

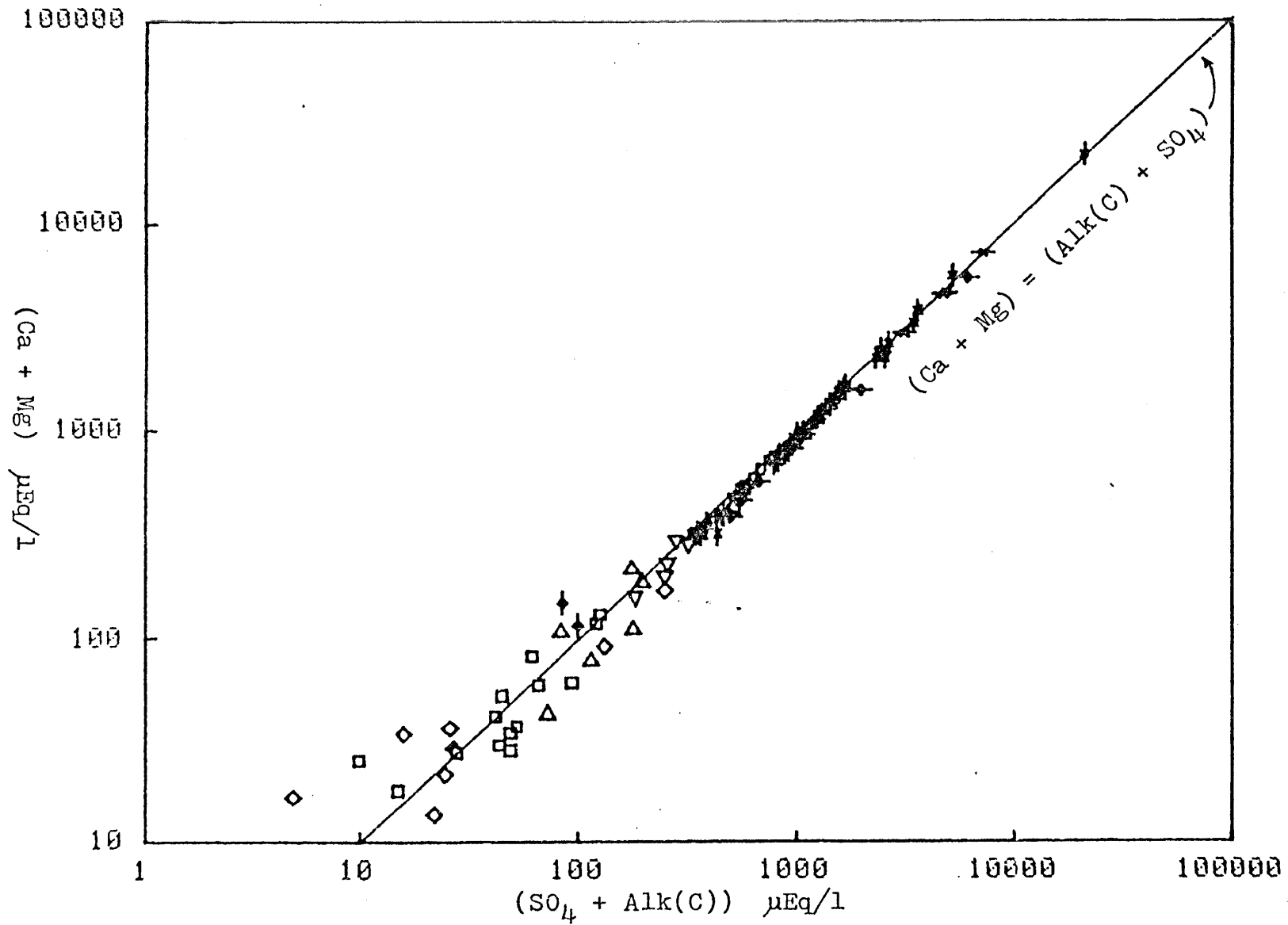


Figure IV.16

Calcium plus magnesium versus carbonate alkalinity ($\mu\text{Eq/l}$). This graph demonstrates that the charge balance seen in the previous graph is between the carbonate species, calcium and magnesium for most of the samples. There are two major exceptions to this, being samples with alkalinities above 1000 $\mu\text{Eq/l}$ which have a major sulfate component from evaporites, and samples from the Madeira Basin, in which sulfuric acid from the weathering of reducing sediments is a significant proton source in the weathering process. The upper limit for alkalinity is roughly 3000 $\mu\text{Eq/l}$. Since the concentration of calcium and magnesium is not similarly limited, it is suggested that carbonate solubility ultimately defines the maximum concentration of carbonate alkalinity in Amazon waters.

Symbol key:

- + - (1) Main Channel
- * - (2) Marañon Drainage
- * - (3) Ucayali Drainage
- * - (4) Madeira Drainage
- † - (5) Other Andean headwater rivers
- ◇ - (6) Negro Drainage
- - (7) Rivers draining shields
- ▽ - (8) Lowland rivers with extensive areas of marine sediments
- △ - (9) Rivers draining only U. Tertiary and Quaternary sediments
- X - (10) Varzêa waters

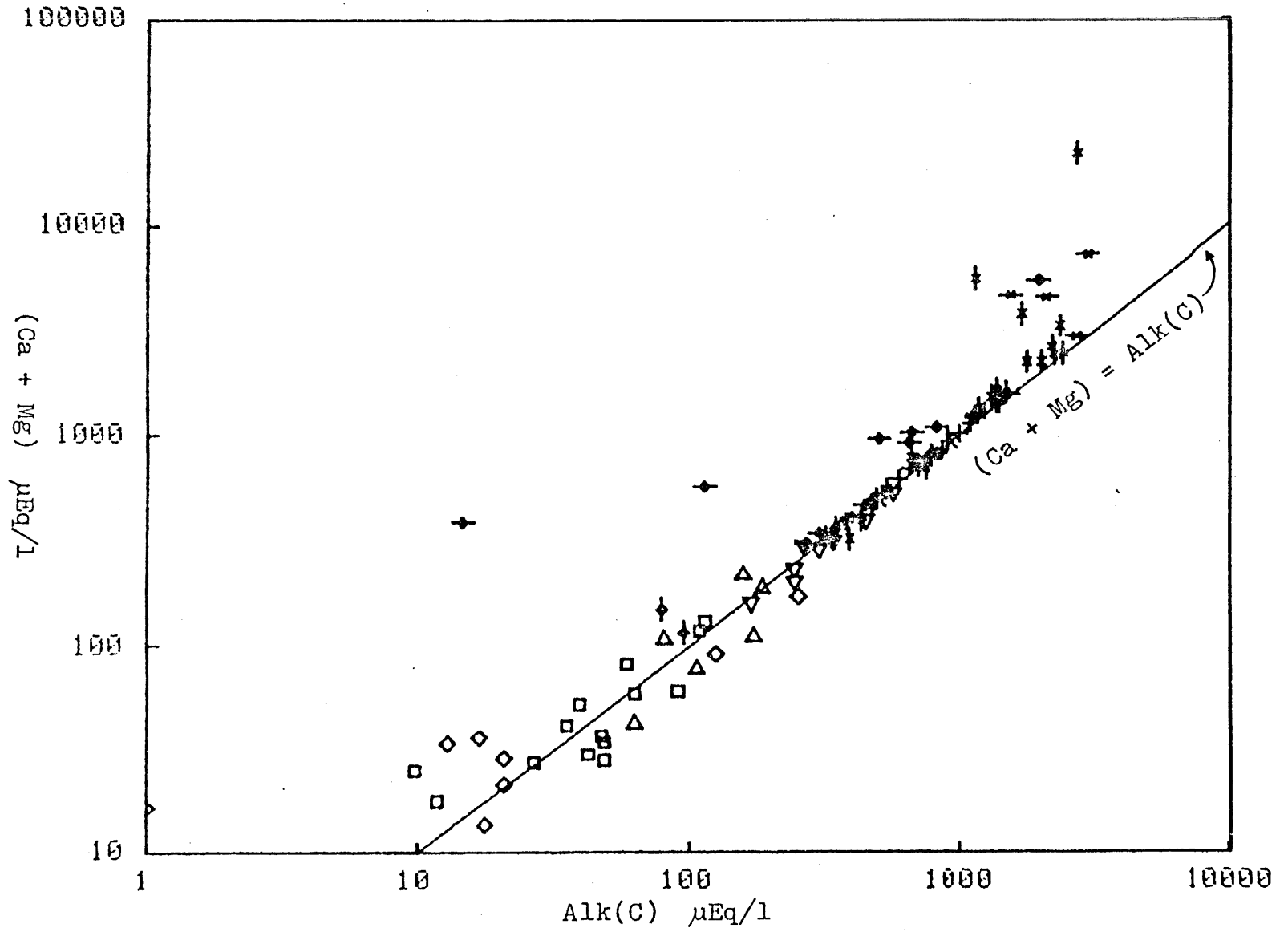
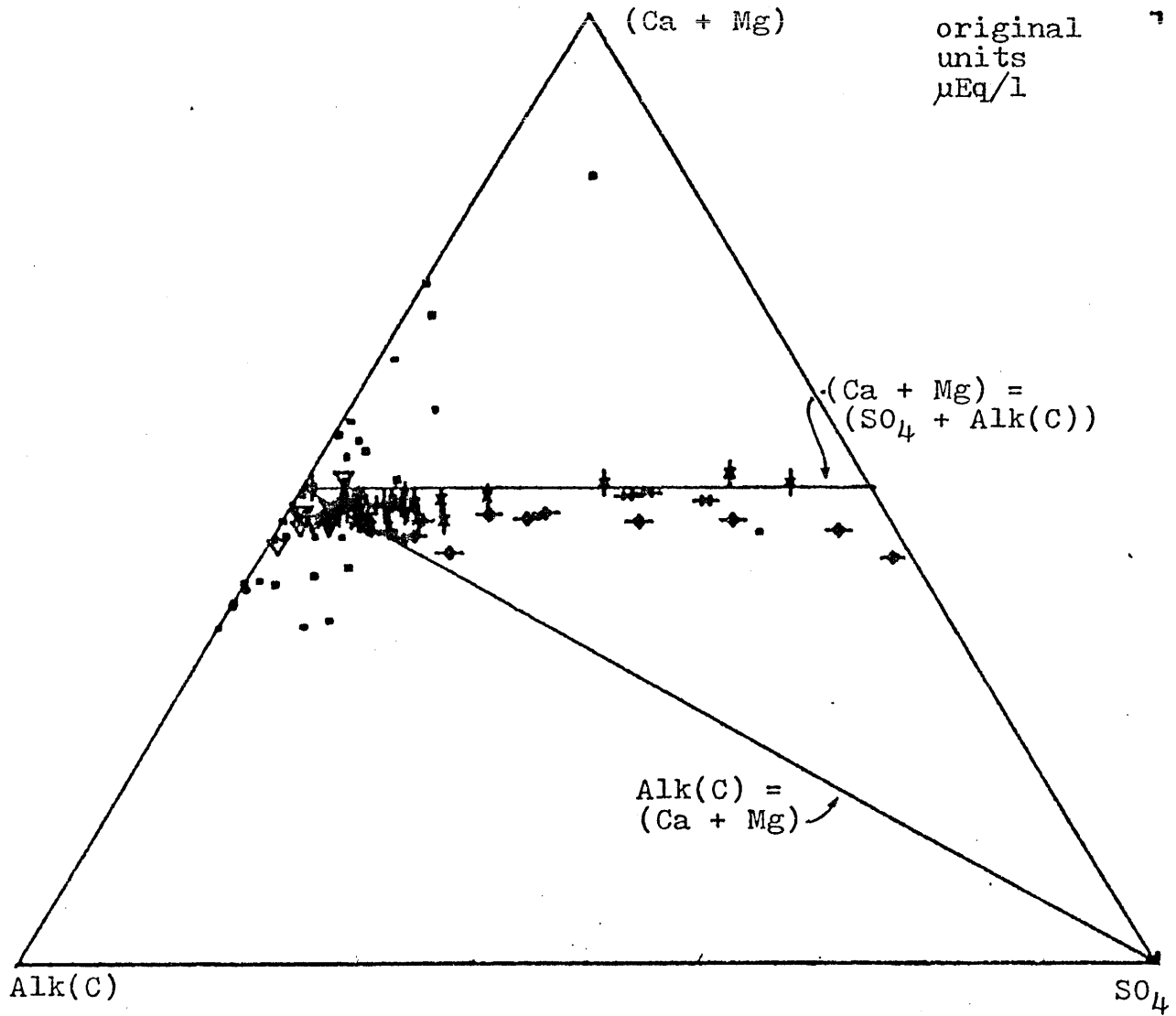


Figure IV.17

Ternary diagram for calcium plus magnesium, carbonate alkalinity, and sulfate, calculated with concentrations in $\mu\text{Eq/l}$. The bulk of the samples draining marine sediments fall within a field bounded by the trends defined by the weathering of carbonate and sulfate minerals (note that the dots are rivers not draining marine sediments).

- + - (1) Main Channel
- * - (2) Marañon Drainage
- * - (3) Ucayali Drainage
- ◆ - (4) Madeira Drainage
- ▽ - (8) Lowland rivers with extensive areas of marine sediments
- X - (10) Varzêa waters
- - Rivers not draining extensive areas of marine sediments



IV.6:1 WEATHERING REACTIONS

This section expands the discussion of water chemistry to include a more detailed examination of weathering reactions occurring in the Amazon Basin. Two interpretative procedures are utilized: (1) thermodynamics is used as a means of delimiting possible weathering reactions, and (2) rock and soil data are used to identify possible chemical relationships between chemical species through use of reaction mass balances.

The use of chemical relationships has been introduced in the previous section, where it is demonstrated that only a few weathering reactions are required to explain the major ion chemistry of high TZ+ surface waters. In low TZ+ waters, complications arise due to contributions of materials from silicate rock weathering. The solution products of silicate weathering are not as well defined because the degradation of silicates generates a variety of solid phases, typically clays and sesquioxides, and dissolved phases (incongruent reaction).

IV.6:2 Applicability of Thermodynamic Models to Amazon Chemistry Data

Despite the complexity of the weathering environment, thermodynamics may provide a means of testing whether a particular (clay) mineral or minerals might be forming as a result of weathering. Examination of Amazon River data using thermodynamic models is rather attractive, however certain qualifications must be discussed prior to application of models.

One might ask if thermodynamics can be validly applied to systems that are so clearly heterogeneous as are the river catchments within the Amazon Basin. This complexity is of course unavoidable, as the only geologically homogeneous basins sampled were in the lowlands. It seems reasonable that in basins which have silicate rocks or carbonate and silicate rocks as dominant lithologies, an assumption of homogeneity would be valid: (1) The wide

distribution of silicate rocks of acid to intermediate composition (which contain roughly the same minerals, but in different proportions) restricts the number of silicate reactions which can occur. (2) Carbonates are very widespread in the Andes, and are commonly associated with shales and other siliceous rock types, furthermore in catchments where carbonates are a major lithology, carbonate weathering controls the chemistry of the river (Section IV.5).

Ultimately, the applicability of thermodynamic calculations to river water can only be validated if thermodynamic models are consistent with independent observations. The validity of the interpretation of any particular sample is often hard to justify due to the lack of detailed environmental data, and the chemical data must be viewed in terms of trends indicating that certain broad controls might be important.

IV.6:3 Carbon Dioxide and pH

A second difficulty in interpreting data thermodynamically is that of possible nonconservative changes in the concentration of species used in the models. Note that thermodynamic models treat data logarithmically, consequently a nonconservative change must be large to have a sensible effect in results. Observations from varzea lakes (Section IV.4:12) suggest that biological effects on the major ions and silica are inconsequential. The most significant changes are seen in the case of hydrogen ion, caused by changes in the carbon dioxide vapor pressure (P_{CO_2}) of the sample.

Garrels (1967) demonstrates that the chemistry of groundwaters draining igneous rocks is best explained by weathering in an environment closed with respect to CO_2 exchange with the atmosphere. High initial CO_2 vapor pressures are involved, perhaps 10 to 100 times the P_{CO_2} of the atmosphere. P_{CO_2} in temperate soils ranges from 5 to >20 times that of the atmosphere (Holland 1978 p.22). Johnson et al. (1975) report soil P_{CO_2} values from a Costa

Rican rainforest, with values averaging 70 times atmospheric.

River P_{CO_2} will be assumed to be in the same range as soil P_{CO_2} . When soil and ground water enter a river, the water becomes an open system with respect to gain and loss of CO_2 . Garrels and Mackenzie (1971, p.125) observe that the P_{CO_2} of rivers averages about ten times that of the atmosphere, comparable to levels observed in soils, and speculate that the high P_{CO_2} is the result of a balance between organic generation of CO_2 by decay in river water and its loss to the atmosphere. These observations indicate that major errors in thermodynamic calculations involving stream water should not occur, as soil and river P_{CO_2} values are comparable.

The distribution of carbon dioxide vapor pressures in Amazon surface waters reflects both productivity and the dynamic state of the river from which the samples were taken (Figure IV.18). Waters from swift Andean rivers and high productivity lakes fall below the range typical of soil P_{CO_2} , suggesting that pH's from these rivers are probably not representative of the soil environment.

The relationship between pH, Alkalinity, and P_{CO_2} for waters having alkalinity and pH values typical of Andean rivers can be approximated by:

$$\log(\text{Alk}) + pK_0 + pK_1 - \text{pH} = \log(P_{CO_2}) \quad \text{or} \quad -\Delta\log(P_{CO_2}) = \Delta\text{pH}$$

where K_0 and K_1 are Henry's law and first association constants for carbon dioxide. The rise in pH of water moving from Andean soils into rivers may be as much as 1 or 2 pH units. As no estimates are available for P_{CO_2} in lowland and Andean soils, no attempt will be made to correct pH values in subsequent calculations.

IV.6:4 Carbonate Rocks

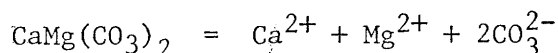
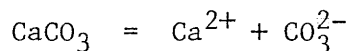
Prior to delving into silicate weathering, the simpler chemistry of carbonates will be examined. With carbonates the problems of varied secondary

solid phases need not be considered; furthermore, samples of interest come only from the Andes.

Several studies have shown that thermodynamic controls of ground water chemistry in carbonate terrains are straightforward. Typically these ground waters are just under or at saturation with respect to calcite, dolomite, or both, and exhibit high P_{CO_2} values (approximately 10 to 100 times the atmospheric value) (Holland et al. 1964, Thraillkill 1972, Langmuir 1971).

The plot of carbonate alkalinity versus magnesium plus calcium (Figure IV.19) suggests that an upper limit to alkalinity exists for the river water. The high (Ca+Mg) waters are from rivers in which carbonate rock and evaporite inputs dominate the chemistry.

The carbonate dissolution reactions to be considered are:



Following Langmuir (1971), the thermodynamic state of the water samples can be parameterized using saturation indices (or saturation or disequilibrium indices) for calcite and dolomite, given by:

$$\text{Calcite: } SI_C = \log(a_{Ca} \cdot a_{CO_3} / K_{sp\text{calcite}})$$

$$\text{Dolomite: } SI_D = \log(a_{Ca} \cdot a_{Mg} \cdot a_{CO_3}^2 / K_{sp\text{dolomite}})$$

Figure IV.18

Histograms of carbon dioxide vapor pressures in selected categories of samples. Productivity information is taken from Wissmar et al.(1979). The figure shows that carbon dioxide vapor pressures in Amazon surface waters are related to the dynamic and biological conditions in the waters. It should be noted that the vapor pressures on the main channel increase down river.

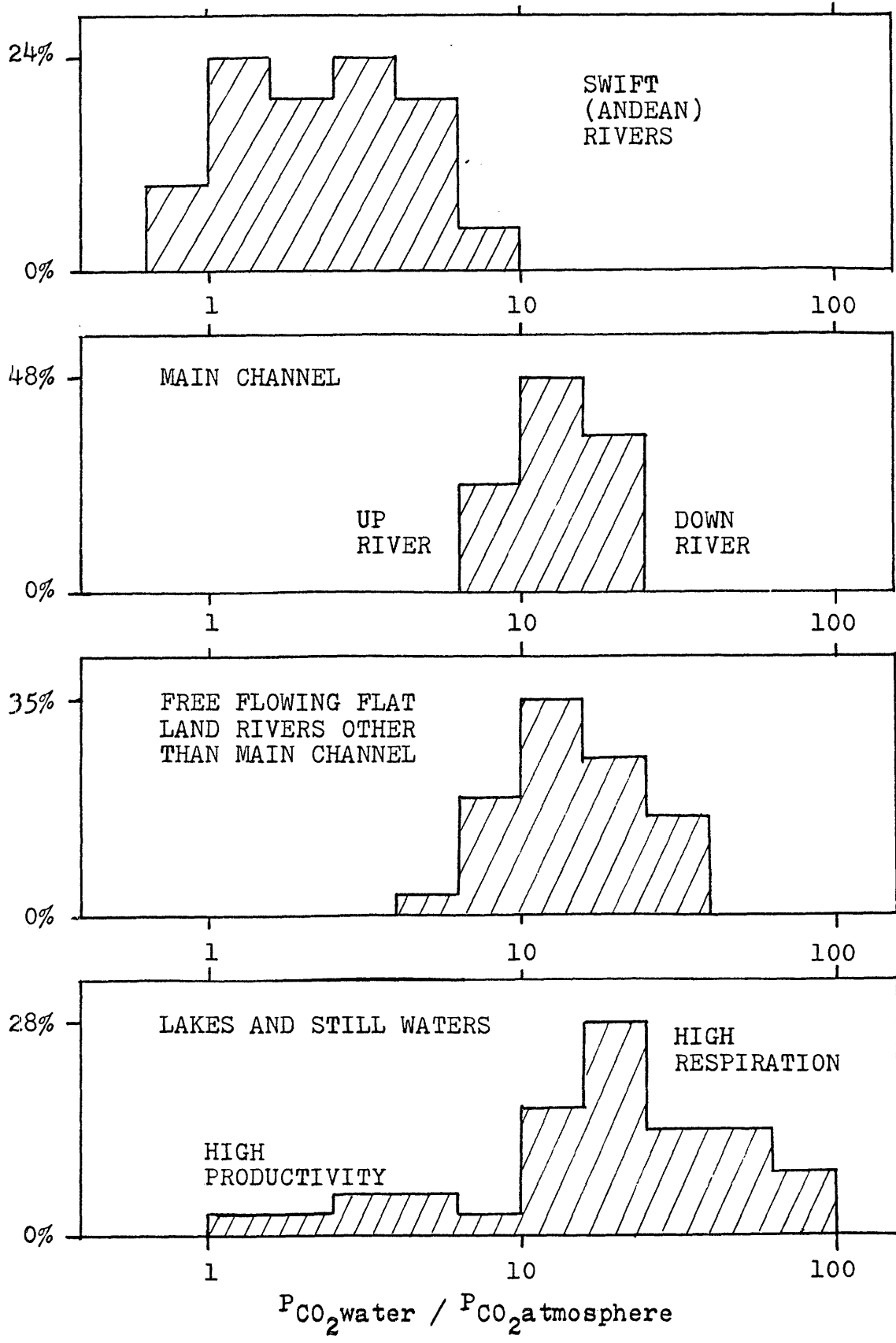
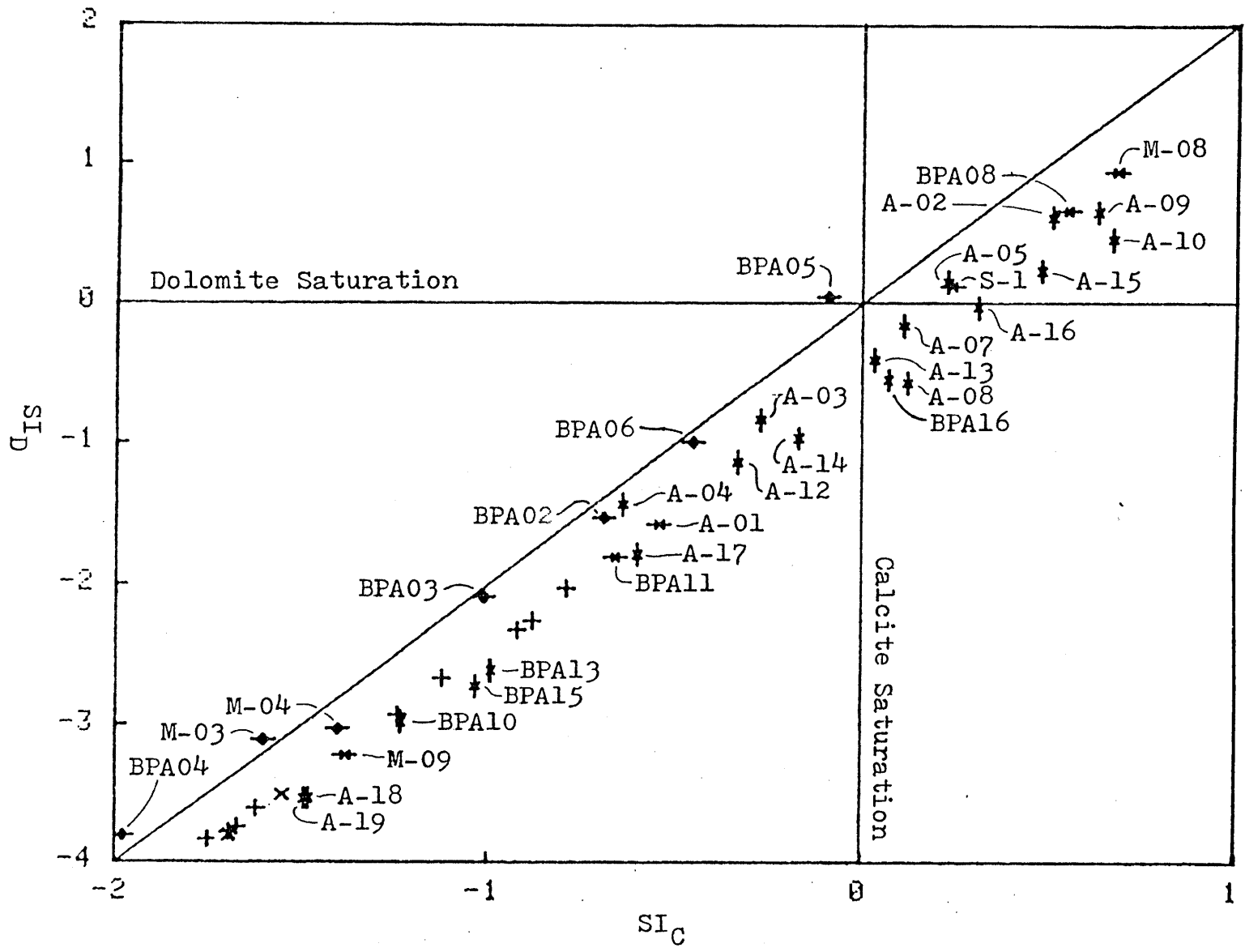


Figure IV.19

Saturation index for dolomite versus saturation index for calcite. Note that most of the samples that are saturated for dolomite are also saturated for calcite. Station numbers have been identified for all the Andean samples to facilitate comparison with Table IV.4. In doing this comparison it should be noted that all of the rivers supersaturated with respect to calcite have limestone as a major lithology in their drainage, while very few of the undersaturated samples have limestone as a major lithology.

Symbol key:

- + - (1) Main Channel
- * - (2) Marañon Drainage
- * - (3) Ucayali Drainage
- ◆ - (4) Madeira Drainage
- X - (10) Varzêa waters



Constants are from Langmuir (1971)².

When SI_D is plotted against SI_C (Figure IV.19), the samples fall on a clearly defined 2:1 trend. The occurrence of a 2:1 trend depends primarily on the limited range of variation in the $\log(Mg/Ca)$ of the samples, as:

$$SI_D = 2SI_C + \log(Mg/Ca) - pK_{sp_{dolomite}} + 2pK_{sp_{calcite}}$$

Any phenomena which change Mg and Ca proportionately (dilution by much fresher waters, evaporation) will shift the sample along a 2:1 trend. In contrast, inputs of $CaSO_4$ (such as those occurring in the Peruvian Andean rivers) would shift data along a 1:1 trend. Waters draining carbonate or siliceous rocks having different Mg:Ca ratios would be expected to fall on different 2:1 trends. The distinct 2:1 trend in Figure (IV.19) reflects the approximately inverse relationship of hydrogen ions with calcium, magnesium, and alkalinity, as can be seen by approximating SI_C and SI_D in terms of these variables:

²Pertinent equations

$$Alk(\text{titration}) = [HCO_3^-] + 2[CO_3^{2-}] + [OH^-] - [H^+] \quad (\text{c.f. Appendix III})$$

$$K_0 = \frac{\gamma_2}{\gamma_1} [H_2CO_3^*] / P_{CO_2} \quad K_1 = \gamma_2 [H^+] [CO_3^{2-}] / [HCO_3^-] \quad K_2 = \gamma_2 [H^+] [CO_3^{2-}] / [HCO_3^-]$$

$$K_w = \frac{\gamma_2}{\gamma_1} [H^+] [OH^-] / [H_2O] \quad H^+ = 10^{-pH} / \gamma_1$$

Activity coefficients, γ , are calculated using the Davies Equation (Butler 1964). Equilibrium constants are from Langmuir (1971). Temperature corrections are included for all samples. Temperatures in some lowland rivers were not measured, and are assumed to be 25°C. Calculations for the most concentrated samples (A-05, A-10, M-08, BPA16) indicate that significant ion pairing for Mg and Ca with SO_4 is occurring, but not with HCO_3 (2%). Consequently only ion pairing for Mg and Ca with SO_4 are considered in the calculations.

$$SI_C = \log(a_{Ca}) + \log(\text{Alk}) + \text{pH} + \text{pK}_2 + \text{pK}_{sp_{\text{calcite}}}$$

$$SI_D = \log(a_{Ca}) + \log(a_{Mg}) + 2\log(\text{Alk}) + 2\text{pH} + 2\text{pK}_2 + \text{pK}_{sp_{\text{dolomite}}}$$

A change in pH caused by a gain or loss of CO_2 due to atmospheric exchange, or a decrease in pH and increase in alkalinity during weathering, would shift a water sample along a 2:1 trend.

The data for Andean rivers (Figure IV.19) clearly fall on two trends. One is a Madeira Basin trend, which intersects both the dolomite and calcite supersaturation fields at the same point. The other trend, including all Peruvian Andean samples (except the Huachipa River, draining Precambrian metamorphic rocks, see Table IV.4), intersects the calcite field first. All of the samples that are supersaturated with respect to calcite have limestones as a dominant lithology in their catchments (compare Figure IV.19 with Table IV.4). Sample BPA05 (Guapay River) of the Madeira group is the only sample saturated solely with respect to dolomite. Redissolution of soil salts is thought to control the chemistry of this sample (see Section IV.4:5). The high magnesium content of the Madeira Basin rivers is thought to be due to the magnesium rich dark shales in the drainage (Section IV.4:5), which may have dolomites in their carbonate component (Section III.3:3). However Peruvian rivers having dolomitic carbonates (Section IV.4:6) do not fall on the Madeira trend.

Figure IV.20

Carbonate alkalinity plotted against the saturation index for calcite.

Symbol key:

- + - (1) Main Channel
- * - (2) Marañon Drainage
- * - (3) Ucayali Drainage
- * - (4) Madeira Drainage
- ‡ - (5) Other Andean headwater rivers
- ◇ - (6) Negro Drainage
- - (7) Rivers draining shields
- ▽ - (8) Lowland rivers with extensive areas of marine sediments
- △ - (9) Rivers draining only U. Tertiary and Quaternary sediments
- X - (10) Varzêa waters

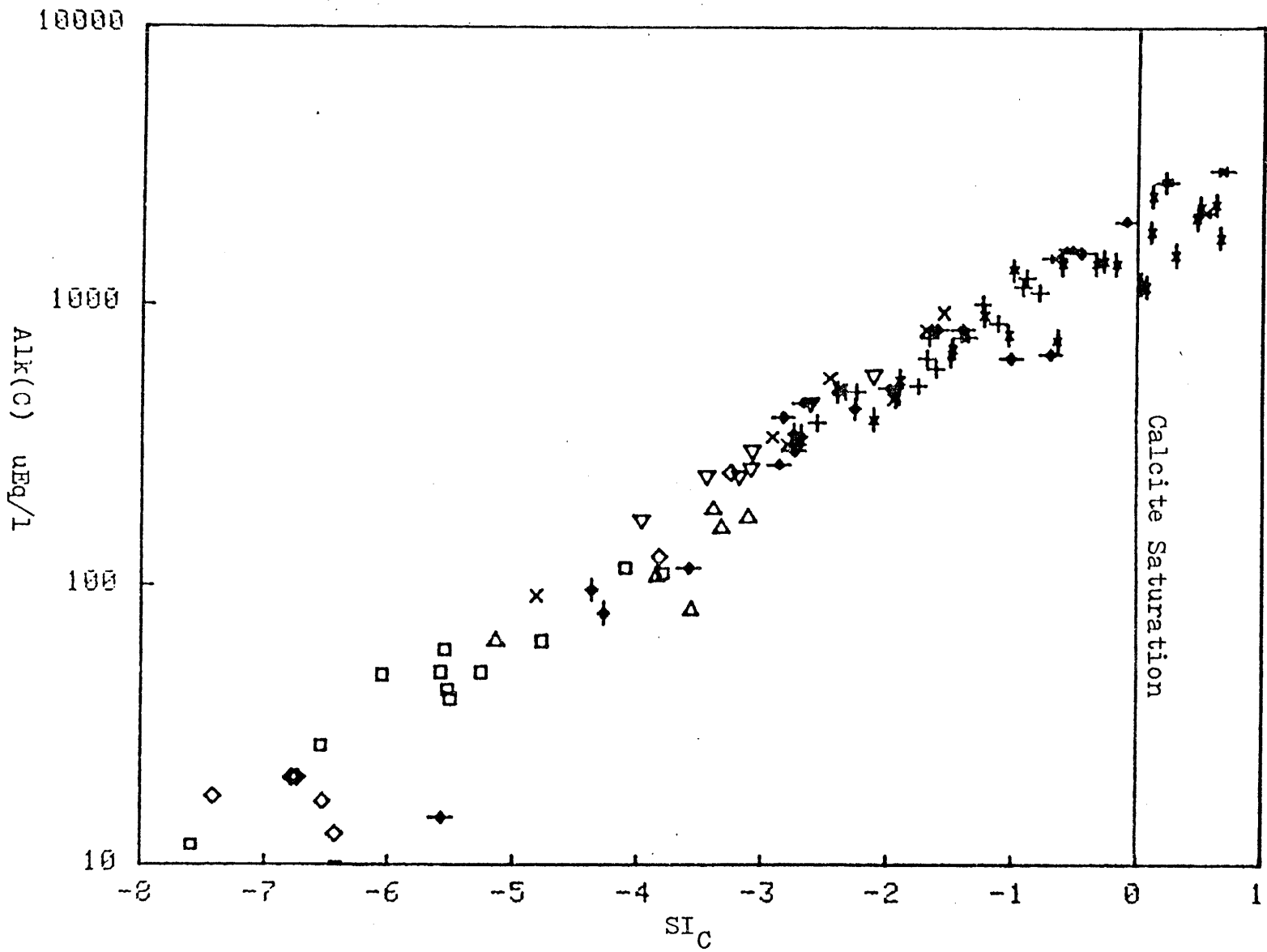
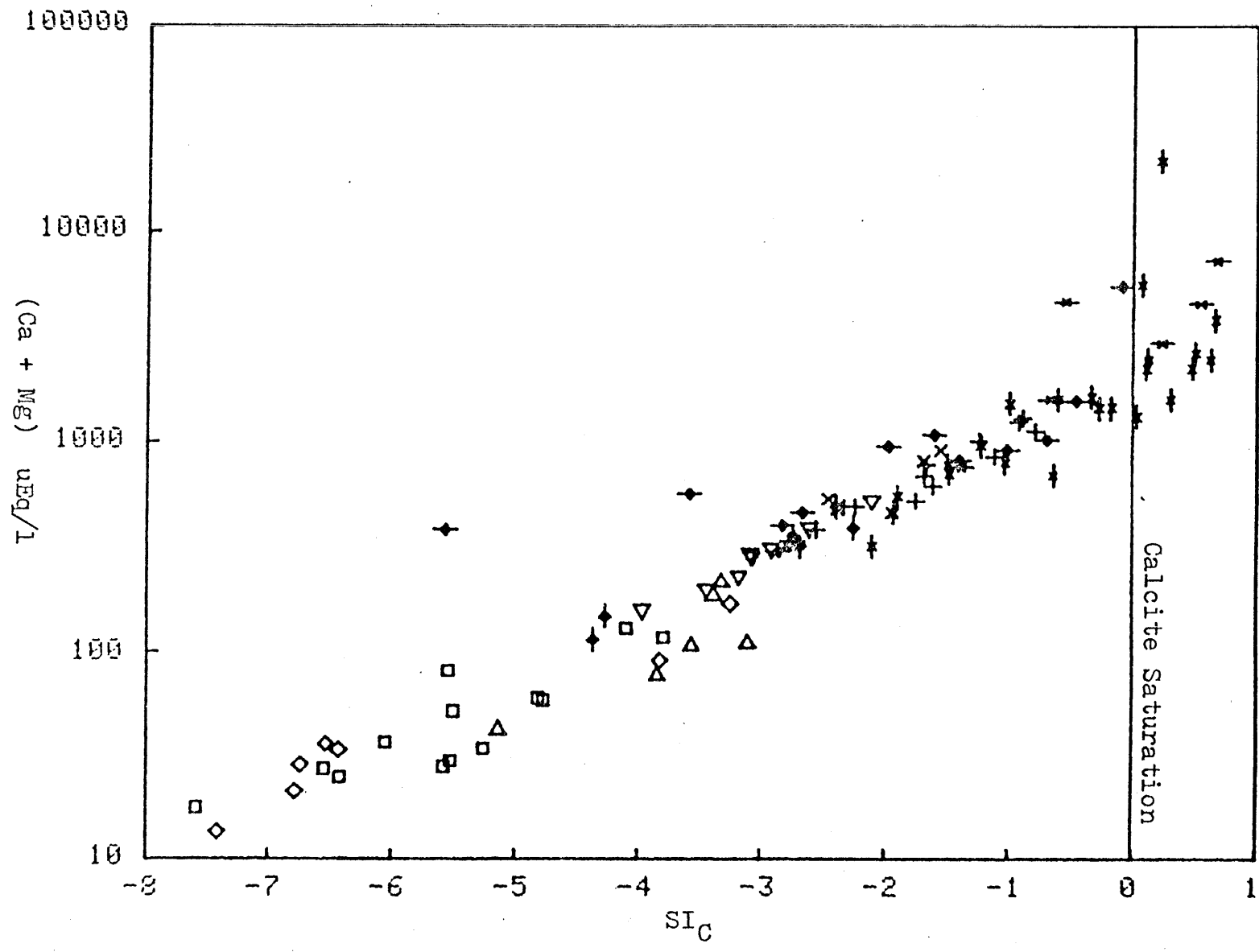


Figure IV.21

Calcium plus magnesium plotted against the saturation index for calcite. Compare this figure with Figures IV.20 and IV.16.

Symbol key:

- + - (1) Main Channel
- * - (2) Marañon Drainage
- * - (3) Ucayali Drainage
- * - (4) Madeira Drainage
- † - (5) Other Andean headwater rivers
- ◇ - (6) Negro Drainage
- - (7) Rivers draining shields
- ▽ - (8) Lowland rivers with extensive areas of marine sediments
- △ - (9) Rivers draining only U. Tertiary and Quaternary sediments
- X - (10) Varzēa waters



The supersaturation seen in these samples is not characteristic of ground waters from carbonate terrains, where saturation or undersaturation is typically observed. Both loss of carbon dioxide in the transition from soil to river environments and addition of CaSO_4 (A-05, A-10, A-16, M-08, BPA08) may bring about supersaturation.

Sample A-05, from a salt spring, is particularly interesting, as carbonate coatings are observed on pebbles in the spring. The calculated P_{CO_2} of the sample is 13 times the atmospheric value, and the sample is supersaturated with both calcite and dolomite. The coatings are likely due to the precipitation of calcite caused by supersaturation induced by losses of carbon dioxide. Similar coatings were not observed elsewhere during this study, however they are reported for a tributary of the Huallaga, Quebrada de Puente Perez, by Patrick (1966), who attributes them to deposition by blue-green algae.

When $\log(\text{Alk}(\text{C}))$ is plotted against SI_{C} (Figure IV.20), a simple linear relationship is observed, while if $\log(\text{Ca}+\text{Mg})$ is plotted against SI_{C} (Figure IV.21), some samples plot independently of SI_{C} once supersaturation is reached. This is taken as indicating that the alkalinity is limited by either saturation with respect to calcite in soils, calcite precipitation in rivers or both. It should be noted that if pH values of supersaturated samples are adjusted so that $\text{SI}_{\text{C}} = 0$, the calculated P_{CO_2} values increase from an average of 2.73 times the atmospheric value to an average of 6.38 times the atmospheric value. The latter value is in the low end of the range of P_{CO_2} levels of soils.

IV.6:5 Silicate Weathering

A general description of the silicate weathering process has been developed over the past two decades. Cation rich primary minerals are dissolved at disequilibrium, releasing the cations, silica, and some iron and aluminum into solution. It is accepted that the weathering rate of primary mineral grains is in part controlled by the availability of a source of protons in solution. The proton source is typically carbonic acid, but may also be sulfuric, nitric, and organic acids. The hydrogen ions displace exchangeable cations and hydrolyze the Si-O-, Al-O-, and Fe-O- bonds.

The interpretation of other controls on the dissolution rate are somewhat controversial, and two groups of models have been developed. The earliest models assume that dissolution rates are partly controlled by diffusion through either a protective weathering rind consisting of cation depleted silicates (clays) (Correns and von Engelhart 1938, Wollast 1967, Helgeson 1971, Busenberg and Clemency 1976), or through cation depleted outer layers of the primary grain (Paces 1973). Recent models suggest that feldspar dissolution is controlled by surface reaction kinetics (Petrovic et al. 1976, Berner and Holdren 1977, Berner 1978), occurring on a surface of minimum lattice energy. This mechanism is supported by observations, including chemical measurements and electron microscopy of the outer layers of soil feldspars, which show no alteration and no weathering rinds, instead the soil feldspars exhibit well developed crystallographically controlled etch pits on otherwise fresh surfaces. These observations parallel those of Pasquali et al. (1972, p.2272, see Section III.6:2) who report fresh appearing microcline in weathered parts of soil profiles in Venezuela. Pasquali et al.

(1972) also observe that unlike microcline, biotite is bleached in soil profiles, an indication that cation loss may occur in some minerals. In certain silicate phases, notably volcanic glasses, rinds are observed to form during the weathering process (Loughnan 1968).

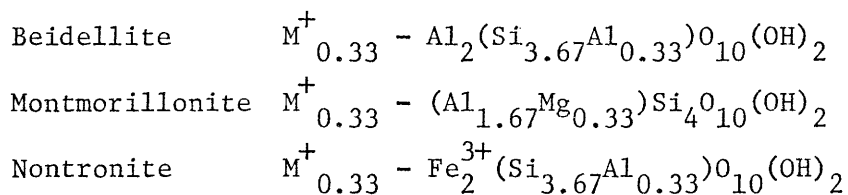
Some of the cations, silica, iron and aluminum released from the degrading primary grains reprecipitate as clay minerals in the immediate vicinity of the primary grains (if not as a weathering rind). These clay minerals are thought to be near to thermodynamic equilibrium with the soil and ground water solutions in contact with them. Thermodynamic equilibration in ground and soil water systems has been subject to numerous studies (Feth et al. 1964, Garrels and Christ 1965, Keller 1967, Polzer 1967, Garrels 1967, Bricker and Garrels 1967, Garrels and Mackenzie 1967, Paces 1972, 1974, Weaver et al. 1971, Norton 1974, Hemley et al. 1977, Nesbitt and Bricker 1978). The usual approach is to construct stability fields for various soil minerals (graphically or as solubility indices) as a function of the activity of dissolved species in the soil solution. Typically iron is assumed to be equilibrated with hydroxides or oxides, and aluminum activity is treated as a dependent variable, with phases being chosen so that it is minimized. Consequently only the major ions, silica, and the hydrogen ion are used in calculations. This standard approach is quite reasonable as no method for measuring or calculating the activity of iron and aluminum in soil solutions exists, due to organic reactions involving Fe and Al. Chemically, water from most soil and groundwater samples falls in kaolinite or montmorillonite fields on stability diagrams.

A major shortcoming of thermodynamic studies of soil and groundwater systems is a failure to adequately characterize clays, particularly the more cation rich clays. Thermodynamic models generally fail to treat amorphous

and mixed layer clays commonly observed in soils. Data exist, however, that suggest that the amorphous clays have similar stoichiometries and occupy similar stability fields as the more crystalline phases (c.f. Weaver et al. 1971, 1976).

Kaolinite represents a class of cation depleted aluminosilicates, which also includes halloysite and metahalloysite, and poorly crystalline aluminosilicates, all having a 1:1 aluminum to silica stoichiometric ratio. Kaolinite is associated with acid, well drained soils. Very little substitution of other elements for silicon and aluminum in its lattice is observed. These clays are representative of forested lowland soils, while savanna soils are more aluminous.

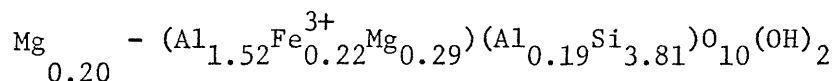
Montmorillonites (smectites) are associated with poorly drained soils (where cations build up due to long residence times), calcareous soils, or soils with a high volcanic ash content. Unlike kaolins, montmorillonites are chemically an extraordinarily heterogeneous group of minerals (Ross and Hendricks 1945). Common montmorillonites have compositions intermediate between three end members:



None of these end members represents a reasonable estimate of the composition of a "typical" montmorillonite, as situations where iron and/or magnesium are lacking in the environment are atypical. Early studies of soils and groundwaters assumed that beidellites were representative of typical montmorillonites, and thermodynamic constants for beidellites were calculated using ground and soil water chemical data (Garrels and Mackenzie 1967, Norton 1974). Most early investigations only examined one exchangeable ion

at a time ($M^+ = \text{Ca}, \text{Na}, \text{or Mg}$), as more complicated situations cannot be treated conveniently on two dimensional diagrams.

Thermodynamic parameters for more complex montmorillonites have been obtained in laboratory equilibration studies (Kittrick 1971a,b, Weaver et al. 1971, 1976). A particularly well studied montmorillonite is the Colony-I montmorillonite from Wyoming (Weaver et al. 1971, 1976, Tardy and Garrels 1974). Laboratory derived thermodynamic constants from the Colony-I have been shown to be applicable to soil systems in which the mineralogy (that is, the presence of kaolinite and/or montmorillonite) and soil water chemistry are known (Weaver et al. 1971). The Colony -I montmorillonite has the following stoichiometry:



Note that beidellite has a low silica to aluminum ratio compared to the Colony-I (1.57 versus 2.23) and a high silica to cation equivalent ratio (11 versus 3.9).

Geologic data suggest that montmorillonites might be forming in the Andes. The Colony-I is assumed to be analogous to modern Andean montmorillonites, as the Colony-I was formed at a time (Early Tertiary) when conditions of climate, geomorphology, structure and volcanism of the North American cordillera and precordillera resembled those of the contemporary Andes and lowlands (c.f. Clark et al. 1967).

The examination of silicate weathering in the Amazon is treated in two steps. Firstly thermodynamic aspects of silicate weathering in the Amazon are examined, and a saturation index for montmorillonite is established. Secondly, the possibility of montmorillonite formation is then tested using an alternative non-thermodynamic reaction mass balance model.

IV.6:6 Recapitulation of Silicate Occurrences in the Amazon

Igneous and metamorphic rocks in the Amazon Basin tend to be intermediate to acid in nature. Siliceous sediments of the Andes and Subandean Trough contain abundant cation rich clays and micas such as illite, chlorite, muscovite, paragonite, biotite, and some montmorillonite (in younger sediments). Andean sands frequently contain unweathered rock fragments and feldspars. Exposed lowland sediments are cation depleted, with the exception of sediments in southwestern Brazil and in Paleozoic outcrops along the lower Amazon. Soils and river sediment loads in the lowlands are kaolinitic (tending to gibbsitic in the savanna areas), while kaolinite, montmorillonite, and other cation rich clays are reported in Andean soils and suspended sediments in rivers.

IV.6:7 Amazon Data and Activity-Activity Diagrams

Stability diagrams for the systems: (Na-H-Si-Al), (K-H-Si-Al), (Ca-H-Si-Al), and (Mg-H-Si-Al-Fe) at 25°C are presented in Figures IV.22, IV.23, IV.24, and IV.25. The reactions and equilibrium constants used are summarized in Table IV.6. All these diagrams, except for Mg, use only standard aluminous end member phases, which are free of other cations and iron. Inspection of these figures shows that most of the data fall in the stability field for kaolinite when the aluminous end member phases are considered. However, in the magnesium stability diagram, a complex montmorillonite (Colony-I) is included. Magnesium and iron are partially substituted for silica and aluminum in the lattice; the effect is to shift the montmorillonite stability field to encompass more data.

Most non-aluminous end member phases cannot be treated on these diagrams, as substitution and ion exchange typically involve several cations. The formulation of stability indices, analogous to the saturation indices

Figure IV.22

Stability diagram for end-member sodium-aluminosilicates.

Symbol key:

- + - (1) Main Channel
- * - (2) Marañon Drainage
- * - (3) Ucayali Drainage
- * - (4) Madeira Drainage
- † - (5) Other Andean headwater rivers
- ◇ - (6) Negro Drainage
- - (7) Rivers draining shields
- ▽ - (8) Lowland rivers with extensive areas of marine sediments
- △ - (9) Rivers draining only U. Tertiary and Quaternary sediments
- X - (10) Varzêa waters

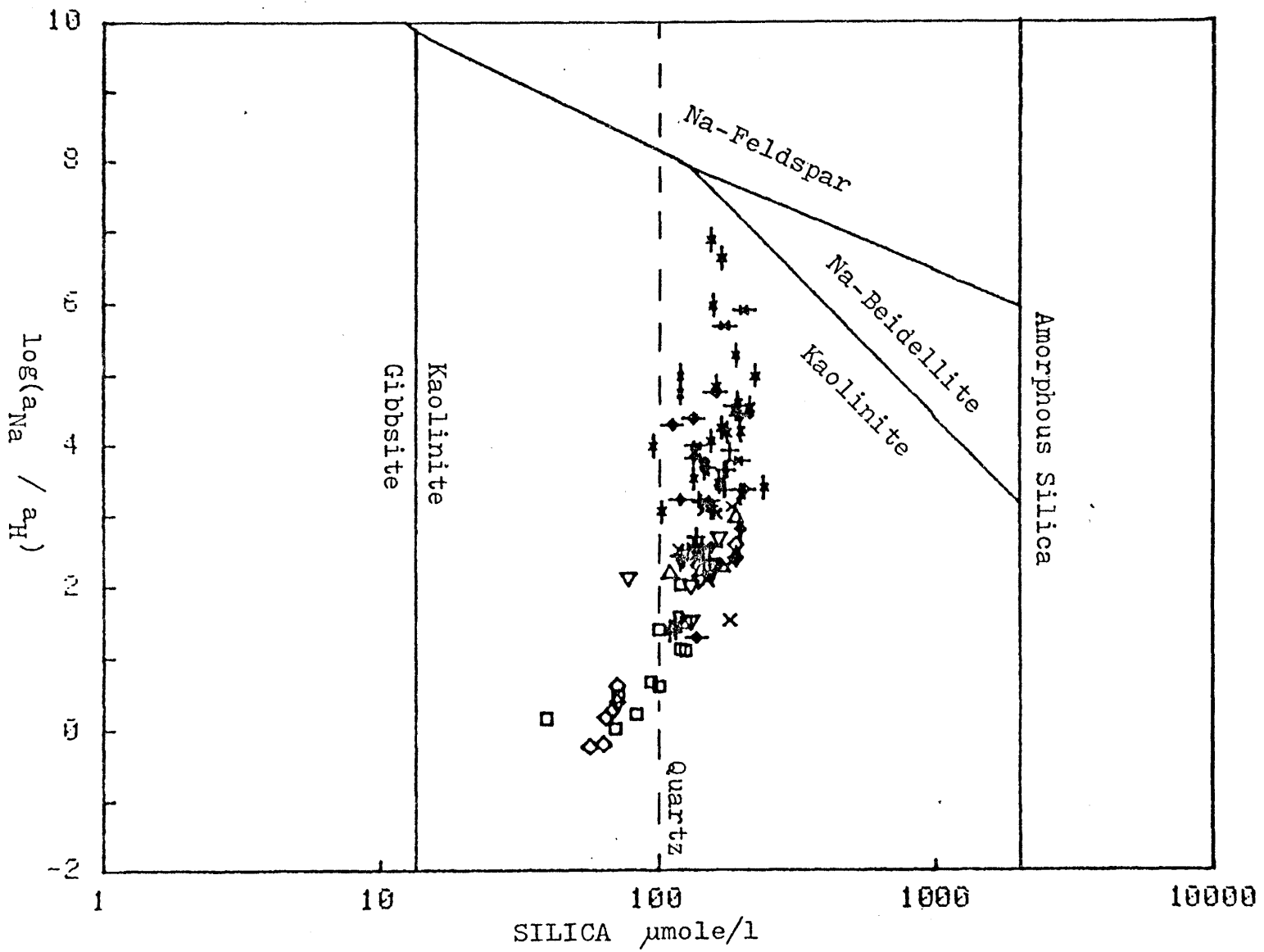


Figure IV.23

Stability diagram for end-member potassium-aluminosilicates.

Symbol key:

- + - (1) Main Channel
- * - (2) Marañon Drainage
- * - (3) Ucayali Drainage
- * - (4) Madeira Drainage
- † - (5) Other Andean headwater rivers
- ◇ - (6) Negro Drainage
- - (7) Rivers draining shields
- ▽ - (8) Lowland rivers with extensive areas of marine sediments
- △ - (9) Rivers draining only U. Tertiary and Quaternary sediments
- X - (10) Varzêa waters

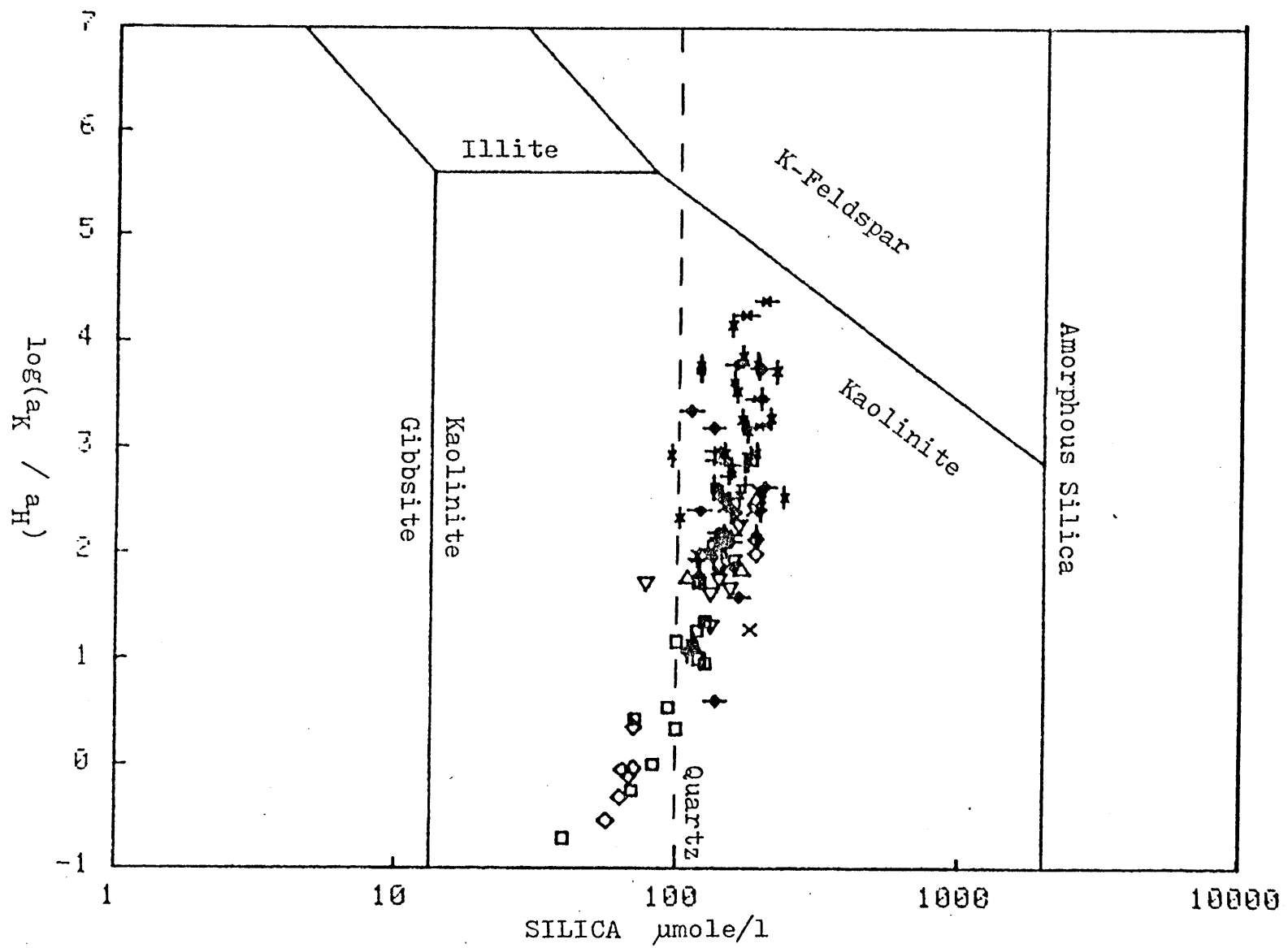


Figure IV.24

Stability diagram for end-member calcium-aluminosilicates.

H-constant from Helgeson (1969)

N-constant from Norton (1974)

Symbol key:

- + - (1) Main Channel
- * - (2) Marañon Drainage
- * - (3) Ucayali Drainage
- * - (4) Madeira Drainage
- † - (5) Other Andean headwater rivers
- ◇ - (6) Negro Drainage
- - (7) Rivers draining shields
- ▽ - (8) Lowland rivers with extensive areas of marine sediments
- △ - (9) Rivers draining only U. Tertiary and Quaternary sediments
- X - (10) Varzêa waters

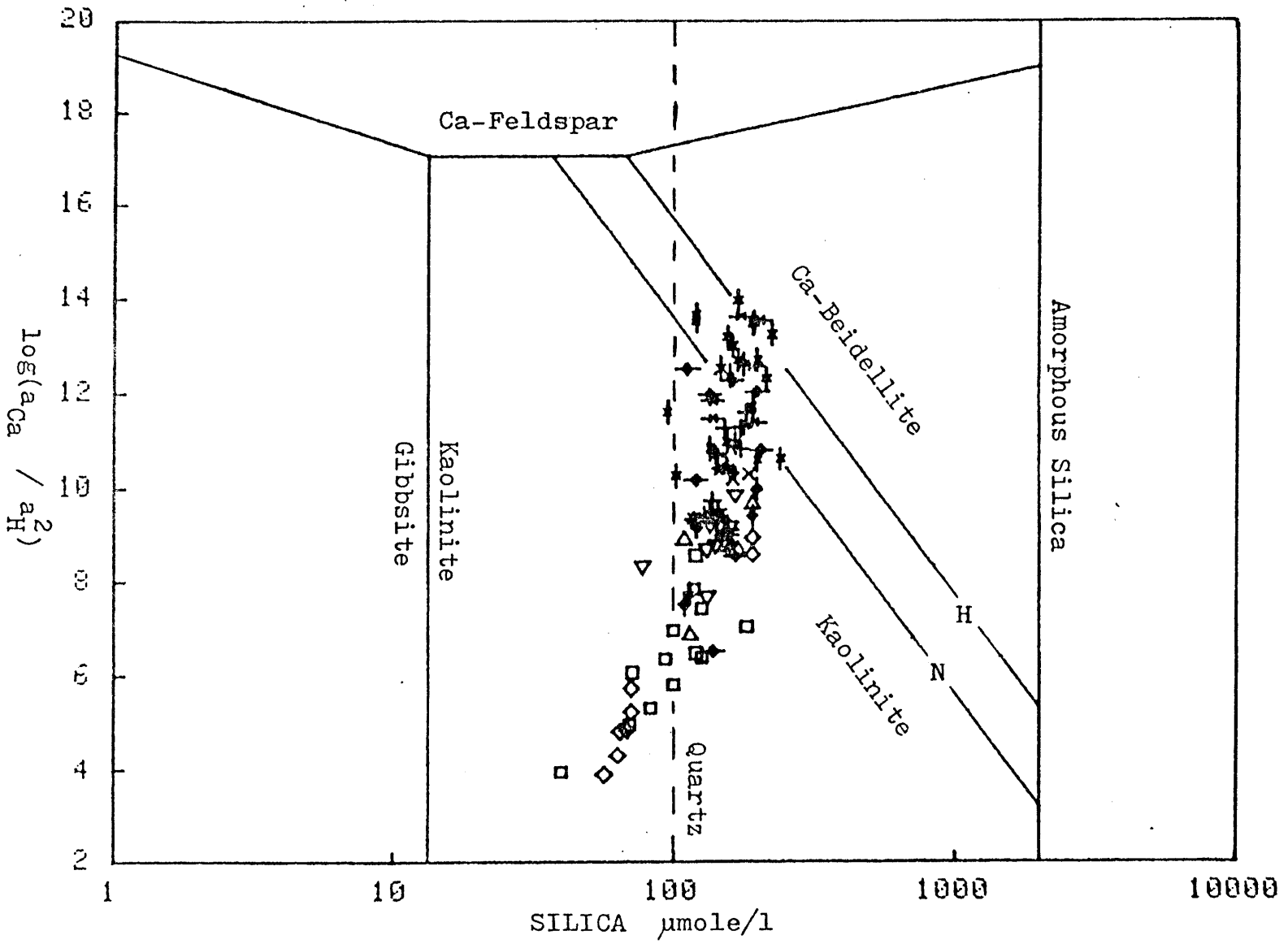


Figure IV.25

Stability diagram for end-member magnesium aluminosilicates, also including thermodynamic data for a complex montmorillonite, the Colony-I montmorillonite (discussed in text). The Colony-I montmorillonite has iron and magnesium substituted into the lattice and probably represents a more realistic composition of montmorillonites occurring in the Andes. Note that the use of a non-idealized phase results in major shifts in the phase boundaries. The montmorillonite phase boundary in this diagram is still idealized in the sense that exchangeable ions other than magnesium are not considered.

Symbol key:

- + - (1) Main Channel
- * - (2) Marañon Drainage
- * - (3) Ucayali Drainage
- * - (4) Madeira Drainage
- † - (5) Other Andean headwater rivers
- ◇ - (6) Negro Drainage
- - (7) Rivers draining shields
- ▽ - (8) Lowland rivers with extensive areas of marine sediments
- △ - (9) Rivers draining only U. Tertiary and Quaternary sediments
- X - (10) Varzêa waters

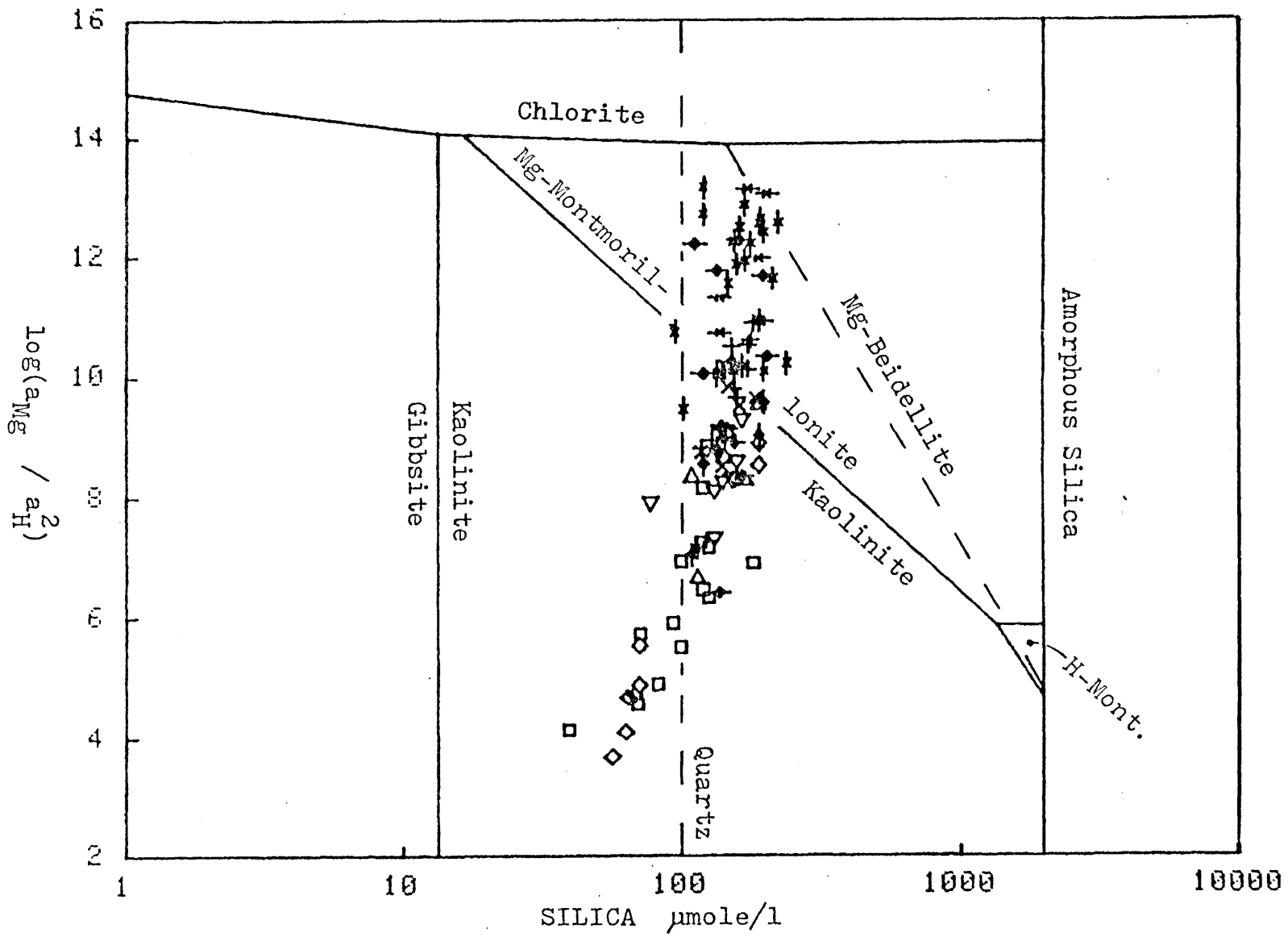


TABLE IV.6

Thermodynamic
Constants used in Text

Reaction	Reactants	Products	log K	Si/(Na+K)	References
<u>Beidellite in products</u>					
(1)	7NaAlSi ₃ O ₈ + 6H ⁺ + 4H ₂ O (Na-feldspar)	= 3Na _{0.33} Al _{2.33} Si _{3.67} O ₁₀ (OH) ₂ + 6Na ⁺ + 10Si(OH) ₄	8.52	1.667	(1)
(2)	7CaAl ₂ Si ₂ O ₈ + 12H ⁺ + 8Si(OH) ₄ (Ca-feldspar)	= 6Ca _{0.167} Al _{2.33} Si _{3.67} O ₁₀ (OH) ₂ + 6Ca ⁺⁺	135.73	-∞	(1)
(3)	7Mg ₅ Al ₂ Si ₃ O ₁₀ (OH) ₈ + 68H ⁺ + Si(OH) ₄ (chlorite)	= 6Mg _{0.167} Al _{2.33} Si _{3.67} O ₁₀ (OH) ₂ + 34Mg ⁺⁺ + 58H ₂ O	475.80	-∞	(1)
<u>Illite in products</u>					
(4)	3KAlSi ₃ O ₈ + 2H ⁺ + 12H ₂ O (K-feldspar)	= KAl ₃ Si ₃ O ₁₀ (OH) ₂ + 2K ⁺ + 6Si(OH) ₄	-13.27	3	(1)
<u>Kaolinite in products</u>					
(5)	2NaAlSi ₃ O ₈ + 2H ⁺ + 9H ₂ O	= Al ₂ Si ₂ O ₅ (OH) ₄ + 2Na ⁺ + 4Si(OH) ₄	0.25	2	(1)
(6)	6Na _{0.33} Al _{2.33} Si _{3.67} O ₁₀ (OH) ₂ + 2H ⁺ 23H ₂ O	= 7Al ₂ Si ₂ O ₅ (OH) ₄ + 2Na ⁺ + 8Si(OH) ₄	-15.29	4	(1)
(7)	2KAlSi ₃ O ₈ + 2H ⁺ + 9H ₂ O	= Al ₂ Si ₂ O ₅ (OH) ₄ + 2K ⁺ + 4Si(OH) ₄	-5.11	2	(1)
(8)	2KAl ₃ Si ₃ O ₁₀ (OH) ₂ + 2H ⁺ + 3H ₂ O	= 3Al ₂ Si ₂ O ₅ (OH) ₄ + 2K ⁺	11.22	0	(1)
(9)	CaAl ₂ Si ₂ O ₈ + 2H ⁺ + H ₂ O	= Al ₂ Si ₂ O ₅ (OH) ₄ + Ca ⁺⁺	17.06	0	(1)
(10)	6Ca _{0.167} Al _{2.33} Si _{3.67} O ₁₀ (OH) ₂ + 2H ⁺ + 23H ₂ O	= 7Al ₂ Si ₂ O ₅ (OH) ₄ + Ca ⁺⁺ + 8Si(OH) ₄	-16.31	∞	(1)
(11)	Mg ₅ Al ₂ Si ₃ O ₁₀ (OH) ₈ + 10H ⁺	= Al ₂ Si ₂ O ₅ (OH) ₄ + 5Mg ⁺⁺ + Si(OH) ₄ + 5H ₂ O	65.57	∞	(1)
(12)	6Mg _{0.167} Al _{2.33} Si _{3.67} O ₁₀ (OH) ₂ + 2H ⁺ + 23H ₂ O	= 7Al ₂ Si ₂ O ₅ (OH) ₄ + Mg ⁺⁺ + 8Si(OH) ₄	-16.81	∞	(1)
(13)	2Mg _{0.20} (Si _{3.81} Al _{0.19})(Al _{1.52} Fe _{0.22} Mg _{0.29})O ₁₀ (OH) ₂ + 8.85H ₂ O + 1.96H ⁺ (Mg-Montmorillonite, Colony I)	= 1.71Al ₂ Si ₂ O ₅ (OH) ₄ + 0.22Fe ₂ O ₃ + 0.98Mg ⁺⁺ + 4.20Si(OH) ₄	-6.304	∞	(2,3,4)
(14)	K _{0.64} (Al _{1.54} Fe _{0.29})(Al _{0.49} Si _{3.51})O ₁₀ (OH) ₂ + 1.02H ⁺ + 3.485H ₂ O (Pethian Illite)	= 1.015Al ₂ Si ₂ O ₅ (OH) ₄ + 0.145Fe ₂ O ₃ + 1.48Si(OH) ₄ + 0.64K ⁺ + 0.19Mg ⁺⁺	-0.327	2.31	(2)
(15)	4Mg ₂ Fe ₂ Al ₂ Si ₃ O ₁₀ (OH) ₈ + 30 ₂ + 16H ⁺	= 4Al ₂ Si ₂ O ₅ (OH) ₄ + 8Mg ⁺⁺ + 4Si(OH) ₄ + 6Fe ₂ O ₃ + 8H ₂ O	279.88	∞	(2)
<u>Gibbsite in products</u>					
(16)	NaAlSi ₃ O ₈ + H ⁺ + 7H ₂ O	= Al(OH) ₃ + Na ⁺ + 3Si(OH) ₄	-4.75	3	(1)
(17)	KAl ₃ Si ₃ O ₁₀ (OH) ₂ + H ⁺ + 9H ₂ O	= 3Al(OH) ₃ + K ⁺ + 3Si(OH) ₄	-9.02	3	(1)
(18)	CaAl ₂ Si ₂ O ₈ + 2H ⁺ + 6H ₂ O	= 2Al(OH) ₃ + Ca ⁺⁺ + 2Si(OH) ₄	7.31	∞	(1)
(19)	Mg ₅ Al ₂ Si ₃ O ₁₀ (OH) ₈ + 10H ⁺	= 2Al(OH) ₃ + 5Mg ⁺⁺ + 3Si(OH) ₄	55.82	∞	(1)
(20)	Al ₂ Si ₂ O ₅ (OH) ₄ + 5H ₂ O	= 2Al(OH) ₃ + 2Si(OH) ₄	-9.75	∞	(1)
<u>Congruent reaction</u>					
(21)	SiO ₂ (quartz) + 2H ₂ O	= Si(OH) ₄	-3.7	∞	(2)
(22)	SiO ₂ (amorphous) + 2H ₂ O	= Si(OH) ₄	-2.7	∞	(2)

(1) Helgeson 1969
(2) Tardy and Garrels 1974
(3) Weaver et al. 1971
(4) Weaver et al. 1976

presented earlier for calcite and dolomite, provides a means of identifying single phase boundaries between complex phases. Stability indices were formulated and tested for the montmorillonite (Colony-I)-kaolinite, illite (Fethian)-kaolinite, and Fe-chlorite ($\text{Mg}_2\text{Fe}_3^{2+}\text{Al}_2\text{Si}_3\text{O}_{10}(\text{OH})_2$)-kaolinite phase boundaries (thermodynamic constants in Table IV.6). Illite and chlorite are not stable in any of the samples from this study. Consequently, only the derivation of a stability index for the montmorillonite-kaolinite boundary is developed below; the main extension from the magnesium stability diagram is the inclusion of exchangeable cations other than magnesium.

IV.6:8 Montmorillonite Stability

Data for the thermodynamic treatment of exchangeable cations is presented in Tardy and Garrels (1974, p. 1108). Using this data it is possible to calculate equilibrium coefficients for exchangeable cations relative to magnesium on montmorillonites:

$$\begin{aligned} K_{\text{Mg}}^{\text{H}} &= 10^{-5.85} \\ K_{\text{Mg}}^{\text{Na}} &= 10^{-1.37} \\ K_{\text{Mg}}^{\text{K}} &= 10^{-1.45} \\ K_{\text{Mg}}^{\text{Ca}} &= 1.0 \end{aligned}$$

$$K_{\text{Mg}}^{\text{M}^{n+}} \text{ is defined by: } \frac{X_{\text{M}}^{n+}}{X_{\text{Mg}}} = K_{\text{Mg}}^{\text{M}^{n+}} \frac{a_{\text{M}}^{2/n}}{a_{\text{Mg}}}$$

where X_{M}^{n+} is the exchanged fraction of M. Sayles and Mangelsdorf (1979, Fig. 3) show a range of $K_{\text{Mg}}^{\text{Ca}}$ of between 0.8 and 1.2 for montmorillonites.

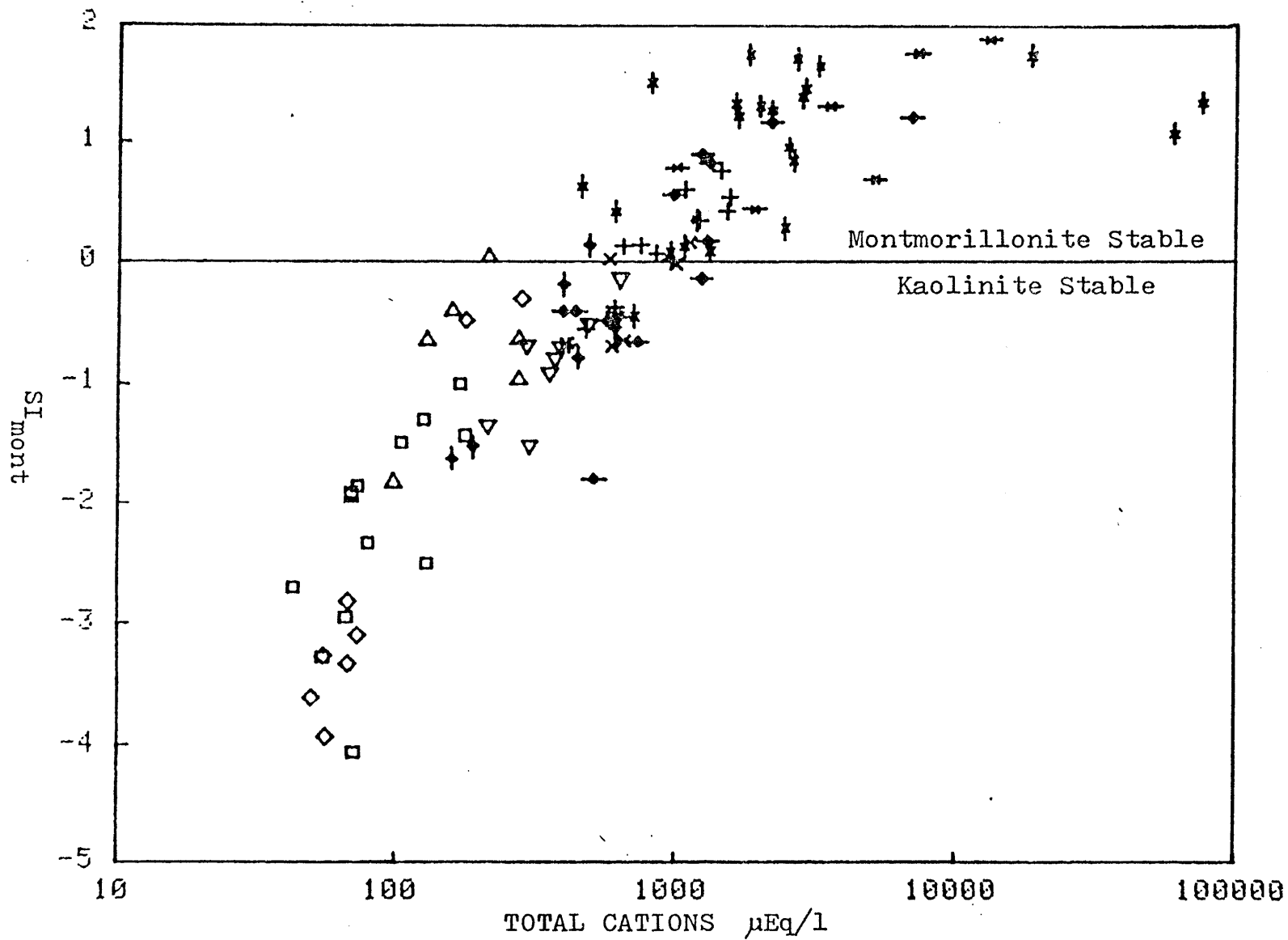
Using these coefficients, the exchanged fractions for other cations relative to magnesium can be determined for montmorillonites equilibrated with Amazon waters. In no case are exchangeable hydrogen ion or potassium

Figure IV.26

Stability index for a complex montmorillonite (Colony-I) plotted against total cations ($\mu\text{Eq/l}$). This saturation index was calculated using both calcium and magnesium as exchangeable ions. Nearly all the samples draining the Andes fall into the montmorillonite stability field with the exception of samples from the Madeira Basin and rivers with Andean headwaters crossing an expanse of lowlands. See Table IV.4 for comparison.

Symbol key:

- + - (1) Main Channel
- * - (2) Marañon Drainage
- * - (3) Ucayali Drainage
- * - (4) Madeira Drainage
- † - (5) Other Andean headwater rivers
- ◇ - (6) Negro Drainage
- - (7) Rivers draining shields
- ▽ - (8) Lowland rivers with extensive areas of marine sediments
- △ - (9) Rivers draining only U. Tertiary and Quaternary sediments
- X - (10) Varzêa waters



significant relative to exchangeable magnesium. Exchangeable sodium is comparable to calculated exchangeable magnesium only in two salt river samples (A-05), BPA16). Exchangeable calcium is greater than or equal to exchangeable magnesium.

Because calcium and magnesium are the dominant exchanged cations, the stability index can be formulated using the simplifying assumption that these are the only exchangeable ions. That is

$$X_{Mg} + X_{Ca} = 1 \quad \text{and} \quad K_{Mg}^{Ca} \text{ will be assumed to be 1.0.}$$

Therefore

$$X_{Mg} = 1 / (1 + a_{Ca} / a_{Mg})$$

The stability indices for magnesium and calcium saturated (Table IV.6,

Reaction 13) montmorillonites on the kaolinite boundary are given by:

$$SI_{Mg} = 0.20 \log (a_{Mg} / a_H^2) + 0.29 \log (a_{Mg} / a_H^2) + 2.10 \log (a_{Si}) + 3.15$$

$$SI_{Ca} = 0.20 \log (a_{Ca} / a_H^2) + 0.29 \log (a_{Mg} / a_H^2) + 2.10 \log (a_{Si}) + 3.15$$

These reactions are combined assuming: $SI_{mont} = X_{Mg} SI_{Mg} + X_{Ca} SI_{Ca}$

Giving:

$$SI_{mont} = 0.20 [X_{Mg} \log (a_{Mg} / a_H^2) + X_{Ca} \log (a_{Ca} / a_H^2)] + 0.29 \log (a_{Mg} / a_H^2) + 2.10 \log (a_{Si}) + 3.15$$

The Mg/(Ca+Mg) ratio of the montmorillonite is given by: $Mg/(Mg+Ca) =$

$$(0.29 + 0.20 X_{Mg}) / 0.49$$

When the montmorillonite saturation index is plotted against total cations (Figure IV.26), it is seen that its value exceeds one (that is montmorillonite is stable) only in basins with significant marine sedimentary deposits in their drainage (TZ+ >400-500). This relationship is reasonable as montmorillonite stability requires a great supply of magnesium and calcium ions.

Thermodynamic parameters such as the stability index have two disadvantages. Firstly, there are all those discussed earlier pertaining to heterogeneous systems and CO_2 exchange. A change of one pH unit will change the stability index for montmorillonite roughly one unit in the opposite sense. Secondly, it is not possible to tell whether montmorillonites are being formed or degraded. The high values for the stability index suggests that montmorillonites are forming, however this cannot be seen as unambiguous evidence.

IV.6:9 Reaction Mass-Balance Relationships

Chemical mass-balance relationships have been used as an independent test of thermodynamic models; in this case they are used to test the plausibility of the montmorillonite saturation index. The most sophisticated application of mass-balance relationships is found in Garrels (1967), who shows that the mineralogical composition of igneous rocks can be calculated from the composition of coexisting ground waters and the composition of the solid weathering products (kaolinite in the case of examples presented by Garrels 1967). Garrels (1967) observes that this approach is not possible in complex terrains, for example many sedimentary and metamorphic terrains (such as the Andean tributary basins).

Two simple mass-balance derived parameters, the alkalinity:silica ratio and the sodium:silica ratio have been used as a test of whether montmorillonites are forming during the weathering process (Feth et al. 1964, Polzer 1967, Garrels 1967). The essential observation is that the alkalinity:silica ratio and sodium:silica ratios are lower in soil solutions, when montmorillonite is the weathering product, than when kaolinite is the weathering product. These two ratio parameters have not been generalized to examine sedimentary terrains (the alkalinity:silica ratio is obviously not usable in carbonate terrains).

The ratio $Si/(Na^* + K^* - Cl^*)$ is the parameter chosen in this study to test if the weathering reactions are producing montmorillonite and/or kaolinite in a particular catchment. Na^* , K^* , and Cl^* are the Na, K, and Cl concentrations corrected for cyclic salt inputs (Section II.5-6). Cl^* is subtracted from Na^* to correct for terrestrial NaCl inputs. It is assumed that $(Na^* - Cl^*)$ and K^* represent material derived solely from silicate rock weathering. In general Na and K are not incorporated in clays produced in Amazonian weathering, with the possible exception of partially degraded illites where potassium is readily reincorporated.

The $Si/(Na+K)$ ratios for a variety of silicate weathering reactions are given in Table IV.6. With the exception of the weathering of paragonite, muscovite, or end member illite, all reactions producing kaolinite have dissolved product $Si/(Na+K)$ ratios near two; reactions producing gibbsite have ratios greater than two; and those producing montmorillonite have ratios of less than two.

The limitation of the $Si/(Na^* + K^* - Cl^*)$ parameter, in interpreting weathering processes, can be best illustrated through model "weathering" of standard lithologies. The "average shield" and "average shale" chemistries of Table III.1 are recalculated into normative igneous rock and micaceous sediment lithologies, respectively (Table IV.7). These are weathered three ways, producing gibbsite, kaolinite, or montmorillonite (of Colony-I composition). It is assumed that no iron, aluminum, or silicon from normative quartz are lost in the weathering. The products of the reactions are itemized in Table IV.8. The $Si/(Na^* + K^* - Cl^*)$ ratio is near two for kaolinite weathering of the igneous lithology, however it is near one for the weathering of the micaceous lithology. If the potassium in the micaceous lithology had been included in normative K-feldspar rather than muscovite, the $Si/(Na^* + K^* - Cl^*)$

ratio would have been nearer two, for the weathering of the average shale to kaolinite. Note that the silica and magnesium concentrations are negative in both examples of montmorillonite formation, as there simply is not enough silicon and magnesium available to produce a montmorillonite of this composition without supplying materials from elsewhere. If montmorillonite were forming, kaolinite would also be expected to form.

When silica is plotted against $(\text{Na}^* + \text{K}^* - \text{Cl}^*)$ for Amazon data, two distinct groups of data are seen (Figure IV.27). Rivers draining igneous and high grade metamorphic rocks and Tertiary fluvio-lacustrine sediments all fall on or above the 2:1, $\text{Si} : (\text{Na}^* + \text{K}^* - \text{Cl}^*)$ trend. This is taken to mean that weathering to kaolinite is occurring, along with weathering to gibbsite or the dissolution of quartz or kaolinite. The higher $\text{Si}/(\text{Na}^* + \text{K}^* - \text{Cl}^*)$ ratios of the lowest silica samples suggests that gibbsite formation, or quartz or kaolinite dissolution are of greater relative importance as a source of silica than the weathering of primary minerals to kaolinite. The most dilute samples are undersaturated with respect to quartz ($K_{\text{sp}} = 100 \mu\text{mole/l}$).

Rivers draining terrains having marine sediments fall on a broad horizontal trend, lying below the 2:1 ratio line (Figure IV.27). As was shown in the model rock weathering (Table IV.8). this could be due either to the weathering of micas or the formation of montmorillonites, and is in fact probably attributable to both processes. Weathering of mica-
ceous Paleozoic shales occurs in the Madeira Basin, where high levels of degraded micas (and usually low levels of montmorillonite) are seen in soils and river sediment. The lithologies in the Peruvian Andes are not notably micaceous, and montmorillonite is typically reported in soils and river load.

The contrast between the Madeira and other Andean rivers is best illustrated by comparing the saturation index for montmorillonite with the

Table IV.7
NORMATIVE MINERALOGIES*

Shield:

<u>mole %</u>	<u>Formula</u>	<u>Name</u>
0.10	CaSO ₄	Anhydrite
0.057	Ca ₅ (PO ₄) ₃ OH	Apatite
0.050	CaCO ₃	Calcite
0.105	FeS ₂	Pyrite
0.649	Fe ₃ O ₄	Magnetite
0.383	NaCa ₂ Fe ₄ ²⁺ Fe ³⁺ Si ₆ Al ₂ O ₂₂ (OH) ₂	} Hornblend
0.623	NaCa ₂ Mg ₄ Al Si ₆ Al ₂ O ₂₂ (OH) ₂	
1.200	CaAl ₂ Si ₂ O ₈	} Plageoclase
5.617	NaAlSi ₃ O ₈	
1.579	K Al Si ₃ O ₈	Microcline
2.091	KAl ₃ Si ₃ O ₁₀ (OH) ₂	Muscovite
22.819	SiO ₂	Quartz

Shale:

<u>mole %</u>	<u>Formula</u>	<u>Name</u>
0.17	NaCl	Halite
0.58	CaSO ₄	Anhydrite
0.057	Ca ₃ (PO ₄) ₃ OH	Apatite
4.647	CaCO ₃	Calcite
0.783	CaMg(CO ₃) ₂	Dolomite
0.480	Mg ₂ Fe ₃ Si ₃ AlO ₁₀ (OH) ₈	} Chlorite
0.437	Mg ₅ Si ₃ Al O ₁₀ (OH) ₈	
3.37	KAl ₃ Si ₃ O ₁₀ (OH) ₂	Muscovite
0.911	NaAl ₃ Si ₃ O ₁₀ (OH) ₂	Paragonite
2.369	NaAlSi ₂ O ₈	Na-Feldspar
32.128	SiO ₂	Quartz
1.49	Fe ₂ O ₃	Hematite

*units are in mole %, calculated from the original analyses found in Table IV.4

Table IV.8
MODEL WEATHERING PRODUCTS*

Shield:

Final Clay →	Gibbsite	Kaolinite	Montmorillonite
Products +			
Na ⁺	6.62	6.62	6.62
K ⁺	3.67	3.67	3.67
Mg ²⁺	2.49	2.49	-2.10
Ca ²⁺	4.09	4.09	0.93
Si(OH) ₄	36.29	17.79	-23.95
HCO ₃ ⁻	22.83	22.83	7.33
SO ₄ ²⁻	0.31	0.31	0.31
SiO ₂ (quartz)	22.82	22.82	22.82
Fe ₂ O ₃ (hemetite)	2.01	2.01	-1.47
Fe ₃ O ₄ (magnetite)	0.65	0.65	0.65
Al(OH) ₃	18.50	--	--
Al ₂ Si ₂ O ₅ (OH) ₄	--	9.25	--
Ca _{0.20} -Mg _{0.29} Al _{1.17} Fe _{0.22} Si _{3.81} O ₁₀ (OH) ₂		--	15.81
Si/(Na + K)	3.5	1.7	-2.3

Shale:

Final Clay →	Gibbsite	Kaolinite	Montmorillonite
Products +			
Na ⁺	3.45	3.45	3.45
K ⁺	3.37	3.37	3.37
Mg ²⁺	3.93	3.93	-0.07
Ca ²⁺	6.32	6.32	3.56
Si(OH) ₄	22.70	6.57	-29.83
HCO ₃ ⁻	25.99	25.99	12.47
SO ₄ ²⁻	0.58	0.58	0.58
Cl	0.17	0.17	0.17
SiO ₂ (quartz)	32.13	32.13	32.13
Fe ₂ O ₃ (hemetite)	2.21	2.21	0.69
Al(OH) ₃	16.13	--	--
Al ₂ Si ₂ O ₅ (OH) ₄	--	8.07	--
Ca _{0.20} -Mg _{0.29} Al _{1.17} Fe _{0.22} Si _{3.81} O ₁₀ (OH) ₂		--	13.78
Si/(Na + K - Cl)	3.4	1.0	4.5

*units are in mole %, calculated from the original analyses found in Table IV.4

$\text{Si}/(\text{Na}^* + \text{K}^* - \text{Cl}^*)$ ratio (Figure IV.28). Samples in which the saturation index is greater than zero and the ratio less than two are considered to be most likely to have montmorillonite forming in their catchments. Observe that about half of the Madeira Basin samples in which the ratios are less than two have saturation indices less than zero; in these samples the weathering of mica (muscovite/illite or paragonite) would be a preferred explanation for the low ratio, as this also agrees with geological observations. The ratios $\text{Si}/(\text{Na}^* - \text{Cl}^*)$ are generally less than two for Madeira samples, indicating that there must be a significant contribution of sodium from paragonite weathering. Montmorillonites must also be forming in the Madeira Basin, as the two samples with the lowest $\text{Si}/(\text{Na}^* + \text{K}^* - \text{Cl}^*)$ ratio are from the Guapay and Piray rivers. The chemistry of these samples is thought to be controlled by the dissolution of soil salts (Section IV.4:5); such cyclic wetting and drying of soils apparently contributes to montmorillonite formation in soils (Drever and Smith 1978). Obviously, in a given area, many different silicate weathering reactions are occurring, and some cannot be unambiguously differentiated from others using only water chemistry data. Available soil and sediment data for the Amazon Basin is clearly inadequate to make this differentiation. To reiterate, the existing data suggest only that the weathering of mica (to degraded micas or kaolinite) is an important process in the Madeira Basin (this does not rule out significant montmorillonite formation), and that montmorillonite formation (along with kaolinite formation) is an important weathering process in the Peruvian Andes (mica degradation can also be occurring). These processes are consistent with observations regarding both the $\text{Si}/(\text{Na}^* + \text{K}^* - \text{Cl}^*)$ ratio and thermodynamic models (SI_{mont}).

The $\text{Si}/(\text{Na}^* + \text{K}^* - \text{Cl}^*)$ ratio provides a means of testing whether mont-

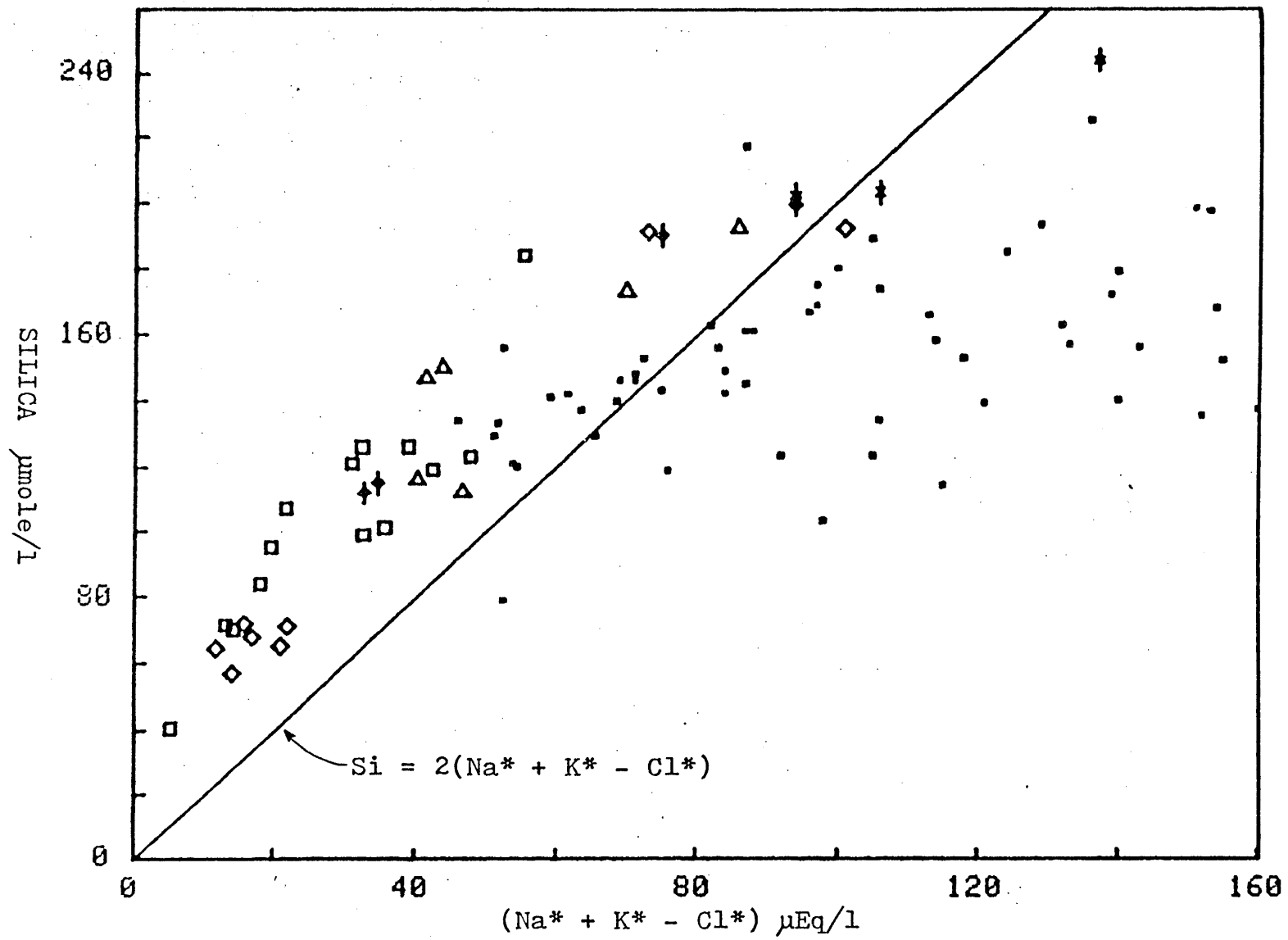
Figure IV.27

Two graphs of silica versus sodium plus potassium minus chloride ($\mu\text{Eq/l}$). The latter species are corrected for cyclic salt inputs, "s". The chloride is included to correct for evaporite inputs, primarily of sodium. In the first graph, only rivers draining terrains having little or no marine sediments are emphasized. In the second graph, rivers draining marine sediments are emphasized. The trend indicated in the graph would result from the weathering of feldspars to kaolinite.

Symbol key:

- + - (1) Main Channel
- * - (2) Marañon Drainage
- * - (3) Ucayali Drainage
- * - (4) Madeira Drainage
- ♦ - (5) Other Andean headwater rivers
- ◇ - (6) Negro Drainage
- - (7) Rivers draining shields
- ▽ - (8) Lowland rivers with extensive areas of marine sediments
- △ - (9) Rivers draining only U. Tertiary and Quaternary sediments
- X - (10) Varzêa waters

- - - Rivers draing marine sediment in the first graph
Rivers not draining marine sediment in the second graph



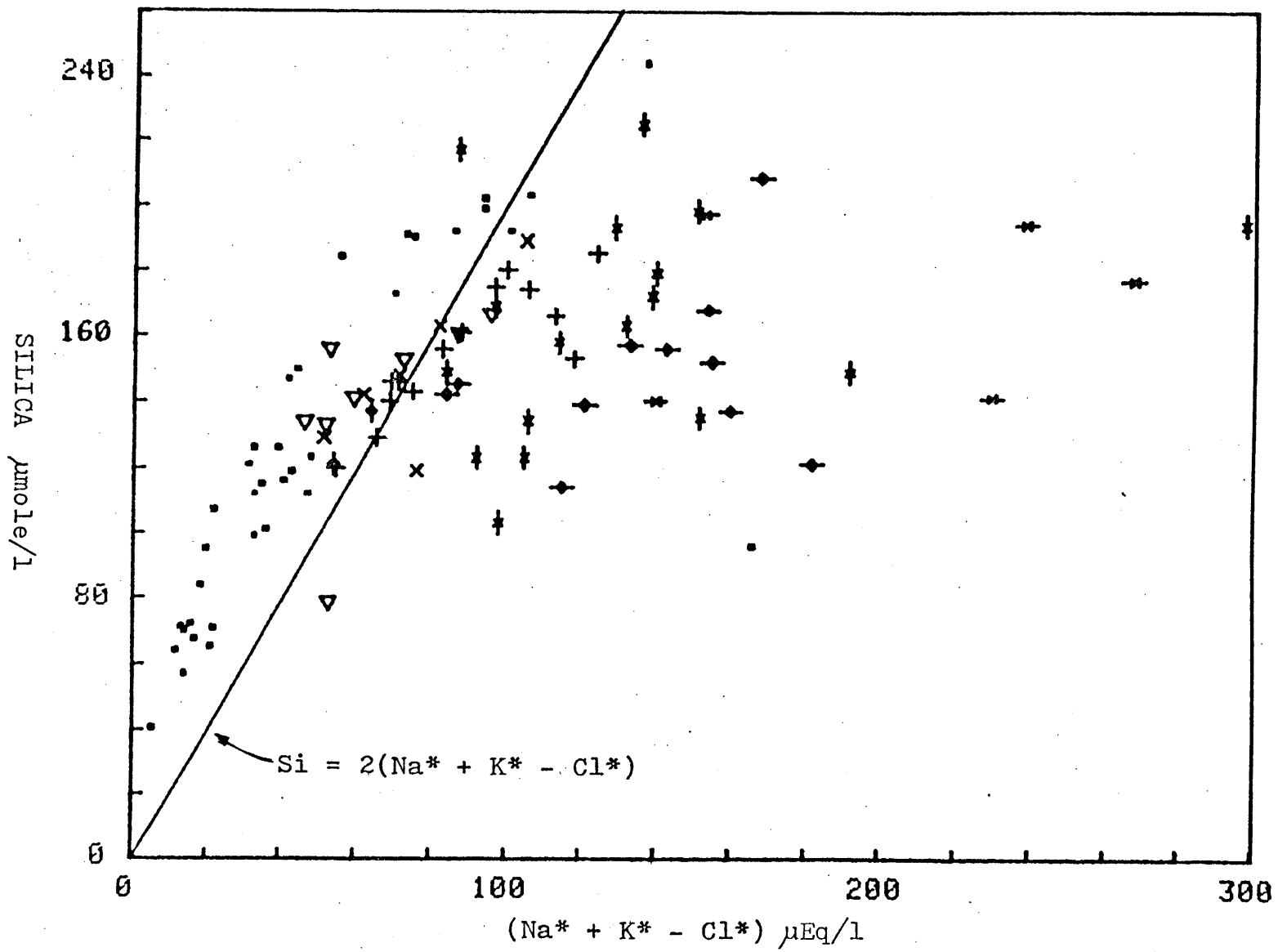


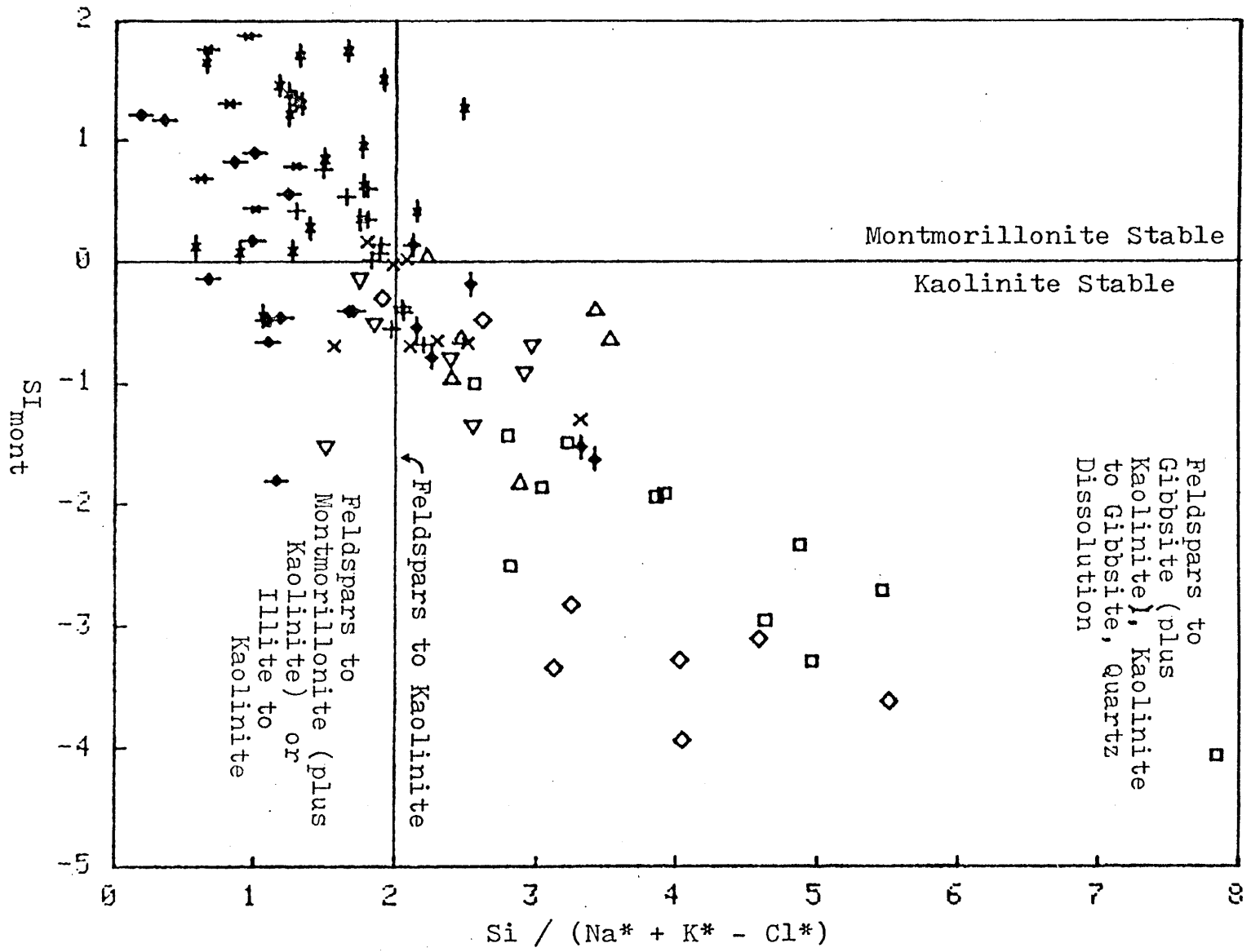
Figure IV.28

The stability index for montmorillonite (Colony-I) plotted against $Si/(Na^*+K^*-Cl^*)$, the "*" signifying cyclic salt corrected data. The two parameters represent independent weathering reaction "indicators", the first based on thermodynamics, the second on reaction mass balances. Both parameters suggest that montmorillonite formation is occurring in the Peruvian Andes.

Symbol key:

- + - (1) Main Channel
- * - (2) Marañon Drainage
- *- - (3) Ucayali Drainage
- ◆ - (4) Madeira Drainage
- ↓ - (5) Other Andean headwater rivers
- ◇ - (6) Negro Drainage
- - (7) Rivers draining shields
- ▽ - (8) Lowland rivers with extensive areas of marine sediments
- △ - (9) Rivers draining only U. Tertiary and Quaternary sediments
- X - (10) Varzēa waters

note that the long axis of the graph is horizontal.



morillonites are forming or are being degraded to a highly cation depleted clay (note that kaolinite is observed in Andean rivers). The Si/TZ+ ratio in solutions associated with degrading montmorillonites is very high (see Table IV.6). Since mostly bivalent ions are in the montmorillonite structure, the Si/(Na+K) ratio would be greater than two (far greater than two, if kaolinite was forming). Si/(Na*+K*-Cl*) ratios much greater than two are not observed in any Andean samples (see Figure IV.28), suggesting that montmorillonite formation is occurring in the Andes, and that significant montmorillonite degradation is not going on.

IV.7 CATION RATIOS AND SILICATE WEATHERING

To this point, the chemical data for the Amazon samples has been used to generate parameters that emphasize that certain silicate weathering reactions are occurring, in spite of variations in chemical composition that might be caused by rock type. Other parameters can be chosen to emphasize differences in lithology, and relate the weathering process to the denudation regimes (transport limited and weathering limited) discussed in Section III.6.

The principal chemical difference between transport and weathering limited conditions is that the physical products of weathering have a longer time to react with soil and ground waters in the former, while partially weathered, disaggregated material is generated in the latter. The erosion of partially weathered material may lead to very significant fractionation of Na, K, Mg, and Ca. Potassium and magnesium are not strongly weathered from saprolite developed on acid to intermediate rocks (Section II.4:3). Solifluction processes and soil sliding act on the the less coherent layers from which Na and Ca have been preferentially removed. As a result, Na and Ca should be partitioned into liquid phases and K and Mg into solid phases. Under weathering limited conditions, this relative mobility trend would be expected of the acid to intermediate rocks. No fractionation is expected for complete weathering to kaolinite or gibbsite, which is expected in the lowlands.

The relative mobility trend is quite unlike the composition trend for common igneous rocks. As one goes from basic (not common in the Amazon) to acidic rocks, the $Mg/(Ca+Mg)$ ratio decreases and the $K/(Na+K)$ ratio increases.

The ratio $(\text{Na}^* + \text{K}^* - \text{Cl}^*) / (\text{TZ}^* - \text{Cl})$, where "*" signifies cyclic salt corrected, represents the ratio of monovalent ions, derived from silicate rock weathering, over the total cations derived from the weathering of silicates, carbonates, and gypsum. This ratio drops systematically with increasing TZ^* (Figure IV.29). Samples derived from terrains free of carbonates and sulfates have a ratio averaging 0.38. This value is reasonable for silicates described for the Amazon region (c.f. Table III.1).

The $\text{K}^* / (\text{Na}^* + \text{K}^* - \text{Cl}^*)$ and $\text{Mg}^* / (\text{Ca}^* + \text{Mg}^*)$ ratios in water samples provide a basis for comparing rock and solute compositions in the Amazon Basin. The $\text{K}^* / (\text{Na}^* + \text{K}^* - \text{Cl}^*)$ ratio represent only siliceous inputs, while the $\text{Mg}^* / (\text{Ca}^* + \text{Mg}^*)$ ratio also includes contributions from carbonates and evaporites. When these ratios for Amazon data and various rock types (Figure IV.29) are plotted against one another, two features can be seen. Firstly, samples from particular regions plot as distinct groupings. Secondly, samples from the lowlands plot in a general field encompassing intermediate to acidic igneous rocks, "average" shield, and "average" shale compositions (reflecting conditions where relative mobility is less important), while Andean samples are sodium and calcium enriched compared to typical igneous rock and shale compositions. The particularly high $\text{K}^* / (\text{Na}^* + \text{K}^* - \text{Cl}^*)$ and $\text{Mg}^* / (\text{Ca}^* + \text{Mg}^*)$ ratios for some lowland rivers must reflect reweathering of soils and fluvio-lacustrine sediments, already enriched in K and Mg (c.f. Sections IV.4:8, IV.4:11).

In the Andean samples, calcium enrichment is largely due to contributions from limestones and evaporites, however the $(\text{Na}^* - \text{Cl}^*)$ enrichment can only be due to the partitioning of potassium, during silicate weathering, into solid phases of soils and river suspended load. This partitioning is particularly pronounced in the case of the Madeira samples, draining Lower Paleozoic shales, where water ratios are quite low compared to "average" shale and black shale ratios, reflecting stability of potassium bearing micas.

Figure IV.29

First graph:

Cation ratios in water samples with cyclic salt and halite corrections. The first graph is of $(Na^*+K^*-Cl^*)/(TZ+*-Cl^*)$ versus total cations (uEq/l). The drop in the ratio with increasing total cations reflects increasing contributions of bivalent ions from carbonates and evaporites.

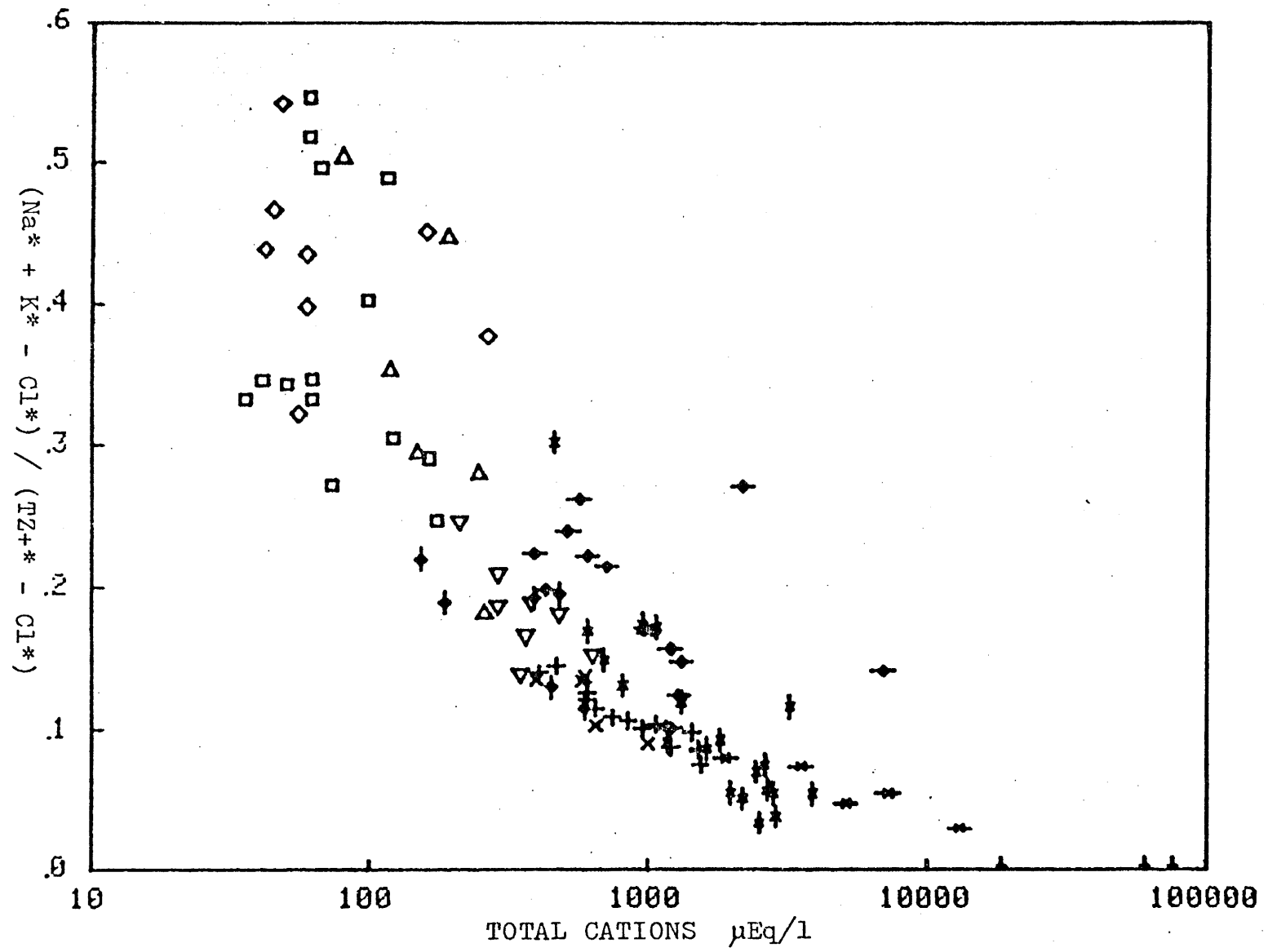
Second graph:

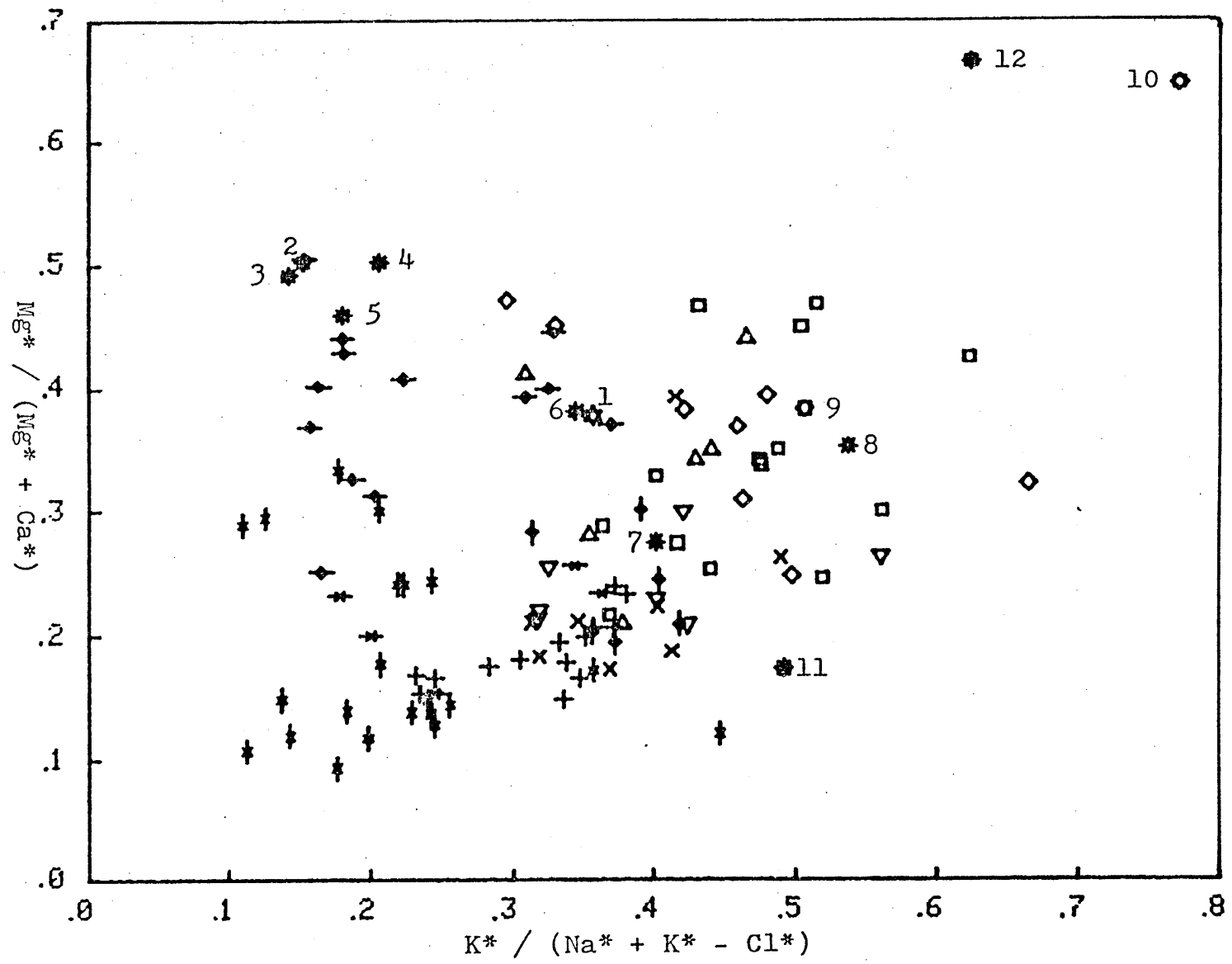
$Mg^*/(Mg^*+Ca^*)$ versus $K^*/(Na^*+K^*-Cl^*)$. Ratios for samples from Amazon surface waters are included along with ratios predicted or the weathering of siliceous lithologies (Table IV.4) to kaolinite. Note that all of the lowland samples fall into a grouping, consistent with lithologies known to be present in their drainages. In contrast Andean samples are strongly sodium and calcium enriched compared to any reasonable silicate lithologies in their drainages. This can be attributed to two factors: (1) the weathering of carbonates and evaporite minerals, rich in calcium (note NaCl inputs have been corrected for), and (2) preferential weathering of calcium and sodium silicate minerals and the transport of potassium and magnesium on solid phases.

- | | | |
|----------------------|--------------------|----------------------|
| 1-average shield | 5-andesite | 9-average shale |
| 2-gabbro | 6-granodiorite | 10-black shale |
| 3-continental basalt | 7-sodic granite | 11-fresh granite |
| 4-diorite | 8-potassic granite | 12-weathered granite |

Symbol key:

- + - (1) Main Channel
- * - (2) Marañon Drainage
- * - (3) Ucayali Drainage
- * - (4) Madeira Drainage
- † - (5) Other Andean headwater rivers
- ◇ - (6) Negro Drainage
- - (7) Rivers draining shields
- ▽ - (8) Lowland rivers with extensive areas of marine sediments
- △ - (9) Rivers draining only U. Tertiary and Quaternary sediments
- X - (10) Varzēa waters





IV.8:1 IRON AND ALUMINUM

Iron and aluminum have not been discussed up to this point as the behavior of these elements is so clearly unlike other species examined (see Figure IV.8), exhibiting an inverse relationship with total cations. Two parameters also showing an inverse relationship are color and hydrogen ion. The decrease in hydrogen ion with increasing TZ+ reflects equilibration with increasing concentrations of bicarbonate. Color in Amazon waters is derived from small molecular weight organics (relative to typical humics) characterized by aromatic nuclei quinone groups, or free-radical groups, (J. Leenheer, U.S.G.S., personal communication). Correlations between color and iron content of rivers has been observed in surface waters of the United States (Lamar 1968).

Organic materials have been shown to be very active chemically in soils and surface waters, serving as chelators, colloid stabilizing agents, reducing agents, and simply as acids. Various studies have shown that soil and water organics possess chelating properties (Deb 1949, Hem 1960, Wright and Schnitzer 1963, Schnitzer and Skinner 1963a, 1963b, 1965, and others). The correlation of iron and aluminum with organics in surface waters is cited as evidence of chelation (Martin et al. 1971, Beck et al. 1974, Reuter et al. 1976). Other studies suggest that trace metals, stabilized in the aqueous phase by organics, exist as colloids and not in true solution. Deb (1949) observes that colloidal iron oxide can be stabilized by humic materials with a Fe:C mole ratio as high as 4:1. Ong and Bisque (1968) note that humic complexes coagulate according to colloid precipitation theory and are likely hydrophobic colloids. Benes et al. (1976) observe that trivalent ions and many trace divalent ions are removed from lake water by ultrafiltration and are therefore either colloids or macromolecular complexes.

In recent work on the estuarine geochemistry of several trace metals (Eckart and Sholkovitz 1976, Sholkovitz 1976, Boyle and Sholkovitz 1977) demonstrate coupled behavior of iron, aluminum, manganese, and phosphorous and experiments using ultracentrifugation and filtration suggest that these elements exist as colloidal material, stabilized by organics. Organics (glucose) have been used as reducing agents to produce material resembling soft laterite in water saturated soils (Beadle and Burgess 1953), and tannic materials (colored products of leaf and bark decay) have been shown to stabilize FeII under oxidizing conditions and to be capable of reducing iron at a pH below 3 (Theis and Singer 1974).

Materials stabilized or dissolved by organics can be destabilized or precipitated by various mechanisms. Precipitation of humic complexes as a result of increasing cation concentrations with depth in soils is thought to be a cause of hydroxide rich layers in podzol soils (Wright and Schnitzer 1963). Ong and Bisque (1968) observe that the effectiveness of the coagulation of humic materials increases greatly with increasing ion valency. Organic acids can be strongly adsorbed on clay minerals and even more so on amorphous aluminium and iron hydroxides (Bloomfield 1953, Greenland 1971). Passage through such materials could immobilize complexes or stabilized colloids; this mechanism is thought to explain the greatly reduced coloration of waters draining terrains having clay rich soils in the Amazon (J. Leenheer, U.S.G.S., personal communication).

IV.8:2 Properties of Amazon Iron and Aluminum Phases

The chemistry of iron and aluminum in Amazon waters will be examined in terms of relationships between these elements and other measured properties. No laboratory experiments were done to characterize their chemistries.

Iron and aluminum samples were treated in two ways:

- (1) One split was treated by filtration followed by acidification in the field (see Appendix II for details).
- (2) Another split was untreated and allowed to settle for several months prior to analysis.

Samples of the first type show very high concentrations in some Andean rivers, thought to be due to dissolution of clays, passing through the (.45 μ) filter. Several lowland samples in the second group show exceptionally high concentrations. This is thought to be due to low density phases which are filterable, but which do not settle out. Procedural blanks for both treatments were satisfactory. Because the high iron and aluminum values are attributed to a particulate phase in treated Andean samples, these cannot be used directly to examine solution properties.

Treated and untreated aluminum in lowland rivers are highly correlated (Figure IV.30), and on this basis it appears that aluminum exists in rather a stable form in lowland river waters. The slope of the trend between treated and untreated samples is 0.93 ± 0.7 with an intercept of 0.00 ± 0.05 $\mu\text{mole/l}$ ($r=0.979$, $S=0.43$), essentially a 1:1 trend.

Treated and untreated iron in lowland samples is also correlated (Figure IV.31). The unusually high values in the untreated samples are thought to be a low density particulate phase which is filterable but which does not settle on storage. A line fit through the trend of data, excepting these high values, has a slope (untreated versus treated) of 1.04 ± 0.16 and an intercept of 0.83 ± 0.16 ($r=0.894$, $s=0.96$). The intercept on the Fe-treated axis is 0.80. This offset is taken to be caused by a form which remains in solution or suspension only upon acidification.

A reasonable explanation for the behavior of iron and aluminum in lowland rivers is that iron exists as both a complex and an organic-stabilized colloid, while aluminum exists exclusively as a complex. Boyle (personal communication) states that the organic-stabilized colloid observed by Boyle

and Sholkovitz (1976) is lost from suspension upon storage. Such loss could therefore explain the non-zero treated iron intercept. Treated iron and treated aluminum are loosely correlated (Figure IV.32) and show the same non-zero iron intercept seen in the graph of treated versus untreated iron (Figure IV.31).

Both iron and aluminum are stable in solution on short time scales under conditions of changing ionic strength. Waters from the Negro River (I=65 $\mu\text{mole/l}$, pH=5.36) mix with those of the main channel (I=873 $\mu\text{mole/l}$, pH=6.74), over a distance of about 200 km, prior to merging with waters from the Madeira. This represents a period of mixing of about 40 to 50 hours prior to sampling, filtration, and acidification. Figure IV.33 presents plots of four parameters Ca, Si, Fe, and Al against alkalinity. Calcium, silica and alkalinity are presumed to be conservative, and simple two-end-member mixing is evidenced by linear plots of one parameter against another. Stations S213 and S214 are from opposite sides of the main channel upriver from the Madeira confluence. Both iron and aluminum show conservative behavior. The scatter on the iron graph is greater than the analytical error, however it is not systematic.

IV.8:3 Relationships of Fe and Al With Other Species

The relationship of iron and aluminum with hydrogen ion and color and net inorganic charge balance (NICB) were examined with the intent of identifying the "best" relationship between parameters in lowland rivers. Since there is no apparent difference between treated and untreated aluminum concentrations the untreated values were used where treated samples were not analyzed. Only analyses of treated iron were used. Lowland iron and aluminum concentrations are plotted against total cations in Figure IV.34.

Figure IV.30

Treated (filtered and acidified) aluminum versus untreated aluminum. Note the excellent, one to one, correlation between these parameters.

Symbol key:

- + - (1) Main Channel
- ⊕ - (5) Other Andean headwater rivers
- ◇ - (6) Negro Drainage
- - (7) Rivers draining shields
- ▽ - (8) Lowland rivers with extensive areas of marine sediments
- △ - (9) Rivers draining only U. Tertiary and Quaternary sediments
- X - (10) Varzêa waters

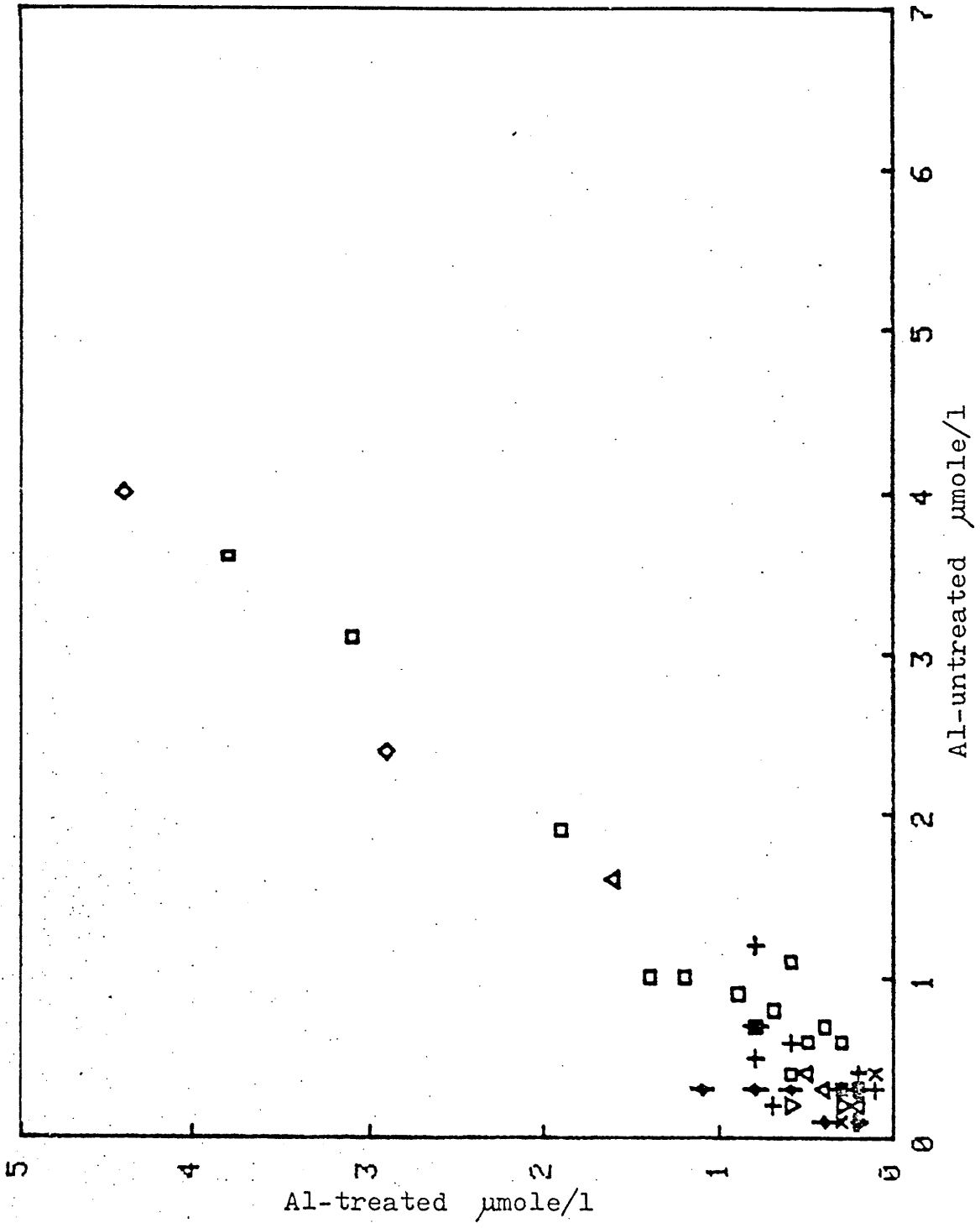


Figure IV.31

Treated iron versus untreated iron ($\mu\text{mole/l}$). Note that a background iron phase apparently is preserved in treated samples, but is not observed in the untreated samples. If the high untreated points are excluded, a reasonable correlation exists between treated and untreated iron.

Symbol key:

- + - (1) Main Channel
- ◆ - (5) Other Andean headwater rivers
- ◇ - (6) Negro Drainage
- - (7) Rivers draining shields
- ▽ - (8) Lowland rivers with extensive areas of marine sediments
- △ - (9) Rivers draining only U. Tertiary and Quaternary sediments
- X - (10) Varzêa waters

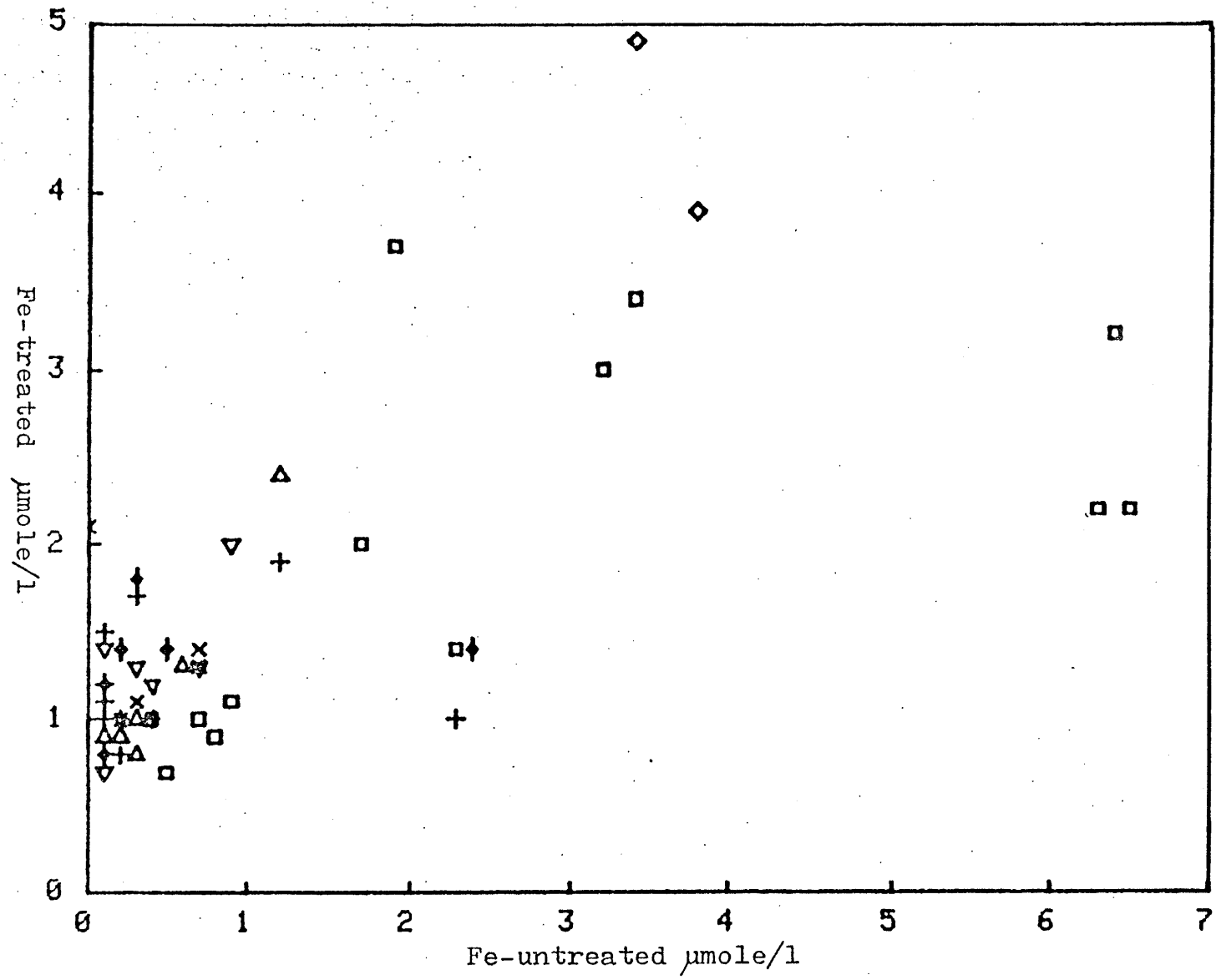


Figure IV.32

Treated aluminum versus treated iron ($\mu\text{mole/l}$).

Symbol key:

- + - (1) Main Channel
- ◆ - (5) Other Andean headwater rivers
- ◇ - (6) Negro Drainage
- - (7) Rivers draining shields
- ▽ - (8) Lowland rivers with extensive areas of marine sediments
- △ - (9) Rivers draining only U. Tertiary and Quaternary sediments
- X - (10) Varzêa waters

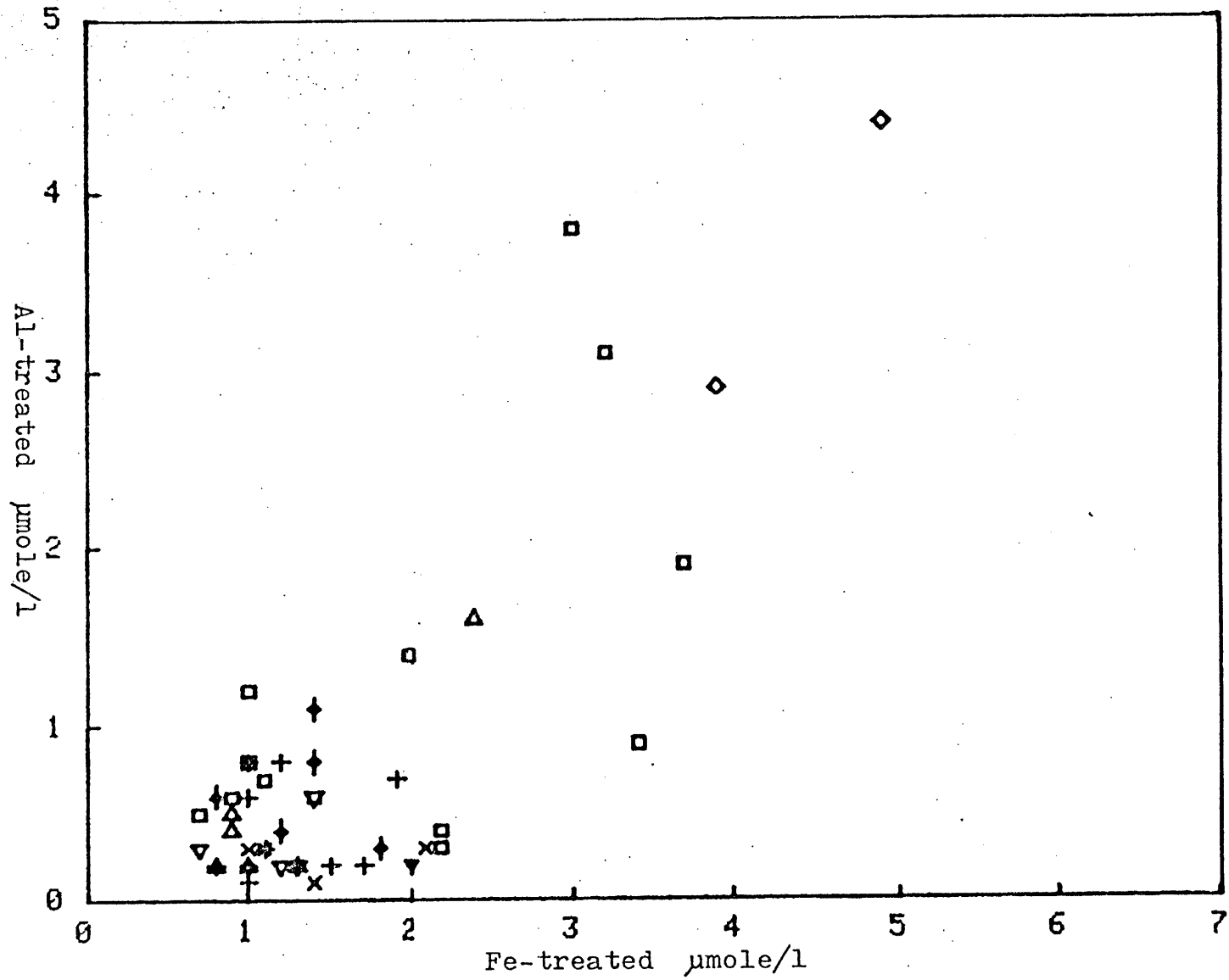


Figure IV.36

Calcium, silica, treated iron, and treated aluminum versus titration alkalinity for samples from the mixing zone for Negro River water with main channel water. The linearity of the first two graphs is taken to mean that the chemistry of conservative species in these samples can be described by simple two end-member mixing. The linearity of the second two graphs suggests that iron and aluminum are conservative on short time scales (40-50 hours). Of all large tributaries, the Negro River shows the greatest chemical contrast to the main channel.

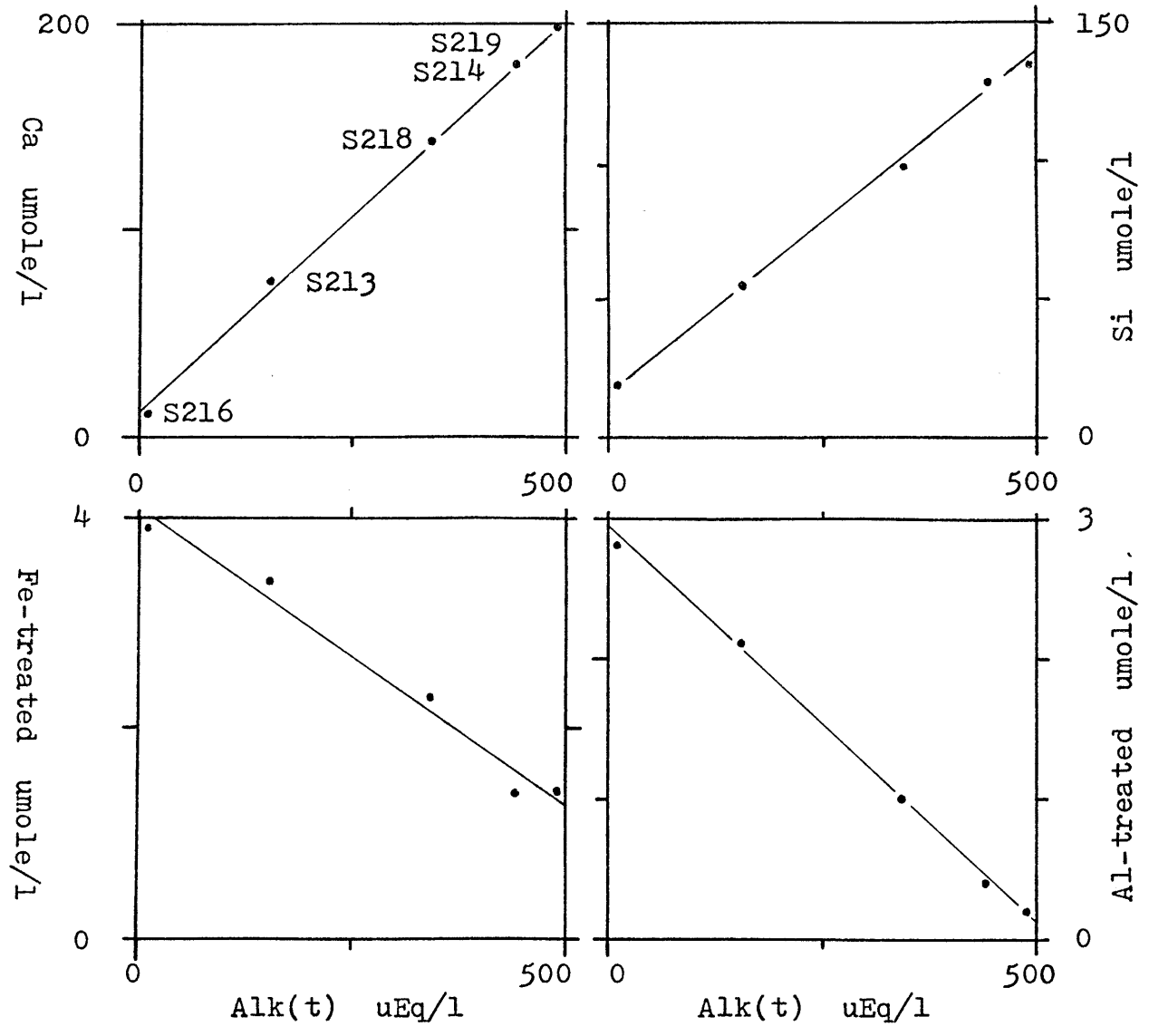
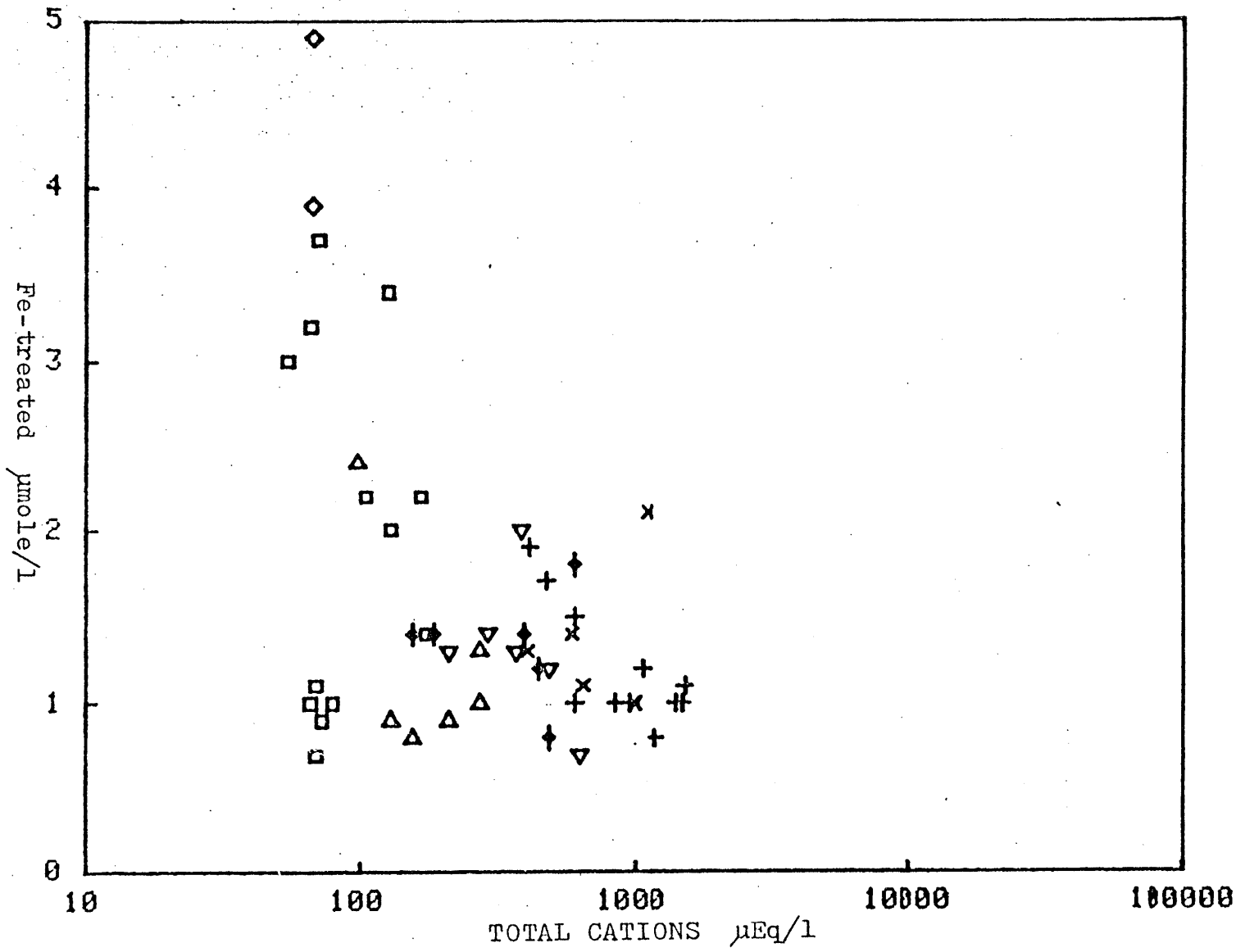


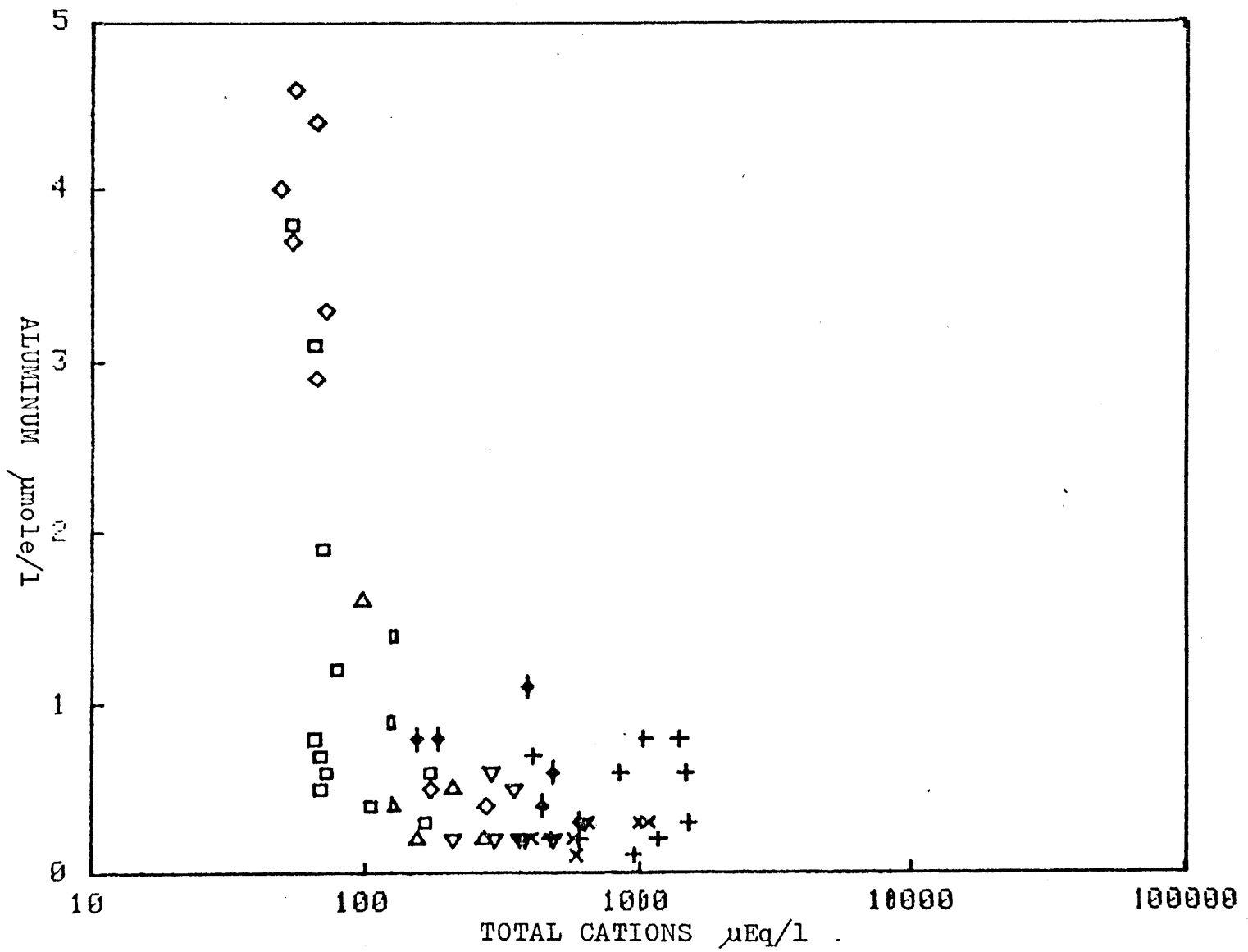
Figure IV.34

Iron and aluminum versus total cations for lowland rivers. Only treated iron samples are included, however because of the good correlation between treated and untreated aluminum, untreated values have been substituted where treated analyses are not available (mostly Negro Basin samples).

Symbol key:

- † - (1) Main Channel
- ◆ - (5) Other Andean headwater rivers
- ◇ - (6) Negro Drainage
- - (7) Rivers draining shields
- ▽ - (8) Lowland rivers with extensive areas of marine sediments
- △ - (9) Rivers draining only U. Tertiary and Quaternary sediments
- X - (10) Varzēa waters





The best correlations observed were between iron and color (Figure IV.35) and between aluminum and hydrogen ion (Figure IV.36), suggesting that slightly different mechanisms are responsible for mobilizing iron and aluminum. In Amazon soils, iron is typically found as amorphous hydroxides and as goethite distributed throughout the profile, with goethite tending not to be present in the surface root-containing zone, when the soil organic carbon content exceeds 5% (see Section III.5).

Aluminum, on the contrary, is typically found in a crystalline form, kaolinite. It may be that the colored soil organics are capable of mobilizing iron over a wider pH range, and that aluminum mobilization is facilitated by higher acidity, which would aid in hydrolyzing the kaolinite lattice. Once mobilized into surface waters, aluminum and iron are stable, on the time scale of a few days, as is seen in the mixing of the Negro and Solimões.

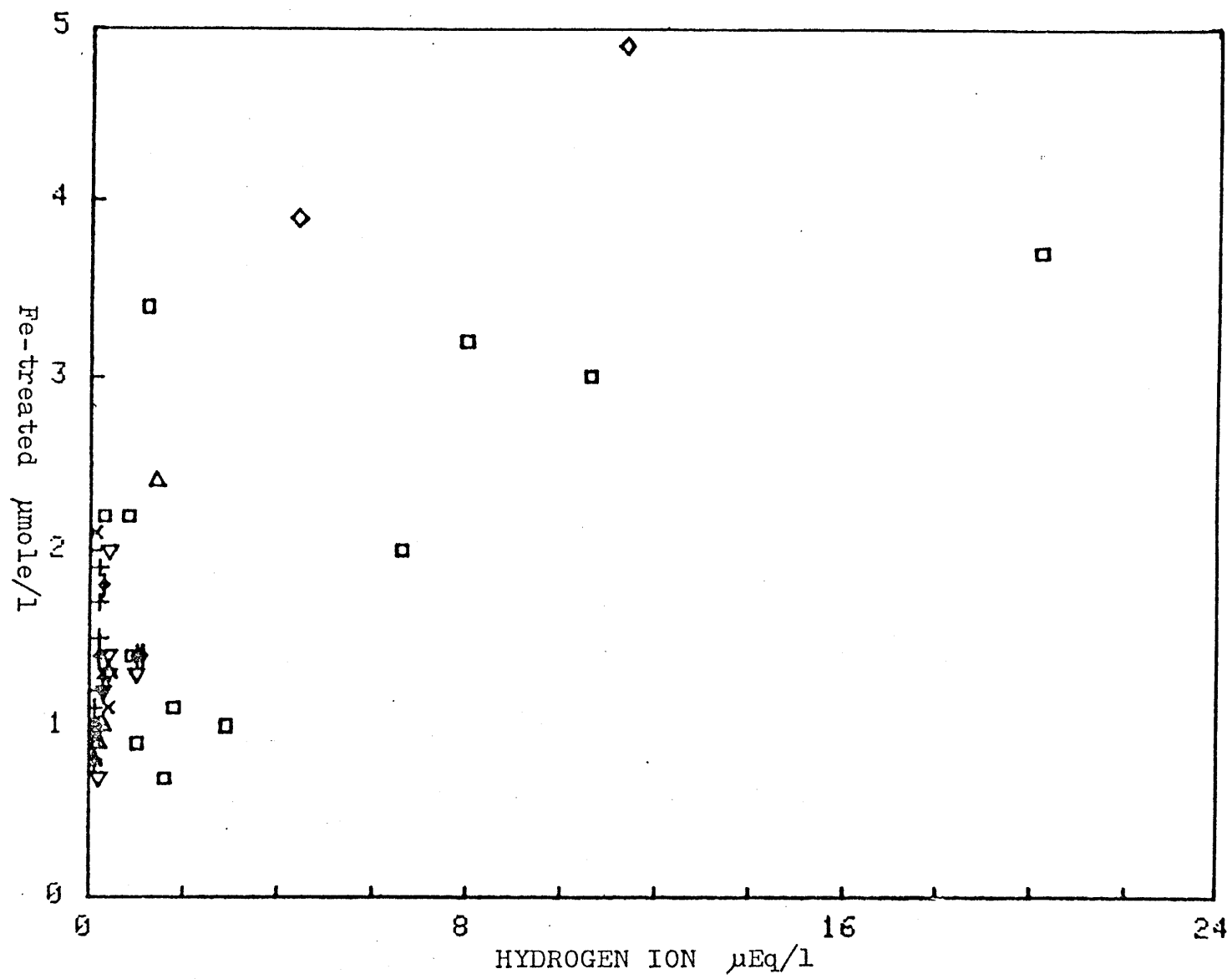
Ultimately, controls on iron and aluminum concentrations are exerted by the presence of cation rich phases in the soil. The weathering of these phases and concomitant hydrogen ion consumption and bicarbonate formation increases the pH. Furthermore, these solid phases serve to bind and immobilize soil organics. Once pH is raised and organics are fixed, iron and aluminum mobility should be low.

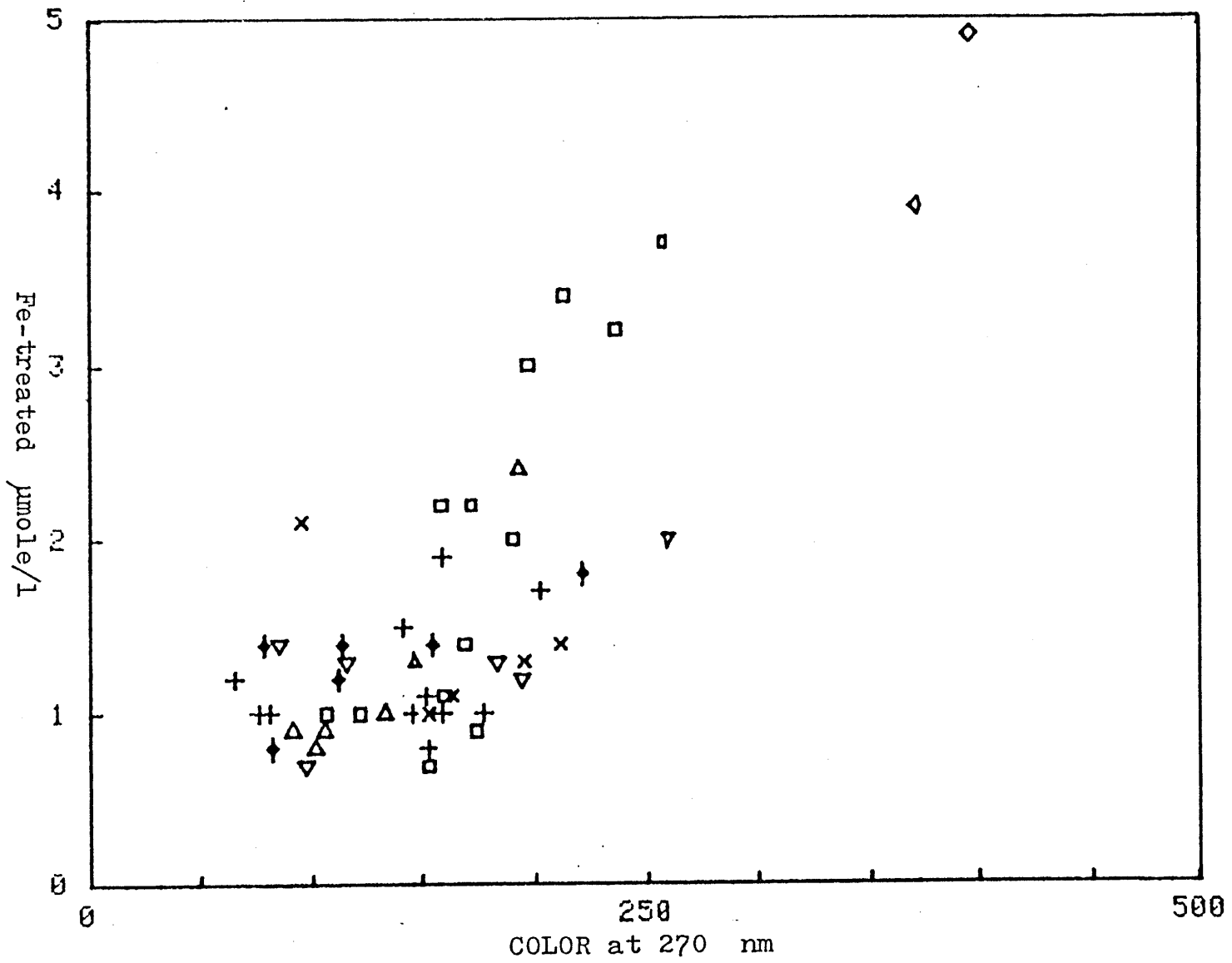
Figure IV.35

Treated iron versus hydrogen ion, color, and net inorganic charge balance (NICB2). The NICB2 is calculated assuming that iron and aluminum are trivalent species. Note that the best correlation is between iron and color.

Symbol key:

- + - (1) Main Channel
- ◆ - (5) Other Andean headwater rivers
- ◇ - (6) Negro Drainage
- - (7) Rivers draining shields
- ▽ - (8) Lowland rivers with extensive areas of marine sediments
- △ - (9) Rivers draining only U. Tertiary and Quaternary sediments
- X - (10) Varzêa waters





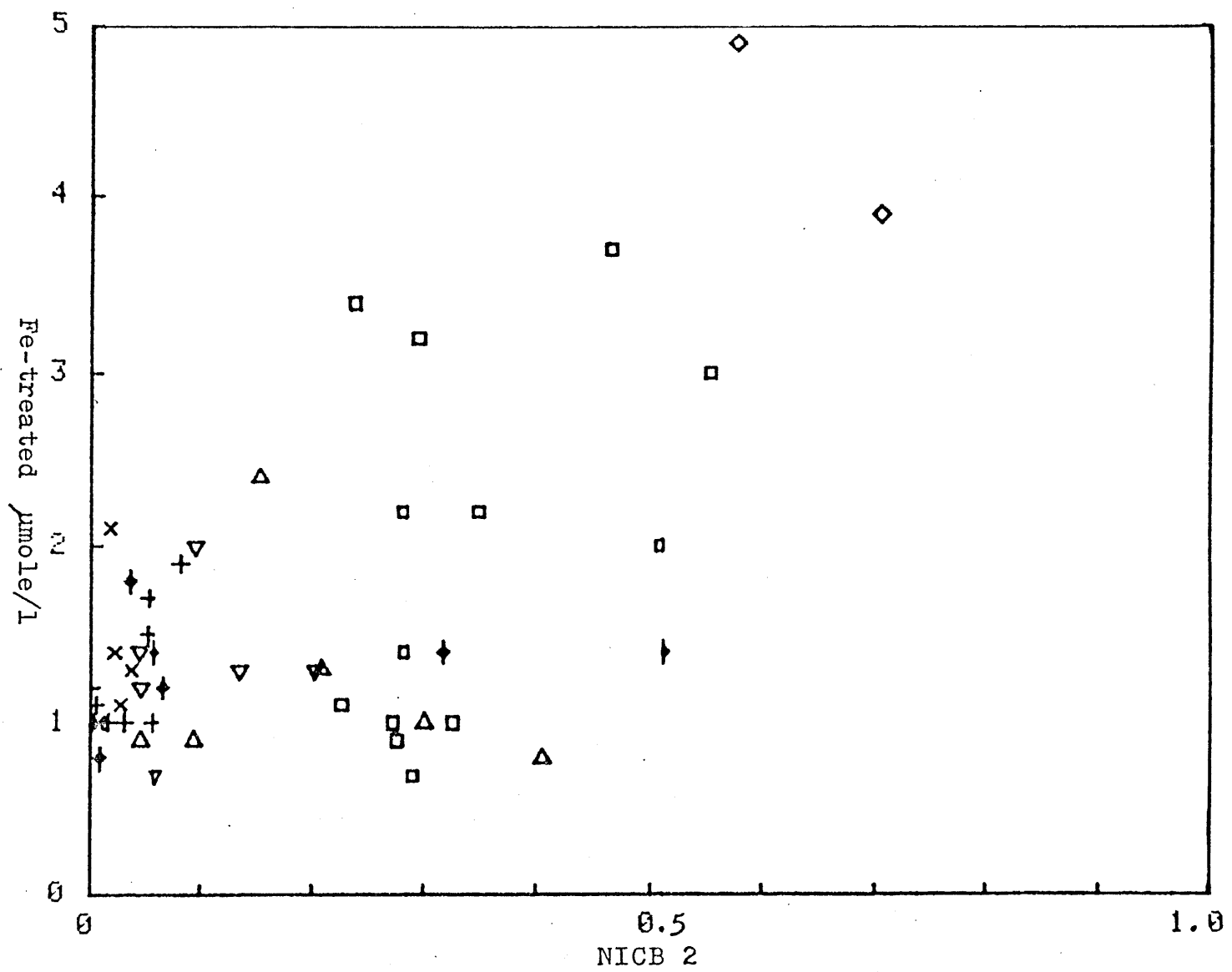
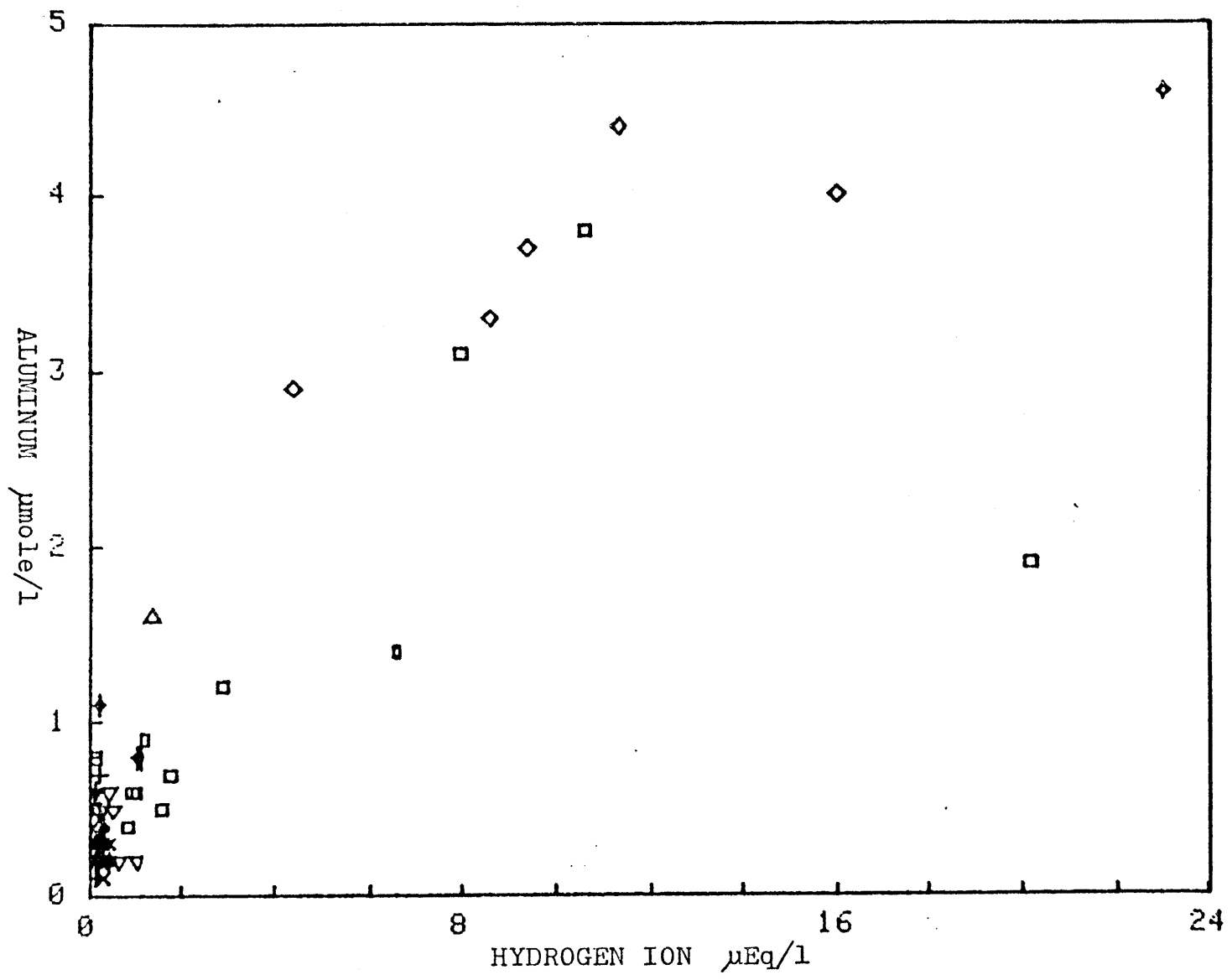


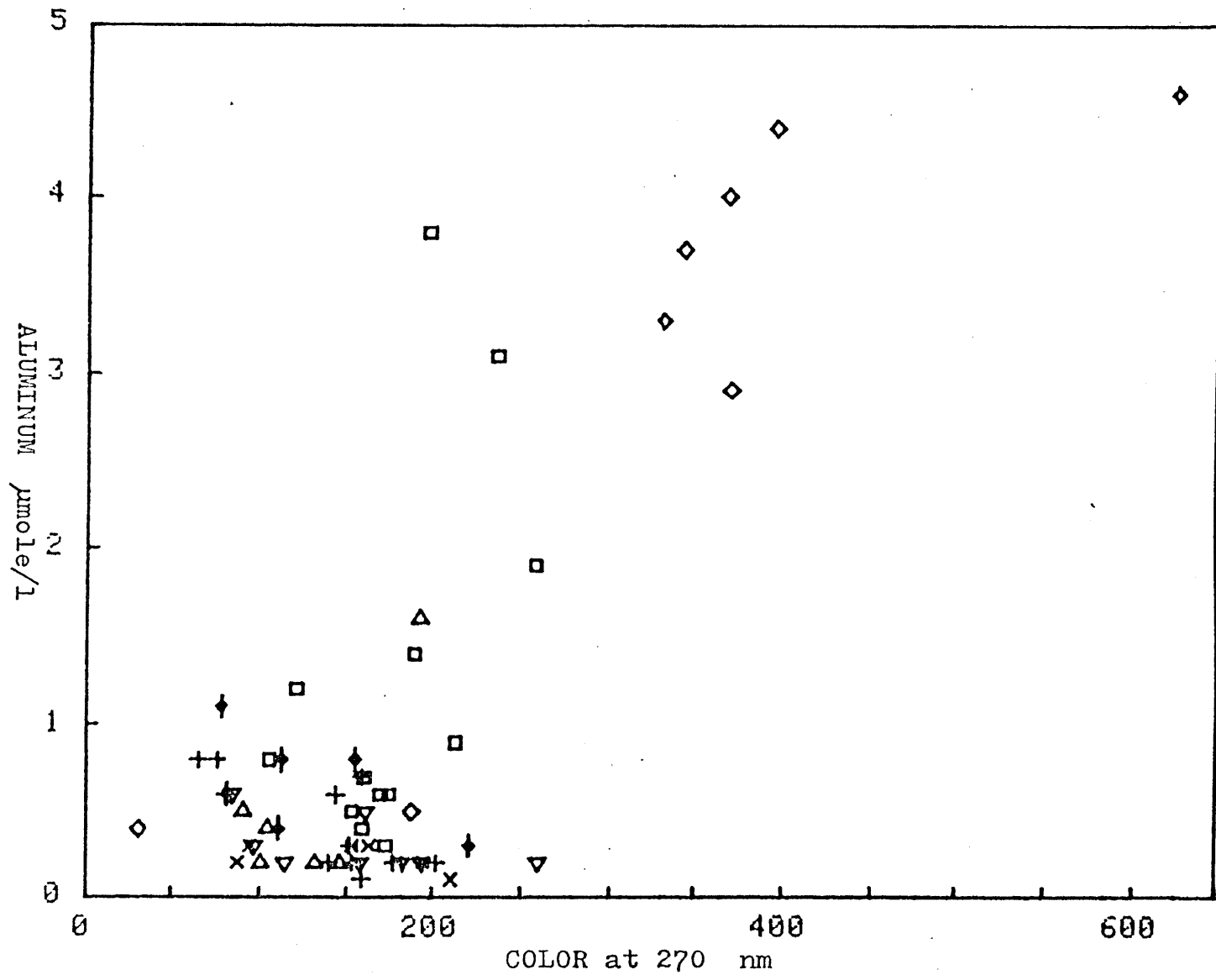
Figure IV.36

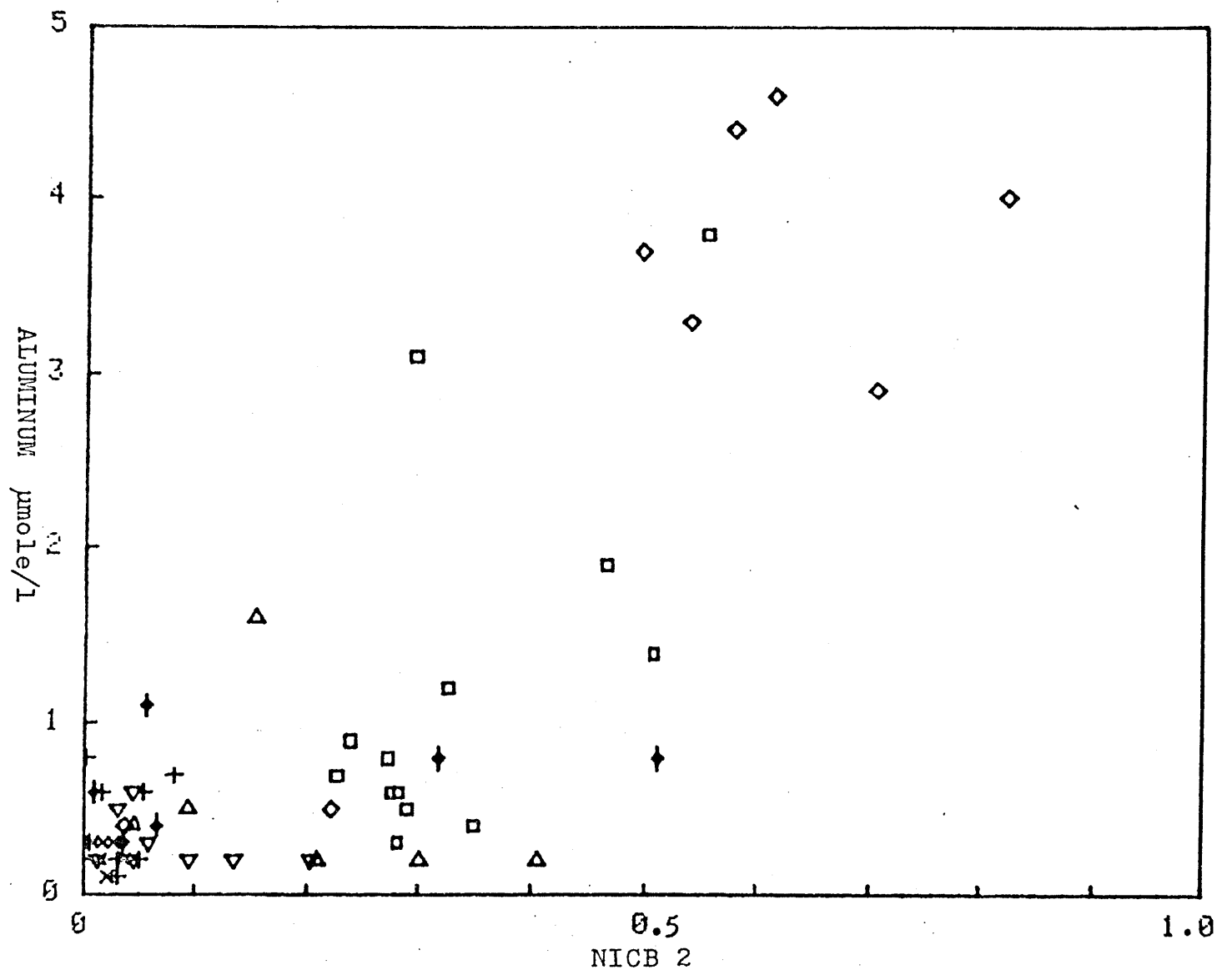
Aluminum versus hydrogen ion, color, and net inorganic charge balance.
Note that the best correlation is between aluminum and hydrogen ion.

Symbol key:

- + - (1) Main Channel
- ⬇ - (5) Other Andean headwater rivers
- ◇ - (6) Negro Drainage
- - (7) Rivers draining shields
- ▽ - (8) Lowland rivers with extensive areas of marine sediments
- △ - (9) Rivers draining only U. Tertiary and Quaternary sediments
- X - (10) Varzēa waters







IV.9 SUMMARY

This chapter demonstrates that to a good approximation, the chemistry of rivers within the Amazon Basin reflects the geology of the terrains which they drain. Secondary effects such as the precipitation of salts in soils and stream beds, biological uptake and generation, and cyclic salt inputs are more difficult to discern, especially in more concentrated samples. With this in mind, the main relationships between dissolved load and geology is summarized:

TZ+ <200 μ Eq/l

Rivers draining the most weathered materials, the Upper Tertiary and the intensely weathered shield in the Negro, and perhaps Tapajos Basins. The (Ca+Mg):(Na+K) equivalent ratio is less than one for the most dilute rivers.

TZ+ <400-500 μ Eq/l

Rivers draining siliceous terrains. Highest silica concentrations are seen in rivers draining igneous or metamorphic rocks.

TZ+ >400-500 μ Eq/l

Rivers in this range drain marine sediments. The high contribution of dissolved material comes primarily from the weathering of carbonate rocks and evaporites in Peruvian rivers, and from the weathering of shales, containing reduced sulfur, in the Madeira Basin.

TZ+ >2000-3000 μ Eq/l

These rivers show the effect of large evaporite inputs (using the term loosely to include dissolution of soil salt of the Guapay and Piray rivers). At highest TZ+, NaCl is the dominant dissolved mineral.

Consequently, the boomerang shape of the Na/(Ca+Na) versus TDS plot (Figure IV.2, Gibbs 1970) can be seen to be the result of

the higher Na:Ca ratio of slower weathering rock types (silicates), the low Na:Ca ratio of more rapidly weathering rock types (carbonates) and the high Na:Ca ratio of extremely rapidly weathering rock types (evaporites).

The relationship between TZ+ and inputs from siliceous, carbonate dominated, and evaporite dominated terrains can be clearly seen in a ternary diagram relating silica, alkalinity, and sulfate plus chloride (Figure IV.37). Silica is taken as an indicator of contributions from siliceous terrains; alkalinity is taken as an indicator of inputs from carbonate terrains, and cation bearing silicates; and the sulfate plus chloride is taken as representing inputs primarily from evaporites, but also from reduced sulfur weathering. The data are corrected for cyclic salts (Section II.6). The TZ+ increases systematically from the Si vertex to the alkalinity vertex, thence to the $(Cl+SO_4)$ vertex. The two less concentrated samples above the Si- $(Cl+SO_4)$ axis are from a river draining black shales (M-05, BPA01, Tables IV.4 and IV.5), where sulfuric acid from the oxidation of reduced sulfur has replaced carbonic acid as the proton source for silicate and carbonate (associated with the shales) rock weathering. The weathering by sulfuric acid is slow compared to evaporite dissolution. These two samples can be seen as defining a separate weathering trend for the black shale terrains, indicated in the insert of Figure IV.37, however the trend not as well defined on this graph as it is in graphs of alkalinity versus $(Ca+Mg)$ and alkalinity versus TZ+ (Figures IV.16 and IV.6, respectively).

The next chapter examines the mixing of tributaries with the main channel to calculate their discharges. This exercise provides the necessary information for the calculation of the relative contribution to the dissolved load made by different terrains and lithologies in the Amazon Basin

Figure IV.37

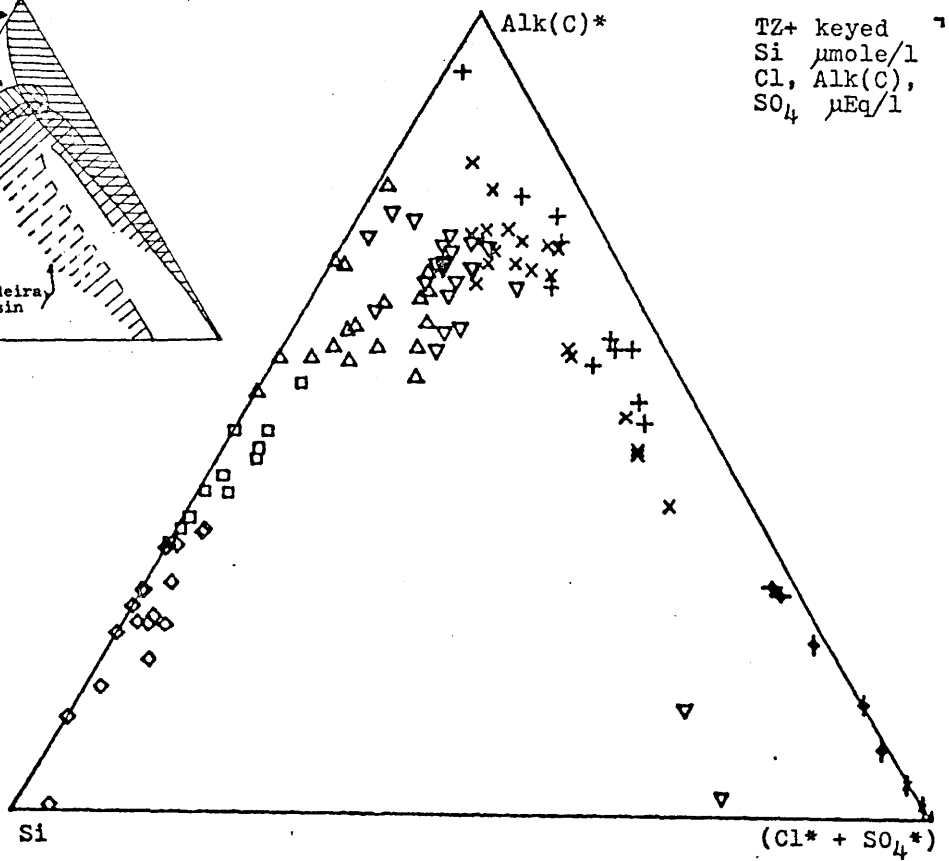
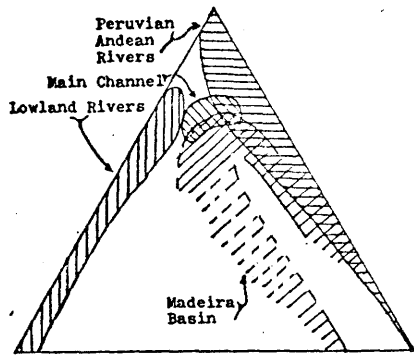
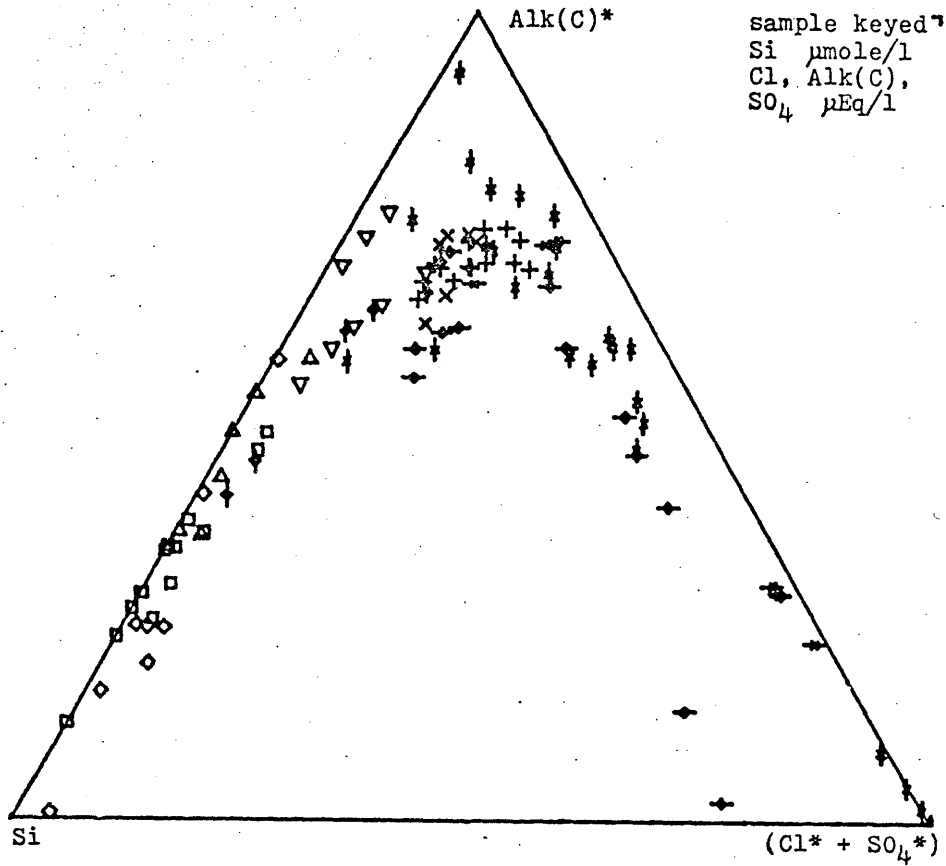
Two ternary diagrams for silica, carbonate alkalinity, and chloride plus sulfate. The data have been corrected for cyclic salt inputs. In the first diagram the samples are keyed to the standard sample-river basin scheme used previously. In the second diagram, samples are keyed to their total cation concentration. These diagrams illustrate the systematic relationship between sample composition, the concentration of total dissolved materials and geology. The major trends are indicated on the insert.

Symbol key, first diagram:

- + - (1) Main Channel
- * - (2) Marañón Drainage
- ✖ - (3) Ucayali Drainage
- ✦ - (4) Madeira Drainage
- ↓ - (5) Other Andean headwater rivers
- ◇ - (6) Negro Drainage
- - (7) Rivers draining shields
- ▽ - (8) Lowland rivers with extensive areas of marine sediments
- △ - (9) Rivers draining only U. Tertiary and Quaternary sediments
- X - (10) Varzêa waters

Symbol key, second diagram; units are TZ+ in $\mu\text{Eq/l}$:

- | | |
|-------------------|----------------------|
| ◇ - 100 | + - 2154. - 4642. |
| □ - 100. - 215. | ✦ - 4642. - 10000. |
| △ - 215. - 464. | ↓ - 10000. - 21544. |
| ▽ - 464. - 1000. | ✖ - 21544. - 46416. |
| X - 1000. - 2154. | * - 46416. - 100000. |



Chapter V

Model of Discharges for the Amazon and its Tributaries Based
on Chemical Data

V.1 FLUX MODEL INTRODUCTION

Geographers and hydrologists have long expressed an interest in determining the absolute and relative discharges of the mainstem and tributaries in the Amazon system. The enormity of the Amazon River was recognized as the result of the Orellana expedition in 1541-42. The basic layout of the principal tributaries along the main channel was understood during the early 17th century as the result of the penetration of missionaries into the Peruvian Amazon and of the Teixeira expedition of 1637-38. The main channel was determined to start at the confluence of the Ucayali and Marañón rivers in Peru, however geographers were unable to decide which of these two rivers was the "mother river" of the Amazon. Many chose the Ucayali, as it is the longer of the two rivers. The matter was confounded in 1879, when Raimondi demonstrated, using the concept of conservation of dissolved load, that the Marañón has the greater discharge. More recently, Matsui et al. (1976), utilized conservation of hydrogen isotopes in water to determine the relative fluxes of the main channel and the Negro tributary, throughout the year.

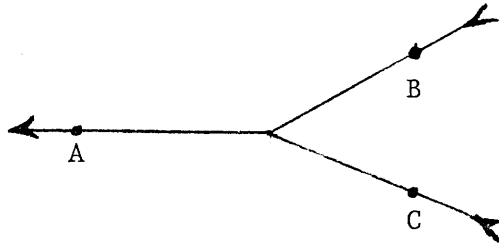
Various observers have tried to indirectly estimate the discharge of the Amazon (c.f. Oltman et al. 1964). The first direct measurements of the discharge were done in 1963 by a U.S.G.S.-Brazilian team (Oltman et al. 1964, Oltman 1968), on the Obidos section. Obidos is the most downstream gageable section on the main channel not strongly affected by tides. Consequently, it is the basic reference point for the entire Amazon system. Oltman (1968) observes that the average discharge at this point is $157,000 \text{ m}^3/\text{sec}$ and that the discharge at the mouth probably averages $175,000 \text{ m}^3/\text{sec}$. Subsequently, a hydrological network was established

through much of the Brazilian Amazon. Efforts to obtain data from this network for the period of this study have, for the most part, been frustrated. However, discharges have been obtained for the dates of sampling of several sections along the main channel. It must be pointed out that the lower courses of the tributaries where samples were taken are not measured for discharge in the network, as the water levels are controlled by the rise and fall of the main channel.

V.2 THEORY

This paper extends the application of mass conservation in determining relative flows to include all the major tributaries of the main channel. To illustrate the concepts, the two river model utilized by Raimondi (1879) and Matsui et al. (1976) will be examined.

Suppose that river B (e.g. Ucayali) and C (e.g. Marañon) mix to form A (e.g. Amazon):



Furthermore, assume that cross sections at A, B, and C are well mixed. The assumption that water discharge (Q_w) is conserved is expressed as:

$$(a) \quad Q_{WA} = Q_{WB} + Q_{WC}$$

The transport of dissolved phase of concentration D is given by:

$$Q_D = DQ_w$$

If D is conserved during mixing:

$$(b) \quad D_A Q_{WA} = D_B Q_{WB} + D_C Q_{WC}$$

Equations (a) and (b) are sufficient to determine the discharges of water past B and C relative to A:

$$\frac{Q_{WB}}{Q_{WA}} = \frac{D_A - D_C}{D_B - D_C} \quad \text{and} \quad \frac{Q_{WC}}{Q_{WA}} = \frac{D_B - D_A}{D_B - D_C}$$

Example:

	Raimondi early June 1876		This study 10 December 1978	
	<u>TDS</u>	<u>relative discharge</u>	<u>TDS</u>	<u>relative discharge</u>
Ucayali	160	.174	156.2	.447
Marañon	45	.826	98.0	.553
Amazon Iquitos	65	1.000	124.0	1.000

If either Q_{WA} , Q_{WB} or Q_{WC} are known, the other two discharges may be determined.

During this study many chemical parameters were measured, and since any conservative chemical parameter can be used in calculations, the problem of estimating discharges is "over determined." Mass conservation equations such as those describing the mixing of two rivers (Eqn. (a) and (b)) are linear equations, and as such can be advantageously treated using simultaneous linear least squares (SLLS) (see Cramer 1945). The use of SLLS will provide not only best estimates of fluxes but also the errors of these estimates.

The procedure for setting up the necessary linear equations can be illustrated using the previous example of two rivers mixing. Suppose that instead of parameter D parameters D_1, D_2, D_3 and so on, are measured. Furthermore, suppose the water discharges at A and B (Q'_{WA} and Q'_{WB} , respectively) are measured directly. The conservation equations can be rewritten with all unknowns on the right hand side:

$$\begin{aligned}
 (1) \quad Q'_{WA} &= Q_{WZ} + e_1 \\
 (2) \quad Q'_{WB} &= Q_{WB} + e_2 \\
 (3) \quad 0 &= -Q_{WA} + Q_{WB} + Q_{WC} + e_3 \\
 (4) \quad 0 &= -Q_{WA}^D 1A + Q_{WB}^D 1B + Q_{WC}^D 1C + e_4 \\
 (5) \quad 0 &= -Q_{WA}^D 2A + Q_{WB}^D 2C + Q_{WC}^D 2C + e_5 \\
 (6) \quad 0 &= -Q_{WA}^D 3A + Q_{WB}^D 3C + Q_{WC}^D 3C + e_6 \\
 &\vdots \\
 &\vdots \\
 &\vdots
 \end{aligned}$$

Where $e_1, e_2 \dots$ are errors to be minimized. As can be seen, all these equations are of the form: $Z = Q_{WA} \cdot W + Q_{WB} \cdot Y + Q_{WC} \cdot Z$ where W, X, Y, and Z are all known.

One refinement is essential, namely all the above equations must be weighted to favor the best measured parameters. For calculations of Amazon data, the inverse of the estimated analytical error of the concentration

(Table IV.2) of the downriver sample at each confluence was used as a weight. i.e., if D_{1A} is measured to $\pm d_{1A}$, the weight is simply $W_1 = 1/d_{1A}$. Equation (4) can be rewritten:

$$(7) \quad 0 = -Q_{WA} (W_1 D_{1A}) + Q_{WB} (W_1 D_{1B}) + Q_{WC} (W_1 D_{1C}) + e_1$$

Leaving coefficients in Equations (1), (2), and (3) as zeros and ones is totally unsatisfactory, as these equations would be diminutively weighted compared to the equation for a well determined chemical parameter. Insufficient weighting is a particularly critical problem in the case of the water conservation equation (Eq. 3), the basis of this model, and in that sense the most fundamental equation of the model. To allow for this, an arbitrary weighting factor (W_0) is applied to Equation (3) that is as great as the combined chemical weights for any station, i.e., W_0 is $\max(W_{0M})$, where $W_{0M} = \sum_n W_n D_{nm}$, over all species, n , for stations, m . Equation (3) can be rewritten as:

$$(8) \quad 0 = -Q_{WA} W_0 + Q_{WB} W_0 + Q_{WC} W_0 + e_3$$

The errors of the measurements Q'_{WA} and Q'_{WB} can be used to determine weighting factors for equations (1) and (2), respectively, however error measurements are not available. If the quality of the regression is good, the resultant model discharges Q_{WB} and Q_{WC} relative to Q_{WA} should not be sensitive to variations in the error of the flux measurement, since the relative fluxes are in theory determined by mass conservation alone. It is assumed that if the relative discharges predicted by the model are dependent on the errors of the measured fluxes, then the mass conservation assumptions are weak (due to poor station selection, time variation of discharge, time variation of chemistry, etc.). Mathematically, a test of the sensitivity of the model to the variation of the errors of the flux measurement can be written as:

$$(9) \quad Q'_{WA} W_0 = Q_{WA} Q_0 = e_1$$

$$(10) \quad Q'_{WB} W_0 r = Q_{WB} W_0 r + e_2$$

where W_0 is the weight defined for Equation (8) and r is the test parameter, which is varied between 0 and 1. The weight on Equation (9) is held at W_0 (i.e., $r = 1$ always) to serve as a fixed reference discharge (anchor point) to which other discharges are compared. Q_{WA} , Q_{WB} , and Q_{WC} are considered well determined, if there is agreement between measured fluxes and fluxes predicted by mass balances alone (that is $r=0$), and if the values of Q_{WB} and Q_{WC} are not sensitive to changes in r .

V.3:1 APPLICATION OF FLUX MODEL OF AMAZON DATA

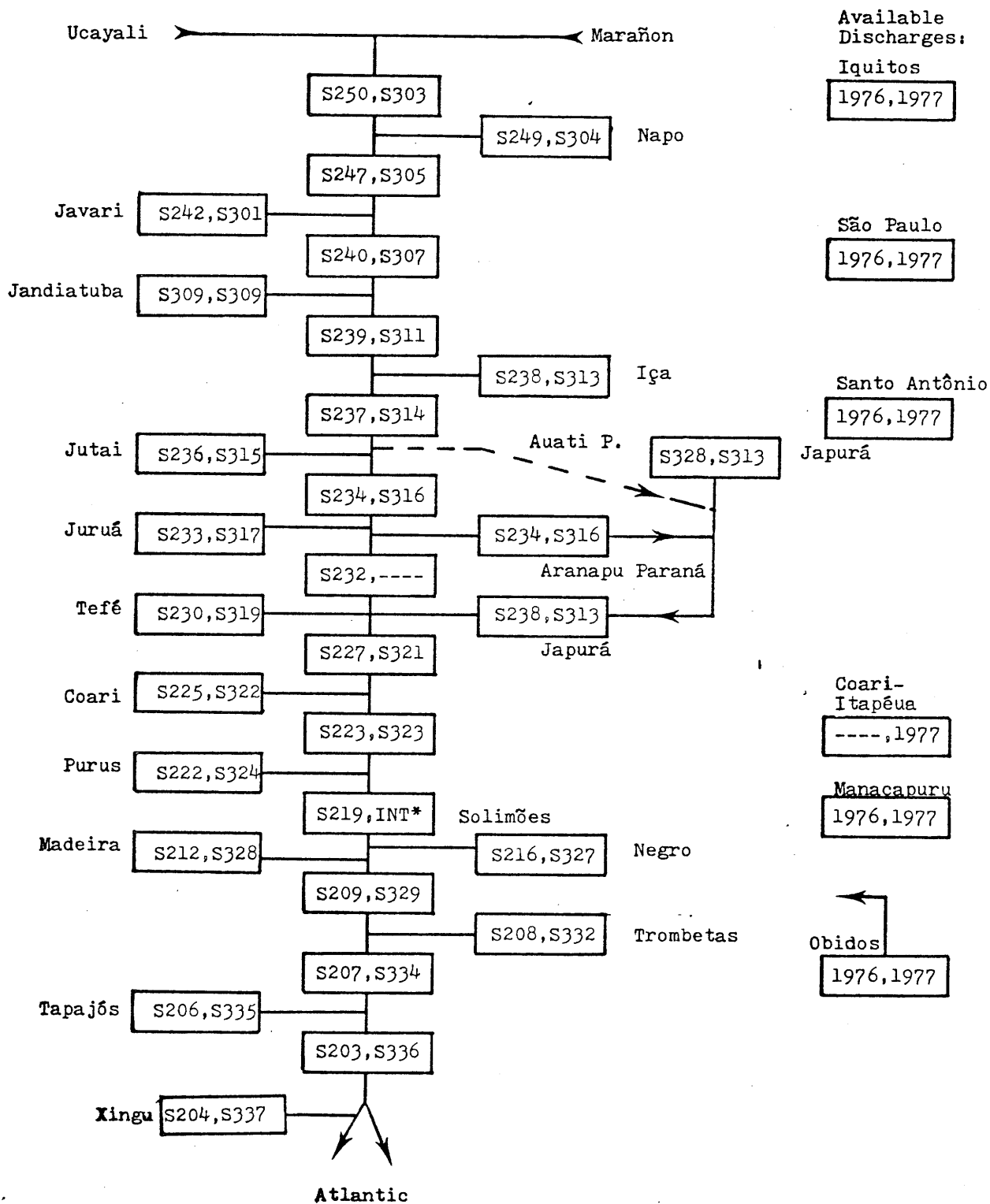
A schematic of the lowland Amazon main channel stations and tributaries used in modeling is shown in Figure (V.1). All of the largest tributaries were sampled, as were several smaller tributaries. The model discharges of smaller tributaries are seen as representing not only their own discharges, but also inputs from other small rivers from the same reach of the main channel. There is no way to distinguish small river inputs of relatively similar chemistry in this model.

The most critical stretch of the main channel for model calculations is that between the mouth of the Jutáí and the Coari. To the left of the main channel, lies a complex system of channels which has been referred to as the "delta" of the Japurá (Tastevin (1928)). According to Tastevin (1920, 1928), water from the main channel feeds into the Japurá through the Auati and Aranapu paranás, with the second being by far the largest of the two main channel distributaries. Water from the Japurá is discharged into the main channel through its primary mouth and its own distributaries with a major secondary discharge point opposite the mouth of the Coari. Geologically the drainage of the Iça and Japurá Rivers is quite similar (Table IV.4), yet the Japurá is much richer in dissolved solids due to main channel inputs (Table IV.5). Only the Aranapu Paranã was included in the model to avoid introducing too many equations, and thereby mathematically destabilizing the solution to the model. As it is, the confluence of the Japurá with the main channel is very complex, being opposite the mouth of the Tefé river. In 1977 no sample was obtained upriver of this confluence, consequently for 1977, the combined effects of the Aranapu distributary and confluence of the Juruá, Japurá, and Tefé rivers is treated as one equation.

Figure V.1

Stations used in constructing the discharge model of the Amazon River system. The stations (numbers in boxes) are described in Appendix III, and analyses are given in Table IV.5.

Stations used in flux model calculations for 1976 and 1977



The main channel also feeds into the Trombetas , and the Madeira has a large distributary which feeds into the main channel (Figure V.2). Sampling coverage was inadequate to examine these features.

Table (V.1) summarizes all the equations used in modeling the Amazon system.

V.3:2 Selection of Stations

The assumption that the main channel is well mixed is not valid and accommodations must be made for this feature. The gradual mixing of the differently colored tributaries with the main channel has been described since the first expedition down the Amazon. Matsui et al. (1976) demonstrate that the waters of the main channel and the Negro River are not fully mixed 100 km downriver of their confluence. The contrasts in color can be traced in satellite photographs for tens of kilometers (Figure V.2).

Figure (V.3) presents alkalinity measurements from several cross sections of the main channel, taken with either Niskin samplers or U.S.G.S. depth integrating samples (Meade et al. 1979). Alkalinity is an ideal measurement because the mainstream alkalinity is always higher than the tributaries, and because alkalinity is measured by titration in the field, it is particularly precise (Appendix III). While no cross section shows complete mixing, only the Santo Antonio section, lying 8 km down river of the Ica River confluence shows extreme variations of alkalinity. The Iquitos section and the Obidos section are similar distances down river of small tributaries, the Nanay and Trombetas respectively, and are not so strongly affected. The Sao Paulo section is far down river of the nearest large river, the Javari, and alkalinity variations must be the influence of small jungle streams.

The samples used in model calculations were taken immediately upriver

Table V.1

CROSS SECTION*	1	2	3	4	5	6	7	8	9	10	11	12	13	14	15	16	17	18	19	20	21	22	23	24	25	26	27	**28	**29	++				
EQUATION*	1	1													1	-1																		
		2														1	-1																	
		3	1														1	-1																
		4		1														1	-1															
		5			1														1	-1														
1976 only		6				1	1	1																										
		7				1																												
**8		8					-1																											
		9							1																									
		10								1																								
		11									1	1																						
		12											1																					
		13												1																				
		14+													1																			
1977 only		15+															1																	
		16+																						1										
		17+																							1									
		18+																																
			.Napo																															
			.Javari																															
			.Jandiatauba																															
			.Iça																															
			.Jutai																															
			.Jurua																															
			.Japurá conf.																															
			.Tefé																															
			.Coari																															
			.Purus																															
			.Negro																															
			.Madeira																															
			.Trombetas																															
			.TapaJós																															
			.Am. ab. Napo																															
			.Am. ab. Javari																															
			.So. ab. Jandia-																															
			.So. ab. Iça																															
			.So. ab. Jutai																															
			.So. ab. Jurua																															
			.So. ab. Japurá																															
			.So. ab. Coari																															
			.So. ab. Purus																															
			.So. ab. Negro																															
			.Am. ab. Trombe-																															
			.Am. ab. TapaJós																															
			.Am. ab. Xingu																															
			.Am. ab. Aran-																															
			.Jurua ab. Aran-																															
			.Aranapu Paraná																															
			.meas. discharge																															

* this table gives coefficients, X_{nA} , of mass conservation equations, where n is the equation number, A is the cross section, and X is either 0, 1 or -1. The equations are in the form:

$$0 = X_{nA} Q_{WA} (W_{nD_{nA}}) + X_{nB} Q_{WB} (W_{nD_{nB}}) + X_{nC} Q_{nC} (W_{nD_{nC}}) + \dots$$

** these equations and cross sections are not utilized when the Aranapu Paraná is not considered.

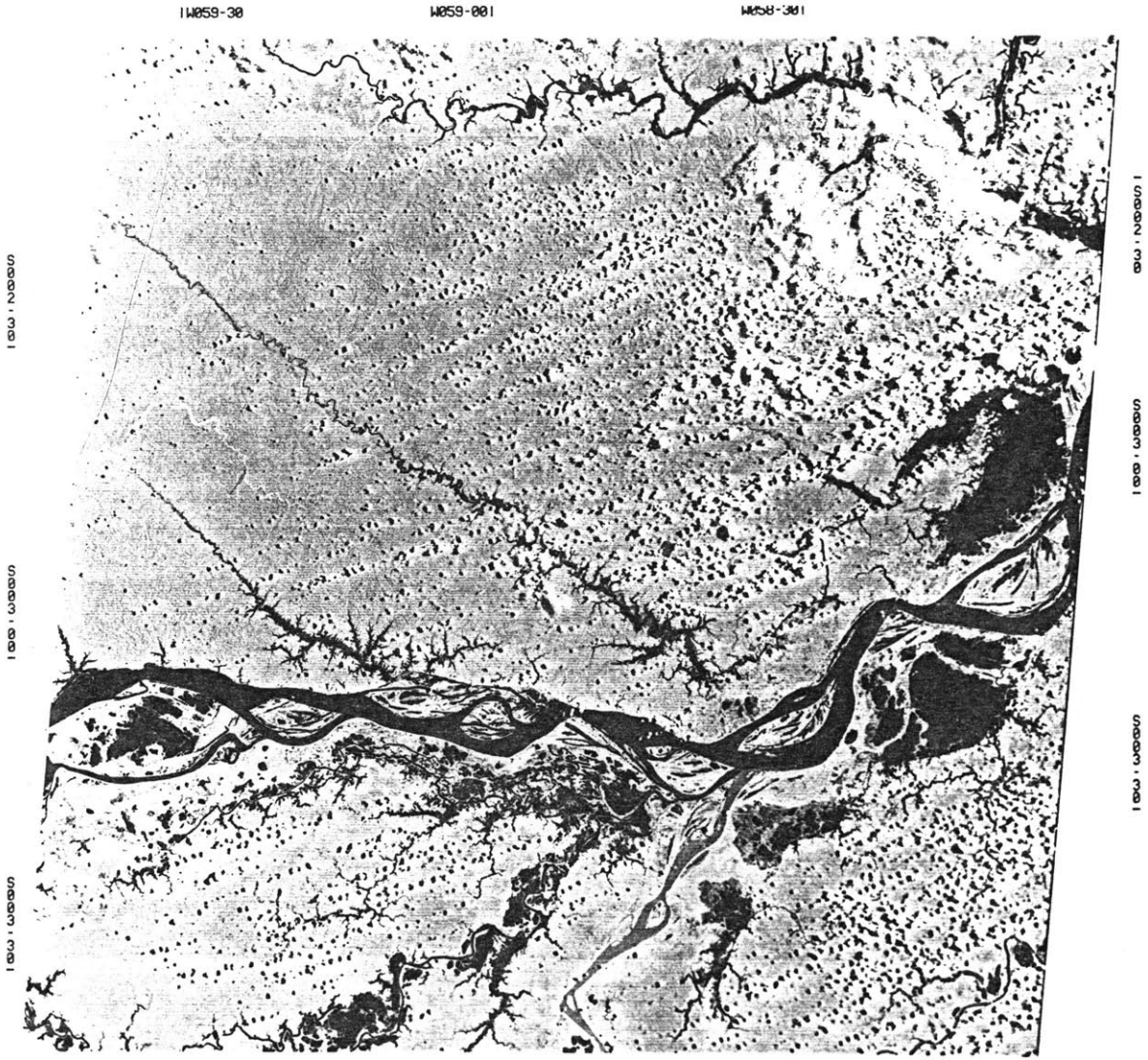
+ these equations represent those with measured discharges

++ measured discharge, the model is forced through the Obidos discharge (Eqn. 18).

abbreviations: ab.-above, conf.-confluence, Am.-Amazon, So.-Solimões

Figure V.2

Photograph of the confluence of the Madeira river with the main channel. The Madeira river is the grey river in the bottom center right of the photograph, the lighter colored waters can be seen occupying the right side of the channel, downstream of the confluence. The confluence of the Negro River with the main channel occurs to the right of the area in the photograph. The very black waters of the Negro can be seen hugging the left bank of the main channel. The river crossing the lower right of the photograph is actually a distributary of the Madeira River, called Paranã Uraria.



21SEP72 C S02-57/14059-00 N S02-58/14058-54 HSS 6 R SUN EL56 AZ004 188-0834-A-1-N-D-2L NASA EXTS E-1868-13362-6 3

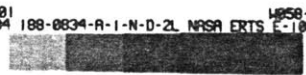


Figure V.3

Titration alkalinity ($\mu\text{Eq/l}$) for various cross sections of the Amazon main channel. Up river contributions are indicated in several cross sections.

Alk(t) μ Eq/l
for various cross
sections of the
Amazon main channel

Nanay 40

	left	middle	right
T	1079	1213	1284
M	1114		
B	1236	1265	1285

IQUITOS

T	1071	1043	977
B	1063	1033	976

SÃO PAULO

Iça 9

T	443	913	992
B	457	914	998

1013 Solimões

SANTO ANTONIO

Solimões 603

T	577	558	438
B	582	557	442

169 Purus

MANACAPURU

576	577	575	562	543	485	438
-----	-----	-----	-----	-----	-----	-----

U.S.G.S. integrated samples

Trombetas 63

T	338	387	390
M	343	388	387
B	342	385	389

386 Amazon

OBIDOS

347	342	388	377	391	387	391
-----	-----	-----	-----	-----	-----	-----

U.S.G.S. integrated samples

of larger tributaries and therefore must represent the most thoroughly mixed sample of upriver tributaries. Every attempt was made to collect samples in the full flow of the main channel, thus minimizing the effect of bank inputs.

The sample upriver of the confluence of the Rio Negro with the mainstem in 1977 (S326) does not give the same alkalinity as is determined from the flux weighted average alkalinity from the Manacapuru section depth integrated samples. The alkalinities are (S326) = 501 $\mu\text{Eq/l}$ and (flux weighted) = 531 $\mu\text{Eq/l}$. Apparently the confluence sample (S326) was sampled from the "Purus side" of the river. A hypothetical sample falling on the mixing curve between the main channel and the Purus, at $\text{Alk} = 531$ $\mu\text{Eq/l}$ was substituted for (S326).

The Obidos section was used as the "anchor point" ($r=1$, always) for the model. The samples (S209 and S329) from this section represent a mixture of water from the Solimoes (mainstem), Negro, and Madeira Rivers, and do not contain water from the Trombetas. The flow measurement includes the effect of the Trombetas. However no location exists where a complete mixture of all four rivers can be found, and one must be satisfied in assuming the flow of the Trombetas is small, as it drains a far smaller region.

The model calculation used Na, K, Mg, Ca, alkalinity, Cl, and SO_4 as conservative parameters. Concentrations are found in Table IV.5; analytical precisions are given in Appendix (III).

V.3:3 Time Variations of Discharge

Time variations of discharge or water chemistry can contribute to apparently nonconservative results for a mass conservation model of a large river system, simply because the output of the system does not respond

instantaneously to inputs. In 1977, the expedition followed the discharge peak downriver, essentially seeing the evolution of the same body of water as a result of tributary inputs. In contrast, the 1976 expedition was longer in duration and travelled upstream. It therefore did not sample a single body of water. Consequently, the effects of time variation in end-member composition are superimposed on effects attributable only to mixing. The effects of time variation are not expected to be serious due to the large number of tributaries and their close spacing, which would lessen the effects of time variations between the sampling of successive tributaries.

V.4 RESULTS OF FLUX MODEL

Model calculations were performed both with and without the Aranapu Paraná for each year. The flux measurement parameter r was varied between 0 and 1 to test the stability of the four sets of calculations. When the Aranapu was included, the Iça composition was assumed for the Japurá on the basis of their similar geology. Model results are presented assuming 5% measurement error on discharges, that is $r_{Wo} = 20$.

When the Aranapu Paraná was not included, the models were unsuccessful (that is, for changes in r , the variations in the predicted discharges exceeded the model errors, and measured and predicted discharges disagreed at $r=0$) for both years, and predicted and measured discharges diverged considerably up river of the Japurá confluence (Figures V.4, V.5).

The two models (Figures V.6, V.7) that included the Aranapu Paraná were both successful. The 1977 model had the smaller errors, but the 1976 model was more stable with respect to changes in r . The 1977 model discharges were in general not sensitive to changes in r , except for the Aranapu Paraná, and Juruá, Japurá, and Tefé rivers; negative fluxes were generated when r was greater than ≈ 0.3 , as a consequence of treating measured fluxes too rigidly (this is equivalent to assuming a discharge measurement error of 0.6%). Time variation of end-members may account for the slightly greater error in the 1976 model.

Main channel concentrations, predicted from Iquitos mainstem and tributary concentration measurements and model Iquitos mainstem and tributary fluxes, agree with observed concentrations for both years (Figure V.8); predicted Na and Cl tend to be high while predicted Ca, Mg, and alkalinity tend to be low. This is best explained by a time variation of relative inputs from evaporite and carbonate rock sources in the Andes, and

variations of Andean versus lowland river inputs. If any particular confluence is examined, down river concentrations agree with concentrations predicted using model discharges with tributary and up river concentrations.

Note that the fluxes of the main channel down river from Obidos are not well determined because a section containing a reasonably homogenous mixture of water from the Trombetas and other left bank tributary inputs does not exist.

Figure V.4

Results of the discharge model (1000 m³/sec) for 1976, not including the Aranapu Paran in the calculations. Errors are one sigma. This model assumed a 5% error on measured discharges, $rW_0 = 20$.

1976 Model Discharges ($10^3 \text{ m}^3/\text{sec}$) without the Aranapu Paraná

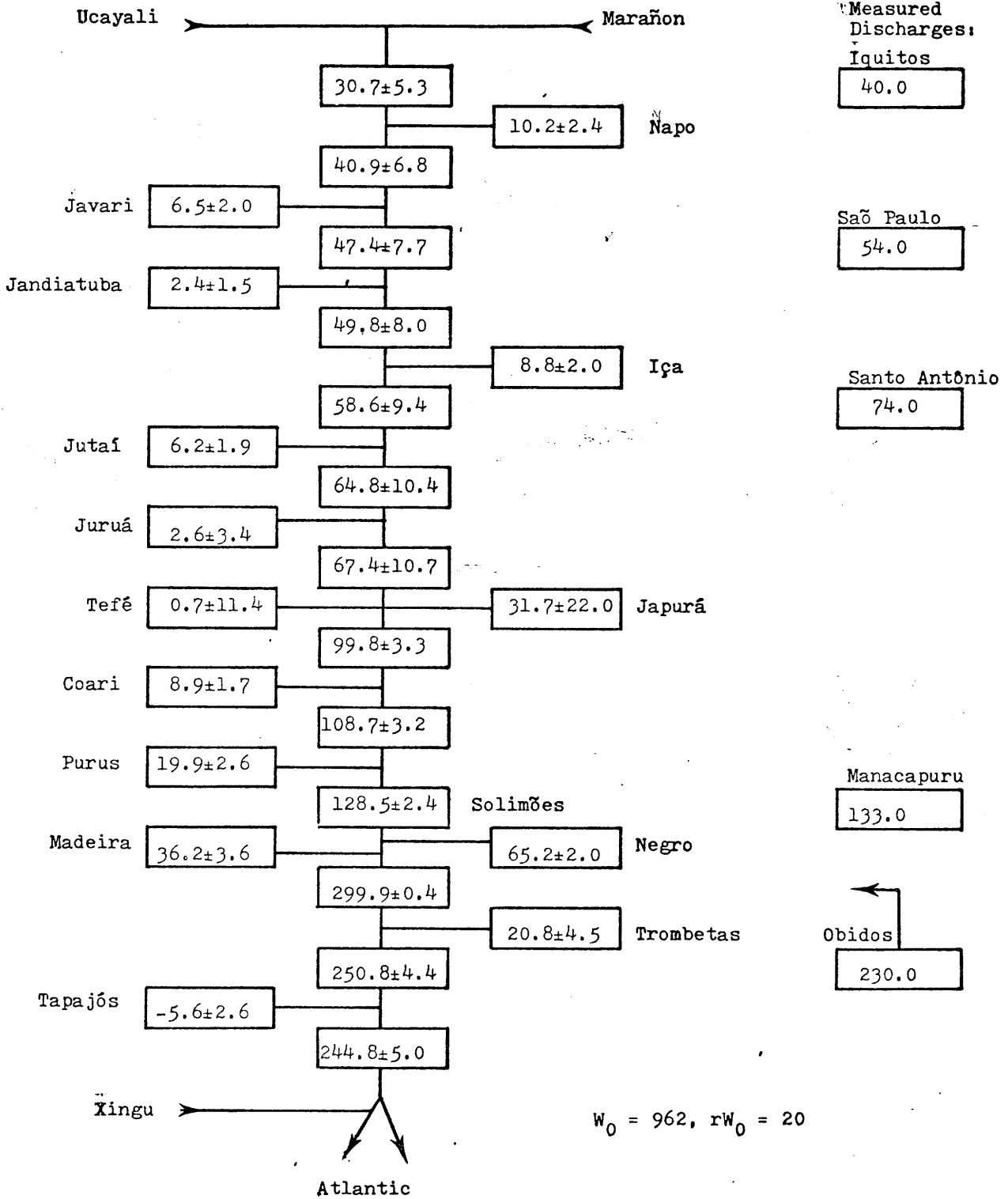


Figure V.5

Results of the discharge model for 1977 without the Aranapu Paraná.

1977 Model Discharges ($10^3 \text{ m}^3/\text{sec}$) without the Aranapu Paraná

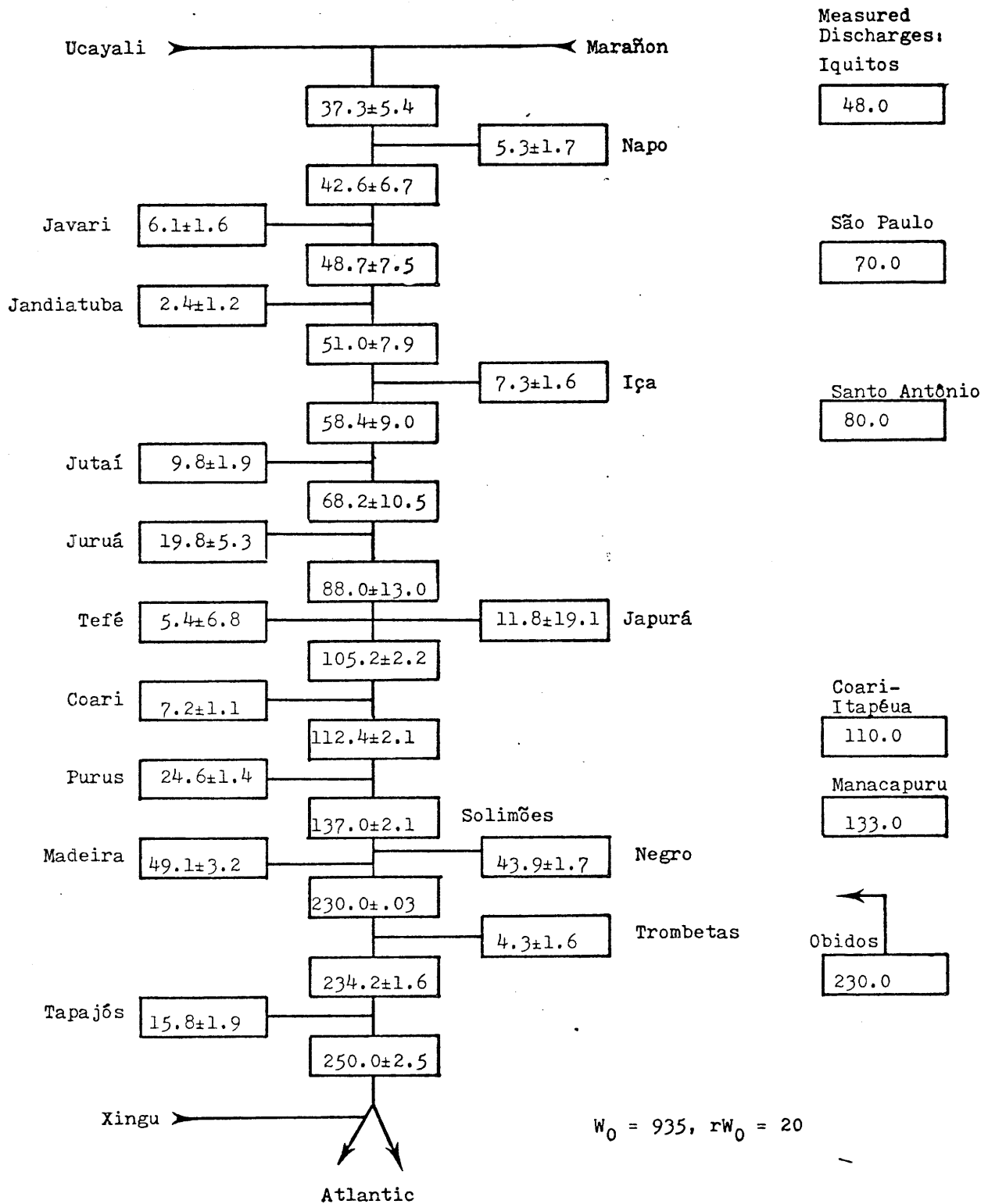


Figure V.6

Results of the 1976 model with the Aranapu Parana. Note that while the errors of the model in the vicinity of the confluence of the Japura are high, the discharge results are coupled through the model and cannot be varied independently. For example if the model discharge for the Tefe is reduced to 1000 m³/sec, the discharges for the other rivers would have to be increased for there to be water conservation.

1976 Model Discharges ($10^3 \text{ m}^3/\text{sec}$) with the Aranapu Paraná

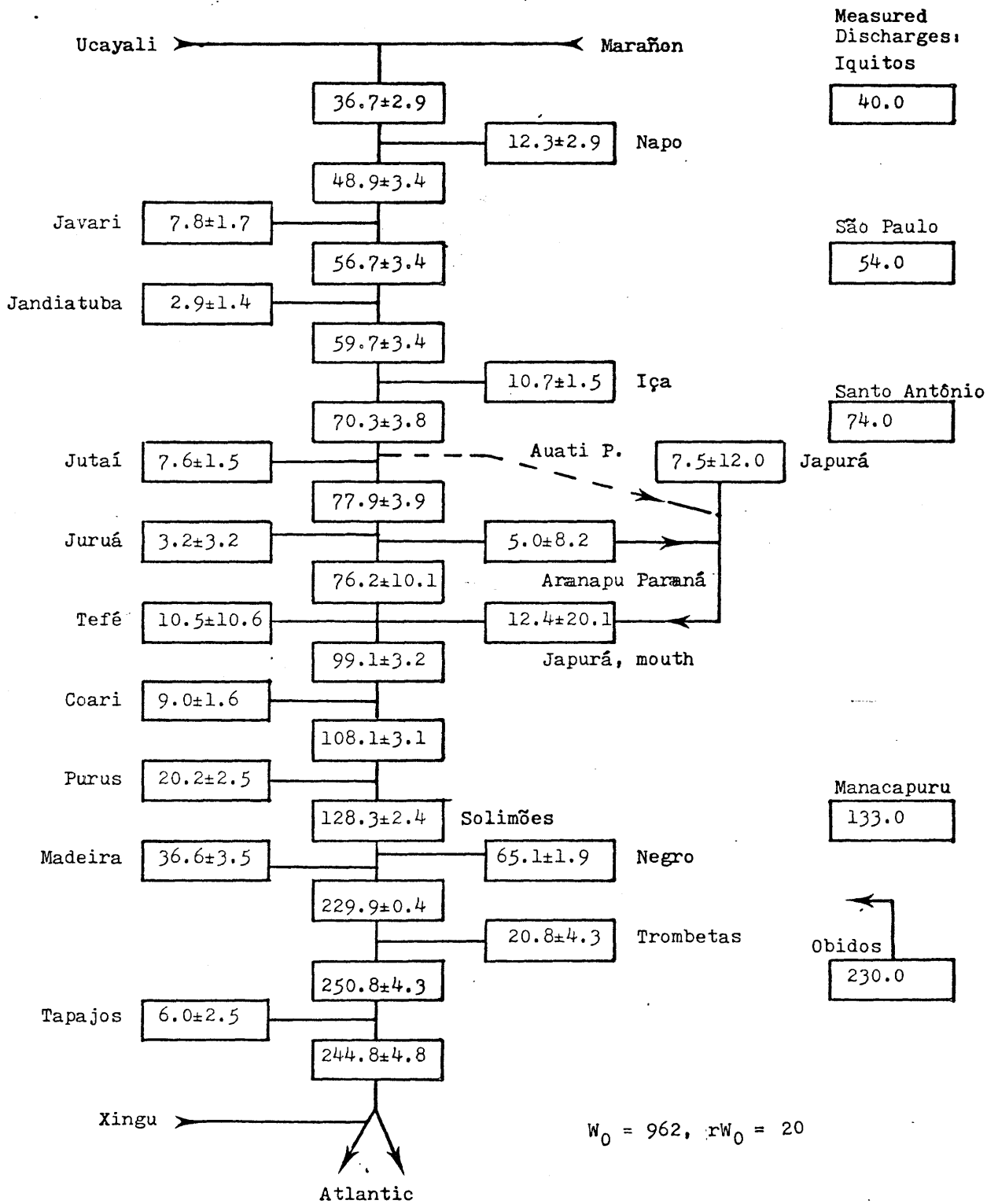


Figure V.7

Results for the discharge model for 1977 with the Aranapu Parana.

1977 Model Discharges ($10^3 \text{ m}^3/\text{sec}$) with the Aranapu Paraná

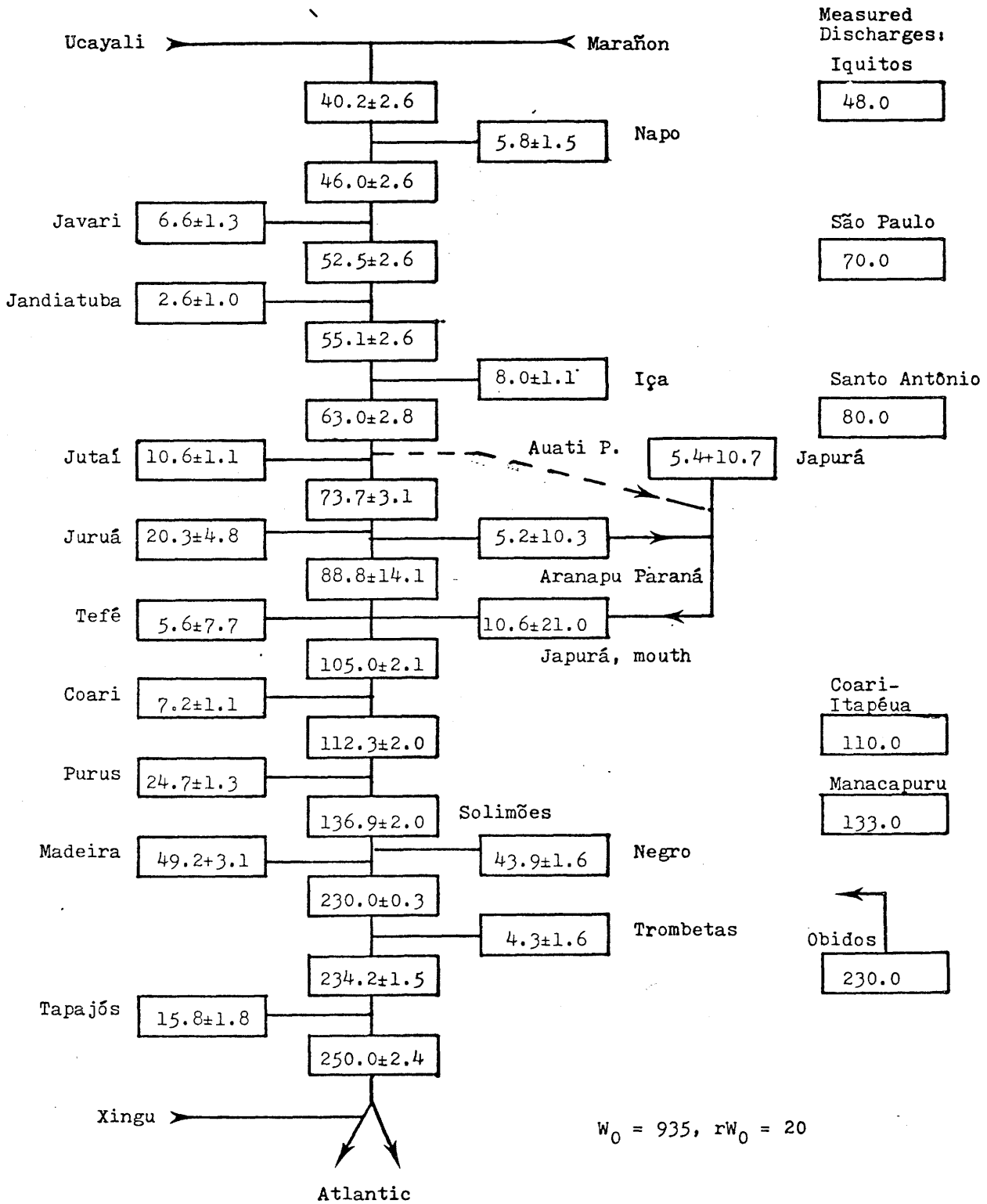
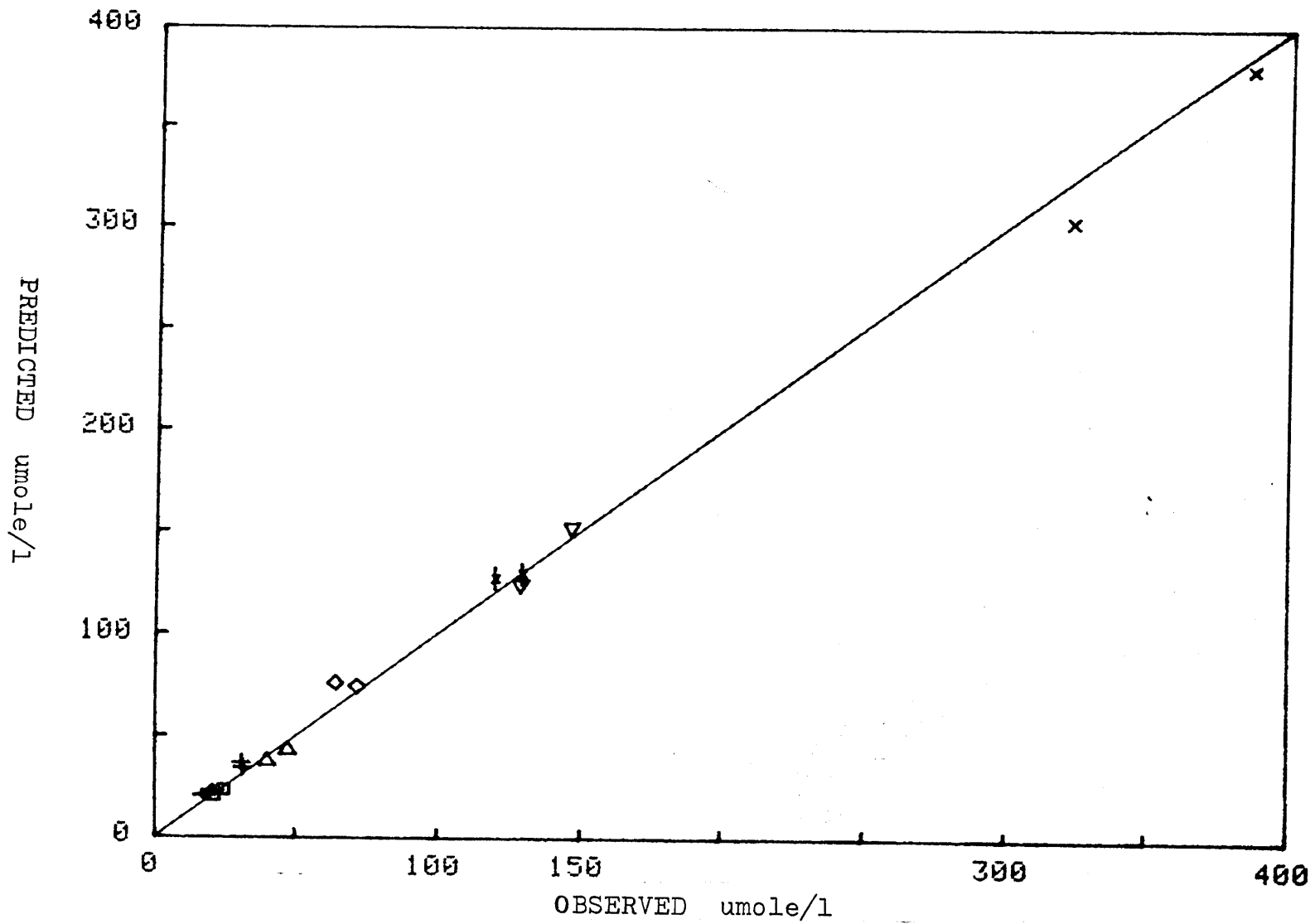


Figure V.8

Concentrations at Obidos predicted by the discharge model, assuming conservative mixing of the tributaries, versus measured concentrations for the respective species.

Symbol key:

Na	- ◊
K	- □
Mg	- Δ
Ca	- ▽
Alk	- X
Cl	- †
SO ₄	- ◆
Si	- *



V.5 SUMMATION

This discussion demonstrates the successful application of chemical mass conservation concepts to the determination of tributary and main channel discharges for the Amazon River system. When a sufficient number of chemical properties are analyzed, major diversions of flow from the main channel, such as the Aranapu Parana can be successfully modeled. It is unlikely that large rivers with major rapid variations of discharge, such as are caused by spring runoff, weirs, cyclonic storms etc., could be modeled along their entire length as instantaneous measurements of flow would not be conservative.

In terms of geochemistry, the discharge model shows that there is no need to hypothesize that the dissolved phase transport of any species used in the model (Na, K, Mg, Ca, Alk(t), Cl, SO₄, Si) is chemically non-conservative. Inspection of the data show that nitrate, total inorganic carbon, and hydrogen ion are not transported conservatively; the iron and aluminum data are ambiguous in this regard.

Chapter VI

GENERAL CONCLUSION

VI GENERAL CONCLUSION

This section summarizes the results of the previous chapters into an estimation of the rates at which various processes contribute dissolved materials to the discharge of the Amazon River system. The standard procedure, to be followed here, is to correct the original data for cyclic salt contributions, and to calculate denudation rates from water discharge. These rates can then be related to geological features. Chapter II establishes the cyclic salt contribution; Chapter IV identifies the relationships between chemistry and geology; and Chapter V provides the rate calibration in terms of water discharge.

Without additional assumptions, the results from this study would not be applicable on an annual basis, as discharge measurements corresponding to samples collected at low discharge during this study are not available. Note that chemical measurements made during different seasons of the year on the larger rivers (Solimões at Manacapuru, Negro at Manaus, Amazon at Iquitos, Huallaga at Yurimaguas) suggest that seasonal variations in chemical composition are small, less than a factor of two, with low discharge concentrations being somewhat higher than high-discharge concentrations. Consequently, reasonable estimates of denudation rates should be obtained using the discharges determined in this study normalized to the mean annual discharge at Obidos (c.f. Oltman 1968). This procedure would tend to underestimate denudation rates for rivers draining from the south of the main channel, as these are at falling stage when the main channel is at peak discharge, and would overestimate denudation rates for regions north of the main channel, which are near peak stage when the main channel is at peak discharge.

Estimated discharges, flux weighted mean concentrations, and denuda-

tion rates are presented in Table (VI.1), for the drainage regions established in Chapter IV. In calculating denudation rates, the model discharges determined in Chapter V, normalized to the annual mean discharge, have been used with the exception of discharges from the Xingu, Tapajós, Trombetas, Tefê, Japurá, and Juruá rivers. The latter discharges were obtained from a regression of model discharge against basin area for the remaining rivers (except for the Negro River basin, a region of exceptionally high precipitation, Hoffman 1975 and runoff, Matsui et al. 1976). The concentration for the Amazon system discharge is a flux-weighted predicted value and includes estimated contributions from the Xingu River and left bank tributaries, which never fully mix with water from the main channel prior to its mixing with salt water, due to islands at the river mouth.

The Peruvian Andes have the greatest denudation rates of any major region of the Amazon Basin. Roughly 40-60% of the dissolved Na, Mg, Ca, Alk(t) (hence inorganic carbon), and S, transported by the Amazon into its estuary and 90% of Cl, after cyclic salt corrections, are derived from the Peruvian Andes. This high contribution is reflected in the denudation rates, where estimates for the Peruvian Andes are about four times the Basin average for Na, Mg, Ca, Alk(t), and S, and about 7 times the basin average for Cl. Other regions draining marine sediments (regions 4, 5, and 8) have denudation rates for Na, Mg, Ca, Alk(t), and S comparable to the basin average, while Cl denudation rates are well below the basin average. Regions 4, 5, and 8 have extensive areas of shields and nonmarine sediments, which lower the basin average. It is expected that the areas of uplifted marine sediments in these regions have denudation rates comparable to those calculated for the Peruvian Andes. In contrast with the above species, the denudation rates for dissolved K and Si are fairly uniform over the entire basin. These results are consistent with the geology of the Basin. Carbonates, sulfates,

Table VI.1

ESTIMATION OF CONTRIBUTIONS FROM VARIOUS SOURCE REGIONS IN THE AMAZON BASIN

percentage of net discharge contributed by various source areas for different species:

Region	TDS	TZ+	Na	K	Mg	Ca	Alk	Cl	SO ₄	Si	H ₂ O
2+3	48.	50.	48.	20.	36.	59.	55.	69.	52.	18.	14.
4	15.	16.	13.	21.	26.	13.	15.	3.3	29.	16.	15.
5	6.3	6.3	4.9	8.9	7.2	6.2	6.0	1.2	3.8	11.	10.
6	3.1	2.8	3.1	8.9	3.0	1.5	0.7	0.0	1.3	9.9	19.
7	11.	8.9	6.3	21.	11.	6.9	4.4	0.0	1.6	24.	21.
8	12.	7.1	8.5	14.	12.	12.	13.	2.7	5.5	14.	13.
9	2.5	2.6	2.4	5.2	2.5	1.9	1.9	0.0	0.9	6.2	7.6
cyclic	1.4	2.4	9.4	0.7	2.2	0.1	-0.4	24.	5.4	0.0	--

flux weighted mean concentrations, and water flux in 10³m³/sec:
TDS-ppm, TZ+, Alk(t)-μEq/l, all others μmole/l (cyclic salt corrected, except for Amazon)

Region	TDS	TZ+	Na	K	Mg	Ca	Alk	Cl	SO ₄	Si	H ₂ O
2+3	127.	1507.	249.	32.0	96.7	514.	1198.	165.	71.	179.	26.9
4	36.2	414.	62.9	29.7	61.8	98.6	289.	7.2	35.7	143.	30.0
5	22.1	246.	33.6	18.2	25.2	70.8	174.	3.9	6.9	137.	20.4
6	5.7	59.5	11.3	10.0	5.7	9.1	11.	0.0	1.1	67.9	38.1
7	19.1	172.	34.3	21.3	18.9	39.2	133.	0.0	1.4	153.	41.6
8	32.1	340.	44.8	23.2	32.7	103.	282.	4.8	7.6	144.	26.4
9	11.1	115.	22.3	14.7	11.7	25.1	64.	0.0	0.9	109.	15.0
Amazon	35.9	411.	71.1	21.8	36.7	120.	301.	32.9	18.6	134.	197.

denudation rates, cyclic salt inputs, water runoff (m/yr):
TDS-tonnes/km²/yr, TZ+, Alk(t)-kEq/km²/yr, all others-kmole/km²/yr

Region	TDS	TZ+	Na	K	Mg	Ca	Alk	Cl	SO ₄	Si	H ₂ O
2+3	132.	1562.	258.	33.2	100.	533.	1241.	171.	73.5	186.	1.04
4	24.5	281.	42.6	20.1	41.9	66.8	196.	4.9	24.2	97.2	0.68
5	25.4	283.	38.7	20.9	29.0	81.4	200.	4.5	8.0	158.	1.15
6	9.0	94.2	17.9	15.8	9.0	14.4	17.	0.0	1.7	108.	1.58
7	16.1	145.	28.9	17.9	16.0	33.0	112.	0.0	1.2	129.	0.84
8	38.3	405.	53.4	27.6	39.0	122.	336.	5.7	9.0	172.	1.19
9	10.5	109.	21.2	14.0	11.1	23.8	61.	0.0	0.8	103.	1.95
cyclic	0.5	9.8	6.6	0.1	0.8	0.1	-1.	7.8	1.0	0.0	--
Amazon	35.2	399.	64.2	21.5	35.7	120.	300.	25.0	17.5	134.	1.00

(cyclic salt component excluded)

denudation rates, above, normalized to Amazon average:

Region	TDS	TZ+	Na	K	Mg	Ca	Alk	Cl	SO ₄	Si	H ₂ O
2+3	3.71	3.92	4.02	1.54	2.80	4.45	4.13	6.85	4.19	1.39	1.04
4	0.69	0.70	0.66	0.93	1.17	0.56	0.65	0.20	1.38	0.73	0.68
5	0.71	0.71	0.60	0.97	0.81	0.68	0.67	0.18	0.45	1.18	1.16
6	0.24	0.23	0.28	0.74	0.25	0.12	0.06	0.0	0.10	0.80	1.59
7	0.45	0.36	0.45	0.83	0.45	0.28	0.37	0.0	0.07	0.97	0.85
8	1.07	1.01	0.83	1.28	1.09	1.02	1.12	0.23	0.52	1.29	1.20
9	0.29	0.27	0.33	0.65	0.31	0.20	0.20	0.0	0.05	0.77	0.95

Region

- 2+3 Marañon Drainage + Ucayali Drainage = Peruvian Amazon
- 4 Madeira Drainage
- 5 Other Andean headwater rivers
- 6 Negro Drainage
- 7 Shield draining rivers
- 8 Lowland rivers draining marine sediments
- 9 Lowland rivers draining U. Tertiary and later sediments

and reduced marine shales are found in regions 2, 3, 4, 5, and 8, which have high denudation rates for Na, Mg, Ca, Alk(t), and S, while halite bearing rocks are particularly concentrated in the Peruvian Andes. In contrast, siliceous lithologies, the principal sources of K and Si, are distributed throughout the basin.

It has been pointed out that much of the halite exposed in the Peruvian Andes is found in rapidly extending salt diapirs (Section III.3:3). The aggregate exposed areas of these salt extrusions is probably 200 km². If the entire flux of chloride from the Peruvian Amazon is attributed to these salt extrusions, a loss of 62 mmoles/cm²/yr of NaCl (1.7 cm/yr) would be required. This figure must be tempered by the observation that significant contributions of NaCl are being derived from salt springs and bedded evaporites, particularly in the Ucayali Basin.

The near average denudation rates for potassium and silica in regions 5, 7, and 9, which are otherwise low contributors in dissolved materials, suggests that the weathering of silicate minerals is important, in well-watered tropical regions, even after thick cation depleted soils have formed. The proportions of major elements in these waters is not too unlike the proportions found in "average" shield or shale, suggesting that the intense weathering is effectively dissolving the basin substrate, perhaps in the most extreme cases, like the Negro Basin, leaving a quartz and aluminous clay residue (Section III.4:1 and IV.4:8, IV.4:11).

In examining these fluxes, it is important to note that the inorganic carbon flux in the river, while large, is comparable to carbon fluxes to the atmosphere from surface waters. An approximate flux of carbon dioxide out of the river is given by a Lewis-Whitman stagnant boundary layer gas exchange model where evasion (moles/m²yr) (E) is given by (c.f. Emerson 1975):

$$E = (P_{\text{CO}_2\text{river}}/P_{\text{CO}_2\text{atmosphere}} - 1) \cdot 600/D$$

where D is the boundary layer thickness in microns. It is assumed that D on the free flowing main channel resembles that of a lake under windy conditions or about 400 microns (c.f. Emerson 1975). No allowance is made for reequilibration in the boundary layer. The P_{CO_2} ratio averages 13. Assuming an area of $3,000,000 \times 3,000 \text{ m}^2$ for the main channel alone, a carbon dioxide flux from the river to the atmosphere of 1.6×10^{11} mole/yr is calculated, compared to a flux of about 1.7×10^{12} mole/yr being discharged from the river. The main channel constitutes only a fraction of the exposed water surface in the Amazon Basin, consequently it is expected that the water-to-atmosphere carbon flux, caused by in situ decay of organic carbon, is comparable to the river to ocean flux of inorganic carbon.

It is possible to estimate the contributions that different lithologies make to the Amazon dissolved load from the observations of Chapter IV, relating river chemistry and geology, and the fluxes given in Table VI.1 after making a cyclic salt correction. There are two major ion groupings for high TZ+ rivers (Section IV.4), Na-Cl and Ca-Mg-SO₄-HCO₃, for which ion relationships can be established on the basis of simple stoichiometry (Section IV.5). The relationship between Si, Na, K, Ca, and Mg can only be determined from field observations (Sections IV.6:5-IV.7). The calculated contributions are given in Table VI.2. In constructing this table the following assumptions were made:

- (1) All silica in the Amazon is derived from silicate rock weathering
- (2) All chloride, after the cyclic salt correction, is derived from halite.
- (3) All potassium, after cyclic salt correction, is derived from silicate rock weathering. The Cl:K ratio of waters derived from evaporites (A-05, A-11, BPA16) averages 360:1 suggesting that the evaporite contribution is insignificant.
- (4) All sodium remaining after a cyclic salt correction and subtraction of a NaCl component is derived from silicate rock weathering.

ESTIMATION OF CONTRIBUTIONS FROM VARIOUS SOURCE LITHOLOGIES IN THE AMAZON BASIN
 expressed as a percentage of the net material discharged from the Amazon system

<u>Region</u>	<u>TDS</u>	<u>TZ+</u>	<u>Na</u>	<u>K</u>	<u>Mg</u>	<u>Ca</u>	<u>Alk</u>	<u>Cl</u>	<u>SO₄</u>	<u>Si</u>
cyclic	1.4	2.4	9.4	0.7	2.2	0.1	-0.4	24.	5.4	0.0
silicates	53.	42.	55.	99.	57.	29.	41.	0.0	34. ⁺	100..
carbonates	38.	44.	0.0	0.0	40.	62.	59.	0.0	0.0	0.0
evaporites	7.9	12.	35.	0.	0.	9.4	0.0	76.	61.	0.0
discharge [#]	2.23	256.	44.	14.	23.	75.	187.	20.	12.	83.

+ reduced sulfur is included with silicates, as geological data suggest that it is most often associated with siliceous lithologies

TDS-10⁸ tonnes/yr TZ+, Alk-10¹⁰ Eq./yr Na,K,Mg,Ca,Cl,SO₄,Si-10¹⁰ moles/yr

Table VI.2

- (5) The average (Na+K):(Ca+Mg)/mole ratio for rivers draining silicate terrains is 1.2:1 (see Section IV.8. It is assumed that this ratio is applicable to calculation of the silicate contribution to (Ca+Mg) in lithologically mixed terrains, using Na and K calculated in (3) and (4) above.
- (6) It is assumed that all SO_4 in rivers which drain regions 2, 3, 5, and 8 (Andean and Subandean of Peru, Ecuador, and Brazil) is from evaporite CaSO_4 (slight overestimate), that all sulfur in region 4 (Madeira Basin) is from reduced shales (a slight overestimate), and that SO_4 from lowland rivers draining regions 6, 7, and 9 is from reduced metamorphic and sedimentary sources (perhaps a major overestimate if the sulfur is largely recycled marine sulfur).
- (7) The Ca:Mg ratio for rivers draining carbonate terrains is assumed to be 6:1, based on averaging this ratio for A-02, A-08, A-09, A-14, A-15, and A-16 after correcting for cyclic salts and a CaSO_4 contribution. This ratio is used in calculating the Ca:Mg ratios from the weathering of silicate rocks in regions 2,3,5, and 8.
- (8) The Ca:Mg ratio for silicate rocks in the Madeira Basin (4) is assumed to be 1.2:1 (average of samples M-05 and BPA01, after cyclic salt correction). The use of the silicate rock ratio in the Madeira Basin is necessitated by the relatively small contribution of Ca and Mg from carbonate rocks.
- (9) The alkalinity derived from carbonate rock weathering is assumed to balance the Ca and Mg calculated as being derived from carbonates. The remaining Alkalinity is assumed to be derived from silicate rock weathering: this will not balance the remaining cations due to the presence of other anions (NO_3 and organic anions).

It is hoped that the reader will not be overzealous in the use of the calculations given in this conclusion. These results will undergo further refinement when more detailed discharge measurements become available and as a greater number of analyses are included in the calculations.

Bear in mind that the Amazon River which is chemically so similar to world average river as it flows past Iquitos, Peru, does not drain a terrain of world average rock, weathering in steady state. Rivers draining adjoining segments of the Andes have very different chemistry; an example is the Madeira, which is the size of the Mississippi. Some inputs are extremely localized and derived from the subsurface. For example, the Amazon (and also the Mississippi and Mackenzie) has remarkably localized chloride

inputs, with salt extrusions and saline springs playing a major role; for these, geologic change has been rapid. Eight m.y.B.P. the Amazon Basin bore little resemblance to its present appearance, being drier and having smaller mountains, probably lacking salt extrusions. Some extrusions today are referred to as "dead salt", having had mineable halite in the historic past but lacking it now. Clearly the Amazon Basin is not in a geochemical steady state.

It is hoped that someday, before the Amazon Basin is completely and irreversibly altered, more work might be done, especially to fill in the vast spatial and temporal gaps in these data, and to apply the results to the benefit of the peoples of the Amazon.

Appendix I

Tabulation of sample locations. To be used in conjunction with
Tables IV.4 and IV.5.

STA.	-SAMPLE LOCATION-	--DATE--	DEPTH	- CHANNEL LOC.	- SAMPLE CATEGORY
S201	PARA RIVER BELOW BREVES	10/06/76	SURFACE	- MID-CHANNEL	- (16) UNANALYZED
S202	AMAZON NEAR ISLA URUTAI	11/06/76	SURFACE	- MID-CHANNEL	- (01) MAIN CHANNEL
S203	AMAZON ABOVE GURUPA BELOW XINGU	11/06/76	SURFACE	- MID-CHANNEL	- (01) MAIN CHANNEL
S204	XINGU RIVER ABOVE CONFLUENCE	11/06/76	SURFACE	- MID-CHANNEL	- (07) SHIELD DRAINING RIVER
S205	AMAZON NEAR ISLA ITUQUI	13/06/76	SURFACE	- MID-CHANNEL	- (15) PARTIALLY MIXED MAIN CH. AND TRIB. WATER
S206	TAPAJOS RIVER ABOVE CONFLUENCE	13/06/76	SURFACE	- MID-CHANNEL	- (07) SHIELD DRAINING RIVER
S207	AMAZON RIVER NEAR APIXUNA	13/06/76	SURFACE	- MID-CHANNEL	- (01) MAIN CHANNEL
S208	R. TROMBETAS RIVER DRIXIMINA	14/06/76	SURFACE	- MID-CHANNEL	- (07) SHIELD DRAINING RIVER
S209	AMAZON RIVER ABOVE OBIDOS	15/06/76	SURFACE	- LEFT SIDE	- (01) MAIN CHANNEL
S210	AMAZON - PARANA URARIA MIX (PARANTINS)	16/06/76	SURFACE	- LEFT SIDE	- (15) PARTIALLY MIXED MAIN CH. AND TRIB. WATER
S211	AMAZON RIVER AT ITACOATIARA	17/06/76	SURFACE	- MID-CHANNEL	- (15) PARTIALLY MIXED MAIN CH. AND TRIB. WATER
S212	MADEIRA RIVER ABOVE CONFLUENCE	17/06/76	SURFACE	- MID-CHANNEL	- (04) MADEIRA DRAINAGE
S213	AMAZON RIVER AT AMATARI	17/06/76	SURFACE	- LEFT SIDE	- (15) PARTIALLY MIXED MAIN CH. AND TRIB. WATER
S214	AMAZON RIVER AT AMATARI	17/06/76	SURFACE	- RIGHT SIDE	- (15) PARTIALLY MIXED MAIN CH. AND TRIB. WATER
S215	AMAZON RIVER, UNANALYZED	17/06/76	SURFACE	- MID-CHANNEL	- (16) UNANALYZED
S216	NEGRO RIVER ABOVE MANAUS	21/06/76	SURFACE	- MID-CHANNEL	- (06) NEGRO DRAINAGE
S217	AMAZON RIVER UNANALYZED	21/06/76	SURFACE	- LEFT SIDE	- (16) UNANALYZED
S218	AMAZON RIVER AT CONFLUENCE OF NEGRO	21/06/76	SURFACE	- LEFT SIDE	- (15) PARTIALLY MIXED MAIN CH. AND TRIB. WATER
S219	SOLIMÕES ABOVE CONFLUENCE WITH NEGRO	21/06/76	SURFACE	- MID-CHANNEL	- (01) MAIN CHANNEL
S220	SOLIMÕES RIVER AT MANACAPURU	23/06/76	SURFACE	- MID-CHANNEL	- (01) MAIN CHANNEL
S221	SOLIMÕES RIVER NEAR ISLA IUARA	23/06/76	SURFACE	- RIGHT SIDE	- (15) PARTIALLY MIXED MAIN CH. AND TRIB. WATER
S222	PURUS RIVER ABOVE CONFLUENCE	23/06/76	SURFACE	- MID-CHANNEL	- (08) LOWLAND RIVER DRAINING MARINE SEDIMENT
S223	SOLIMÕES RIVER NEAR ANORI	23/06/76	SURFACE	- MID-CHANNEL	- (01) MAIN CHANNEL
S224	SOLIMÕES RIVER NEAR CAMARA	24/06/76	SURFACE	- MID-CHANNEL	- (01) MAIN CHANNEL
S225	COARI RIVER NEAR COARI	24/06/76	SURFACE	- MID-CHANNEL	- (09) RIVER DRAINING U. TERT. AND LATER SED.
S226	SOLIMÕES RIVER-PARANA COPEA CONFLUENCE	24/06/76	SURFACE	- LEFT SIDE	- (16) UNANALYZED
S227	SOLIMÕES RIVER NEAR LARANJAI	24/06/76	SURFACE	- MID-CHANNEL	- (01) MAIN CHANNEL
S228	SOLIMÕES RIVER NEAR JUTICA	25/06/76	SURFACE	- MID-CHANNEL	- (01) MAIN CHANNEL
S229	SOLIMÕES ABOVE TEFE RIVER CONFLUENCE	25/06/76	SURFACE	- RIGHT SIDE	- (16) UNANALYZED
S230	TEFE RIVER AT TEFE	25/06/76	SURFACE	- MID-CHANNEL	- (09) RIVER DRAINING U. TERT. AND LATER SED.
S231	JAPURA RIVER ABOVE CONFLUENCE	26/06/76	SURFACE	- MID-CHANNEL	- (05) ANDEAN HEADWATER RIVER
S232	SOLIMÕES RIVER ABOVE ALVAREZ	26/06/76	SURFACE	- MID-CHANNEL	- (01) MAIN CHANNEL
S233	JURUA RIVER ABOVE CONFLUENCE	27/06/76	SURFACE	- MID-CHANNEL	- (08) LOWLAND RIVER DRAINING MARINE SEDIMENT
S234	SOLIMÕES RIVER AT FONTE BOA	27/06/76	SURFACE	- MID-CHANNEL	- (01) MAIN CHANNEL
S235	SOLIMÕES RIVER BELOW JUTAI CONFLUENCE	08/06/76	SURFACE	- MID-CHANNEL	- (01) MAIN CHANNEL
S236	JUTAI RIVER ABOVE CONFLUENCE	28/06/76	SURFACE	- MID-CHANNEL	- (09) RIVER DRAINING U. TERT. AND LATER SED.
S237	SOLIMÕES RIVER ABOVE JUTAI CONFLUENCE	28/06/76	SURFACE	- MID-CHANNEL	- (01) MAIN CHANNEL
S238	ICA RIVER ABOVE CONFLUENCE	30/06/76	SURFACE	- MID-CHANNEL	- (05) ANDEAN HEADWATER RIVER
S239	SOLIMÕES RIVER NEAR AMATAURA	30/06/76	SURFACE	- LEFT SIDE	- (15) PARTIALLY MIXED MAIN CH. AND TRIB. WATER
S240	SOLIMÕES RIVER AT SAO PAULO DE OLIVENCA	01/07/76	SURFACE	- MID-CHANNEL	- (01) MAIN CHANNEL
S241	SOLIMÕES RIVER NEAR ISLA ASSACAID	01/07/76	SURFACE	- MID-CHANNEL	- (01) MAIN CHANNEL
S242	JAVARI RIVER ABOVE CONFLUENCE	02/07/76	SURFACE	- MID-CHANNEL	- (08) LOWLAND RIVER DRAINING MARINE SEDIMENT
S243	AMAZON RIVER NEAR LETICIA	03/07/76	SURFACE	- RIGHT SIDE	- (01) MAIN CHANNEL
S244	VARZEA LAKE NEAR LETICIA	04/07/76	SURFACE	- MIDDLE	- (10) VARZEA WATERS
S245	VARZEA LAKE NEAR LETICIA	04/07/76	SURFACE	- MIDDLE	- (10) VARZEA WATERS
S246	CAYARU RIVER ABOVE CONFLUENCE	04/07/76	SURFACE	- MID-CHANNEL	- (10) VARZEA WATERS
S247	AMAZON RIVER NEAR PEVAS	07/07/76	SURFACE	- MID-CHANNEL	- (01) MAIN CHANNEL
S248	AMAZON RIVER BELOW NAPO CONFLUENCE	07/07/76	SURFACE	- MIDDLE LEFT	- (15) PARTIALLY MIXED MAIN CH. AND TRIB. WATER
S249	NAPO RIVER ABOVE CONFLUENCE	08/07/76	SURFACE	- MID-CHANNEL	- (05) ANDEAN HEADWATER RIVER
S250	AMAZON RIVER AT IQUITOS	08/07/76	SURFACE	- MID-CHANNEL	- (01) MAIN CHANNEL

STA.	--SAMPLE LOCATION--	--DATE--	DEPTH	-- CHANNEL LOC.	-- SAMPLE CATEGORY
S301	JAVARI RIVER ABOVE CONFLUENCE	17/05/77	SURFACE	- MID-CHANNEL	- (08) LOWLAND RIVER DRAINING MARINE SEDIMENT
S302	AMAZON RIVER AT IQUITOS	20/05/77	SURFACE	- MID-CHANNEL	- (01) MAIN CHANNEL
S303	AMAZON RIVER ABOVE NAPO CONFLUENCE	20/05/77	SURFACE	- MID-CHANNEL	- (01) MAIN CHANNEL
S304	NAPO RIVER ABOVE CONFLUENCE	20/05/77	SURFACE	- MID-CHANNEL	- (05) ANDEAN HEADWATER RIVER
S305	AMAZON RIVER BELOW PEVAS	20/05/77	SURFACE	- MID-CHANNEL	- (01) MAIN CHANNEL
S306	AMAZON RIVER AT LETICIA	21/05/77	SURFACE	- MID-CHANNEL	- (01) MAIN CHANNEL
S307	SOLIMÕES ABOVE SAO PAULO DE OLIVENCA	22/05/77	SURFACE	- MID-CHANNEL	- (01) MAIN CHANNEL
S308	VARZEA LAKE NEAR S. PAULO DE OLIVENCA	22/05/77	SURFACE	- MIDDLE	- (10) VARZEA WATERS
S309	JANDIATUBA RIVER ABOVE CONFLUENCE	22/05/77	SURFACE	- MID-CHANNEL	- (09) RIVER DRAINING U. TERT. AND LATER SED.
S309A	LAKE ON THE JANDIATUBA RIVER	22/05/77	SURFACE	- MIDDLE	- (09) RIVER DRAINING U. TERT. AND LATER SED.
S310	SOLIMÕES AT SAO PAULO DE OLIVENCA	22/05/77	SURFACE	- RIGHT SIDE	- (16) UNANALYZED
S311	SOLIMÕES RIVER ABOVE ICA CONFLUENCE	23/05/77	SURFACE	- MID-CHANNEL	- (01) MAIN CHANNEL
S312	VARZEA LAKE IN FRONT OF TONANTINS	23/05/77	SURFACE	- MIDDLE	- (10) VARZEA WATERS
S313	ICA RIVER ABOVE CONFLUENCE	23/05/77	SURFACE	- MID-CHANNEL	- (05) ANDEAN HEADWATER RIVER
S314	SOLIMÕES RIVER ABOVE JUTAI CONFLUENCE	24/05/77	SURFACE	- MID-CHANNEL	- (01) MAIN CHANNEL
S315	JUTAI RIVER ABOVE CONFLUENCE	24/05/77	SURFACE	- MID-CHANNEL	- (09) RIVER DRAINING U. TERT. AND LATER SED.
S316	SOLIMÕES ABOVE JURUA CONFLUENCE	24/05/77	SURFACE	- MID-CHANNEL	- (01) MAIN CHANNEL
S317	JURUA RIVER ABOVE CONFLUENCE	24/05/77	SURFACE	- MID-CHANNEL	- (08) LOWLAND RIVER DRAINING MARINE SEDIMENT
S317A	MINERUA PARANA ABOVE JURUA CONFLUENCE	24/05/77	SURFACE	- MID-CHANNEL	- (10) VARZEA WATERS
S318	JAPURA RIVER ABOVE CONFLUENCE	25/05/77	SURFACE	- MID-CHANNEL	- (05) ANDEAN HEADWATER RIVER
S319	TEFE RIVER IN MIDDLE OF MOUTH BAY LAKE	25/05/77	SURFACE	- MIDDLE	- (09) RIVER DRAINING U. TERT. AND LATER SED.
S319A	TEFE RIVER AT TEFE	25/05/77	SURFACE	- MID-CHANNEL	- (09) RIVER DRAINING U. TERT. AND LATER SED.
S320	LAKE CAIAMBÉ	25/05/77	SURFACE	- MIDDLE	- (10) VARZEA WATERS
S321	SOLIMÕES ABOVE COARI CONFLUENCE	26/05/77	SURFACE	- MID-CHANNEL	- (01) MAIN CHANNEL
S322	COARI R. IN LOWER MIDDLE OF MOUTH BAY L.	26/05/77	SURFACE	- MIDDLE	- (09) RIVER DRAINING U. TERT. AND LATER SED.
S323	SOLIMÕES ABOVE PURUS CONFLUENCE	06/05/77	SURFACE	- MIDDLE RIGHT	- (01) MAIN CHANNEL
S324	PURUS RIVER ABOVE CONFLUENCE	26/05/77	SURFACE	- MID-CHANNEL	- (08) LOWLAND RIVER DRAINING MARINE SEDIMENT
S325	CABOLIANA LAKE NEAR MANACAPURU	27/05/77	SURFACE	- MIDDLE	- (10) VARZEA WATERS
S326	SOLIMÕES RIVER ABOVE NEGRO CONFLUENCE	27/05/77	SURFACE	- MIDDLE RIGHT	- (01) MAIN CHANNEL
S327	NEGRO RIVER AT NARROWS ABOVE MANAUS	28/05/77	SURFACE	- MID-CHANNEL	- (06) NEGRO DRAINAGE
S328	MADEIRA RIVER ABOVE CONFLUENCE	01/06/77	SURFACE	- MID-CHANNEL	- (04) MADEIRA DRAINAGE
S329	AMAZON RIVER AT OBIDOS	02/06/77	SURFACE	- MID-CHANNEL	- (01) MAIN CHANNEL
S330	MAMAURU LAKE	02/06/77	SURFACE	- MIDDLE	- (10) VARZEA WATERS
S331	SMALL STREAM ENTERING AMAZON AT OBIDOS	02/06/77	SURFACE	- MID-CHANNEL	- (08) LOWLAND RIVER DRAINING MARINE SEDIMENT
S332	TROMBETAS RIVER ABOVE ORIXIMINA	03/06/77	SURFACE	- MID-CHANNEL	- (07) SHIELD DRAINING RIVER
S333	AMAZON RIVER BELOW OBIDOS (UNANALYZED)	03/06/77	SURFACE	- MIDDLE LEFT	- (16) UNANALYZED
S334	AMAZON RIVER ABOVE TAPAJOS CONFLUENCE	03/06/77	SURFACE	- MID-CHANNEL	- (01) MAIN CHANNEL
S335	TAPAJOS R. IN MIDDLE OF MOUTH BAY LAKE	04/06/77	SURFACE	- MID-CHANNEL	- (07) SHIELD DRAINING RIVER
S336	AMAZON ABOVE XINGU CONFLUENCE	05/06/77	SURFACE	- MID-CHANNEL	- (01) MAIN CHANNEL
S337	XINGU RIVER AT PORTO DE MOZ	05/06/77	SURFACE	- MID-CHANNEL	- (07) SHIELD DRAINING RIVER
S337A	MATARI RIVER AT CONFLUENCE WITH XINGU	05/06/77	SURFACE	- MID-CHANNEL	- (09) RIVER DRAINING U. TERT. AND LATER SED.
UN1	UPPER NEGRO ABOVE BRANCO CONFLUENCE	/08/77	SURFACE	- MID-CHANNEL	- (06) NEGRO DRAINAGE
UN2	UPPER NEGRO ABOVE BRANCO CONFLUENCE	/04/78	SURFACE	- MID-CHANNEL	- (06) NEGRO DRAINAGE
BR1	BRANCO RIVER ABOVE CONFLUENCE	/08/77	SURFACE	- MID-CHANNEL	- (06) NEGRO DRAINAGE
BR2	BRANCO RIVER ABOVE CONFLUENCE	/04/78	SURFACE	- MID-CHANNEL	- (06) NEGRO DRAINAGE
LN1	NEGRO RIVER AT MANAUS	/01/78	SURFACE	- MID-CHANNEL	- (06) NEGRO DRAINAGE
LN2	NEGRO RIVER AT MANAUS	/04/78	SURFACE	- MID-CHANNEL	- (06) NEGRO DRAINAGE
SOL1	SOLIMÕES ABOVE CONFLUENCE WITH NEGRO	/01/78	SURFACE	- MID-CHANNEL	- (01) MAIN CHANNEL
SOL2	SOLIMÕES RIVER ABOVE NEGRO CONFLUENCE	/04/78	SURFACE	- MID-CHANNEL	- (01) MAIN CHANNEL
LJ1	JANAUARY LAKE	/01/78	SURFACE	- MIDDLE	- (10) VARZEA WATERS

STA.	-SAMPLE LOCATION-	--DATE--	DEPTH	- CHANNEL LOC.	- SAMPLE CATEGORY
AM101	AMAZON RIVER AT IQUITOS	15/10/78	SURFACE	- LEFT BANK	- (01) MAIN CHANNEL
NAN01	NANAY RIVER AT IQUITOS	15/10/78	SURFACE	- RIGHT BANK	- (09) RIVER DRAINING U. TERT. AND LATER SED.
S-1	UCAYALI RIVER AT PUCALLPA	11/07/76	SURFACE	- LEFT BANK	- (03) UCAYALI DRAINAGE
S-2	HUALLAGA RIVER AT HUANUCO	13/07/76	SURFACE	- RIGHT BANK	- (02) MARANON DRAINAGE
A-01	MONTARO RIVER AT CHULEC	04/05/77	SURFACE	- LEFT BANK	- (03) UCAYALI DRAINAGE
A-02	HUALLAGA ABOVE HUIGUERAS (HUANUCO)	05/05/77	SURFACE	- LEFT BANK	- (02) MARANON DRAINAGE
A-03	HUIGUERAS RIVER AT HUANUCO	05/05/77	SURFACE	- LEFT BANK	- (02) MARANON DRAINAGE
A-04	HUACHIPA RIVER-LOWER COURSE	06/05/77	SURFACE	- RIGHT BANK	- (02) MARANON DRAINAGE
A-05	SALT SPRING, LEFT BANK OF MONZON R.	07/05/77	SURFACE	- BANK	- (02) MARANON DRAINAGE
A-06	MONZON RIVER ABOVE CONFLUENCE	07/05/77	SURFACE	- LEFT BANK	- (02) MARANON DRAINAGE
A-07	HUALLAGA ABOVE MONZON (TINGO MARIA)	07/05/77	SURFACE	- RIGHT BANK	- (02) MARANON DRAINAGE
A-08	ASPASARTA RIVER-LOWER COURSE	07/05/77	SURFACE	- RIGHT BANK	- (02) MARANON DRAINAGE
A-09	UCHIZA RIVER-LOWER COURSE	07/05/77	SURFACE	- RIGHT BANK	- (02) MARANON DRAINAGE
A-10	CACHIYACU RIVER-LOWER COURSE	07/05/77	SURFACE	- LEFT BANK	- (02) MARANON DRAINAGE
A-11	TOCACHE RIVER-LOWER COURSE	08/05/77	SURFACE	- RIGHT BANK	- (02) MARANON DRAINAGE
A-12	HUALLAGA ABOVE TOCACHE R. (TOCACHE)	08/05/77	SURFACE	- LEFT BANK	- (02) MARANON DRAINAGE
A-13	HUALLAGA AT BALSAYACU	10/05/77	SURFACE	- LEFT BANK	- (02) MARANON DRAINAGE
A-14	HUALLABAMBA RIVER AT CONFLUENCE	10/05/77	SURFACE	- RIGHT BANK	- (02) MARANON DRAINAGE
A-15	SAPOSOA RIVER-LOWER COURSE	11/05/77	SURFACE	- LEFT BANK	- (02) MARANON DRAINAGE
A-16	MAYO RIVER-LOWER COURSE	11/05/77	SURFACE	- LEFT BANK	- (02) MARANON DRAINAGE
A-17	HUALLAGA ABOVE SHANUSI R. (YURIMAGUAS)	12/05/77	SURFACE	- MID-CHANNEL	- (02) MARANON DRAINAGE
A-18	SHANUSI RIVER YURIMAGUAS	12/05/77	SURFACE	- MID-CHANNEL	- (02) MARANON DRAINAGE
A-19	PARANAPURA RIVER YURIMAGUAS	12/05/77	SURFACE	- MID-CHANNEL	- (02) MARANON DRAINAGE
A-21	NANAY RIVER IQUITOS	14/05/77	SURFACE	- MID-CHANNEL	- (09) RIVER DRAINING U. TERT. AND LATER SED.
M-01	MADEIRA RIVER AT PORTO VELHO	15/06/77	SURFACE	- RIGHT BANK	- (04) MADEIRA DRAINAGE
M-02	MAMORE RIVER AT GUAYARAMERIN	17/06/77	SURFACE	- LEFT BANK	- (04) MADEIRA DRAINAGE
M-03	BENI RIVER ABOVE MADRE DE DIOS RIVER	18/06/77	SURFACE	- MID-CHANNEL	- (04) MADEIRA DRAINAGE
M-04	MADRE DE DIOS RIVER ABOVE BENI RIVER	18/06/77	SURFACE	- MID-CHANNEL	- (04) MADEIRA DRAINAGE
M-05	ICHILO RIVER AT PUERTO VILLARROEL	25/06/77	SURFACE	- LEFT BANK	- (04) MADEIRA DRAINAGE
M-06	CHACALTAYA SNOW	10/07/77			- (14) SNOW
M-08	URUBAMBA RIVER AT MACHU PICCHU	22/07/77	SURFACE	- MID-CHANNEL	- (03) UCAYALI DRAINAGE
M-09	STREAM AT AGUAS CALIENTES	22/07/77	SURFACE	- MID-CHANNEL	- (03) UCAYALI DRAINAGE
BPA01	ICHILO RIVER AT PUERTO VILLARROEL	22/11/78	SURFACE	- LEFT BANK	- (04) MADEIRA DRAINAGE
BPA02	SAN MATEO RIVER AT VILLA TUNARI	23/11/78	SURFACE	- LEFT BANK	- (04) MADEIRA DRAINAGE
BPA03	ESPIRITU SANTO RIVER AT VILLA TUNARI	23/11/78	SURFACE	- RIGHT BANK	- (04) MADEIRA DRAINAGE
BPA04	MAMORE RIVER AT TRINIDAD	26/11/78	SURFACE	- RIGHT BANK	- (04) MADEIRA DRAINAGE
BPA05	GUAPAY RIVER AT PAILAS	28/11/78	SURFACE	- LEFT BANK	- (04) MADEIRA DRAINAGE
BPA06	PIRAY RIVER AT SANTA CRUZ	29/11/78	SURFACE	- RIGHT BANK	- (04) MADEIRA DRAINAGE
BPA07	CHACALTAYA SNOW	30/11/78			- (14) SNOW
BPA08	URUBAMBA RIVER AT MACHU PICCHU	06/12/78	SURFACE	- LEFT BANK	- (03) UCAYALI DRAINAGE
BPA09	AMAZON RIVER AT IQUITOS	10/12/78	SURFACE	- MID-CHANNEL	- (01) MAIN CHANNEL
BPA10	MARANON RIVER AT CONFLUENCE (NAUTA)	10/12/78	SURFACE	- MID-CHANNEL	- (02) MARANON DRAINAGE
BPA11	UCAYALI RIVER AT CONFLUENCE	10/12/78	SURFACE	- MID-CHANNEL	- (03) UCAYALI DRAINAGE
BPA12	NANAY RIVER AT IQUITOS	11/12/78	SURFACE	- RIGHT BANK	- (09) RIVER DRAINING U. TERT. AND LATER SED.
BPA13	HUALLAGA ABOVE SHANUSI R. (YURIMAGUAS)	13/12/78	SURFACE	- MID-CHANNEL	- (02) MARANON DRAINAGE
BPA14	SHANUSI RIVER AT YURMAGUAS	13/12/78	SURFACE	- MID-CHANNEL	- (02) MARANON DRAINAGE
BPA15	PARANAPURA RIVER AT YURIMAGUAS	13/12/78	SURFACE	- MID-CHANNEL	- (02) MARANON DRAINAGE
BPA16	CANA STREAM BY MINES, PILLUANA SALT DOME	15/12/78	SURFACE	- RIGHT BANK	- (02) MARANON DRAINAGE

STA.	-SAMPLE LOCATION-	--DATE--	DEPTH	- CHANNEL LOC.	- SAMPLE CATEGORY
RA01	PRECIPITATION (MARINE)	31/05/76			- (13) RAIN
RA02	PRECIPITATION (MARINE)	05/06/76			- (13) RAIN
RA03	PRECIPITATION (SANTAREM)	13/06/76			- (13) RAIN
RA04	PRECIPITATION (SANTAREM)	13/06/76			- (13) RAIN
RA05	PRECIPITATION (SANTAREM)	13/06/76			- (13) RAIN
RA06	PRECIPITATION (SANTAREM)	13/06/76			- (13) RAIN
RA07	PRECIPITATION (SANTAREM)	13/06/76			- (13) RAIN
RA08	PRECIPITATION (SANTAREM)	13/06/76			- (13) RAIN
RA09	PRECIPITATION (SANTAREM)	13/06/76			- (13) RAIN
RA10	PRECIPITATION (SANTAREM)	13/06/76			- (13) RAIN
RA11	PRECIPITATION (ABOVE JURUA)	27/06/76			- (13) RAIN
RA12	PRECIPITATION (SANTO ANTONIO)	29/06/76			- (13) RAIN
RA13	PRECIPITATION (SANTO ANTONIO)	29/06/76			- (13) RAIN
RA14	PRECIPITATION (SANTO ANTONIO)	29/06/76			- (13) RAIN
RA15	PRECIPITATION (SANTO ANTONIO)	29/06/76			- (13) RAIN
RA16	PRECIPITATION (SANTO ANTONIO)	29/06/76			- (13) RAIN
RA17	PRECIPITATION (SANTO ANTONIO)	29/06/76			- (13) RAIN
RA18	PRECIPITATION (SANTO ANTONIO)	29/06/76			- (13) RAIN
RA19	PRECIPITATION (SANTO ANTONIO)	29/06/76			- (13) RAIN
RA20	PRECIPITATION (TOCACHE)	08/05/77			- (13) RAIN
RA21	PRECIPITATION (LETICIA)	17/05/77			- (13) RAIN
RA22	PRECIPITATION (LETICIA)	17/05/77			- (13) RAIN
RA23	PRECIPITATION (LETICIA)	17/05/77			- (13) RAIN
RA24	PRECIPITATION (LETICIA)	17/05/77			- (13) RAIN
RA25	PRECIPITATION (LETICIA)	17/05/77			- (13) RAIN
RA26	PRECIPITATION (LETICIA)	17/05/77			- (13) RAIN
RA27	PRECIPITATION (LETICIA)	17/05/77			- (13) RAIN
RA28	PRECIPITATION (LETICIA)	17/05/77			- (13) RAIN
RA29	PRECIPITATION (LETICIA)	17/05/77			- (13) RAIN
RA30	PRECIPITATION (LETICIA)	17/05/77			- (13) RAIN
RA31	PRECIPITATION (LETICIA)	17/05/77			- (13) RAIN
RA32	PRECIPITATION (SAO PAULO)	22/05/77			- (13) RAIN
RA33	PRECIPITATION (SAO PAULO)	22/05/77			- (13) RAIN
RA34	PRECIPITATION (CHACALTAYA SNOW)	10/07/77			- (14) SNOW
RA35	PRECIPITATION (CHACALTAYA SNOW)	30/11/78			- (14) SNOW

Appendix II

Collection procedures

Appendix II Sample Collection

The philosophy of sample collection was to obtain samples in a variety of ways so as to eliminate concentration changes during storage. Previous investigations have indicated (Section IV.2) that all major elements are found at trace levels in at least some Amazon surface waters. Thus, bottle preparation and sample handling procedures are crucial in obtaining good results. For example, one would not want to analyze chloride in a HCl leached bottle. Sample collection differed slightly between the shipboard work and ground-based studies, however all attempts were made to establish similar procedures for the two.

Shipboard Samples

Sampling from the R.V. Alpha Helix utilized a shipboard system for collecting uncontaminated underway samples. A polyethylene tube led from a "fish", towed on a boom extended from the side of the ship, to a collection container. Samples were collected by suction. The system was rinsed, prior to collection, by pumping water through it.

When sampling from a Boston Whaler, bottles were submerged, shaken, then emptied three times before collecting the sample.

Alkalinity, pH, Si, PO₄, Total-P, NO₃, NO₂, and NH₄ were all run within 24 hours of collection. Temporary storage was in glass at near zero temperatures. Alkalinity, Si, and NO₃ were also run on stored samples, and provided a method for checking the stability of these samples. Samples analyzed for pH, TCO₂ and TOC were processed immediately upon receipt of the samples. The remaining subsamples were typically split from a single Gerry-jug. Four classes of subsamples were split into 500 ml polyethylene bottles:

- (1) Untreated sample - this split was stored in a bottle which had been nitric then distilled water leached. This subsample was taken separately if collected from a whaler. It was analyzed for Na, K, Mg, Ca, Alk, Cl, SO₄, Si, Fe, Al.

- (2) Trace element sample - this split was filtered through a preweighed .45 μ Nucleopore © filter, into a HCl or HNO₃ leached bottle, then acidified with 1 ml, 6N, 2x distilled, HCl. The subsample was analyzed for Fe, Al and other trace elements.
- (3) Acidified sample - this split was filtered through a rinsed .45 μ millipore © filter, into an HCl leached bottle, then spiked with 1 ml, 6N 2x distilled HCl. It was analyzed for cations and NO₃.
- (4) Unacidified sample - this split was filtered through a .45 μ glass fiber filter into a hot-distilled-water leached bottle. The subsample was analyzed for Na, K, Mg, Ca, Alk, Cl, SO₄, Si.

Ground-Based

The only ground-based field measurements were of pH and temperature, which were done in situ. Remaining analyses were done in the laboratory.

An analagous set of four bottles was collected, however all volumes were halved to increase portability during numerous public transportation connections. In addition a sample was collected for PO₄ in a 50ml ground glass milk sampling bottle and spiked with 200 μ l of chloroform. It should be noted that sediment passed throught the .45 μ filters, evidenced by haze and color. This sediment apparently dissolved upon acidification.

Storage

Storage for Fe and Al is discussed in detail in section IV.8. Alkalinity and silica measured on shipboard agreed with the unacidified sample and , in the case of sediment poor rivers, with the untreated samples. For Na, K, Mg, Ca, Cl, SO₄ the unacidified sample was stable over several years, if stored in the dark. Slight increases (5%) in cation concentrations are seen in untreated samples from sediment-rich waters. pH appears to be stable in untreated samples where the initial pH is below about 5.5. NO₃ was not as stable on storage, and it appears that storage in excess of about 6 months involves increased scatter and some, apparently systematic loss of NO₃.

Appendix III

Analytical methods

APPENDIX III ANALYTICAL METHODS

Analytical methods were selected and modified for the low concentrations encountered, yet adaptable to a wide concentration range without undue handling of samples. Concentration ranges for waters from the Amazon Basin, analytical ranges, and measurement precisions are presented in Table (IV. 2).

Most of the analyses followed a basic scheme. All labware was leached in 20% nitric acid. Blanks and standards were prepared using water that had been distilled in a Barnsted metal still, passed through an ion exchanger, and then distilled in a Corning borosilicate glass still. The concentrations of the primary standards were selected such that multipoint standard curves for the analytical ranges in Table (IV.2) could be prepared using the same volumetric apparatus and dilution procedures (exceptions being alkalinity and shipboard analyses). Blanks and (at least partial) standard curves were run after every 5 to 15 samples. All runs were bracketed by complete standard curves. If necessary, quadratic fits were used to account for nonlinearity in standard curves. Drift in instrument readings, if observed, was assumed to be smooth, and concentrations were calculated using linear interpolation. Most dilutions were done gravimetrically, except for samples whose concentrations fell into the range of the primary standards. These were diluted with the same equipment as was used for preparing the primary standards. In addition to prepared standards, certain samples, covering the range of concentrations found in lowland rivers, were rerun with most analyses. These were used to check the consistency of the data, and to provide an estimate of analytical variability.

Sodium, Potassium, Magnesium, Calcium

These elements were analyzed using a Perkin-Elmer 403 Atomic Absorption Spectrophotometer, following Fishman and Downs (1966). Interference suppres-

sors were adjusted to the following concentrations in the samples and standards:

<u>Element</u>	<u>Suppressor</u>
Sodium	Potassium 20 mmole/l
Potassium	Sodium 20 mmole/l
Magnesium	Lanthanum 36 mmole/l* + (0.1N) HCl
Calcium	Lanthanum 36 mmole/l* + (0.1N) HCl

* higher concentrations caused deposits on the burner head

Samples containing the lowest concentrations of the above elements were also run without suppressors to reduce noise in the blanks, and this proved significant for only precipitation samples.

Silica

Silica was analyzed according to the molybdenum blue method of Strickland and Parsons (1968). All samples and standards were diluted simultaneously by a factor of four prior to analysis. Precisions for laboratory analysis were an order of magnitude better than shipboard analyses, consequently the former are utilized in this study; laboratory and shipboard analyses agree within the analytical precisions. Sample concentrations are reported relative to a Baker Dilut-it standard. These concentrations are 1.089 times values calculated relative to sodium silicon hexafluoride standards. A Beckman DU-2 was used onboard ship and a Perkin-Elmer Model 55E Spectrophotometer was used in the lab.

pH

pH measurements were either done in situ or in a closed system, consisting of a 125 ml ground glass-stoppered flask with electrode ports, due to high CO₂ vapor pressures in the samples. Samples were siphoned from the ground glass collection bottles into the bottom of the flask; 100 to 200

ml of the sample was allowed to overflow. Shipboard measurements utilized Corning model 110 and 130 digital meters. Andean rivers (stations S-1 and A1-A21) were measured using an Orion model 401 pH meters; (stations M01-M09) were measured using Merck pH strips; and (stations BPA01-BPA16) were measured using a Chemtrix model 600 digital pH meter. Precipitation samples were measured on 5 ml volumes, in an open 10 ml beaker. Measurements were done at $25 \pm 3^{\circ}\text{C}$. Corning or Fisher prepared standards were used. Estimated precisions are:

<u>Stations</u>	<u>Precision (est 2σ)</u>
S201-S328	0.03
S-1, A01-A21	0.1
M01-M09	0.3
BPA01-BPA16	0.05
Precipitation	0.05

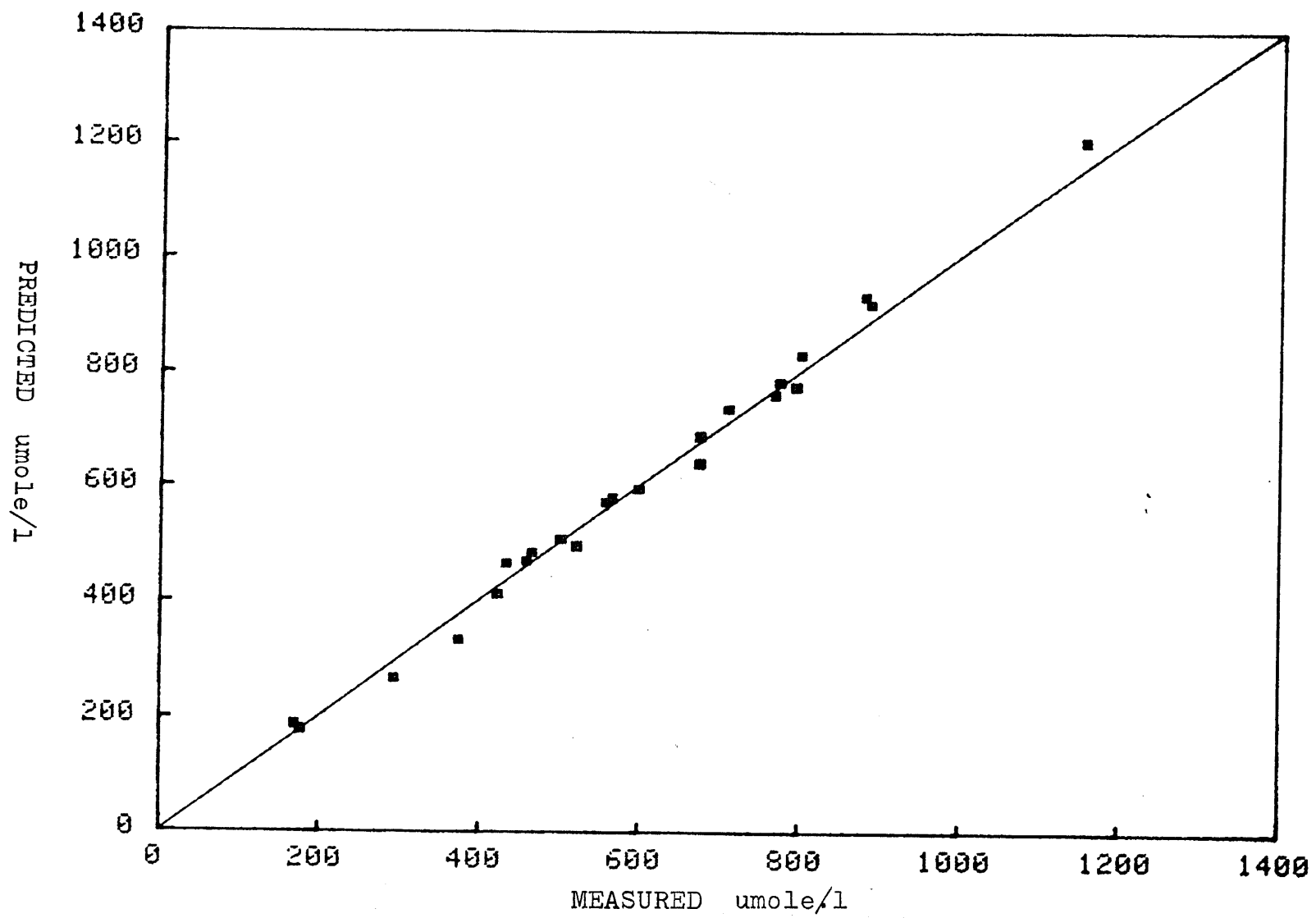
Alkalinity and Total Carbon Dioxide

All alkalinities were measured in duplicate or triplicate, modified from the titration method of Edmond (1970), for an open system and 100 ml volumes for lowland samples and 50 ml volumes for remaining samples.

Total carbon dioxide was measured using Beckman models 215 and 865 non-dispersive infrared analyzers. Samples, collected in ground glass-stoppered bottles, were transferred to 20 ml ampoules using a syringe. Care was taken to remove bubbles from the syringe and to introduce the samples slowly into the bottom of the ampoule. The samples were then poisoned using 100 μl saturated HgCl_2 , acidified with 100 μl of concentrated H_3PO_4 , and promptly flame sealed. The samples were introduced into the CO_2 analyzer through a closed loop recycling system, in which the ampoule was sealed into the system; the neck was broken; and air was recycled through the sample until

Figure AIII.1

Graph of total CO_2 predicted from $\text{Alk}(t)$ and pH versus
measured total CO_2



the instrument reading stabilized. Standards were prepared with individually weighed calcite crystals and 20 ml of CO₂-free distilled water, treated and sealed in the same manner as the samples.

TCO₂ can be calculated from pH and alkalinity, assuming that the alkalinity is derived from bicarbonate and carbonate ions:

$$\text{TCO}_2 = \frac{(\text{Alk} + (\text{H}) - K_w/(\text{H})) \cdot ((\text{H})/K_1 + 1 + K_2/(\text{H}))}{(1 + 2/K_2/(\text{H}))}$$

$pK_w = 14$
 $pK_1 = 6.352 \quad 25^\circ\text{C}$
 $pK_2 = 10.329$

Alk (H), in practice calculated TCO₂ agrees with measured TCO₂ (Figure AIII.1), demonstrating that the titration alkalinity involves dominantly CO₂ system species, the effects of other weak acids being unimportant.

Sulfate and Chloride

Most methods for sulfate and chloride analysis cannot be used reliably for Amazonian waters. Both species are often found near the detection limit for many techniques, furthermore organic materials in the samples interfere with many sulfate procedures. To raise detection limits samples were preconcentrated by evaporation, and to eliminate organic interferences all samples analyzed for sulfate were completely evaporated and heated to 525^oC. Chloride was also measured in the latter samples. Batches of 20 to 40 samples were processed at one time, the entire procedure, including analysis taking 3-4 days. Samples were treated with base to avoid losses of volatile salts.

Preliminary chloride concentrations were obtained by direct analysis of samples, and initial estimates of the sulfate concentrations were calculated from charge balances of all other species. All samples

whose concentrations did not fall into the middle of the analytical range (Table AIII.1) were adjusted into that range by preconcentration (up to 15 fold) or by dilution. The preconcentration was done on a hotplate in a laminar flow bench. Samples to be preconcentrated were measured into 50 ml borosilicate flasks. Samples were evaporated in borosilicate

vials, which were periodically brought up to about 10 ml with sample from the flask. Five umoles of NaCO_3 were added to the samples in the vials to prevent the loss of chloride, if the samples were dried to dryness (Howard 1933). The hotplate temperatures were adjusted such that the samples were held at the boiling point, with at the most very slight bubbling. Sixteen to eighteen hours were required to reduce 100 ml to 10 ml. After the sample was transferred from the flask to the vial, the flask was rinsed with 5 ml distilled water. Blanks for this distilled water (important for Cl) were determined by preconcentrating the distilled water along with the samples. Concentration factors for chloride samples not evaporated to dryness were determined gravimetrically.

Samples analyzed for sulfate were heated to 525°C in a Lindburg muffle furnace. These were heated from a cool start, taking one half hour to reach temperature, where they were maintained for another half hour. Samples were covered with a glass plate during heating. If samples were placed directly in the hot oven, they lost chloride, perhaps due to a thermal over-shoot or to sputtering. This phenomenon shows on the glass plate as a film, and was not observed in slowly heated samples. For both chloride and sulfate, standards and samples spiked with standards showed 100% recovery to within the analytical error. In addition, chloride samples that were heated in the oven agreed with samples which were not.

After samples were cooled, they were redissolved in 10 ml of 0.02N acetic acid solution. Dissolution was aided with an ultrasonic bath (2 minutes) and a shaker table (1 hour). The acetic acid, combined with the added NaCO_3 , and the alkalinity of the samples, served to buffer the samples into the pH range of 4.0-4.3. This 10 ml could be analyzed 2-3 times for sulfate and 1-2 times for chloride. Blanks and standards were prepared with the same NaCO_3 -acetic acid mixture.

Sulfate was analyzed by the indirect colorimetric method of Archer (1975), using 2-aminoperimidine (2-AP), modified for high molar absorptivity. This method was particularly advantageous as it offered potential for resolving small variations in concentration, and required a small (2 ml) sample, however in untreated samples organics inhibited the precipitation of 2-AP sulfate. This was circumvented by the above heat treatment. A second major problem stemmed from this being an indirect method in which the maximum volume error for transfer and spiking occurred at lowest concentrations. To circumvent this problem samples were transferred with an Eppendorf pipette, and reagents were added with microburettes. 200 μl of 550 $\mu\text{mole/l}$ K_2SO_4 was added prior to the 2-AP bromide to insure precipitation of 2-AP sulfate and to test recovery (a highly recommended step if this method is to be used on unprocessed samples). The variance of the standard curve (0-300 $\mu\text{moles/l}$) was typically 2-3 $\mu\text{moles/l}$. All samples were run in duplicate, and if these did not agree within the variance, they were rerun.

Chloride was analyzed on a Butchler Chloridimeter. Three ml of sample were spiked with one ml of reagent. The reagent consisted of 40% acetic acid, 0.4 N nitric acid, and 280 $\mu\text{mole/l}$ NaCl . The NaCl was added to insure an inflection in the titration curve at low concentrations. The variance of a standard curve (0-1000 $\mu\text{mole/l}$) was typically 2-3 $\mu\text{mole/l}$.

Iron and Aluminum

Iron and aluminum were analyzed using colorimetric methods modified from Stookey (1970) and Dougan and Wilson (1974) respectively. Modifications were done to ensure that similar phases were being analyzed for both elements.

The principal modification involved extending the heating step of the above iron method and adding an identical heating step to the above aluminum procedure. Both original procedures utilized an initial step which involved complexing the iron present in the sample under acid (0.2 N HCl) conditions, in the presence of a reducing agent (hydroxylamine hydrochloride). The Fe II complex is analyzed in the iron method, and is used to eliminate iron interference in the aluminum method. In the iron analysis the initial step is assisted by heating. Boyle et al. (1977) observe that if the heating is extended from the recommended 10 minutes to at least one half hour, colorimetric results agreed with atomic absorption results. Iron released by the additional heating may be initially bound or stabilized by organics in the sample, furthermore clays, not eliminated by filtration, would be more thoroughly digested.

Volumes for both methods were changed so that analyses could be done using preweighed borosilicate scintillation vials. Samples to be analyzed for aluminum were acidified to the recommended concentration. Following the addition of the reducing and complexing agents, all samples were heated for one hour in a 110^oC oven. Samples were cooled and brought to their initial volume gravimetrically. Remaining steps conformed to the published procedures. Standards were processed identically to the samples.

Color

Color (being the absorbance of the water sample at a certain wavelength)

has been measured in Amazonian water samples at a variety of wavelengths (Klinge and Ohle 1964, Santos and Santos 1970) as a guide to the organic carbon content and the humic acid content. In reality it is a direct measure of neither, and is instead the measure of one particular component of the dissolved organics in the sample (J. Leenher, U.S.G.S., personal communication), that is, to a degree, independent of the total organic carbon content.

A wavelength of 270 nm was chosen for the color measurement in this study. The absorbance of a typical sample is sufficiently high to be easily measured in a 1 cm quartz cell, and the ultraviolet absorbance of nitrate is insignificant. This permits extremely rapid measurements, using the sipper system of the Perkin-Elmer spectrophotometer.

Samples were generally not measured in the field, so the slight decay of color with time was corrected using an empirical formula determined from measurements of the samples separated by about 1.5 years. The formulae are:

$$\text{Abs.} = \text{Abs.}_{(t=0)} \times e^{(at)}$$

$$a(\text{filtered samples}) = 7.1 \times 10^{-5} \text{ d}^{-1}$$

$$a(\text{unfiltered samples}) = 3.3 \times 10^{-4} \text{ d}^{-1}$$

Comparison with shipboard measurements of the Rio Negro suggest that the corrected absorbances are within 5% of their original values.

Nutrients

Phosphate, nitrate, nitrite, and ammonia were run according to standard methods:

Phosphate: molybdenum blue method of Strickland and Parsons (1968)
Total P: persulfate oxidation following Menzel and Corwin (1965)

Nitrate: reduction to nitrite on cadmium columns,
pre-1978, Strickland and Parsons (1968)
subsequent, Gardner, Wynne, and Dunstan (1976)

Nitrite: Sulfanilamide and N-1-N, Strickland and Parsons (1968)

Ammonia: indophenol blue method
pre-1977, Solorzano (1969)
subsequent, Scheiner (1976)

Notes: The nitrate method was changed as the second method used a smaller volume, 15 ml versus 50 to 150 ml

The ammonia method was changed because the first method proved somewhat erratic in the river samples

Organic Carbon

Organic carbon was measured using the wet oxidation method of Menzel and Vaccaro (1964). Briefly, samples were glass pipetted into 20 ml ampoules, spiked with 100 ul concentrated H_3PO_4 , bubbled with CO_2 free N_2 , spiked with a small scoop of potassium persulfate, and promptly sealed. Samples were then run like TCO_2 .

BIBLIOGRAPHY, CHAPTER I

- Clarke, F.W. (1924) The Data of Geochemistry, 5th ed.: U.S. Geological Survey Bull. 770.
- Conway, E.J. (1942) Mean geochemical data in relation to oceanic evolution: Royal Irish Acad. Proc.; v. 48, sec. B, p. 119-159.
- Curtis, W.F., Culbertson, J.K., and Chase, E.B. (1973) Fluvial sediment discharge to the oceans from the conterminous United States: U.S. Geological Survey Circular 670.
- Durum, W.H., Heidel S.G., and Tison, L.J. (1960) World-wide runoff of dissolved solids: I.A.S.H. Publication No. 51, 618-628.
- Eriksson, E. (1959) The Yearly Circulation of Chloride and Sulfur in Nature; Meteorological, Geochemical, and Pedological Implications, Part II: Tellus, v. 11, p. 375-403.
- Eriksson, E. (1960) The Yearly Circulation of Chloride and Sulfur in Nature; Meteorological, Geochemical, and Pedological Implications. Part I: Tellus, v. 12, p. 63-109.
- Feth, J.H. (1971) Mechanisms Controlling World Water Chemistry: Evaporation-Crystallization Process: Science, v. 172, p. 870-871.
- Fournier, F. (1960) Climat et érosion: Presses Universitaires de France, Paris, 201p.
- Fournier, F. (1969) Transports solides effectués par les cours d'eau: I.A.S.H. Bull., v. 14, p.7-47.
- Garrels, R.M. and Mackenzie (1971) Evolution of Sedimentary Rocks: W.W. Norton & Co., Inc. N.Y. 397p.
- Gibbs, R.J. (1965) The Geochemistry of the Amazon River Basin: PhD. Thesis, Geology, U. California, San Diego, 96p.
- Gibbs, R.J. (1967) The Geochemistry of the Amazon River System: Part I. The Factors that Control the Salinity and the Composition and Concentration of the Suspended Solids: Geol. Soc. America. Bull., v. 78, p.1203-1232.
- Gibbs, R.J. (1970) Mechanisms Controlling World Water Chemistry: Science, v. 170, p. 1088-1090.
- Gibbs, R.J. (1971) Mechanisms Controlling World Water Chemistry: Evaporation-Crystallization Process: A Reply: Science, v. 172, p.871-872.

- Gibbs, R.J. (1972) Water chemistry of the Amazon River: *Geochimica et Cosmochimica Acta*, v. 36, p. 1061-1066.
- Hitchon, B., Levinson, A.A., and Reeder, S.W. (1969) Regional variations of river water composition resulting from halite solution, Mackenzie River drainage basin, Canada: *Water Resour. Res.*, v. 5, p. 1395-1403.
- Hitchon, B. and Krouse, H.R. (1972) Hydrochemistry of the surface waters of the Mackenzie River drainage basin, Canada-III. Stable isotopes of oxygen, carbon, and sulphur: *Geochim. Cosmochim. Acta.*, v.36, p.1337-1357.
- Holeman, J.N. (1968) The sediment yield of major rivers of the world: *Water Resour. Res.*, v.4, p.737-747.
- Holland, H.D. (1978) The Chemistry of the Atmosphere and Oceans: John Wiley and Sons: N.Y., 351p.
- Livingstone, D.A. (1963) Chemical composition of rivers and lakes, Data of geochemistry, 6th ed.: U.S. Geological Survey Profess. Paper, 440-G, 64p.
- Martin, J.M., and Meybeck, M. (1979) Elemental mass-balance of material carried by major world rivers: *Marine Chemistry*, v.7, p.173-206.
- Meybeck, M. (1976) Total Mineral Dissolved Transport by World Major Rivers: *Hydrological Sciences Bull.*, v.21, p.265-284.
- Meybeck, M. (1977) Dissolved and suspended matter carried by rivers: composition, time and space variation, and world balance, In: H.L. Golterman, ed., *Interaction between sediments and fresh waters*, Amsterdam: Junk and Pudoc, p.25-32.
- Meybeck, M. (1979) Pathways of major elements from land to ocean through rivers: In, *Extended Abstracts of Invited Papers, Review and Workshop on River Inputs To Ocean Systems (RIOS)*, FAO: Rome, 26-30, March 1979.
- Peake, E., Baker, B.L., and Hodgson, G.W. (1972) Hydrochemistry of the surface waters of the Mackenzie River drainage basin, Canada-II. The contribution of amino acids, hydrocarbons, and chlorins to the Beufort Sea by the Mackenzie River system: *Geochim. Cosmochim. Acta*, v.36, p.867-883.
- Potter, P.E. (1978) Petrology and Chemistry of modern big river sands: *Journal of Geology*, v.86, p.423-449.
- Reeder, S.W., Hitchon, B., and Levinson, A.A. (1972) Hydrochemistry of the surface waters of the Mackenzie River drainage basin, Canada-I. Factors controlling inorganic composition: *Geochim. Cosmochim. Acta*, v.36, p.825-865.

Sioli, H. (1954a) Beiträge zur regionalen Limnologie des Amazonasgebietes. I. Vorwort: Arch. Hydrobiol., v.49, p.441-447.

Sioli, H. (1954b) Beiträge zur regionalen Limnologie Amazonasgebietes. II. Der Rio Arapiuns. Limnologische Untersuchung eines Gewässers des Tertiärgebietes., Serie der "Barreiras", des unteren Amazonas: Arch. Hydrobiol., v.49, p.448-518.

Sioli, H. (1955) Beiträge zur regionalen Limnologie Amazonasgebietes. III Über einige Gewässer des oberen Rio-Negro-Gebietes: Arch. Hydrobiol., v.50, p.1-32.

Sioli, H. (1957a) Beiträge zur regionalen Limnologie des Amazonasgebietes. IV. Limnologische Untersuchungen im Gebiet der Eisenbahnlinie Belém-Bragança, Staat Para, Brasilien: Arch. Hydrobiol., v.53, p.161-222.

Sioli, H. (1957b) Sedimentation im Amazonasgebiet: Geol. Rundschau, v.45, p.608-633.

Sioli, H. (1963) Beiträge zur regionalen Limnologie Amazonasgebietes. V. Die Gewässer der Karbonstreifen Unteramazoniens: Arch. Hydrobiol., v. 59, p.311-350.

Sioli, H. (1964) General features of the limnology of Amazônia: Verh. Internat. Verein. Limnol., v.15, p.1053-1060.

Sioli, H. (1968) Hydrochemistry and Geology in the Brazilian Amazon Region: Amazoniana, v.1, p.267-277.

BIBLIOGRAPHY, CHAPTER II

- Anderson et al. (1974) Diurnal Cloud Changes in the Tropics; in Application of Meteorological Satellite Data in Analysis and Forecasting, ESSA TECHNICAL REPORT NES-51, p.4-I-1.
- Anonymous (1972a) Die Ionfracht des Rio Negro, Staat Amazonas, Brasilien nach Untersuchungen von Dr. Harald Ungemach: Amazoniana, v.3, p.175-185
- Anonymous (1972b) Regenwasseranalysen aus Zentralamazonien ausgeführt in Manaus, Amazonas, Brasilien, von Dr. Harald Ungemach: Amazoniana, v.3, p.186-198.
- Bolin, B., G. Aspling, and Persson (1974) Residence time of atmospheric pollutants as dependent on source characteristics, atmospheric diffusion processes and sink mechanisms: Tellus, v.26, p.185-195.
- Brinkmann, W.L.F., and A.dos Santos (1973) Natural Waters in Amazonia, VI-Soluble Calcium Properties: Acta Amazonica, v.3, n.2, p.33-40.
- Brinkmann, W.L.F. and U.M. Santos (1974) The emission of biogenic hydrogen sulfide from Amazonian floodplain lakes: Tellus, v.25, p.261-267
- Calvert, J.G., F. Su, J.W. Bottenheim, and O.P. Strausz (1978) Mechanism of the homogeneous oxidation of sulfur dioxide in the troposphere: Atmos. Environ., v.12, p.197-226.
- Cleaves, E.T., A.E. Godfrey, and O.P. Bricker (1970) Geochemical Balance of a Small Watershed and Its Geomorphic Implications: Geological Society of America Bull., v.81, p.3015-3032.
- Conway, E.J. (1942) Mean geochemical data in relation to oceanic evolution: Royal Irish Acad. Proc., v.48, sec.B, p.119-159.
- Crozat, G. (1979) Sur L'émission d'un aérosol riche en potassium par la forêt tropicale: Tellus, v. 31, p.52-57.
- Delmas, R., J. Baudet, and J. Servant (1978) Mise en évidence des sources naturelles de sulfate en milieu tropical humide: Tellus, v.30, p.158-168.
- Eriksson, E. (1952) Composition of atmospheric precipitation II. Sulphur, chloride, iodine compounds. Bibliography; Tellus, v.4, p.280-303.
- Eriksson, E. (1955) Air Borne Salts and the Chemical Composition of River Waters: Tellus, v.7, p.243-250.
- Eriksson, E. (1959) The Yearly Circulation of Chloride and Sulfur in Nature; Meteorological, Geochemical, and Pedological Implications. Part I: Tellus, v.11, p.375-403.

- Eriksson, E. (1960) The Yearly Circulation of Chloride and Sulfur in Nature; Meteorological, Geochemical, and Pedological Implications, Part II: *Tellus*, v. 12, p. 63-109
- Galloway, J.N. and G.E. Likens (1976) Calibration of collection procedures for the determination of precipitation chemistry: *Water Air Soil Pollut.*, v.6, p.241-258.
- Galloway, J.N., and G.E. Likens (1978) The collection of precipitation for chemical analysis: *Tellus*, v.30, p.71-82.
- Garrels, R.M. and Mackenzie (1971) Evolution of Sedimentary Rocks: W.W. Norton and Co., Inc.: N.Y., 397p.
- Gibbs, R.J. (1970) Mechanisms Controlling World Water Chemistry: *Science*, v.170, p.1088-1090.
- Gibbs, R.J. (1972) Water chemistry of the Amazon River: *Geochimica et Cosmochimica Acta*, v.36, p.1061-1066.
- Goodland, R.J.A., and H.S. Irwin (1975) Amazon Jungle: Green Hell to Red Desert?: Elsevier: Amsterdam, 155p.
- Gorham, E. (1961) Factors influencing supply of major ions to inland waters, with special reference to the atmosphere: *Geol. Soc. Am. Bull.*, v.72, p.795-840.
- Graedel, T.E. (1978) The oxidation of atmospheric sulfur compounds; in The Questions of Atmospheric Sulfates, APCA spec. Conf., Air Pollut. Control Assoc.: Pittsburgh.
- Graedel, T.E. (1979) Reduced sulfur emission from the open oceans: *Geophysical Research Letters*, v.6, p.329-331.
- Hegg, D.A., and P.V. Hobbs (1978) Oxidation of sulfur dioxide in aqueous systems with particular reference to the atmosphere; *Atmos. Environ.*, v.12, p.241-253.
- Herrera, R., C.F. Jordan, H. Klinge, and E. Medina (1978) Amazon ecosystems. Their structure and functioning with particular emphasis on nutrients: *Interciencia*, v.3, p.223-231,
- Hjelmfelt Jr., A.T. (1978) Amazon Basin Hydrometeorology: *Journal of the Hydraulic Division, Proc. Am. Soc. Civil Eng.*, v.104, p.887-897
- Hoffmann, J.A.J. (1975) Climatic Atlas of South America: WMO: Hungary
- Holland, H.D. (1978) The Chemistry of the Atmosphere and Oceans: John Wiley and Sons: N.Y., 351 p.

- Jackson, D.D. (1905) The normal distribution of chlorine in natural waters of New York and New England: U.S. Geol. Survey Water Supply and Irrigational Paper 144, 31p.
- Jahoda, J.C. and O'Hearn (1975) The Reluctant Amazon Basin: Environment, v.17, n.7, p.16-30.
- Jones, T.A. (1979) Fitting straight lines when both variables are subject to error I. Maximum likelihood and least-squares estimation: Mathematical Geology, v.11, p.1-25.
- Jordan, G.F. and Medina, E. (1977) Ecosystem research in the tropics: Ann. Missouri Bot. Gard., v.64, p.737-745.
- Junge, C.E. (1958) The distribution of ammonia and nitrate in rain water over the United States: Trans. Am. Geophys. Union, v.39, p.241-248.
- Junge, C.E. (1963) Air Chemistry and Radioactivity: Academic Press: N.Y., 382p.
- Junge, C.E. (1974) Residence time and variability of tropospheric trace gases: Tellus, v.26, p.477-488.
- Junge, C.E. and P.E. Gustafson (1957) On the Distribution of Sea Salt over the United States and its Removal by Precipitation: Tellus, v.9, p.164-173.
- Junge, C.E. and R.T. Werby (1958) The Concentration of Chloride, Sodium, Potassium, Calcium, and Sulfate in Rain Water over the United States: Journal of Meteorology, v.15, p.417-425.
- Klinge, H. (1977) Preliminary data on nutrient release from decomposing leaf litter in a neotropical rain forest: Amazoniana, v.6, p.193-202.
- Koyama, T. and K. Sugawara (1953) Separation of the components of atmospheric salt and their distribution (cont.): Chem. Soc. Japan Bull., v.26, p.123-126.
- Lawson, D.R. and J.W. Winchester (1979) Sulfur, potassium, and phosphorus associations in aerosols from South American tropical rain forests: Jour. Geophys. Res., in press
- Lettau, H., K. Lettau, and L.C.B. Molion (1979) Amazonia's Hydrologic Cycle and the Role of Atmospheric Recycling in Assessing Deforestation Effects: Monthly Weather Review, v.107, p.227-238

- Likens, G.E., F.H. Bormann, R.S. Pierce, J.S. Eaton, and N.M. Johnson (1977) Biogeochemistry of a Forested Ecosystem: Springer-Verlag Inc.: N.Y., 146p.
- Lodge, J.P., A.J. MacDonald, and E. Vihman (1960) A Study of the Composition of Marine Atmospheres: *Tellus*, v.12, p.184-187.
- Lovelock, J.E., R.J. Maggs, and R.A. Rasmussen (1972) Atmospheric dimethyl sulfide and the natural sulfur cycle: *Nature* v.239, p.452-453.
- MacIntyre, F. (1974) The Top Millimeter of the Ocean: *Scientific American*, v.230, n.5, p.62-77.
- Maroulis, P.J. and A.R. Bandy (1977) Estimate of the contribution of biologically produced dimethyl sulfide to the global sulfur cycle: *Science*, v.196, p.647-648.
- Maroulis, P.J., A.L. Torres, A.B. Goldberg, and A.R. Bandy (1978) Measurements of tropospheric background levels of SO₂ on Project GAMETAG, *Trans. Am. Geophys. Union*, v.59, p.1081
- Meinert, D.L. and J.W. Winchester (1977) Chemical Relationships in the North Atlantic Marine Aerosol: *Jour, Geophys. Res.*, v.82, p.1778-1782
- Miller, D.B. (1971) Global Atlas of Relative Cloud Cover: USAF/ETAC, NOAA/NESS
- Molion, L.C.B. (1975) A Climatonic Study of the Energy and Moisture Fluxes of the Amazonas Basin with Considerations of Deforestation Effects: PhD Thesis, University of Wisconsin, 133p.
- Nortcliff, S. and J. B. Thornes (1978) Water and cation movement in a tropical rainforest environment. I: *Acta Amazonica*, v.8, p.245-258.
- Rahn, K.A., R.D. Borys, and R.A. Duce (1976) Tropospheric Halogen Gases: Inorganic and Organic Components: *Science*, v.192, p.549-550.
- Rasmussen, R.A. (1974) Emission of biogenic hydrogen sulfide: *Tellus*, v.26, p.254-260.
- Ratisbona, L.R. (1976) The climate of Brazil; in Climates of Central and South America, W. Schwerdtfeger, Elsevier: N.Y., p.219-294.
- Schlegel, H.C. (1974) Production, modification, and consumption of atmospheric trace gases by microorganisms: *Tellus*, v.26, p.11-20.
- Scott, G. (1977) The importance of old-field succession biomass increments to shifting cultivation: *Great Plains - Rocky Mountain Geographical Journal*, v.6, p.318-327.

Salati, E., J. Marques, and L.C.B. Molion (1978) Origem e distribuição das chuvas na Amazônia: Interciencia, v.3, p.200-206

Sioli, H. (1963) Beiträge Zur regionalen Limnologie Amazonasgebietes. V. Die Gewässer der Karbonstreifen Unteramazoniens: Arch. Hydrobiol., v.59, p.311-350.

Sioli, H. (1977) Amazonasgebiet - Zerstörung des ökologischen Gleichgewichtes?: Geol. Rundschau, v.66, p.782-795.

Slatt, B.J., D.F.S. Natusch, J.M. Prospero, and D.L. Savoie (1978) Hydrogen sulfide in the atmosphere of the northern equatorial Atlantic Ocean and its relationship to the global sulfur cycle: Atmos. Environ. v.12, p.981-991.

Stark, N. (1971b) Nutrient Cycling II. Elemental contents of plants from South America: Int. J. Tropical Ecol., v.12, p.177-201.

Ungemach, H. (1967) Sobre o balanço metabólico de íônios inorgânicos da área do sistema do Rio Negro: Atas do Simpósio sobre a Biota Amazônica, v.3 (Limnologia), p.221-226.

Ungemach, H. (1969) Chemical rain water studies in the Amazon region; in II Simposio y Foro de Biología Tropical Amazónica, Idrobo, J.M. ed., Bogotá, p.354-359.

Went, F.W. and N. Stark (1968) Mycorrhiza: BioScience, v.18, p.1035-1039.

BIBLIOGRAPHY, CHAPTER III

Ahlfeld, F. (1972) *Geología de Bolivia*: Ed. Los Amigos del Libro: La Paz, 190p.

Anonymous (1972a) Die Ionenfracht des Rio Negro, Staat Amazonas, Brasilien nach Untersuchungen von Dr: Harald Ungemach: *Amazoniana*, v.3, p.175-185.

Audebaud, E., C. Capdevila, B. Dalmayrac, J. Debelmas, G. Laubacher, C. Lefevre, R. Marocco, C. Martinez, M. Mattauer, F. Megard, J. Paredes, and P. Tomasi (1973) *Les Traits Géologiques, Essentiels des Andes Centrales (Pérou-Bolivie)*: *Revue de Géographie Physique et de Géologie Dynamique*, v.15, p.73-114.

Ballivián, O., J.L. Bles, M. Servant (1978) *El Plio-Cuaternario de la region de La Paz (Andes Orientales, Bolivia)*: *Cah. ORSTOM, sér Géol.*, v.10, p.101-113.

Bellido, B.E. (1969) *Sinopsis de la Geologia del Perú*: Servicio de la Geología del Perú Bol. 22, 54p.

Benavides, V. (1968) *Saline Deposits for South America*: Geological Society of America, Special Paper 88, p.249-290.

Bigarella, J.J. (1973) *Geology of the Amazon and Parnaiba Basins*; in *The Ocean Basins and Margins*, Nairn, A.E.M. and F.G. Stehli, eds., Plenum Pub. Co.: N.Y., v.1, p.25-86.

Brinkmann, W.L.F. and J.C. de Nascimento (1973) *The effect of slash and burn agriculture on plant nutrients in the Tertiary region of Central Amazonia*: *Turrialba*, v.23, p.284-290.

Brockmann, C., A. Castaños, R. Suarez, and P. Tomasi (1972) *Estudio Geológico de la Cordillera Oriental de los Andes en la Zona Central de Bolivia*: *Sociedad Geologica Bolivia Bol.*, No.18, p.3-36.

Camargo, M.N. and I.C. Falesi (1975) *Soils of the Central Plateau and Transamazonic Highway*: in *Soil Managemant in Tropical America*, E. Bornemisza and A. Alvarado, ed.: *University Consortium on Soils of the Tropics*: Raleigh, N.C., p.25-45

Carson, M.A., and M.J. Kirby (1972) *Hillslope, Form and Process*: Cambridge University Press: Cambridge, p.

Colby, B.R., C.H. Hembree, and F.H. Rainwater (1956) *Sedimentation and the chemical quality of surface waters in the Wind River Basin, Wyoming*: U.S. Geological Survey Water-Supply Paper 1373.

Dunne, T. (1978) Rates of chemical denudation of silicate rocks in tropical catchments; *Nature* v.274, p.244-246

Ernst, W.G. (1969) Earth Materials: Prentice-Hall, Inc.: Englewood Cliffs

FAO/UNESCO (1971) Soil Map of the World, Volume IV South America, explanatory note: UNESCO: Paris, 193p.

Gansser, A. (1973) Facts and theories on the Andes: *J. Geol. Soc. London*, v. 129, p.93-131.

Garner, H.F. (1959) Stratigraphic-Sedimentary Significance of Contemporary Climate and Relief in Four Regions of the Andes Mountains: *Geol. Soc. Am. Bull.*, v.70, p.1327-1368.

Garner, H.F. (1968) Tropical Weathering and Relief; in The Encyclopedia of Geomorphology, Fairbridge, R.W. ed., p. 1161-1172.

Garrels, R.M. and Mackenzie (1971) Evolution of Sedimentary Rocks: W.W. Norton & Co. Inc.: N.Y., 397p.

Garwood, N.C., D.P. Janos, and N. Brokaw (1979) Earthquake-Caused Landslides: A Major Disturbance to Tropical Forests: *Science*, v.205, p.997-999.

Gibbs, R.J. (1965) The Geochemistry of the Amazon River Basin: Ph.D. Thesis, Geology, U. California, San Diego, 96p.

Goldich, S.S. (1938) A Study in rock weathering; *J. Geol.*, v.46, p.17-58

Grubb, P.L.C. (1979) Genesis of Bauxite Deposits in the Lower Amazon Basin and Guianas Coastal Plain; *Economic Geology*, v.74, p.735-750.

Guerrero, M.R. (1975) Soils of the Llanos Orientales of Colombia; in Soil Management in Tropical America, Bornemisza, E. and Alvarado, A. ed.: University Consortium of Soils in the Tropics: Raleigh, N.C. p.61-91.

Hem, J.D. and C.J. Lind (1974) Kaolinite Synthesis at 25°C: *Science*, v.184, p.1171-1173.

Hembree, C.H. and F.H. Rainwater (1961) Chemical Degradation on Opposite Flanks of the Wind River Range Wyoming: U.S. Geological Survey Water-Supply Paper 1535-E.

Herrera, R., C.F. Jordan, H. Klinge and E. Medina (1978) Amazon ecosystems. Their structure and functioning with particular emphasis on nutrients: *Interciencia*, v.3, p.223-231.

Herrera, R., T. Merida, N. Stark, and C.F. Jordan (1978b) Direct Phosphorus Transfer from Leaf Litter to Roots: *Naturwissenschaften*, v.65, p.208-209.

- Holeman, J.N. (1968) The sediment yield of major rivers of the world: *Water Resour. Res.*, v.4, p.737-747.
- Holland, H.D. (1978) The Chemistry of the Atmosphere and Oceans: John Wiley & Sons: N.Y., 351p.
- Holm, V.T. (1977) Geomorphology and Landscape Development at Mucajai, Roraima Territory, Brazil: unpublished report for ITAIBA: Manaus, 18p.
- Hueck, K., and P. Seibert (1972) Vegetations-karte von Sudamerika: Gustav Fischer Verlag: Stuttgart, 71p.
- Irion, G. (1975) Los primeros resultados de las investigaciones de sedimentación y perfiles de erosión en la región amazónica: *Unversitas*, v.12, p.256-257.
- Irion, G. (1976) Mineralogisch-geochemische Untersuchungen an der pelitischen Fraktion amazonischer Oberboden und Sedimente: *Bio-geographica*, n.7, p.7-25.
- Klammer, G. (1971) Uber plio-pleistozäne Terrassen und ihre Sedimente im unteren Amazonasgebiet: *Z. Geomorph. N.F.* v.15, p.62-;06.
- Klinge, H. (1965) Podzol soils in the Amazon Basin: *J. Soil Science*, v.16, p.95-103.
- Klinge, H. (1967) Podzol soils: A source of blackwater rivers in Amazonia: *Atas do Simpósio sobre a Biota Amazônica*, v.3, p.117-125.
- Klinge, H. (1973) Root mass estimation in lowland tropical rain forests of Central Amazonia, Brazil. I. Fine root masses of a pale yellow latosol and a giant humus podzol: *Torp. Ecol.*, v.14, p.29-38.
- Klinge, H. and W. Olhe (1964) Chemical properties of rivers in the Amazonian area in relation to soil conditions: *Verh. Internat. Verein. Limnol.*, v.15, p.1067-1076.
- Klinge, H. and W.A. Rodrigues (1973) Biomass estimation in a central Amazonian rain forest: *Acta Cient. Venezolana*, v.24, p. 225-237.
- Kodama, H. and M. Schnitzer (1977) Effect of Fulvic Acid on the Crystallization of Fe(III) oxides: *Geoderma*, v.19, p.279-291.
- Kronberg, B.I., W.S. Fyfe, O.H. Leonardos, Jr. and A.M. Santos (1979) The chemistry of some Brazilian soils: Element mobility during intense weathering: *Chemical Geology*, v.24, p.211-229.
- Kummel, B. (1948) Geological reconnaissance of the Contamana region, Peru: *Geol. Soc. Am. Bull.*, v.59, p.1217-1266.
- Likens, G.E., F.H. Bormann, R.S. Peirce, J.S. Eaton, and N.M. Johnson (1977) Biogeochemistry of a Forested Ecosystem: Springer-Verlag Inc.: New York, 146p.

- Linares, J. and F. Huetras (1971) Kaolinite: Synthesis at Room Temperature: *Science*, v.171, p.896-897.
- Loczy, L. de (1968) Geotectonic Evolution of the Amazon, Parnaíba, and Paraná Basins: *An. Acad. brasil. Ciênc.*, v.40 (sup.), p.231-249.
- Lopez-Eyzaquirre, C. and R.E. Bisque (1975) Study of the weathering of basic, intermediate, and acidic rocks under tropical humid conditions: *Quarterly of the Colorado School of Mines*, v.70, p.1-59.
- Loughnan, F.C. and P. Bayliss (1961) The mineralogy of the bauxite deposits near Weipa, Queensland: *Am. Mineralogist*, v.40, p.209-217.
- Marlier, G. (1973) Limnology of the Congo and Amazon Rivers; in Tropical Forest Ecosystems in Africa and South America: A Comparative Review, Meggers, B.J., E.S. Ayensu, and W.D. Duckworth, eds., Smithsonian Inst. Press: Washington D.C., p.223-238.
- Maribe, B., W. Ruegg, and R. Pougnet (1975) Grandes failles visibles de satellite au Pérou: *Revue de Géographie Physique et de Géologie Dynamique* (2), v.16, p.399-412
- Martin, J.M. and M. Meybeck (1979) Elemental mass-balance of material carried by major world rivers: *Marine Chemistry*, v.7, p.173-206
- McFarlane, M.J. (1976) Laterite and Landscape: Academic Press: London, 151p.
- Meade, R.H., C.F. Nordin, Jr., W.F. Curtis, F.M.C. Rodrigues, C.M. doVale, and J.M. Edmond (1979) Sediment loads in the Amazon River: *Nature*, v.278, p.161-163.
- Meybeck, M. (1976) Total Mineral Dissolved Transport by World Major Rivers: *Hydrological Sciences Bull.*, v.21, p.265-284.
- Mousinho de Meis, M.R. (1971) Upper Quarternary process changes of the Middle Amazon area: *Geol. Soc. Am. Bull.*, v.82, p.1073-1078.
- Nortcliff, S. and J.B. Thornes (1978) Water and cation movement in a tropical rainforest environment. I: *Acta Amazonica*, v.8, p.245-258.
- Nortcliff, S., J.B. Thornes, and M.J. Waylen (1979) Tropical Forest Systems: A Hydrological Approach: *Amazoniana*, v.6, p.557-568.
- Oltman, R.E. (1968) Reconnaissance Investigations of the Discharge and Water Quality of the Amazon River: *U.S.G.S. Circ.* 552, 16p.
- Pain, C.F. (1972) Characteristics and geomorphic effects of earthquake initiated landslides in the Albert Range in Papua, New Guinea: *Engineering Geology*, v.6, p.261-274.

Pasquali Z., J., C. López E., & H. Meinhard (1972) Meteorización de rocas del escudo de Guayana en ambiente tropical: Congreso Geológico Venezolano, Memoria IV, Tomo IV, Boletín de Geología, Publicación Especial n.5.

Pettijohn, F.J. (1975) Sedimentary Rocks, Third Ed.: Harper and Row Publishers: NY, 628p.

Potter, P.E. (1978) Petrology and chemistry of modern big river sands: *Journal of Geology*, v.86, p.423-449.

Reichardt, K., A. dos Santos, V.F. do Nascimento F., and O.O.S. Bacchi (1975) Movimento de água subterrânea em ecossistema Campina Amazônica: *Acta Amazonica*, v.5, p.287-290.

Reynolds, R.C., Jr. and N.M. Johnson (1972) Chemical weathering in the temperate glacial environment of the Northern Cascade Mountains: *Geochim. Cosmochim. Acta*, v.36, p.537-554.

Rigo de Righi, M. and G. Bloomer (1975) Oil and Gas Developments in the Upper Amazon Basin -- Colombia, Ecuador, and Peru: 9th World Petrol. Cong. Proc., v.3, p.181-192.

Rüegg, W. and A. Rosenzweig (1949) Contribución a la Geología de las formaciones modernas de Iquitos y de la Amazonia Superior: *Soc. Geol. Perú, Volumen Jubilar, parte II, fascículo 3*, p.1-24.

Sarmeinto, G. and M. Monasterio (1975) A critical consideration of the environmental conditions associated with the occurrence of savanna ecosystems in Tropical America; in *Tropical Ecological Systems*, Golley, E.B.

Scott, G.A.J. (1975) Soil profile changes resulting from the conversion of forest to grassland in the montaña of Peru: *Great Plains-Rocky Mountain Geogr. J.*, v.4, p.124-130.

Scott, G.A.J. (1975b) Relationships Between Vegetation Cover and Soil Avalanching in Hawaii: *Proc. Assoc. Am. Geog.*, v.7, p.208-212.

Scott, G.A.J. (1977) The role of fire in the creation and maintenance of savanna in the montana of Peru: *J. Biogeography*, v.4, p.143-167.

Scott, G.A.J. and J.M. Street (1976) The role of chemical weathering in the formation of Hawaiian Amphitheatre-headed Valleys: *Z. Geomorph. N.F.*, v.20, p.171-189.

Sherman, G.P. (1949) Factors influencing the development of lateritic and laterite soils in the Hawaiian Islands: *Pac. Sci.*, v.3, p.307-314.

Sherman, G.P. (1952) The genesis and morphology of the aluminum-rich laterite clays; Clay and Laterited Genesis: *Am. Ist. Min. Met.*, p.154-161.

Sioli, H. (1954) Betrachtungen über den Begriff der "Fruchtbarkeit" eines Gebietes anhand der Verhältnisse in Böden und Gewässer Amazoniens: Porsch. Fortschr., v.28, p.65-72.

Sioli, H. (1968) Hydrochemistry and Geology in the Brazilian Amazon Region: Amazoniana, v.1, p.267-277.

Sioli, H. and H. Klinge (1961) Über Gewässer und Boden des brasilianischen Amazonasgebietes: Die Erde, v.3, p.205-219.

Sombroek, W.G. (1966) Amazon Soils: Centre for Agricultural Publications and Documentation: Wageningen, 292p.

Stark, N. (1971a) Nutrient Cycling I. Elemental content of soils from South America: Int. J. Tropical Ecol., v.12, p.24-50.

Stark, N. (1971b) Nutrient Cycling II. Elemental contents of plants from South America: Int. J. Tropical Ecol., v.12, p.177-201.

Stark, N. (1972) Nutrient pathways and litter fungi: BioScience, v.22, p.355-360.

Stark, N. (1978) Man, Tropical Forests, and the Biological Life of a Soil: Biotropica, v.10, p.1-10.

Stark, N. and C. Holley (1975) Final report on studies of nutrient cycling on white and black water areas in Amazonia; Acta Amazonica v5 p.51-76

Stark, N.M. and C.F. Jordan (1978) Nutrient retention by the root mat of an Amazonian rain forest: Ecology, v.59, p.434-437.

Tschopp, H.J. (1953) Oil explorations in the Oriente of Ecuador: Am. Assoc. Petrol. Geologists Bull., v.37, p.2303-2347.

Ungemach, H. (1967) Sobre o balanço metabólico do iônios inorgânicos da área do sistema do Rio Negro: Atas do Simposio sobre a Biota Amazônica, v.3, (Limologia), p.221-226.

Van Wambeke, A. (1978) Properties and potentials of soils in the Amazon Basin: Interciencia, v.3, p.233-242.

Verhoogen, J., F.J. Turner, L.E. Weiss, C. Wahrhaftig, and W.S. Fyfe (1970) the earth: Holt, Rinehart and Winston Inc.. NY

Violante, A. and M.L. Jackson (1979) Crystallization of Nordstrandite in Citrate Systems and in the Presence of Montmorillonite; in International Clay Conference 1978, Mortland, M.M. and V.C. Farmer, eds. Elsevier: Amsterdam, p.517-525.

Walter, H. (1973) Vegetation of the Earth: Springer-Verlag: New York, 273p.

Went, F.W. and N. Stark (1968) Mycorrhiza: BioScience, v.18, p.1035-1039.

Zonneveld, J.I.S. (1975) Some problems of tropical geomorphology: Z. Geomorph. N.F., v.19, p.377-392.

BIBLIOGRAPHY, CHAPTER IV

- Anonymous (1972a) Die Ionenfracht des Rio Negro, Staat Amazonas, Brasilien nach Untersuchungen von Dr. Harald Ungemach; Amazoniana, v. 3, p. 175-185.
- Beadle, N.C.W. and A. Burgess (1953) A further note on laterites, Australian J. Sci., v.15, p.170-171 .
- Beck, K.C., Reuter, J.H., and Perdue, J.H. Organic and inorganic geochemistry of some coastal plain rivers of the southeastern United States; Geochim. Cosmochim. Acta, v. 38, p. 341-364.
- Benes, P., E.T. Gjessing and E. Steinnes (1976) Interaction between humus and trace elements in fresh water; Water Research, v.10, p.711-716
- Benavides, V. (1968) Saline Deposits of South America; Geological Society of America, Special Paper 88, p. 249-290.
- Berner, R.A. (1978) Rate control of mineral dissolution under earth surface conditions; Am. J. Sci., v. 278, p. 1235-1252.
- Berner, R.A. and Holdren, G.R. (1977) Mechanism of feldspar weathering: some observations and evidence; Geology, v. 5, p. 369-372.
- Bloomfield, C. (1953) Sesquioxide Immobilization and Clay Movement in Podzolized Soils, Nature, v.172, p.958
- Boyle, E.A., Edmond, J.M. and Sholkovitz, E.R. (1977) The mechanism of iron removal in estuaries; Geochim. Cosmochim. Acta, v. 41, p. 1313-1324.
- Bricker, O.P. and Garrels, R.M. (1967) Mineralogical factors in natural water equilibria; in Principals and Applications of Water Chemistry, Faust, S.P. and Hunter, J.V. eds., John Wiley & Sons: N.Y., p. 449-469.
- Butler, J.N. (1964) Ionic Equilibrium; Addison-Wesley Inc.: Reading, MA., 547 p.
- Busenberg, E. and Clemency, C.V. (1976) The dissolution kinetics of feldspars at 25°C and 1 atm CO₂ partial pressure; Geochim. Cosmochim. Acta, v. 40, p. 41-49.
- Clark, J., Berbower, J.R., and Kietzke, K.K. (1967) Oligocene Sedimentation, Paleoecology and Paleoclimatology in the Badlands of South Dakota; Fieldiana, Geology Memoirs, v.5, 158 p.

- Clarke, F.W. (1924) *The Data of Geochemistry*, 5th ed.: U.S. Geological Survey Bull. 770
- Correns, C.W. and von Engelhardt, W. (1938) Neue untersuchungen uber die verwitterung des kalifeldspats; *Chem. Erde*, v. 12, p. 1-22.
- Cronan, C.S., Reiner, W.A., Reynolds, R.C., Jr. and Lang, G.E. (1978) Forest floor Leaching: Contributions from mineral, organic, and carbonic acids in New Hampshire subalpine forests, *Science*, v. 200, p. 309-311.
- Deb, B.C. (1949) The movement and precipitation of iron oxides in podzol soils; *J. Soil Sci.*, v. 1, p. 112-122.
- Drever, J.I. and Smith, C.L. (1978) Cyclic wetting and drying of the soil zone as an influence on the chemistry of ground water in arid terrains; *Am. J. Sci.*, v. 278, p. 1448-1454.
- Eckert, J.M. and Sholkovitz, E.R. (1976) The flocculation of iron, aluminum, and humates from river water by electrolytes; *Geochim. Cosmochim. Acta*, v. 40, p. 847-848.
- FAO/UNESCO (1971) *Soil Map of the World, Volume IV South America*, explanatory note; Unesco: Paris, 193 p.
- Feth, J.H. (1971) Mechanisms Controlling World Water Chemistry: Evaporation-Crystallization Process: *Science*, v. 172, p. 870-871.
- Feth, J.H., Roberson, C.E., and Polzer, W.L. (1964) Sources of mineral constituents in water from granitic rocks of Sierra Nevada California and Nevada; U.S. Geol. Surv. Water-Supply Paper 1535-I, 70 p.
- Fittkau, E.J., Ilmer, U., Junk, W.J., Reiss, F., and Schmidt, G.W. (1975) Productivity, Biomass, and Population Dynamics of Amazonian Water Bodies; in Tropical Ecological Systems, Trends in Terrestrial and Aquatic Research, Golley, F.B. and Medina, E. eds., Springer-Verlag: N.Y.
- Furch, K. (1976) Haupt- und Spurenmetallgehalte zentralamazonischer Gewassertypen (Erste Ergebnisse); *Biogeographica*, v. 7, p. 27-43.
- Garrels, R.M. (1967) Genesis of some ground waters from igneous rocks; in Researches in Geochemistry, Abelson, P.H. ed., John Wiley & Sons: N.Y., v. 2, p. 405-420.
- Garrels, R.M. and Christ, C.L. (1965) Solutions, Minerals, and Equilibria; Harper and Row: N.Y., 450 p.

- Garrels, R.M. and Mackenzie, F.T. (1967) Origin of the chemical composition of some springs and lakes; *Adv. Chem. Ser.*, v. 67, p. 222-242.
- Garrels, R.M. and Mackenzie (1971) Evolution of Sedimentary Rocks: W.W. Norton & Co. Inc.: N.Y., 397 p.
- Gibbs, R.J. (1965) The Geochemistry of the Amazon River Basin: Ph.D. Thesis, Geology, U. California, San Diego, 96 p.
- Gibbs, R.J. (1967) The Geochemistry of the Amazon River System: Part I. The Factors that Control the Salinity and Composition and Concentration of the Suspended Solids: *Geol. Soc. America Bull.*, v.78, p.1203-1232
- Gibbs, R.J. (1970) Mechanisms Controlling World Water Chemistry: *Science*, v. 170, p. 1088-1090.
- Gibbs, R.J. (1972) Water Chemistry of the Amazon River: *Geochimica et Cosmochimica Acta*, v.36, p.1061-1066
- Greenland, D.J. (1971) Interactions between humic and fulvic acids and clay; *Soil Sci.*, v. 111, p. 34-41.
- Hegewald, E., Aldave, A. and Hakuli (1976) Investigations of the lakes of Peru and their phytoplankton I. Review of the literature, description of the investigated waters and chemical data; *Arch. Hydrobiol.*, v. 78, p. 494-506.
- Helgeson, H.C. (1969) Thermodynamics of hydrothermal systems at elevated temperatures and pressures; *Am. J. Sci.*, v. 267, p. 729-804.
- Helgeson, H. (1971) Kinetics of mass transfer among silicates and aqueous solutions; *Geochim. Cosmochim. Acta*, v. 35, p. 421-469.
- Hem, J.D. (1960) Complexes of ferrous iron with tannic acid, U.S. Geol. Survey Water-Supply Paper 1459-D.
- Hemley, J.J., Montoya, J.W., Christ, C.L., and Hostetler, P.B. (1977) Mineral equilibria in the $MgO-SiO_2-H_2O$ system: I talc-chrysotile-forsterite-brucite stability relations; *Am. J. Sci.*, v. 227, p. 322-351.
- Herndon, W.L. (1854) Exploration of the Valley of the Amazon; Robert Armstrong, Public Printer: Washington, D.C., 417 p.
- Hill, R.A. (1942) Geochemical patterns in Coachella Valley; *Trans. Am. Geophys. Union*, Pt. 1, p. 46-49.
- Hitchon, B., Billings, G.K. and Klován, J.E. (1971) Geochemistry and origin of formation waters in the western Canada sedimentary basin-III. Factors controlling chemical composition; *Geochim. Cosmochim. Acta*, v. 35, p. 567-598.

- Hoffman, J.A.J. (1975) Climatic Atlas of South America; WMO: Hungary.
- Holland, H.D. (1978) The Chemistry of the Atmosphere and Oceans: John Wiley & Sons: N.Y., 351 p.
- Holland, H.D., Kirsipu, T.V., Huebner, J.S., and Oxburgh (1964) On some aspects of the chemical evolution of cave waters; *J. Geol.*, v. 72, p. 36-67.
- Imbrie, J., and T.H. Van Andel (1964) Vector Analysis of Heavy Mineral Data: *Geological Society of America Bulletin*, v. 75, p. 1131-1156.
- Irion, G. (1976) Mineralogisch-geochemische Untersuchungen an der pelitischen Fraktion amazonischer Oberboden and Sedimente: *Biogeographica*, n. 7, p. 7-25.
- Johnson, D., Cole, D.W., and Gesses, S.P. (1975) Processes of Nutrient Transfer in a Tropical Rain Forest; *Biotropica*, v. 7, p. 208-215.
- Joreskog, K.G., J.E. Klován, R.A. Reymont (1976) Geological Factor Analysis: Amsterdam: Elsevier Scientific Publishing Company, 178 p.
- Katzer, F. (1897) Das Wasser des unteren Amazonas; *Sitz. bohm. Ges. Wiss. Math. - naturw.*, cl. 17, p. 1-38.
- Katzer, F. (1903) Geologie des unteren Amazonasgebietes (des Staates Para in Brasilien): Max Weg: Leipzig, 296 p.
- Keller, W.D. (1967) Geologic occurrences of the clay-mineral layer silicates; in Layer Silicates, *Am. Geol. Inst.*: Washington, D.C.
- Kittrick, J.A. (1971) Stability of montmorillonites. I. Belle Fourche and Clay Spur montmorillonites; *Soil Sci. Soc. Am. Proc.*, v. 35, p. 140-145.
- Klinge, H. (1965) Podzol Soils in the Amazon Basin: *J. Soil Science*, v.16, p.95-103
- Klinge, H. (1967) Podzol soils: A source of blackwater rivers in Amazonia: *Atas do Simpósio sobre a Biota Amazônica*, v.3., p.117-125
- Klinge, H. and Olhe, W. (1964) Chemical properties of rivers in the Amazonian area in relation to soil conditions; *Verh. Internat. Verein. Limnol.*, v. 15, p. 1067-1076.
- Lamar, W.L. (1968) Evaluation of organic color and iron in natural surface waters, U.S. Geol. Survey Prof. Paper 600-D, p. D24-D29.
- Langmuir, D. (1971) The geochemistry of some carbonate ground waters in central Pennsylvania; *Geochim. Cosmochim. Acta*, v. 35, p. 1023-1045.

- Leenheer, J. and Santos, U. (1979) *Acta Amazonica*, in press.
- Loughnan, F.C. (1969) Chemical Weathering of Silicate Minerals; American Elsevier: N.Y., 154 p.
- Martin, D.F., Doig, M.T., and Pierce, R.H., Jr. (1971) Distribution of naturally occurring chelators (humic acids) and selected trace metals in some west coast Florida streams, 1968-1969; University of South Florida Professional Papers Series.
- Martin, J.M. and M. Meybeck (1979) Elemental mass-balance of material carried by major world rivers: *Marine Chemistry*, v.7, p.173-206
- Meybeck, M. (1979) Pathways of major elements from land to ocean through rivers: In, *Extended Abstracts of Invited Papers, Review and Workshop on River Inputs To Ocean Systems (RIOS)*, FAO: Rome. 26-30 March, 1979.
- Nesbitt, H.W. and Bricker, O.P. (1978) Low temperature alteration processes affecting ultramafic bodies; *Geochim. Cosmochim. Acta*; v. 42, p. 403-409.
- Norton, D. (1974) Chemical mass transfer in the Rio Tanama system, west-central Puerto Rico; *Geochim. Cosmochim. Acta*, v. 38, p. 267-277.
- Ong, H.L. and Bisque, R.E. (1968) Coagulation of humic colloids by metal ions; *Soil Sci.*, v. 106, p. 220-224.
- Paces, T. (1972) Chemical characteristics and equilibrium in natural water-felsic rock-CO₂ system; *Geochim. Cosmochim. Acta*, v. 36, p. 217-240.
- Paces, T. (1973) Steady-state kinetics and equilibrium between ground water and granitic rock; *Geochim. Cosmochim. Acta*, v. 37, p. 2641-2663.
- Palmer, C. (1911) The geochemical interpretation of water analyses; *U.S. Geological Survey Bull.* 479, 31 p.
- Pasquali, Z., J., C. López E., and H. Meinhard (1972) Meteorización de rocas del escudo de Guayana en ambiente tropical: Congreso Geológico Venezolano, Memoria IV, Tomo IV, Boletín de Geología, Publicación Especial n. 5.
- Patrick, R. (1966) Limnological observations and discussion of results; in The Catherwood Foundation Peruvian-Amazon Expedition: Limnological and Systematic Studies; Academy of Natural Sciences Philadelphia: Philadelphia, p. 5-40.
- Perdue, E.M., Beck, K.C., and Reuter (1976) Organic complexes of iron and aluminum in natural waters; *Nature*, v. 260, p. 418-420.

- Petrovic, R. Berner, R.A., and Goldhaber, M.B. (1976) Rate control in dissolution of alkali feldspars-I. Study of residual feldspar grains by X-ray photoelectron spectroscopy; *Geochim. Cosmochim. Acta*, v. 40, p. 537-548.
- Pettijohn, F.J. (1975) Sedimentary Rocks, Third Ed.; Harper and Row: N.Y., 628 p.
- Piper, A.M. (1944) A graphic procedure in the geochemical interpretation of water analyses; *Trans. Am. Geophys. Union*, 25th aniv. mtg., pt. 6, p. 914-923.
- Polzer, W.L. (1967) Geochemical control of solubility of aqueous silica; in *Principals and Applications of Water Chemistry*, Faust, S.D. and Hunter, J.V. eds., John Wiley & Sons, Inc.: N.Y., p. 505-519.
- Potter, P.E. (1978) Petrology and chemistry of modern big river sands: *Journal of Geology*, v. 86, p. 423-449.
- Price, N.B. and Sholkovitz, E.R. (1978) Composition of suspended matter in the Amazon River and Estuary; *Trans. Am. Geophys. Union*, v. 59, p. 276-277.
- Raimondi, A. (1879) Resolución del problema: Cual de los ríos que forman el Amazonas, se puede reputar como el río madre?; El Perú, Imprenta del Estado: Lima, t. III, p. 577-584.
- Raimondi, A. (1884) Aguas Potables del Perú; F. Masias y Ca.: Lima, p. 127-134.
- Reeder, S.W., Hitchon, B., and Levinson, A.A. (1972) Hydrochemistry of the surface waters of the Mackenzie River drainage basin, Canada-I. Factors controlling inorganic composition: *Geochim. Cosmochim. Acta*, v. 36, p. 825-865.
- Rigo de Righi, M. and Bloomer, G. (1975) Oil and Gas Developments in the Upper Amazon Basin-Colombia, Ecuador, and Peru; 9th World Petrol. Cong. Proc., v. 3, p. 181-192.
- Ross, C.S. and Hendricks, S.B. (1945) Minerals of the montmorillonite group: their origin and relation to soil clays; U.S. Geol. Surv. Prof. Paper 250B.
- Sayles, F.L. and P.C. Mangelsdorf Jr. (1979) Cation-exchange characteristics of Amazon River suspended sediment and its reaction with seawater: *Geochim. Cosmochim. Acta*, v.43, p.

Schnitzer, M. and S.I.M. Skinner (1963a) Organo-metalic interactions in soils: 1. Reactions between a number of metal ions and the organic matter of a podzol Bn horizon, Soil Sci., v.96, p.86-93

Schnitzer, M. and S.I.M. Skinner (1963b) Organo-metalic interactions in soils: 2. Reactions between different forms of iron and aluminum and the organic matter of a podzol Bn horizon: Soil Sci., v.96, p.181-186

Schnitzer, M. and S.I.M. Skinner (1965) Organo-metalic interactions in soils: 4. Carboxyl and hydroxyl groups on organic matter and metal retention: Soil Sci., v.99, p.278-284

Schmidt, G.W. (1972a) Amounts of suspended solids and dissolved substances in the middle reaches of the Amazon over the course of one year (August, 1969-July, 1970); Amazoniana, v. 3, p. 208-223.

Schmidt, G.W. (1972b) Chemical properties of some waters in the tropical rain-forest region of Central-Amaonia along the new road Manaus-Caracarai; Amazoniana, v. 3, p. 199-207.

Sholkovitz, E.R. (1976) Flocculation of dissolved inorganic matter during the mixing of river water and seawater; Geochim. Cosmochim. Acta, v. 40, p. 831-845.

Sioli, H. (1951) Sobre a sedimentacao na Varzea do Baixo Amazonas; Bol. Tech. Inst. Agr. Norte, v. 24, p. 45-65.

Sioli, H. (1954a) Beitrage zur regionalen Limnologie Amazonasgebietes. II. Der Rio Arapiuns. Limnologische Untersuchung eines Gewassars des Tertiargebietes., Serie der "Barreiras", des unteren Amazonas: Arch. Hydrobiol., v.49, p.448-518

Sioli, H. (1954b) Betrachtungen uber den Begriff der "Fruchtbarkeit" eines Gebietes anhand der Verhaltnisse in Boden und Gewasser Amazoniens: Forsch. Fortschr., v.28, p.65-72

Sioli, H. (1955) Beitrage zur regionalen Limnologie Amazonasgebietes, III Uber einige Gewasser des oberen Rio-Negro-Gebietes: Arch. Hydrobiol. v. 50, p. 1-32.

Sioli, H. (1957) Beitrage zur regionalen Limnologie des Amazonasgebietes. IV. Limnologische Untersuchungen im Gebiet der Eisenbahnlinie Belém-Braganca, Staat Pará, Brasilien: Arch. Hydrobiol., v. 53, p. 161-222.

Sioli, H. (1963) Beitrage zur regionalen Limnologie Amazonasgebietes. V. Die Gewasser der Karbonstreifen Unteramazoniens: Arch. Hydrobiol., v. 59, p. 311-350.

Sioli, H. (1964) General features of the limnology of Amazonia: Verh. Internat. Verein. Limnol., v. 15, p. 1053-1060.

- Sioli, H. (1967) Studies in Amazon Waters; Atas do Simposio sobre a Biota Amazonica; v. 3, p. 9-50.
- Sioli, H. (1968) Hydrochemistry and Geology in the Brazilian Amazon Region: Amazoniana, v. 1, p. 267-277.
- Sioli, H. (1975) Tropical Rivers as Expressions of Their Terrestrial Environments; in Tropical Ecological Systems, Trends in Terrestrial and Aquatic Research, Golley, F.B. and Medina, E. eds., Springer-Verlag: N.Y., p. 275-288.
- Sioli, H. and Klinge, H. (1961) Uber Gewasser und Boden des brasilianischen Amazonasgebietes; Die Erde, v. 3, p. 205-219.
- Sombroek, W.G. (1966) Amazon Soils; Centre for Agricultural Publications and Documentation: Wageningen, 292 p.
- Spruce, R. (1908) Notes of a Botanist on the Amazon and Andes, ed. by Wallace, A.R., MacMillan: London, v. 2.
- Swabey, Y.H. (1966) Chemical, Physical, and bacterial characteristics; in The Catherwood Foundation Peruvian-Amazon Expedition: Limnological and Systematic Studies: Academy of Natural Sciences Philadelphia; Philadelphia, p. 41-51.
- Tardy, Y. and Garrels, R.M. (1974) A method of estimating the Gibbs energies of formation of layer silicates; Geochim. Cosmochim. Acta, v. 38, p. 1101-1116.
- Tastevin, C. (1929) Le delta du Japurá et le Piuriny; Géographie; Paris, v. 51, p. 280-298.
- Theis, T.L. and Singer, P.C. (1974) Complexation of iron (II) by organic matter and its effect on iron (II) oxygenation; Env. Sci. Tech., v. 8, p. 569-573.
- Thraillkill, J. (1972) Carbonate chemistry of aquifer and stream water in Kentucky; J. Hydrol., v. 16, p. 93-104.
- Tschopp, H.J. (1953) Oil explorations in the Oriente of Ecuador: Am. Assoc. Petrol. Geologists Bull., v. 37, p. 2303-2347.
- Ungemach, H. (1967) Sobre o balanço metabólico de íonios inorgânicos da área do sistema do Rio Negro: Atas do Simposio sobre a Biota Amazonica, v. 3 (Limnologia), p. 221-226.

Weaver, R.M., Jackson, M.L., and Syers, J.K. (1971) Magnesium and Silicon Activities in Matrix Solutions of Montmorillonite-Containing Soils in relation to Clay Mineral Stability; Soil Sci. Soc. Am. Proc., v. 35, p. 823-830.

Weaver, R.M., Jackson, M.L. and Syers, J.K., (1976) Clay mineral stability as related to activities of aluminum, silicon, and magnesium in matrix solution of montmorillonite-containing soils; Clays and Clay Minerals, v. 24, p. 246-252.

Wissmar, R., J. Richey, R. Stallard, and J. Edmond (1980) in press Limnology and Oceanography

Wollast, R. (1967) Kinetics of the alteration of K-feldspar in buffered solutions at low temperature; Geochim. Cosmochim. Acta, v. 31, p. 635-648.

Wright, J.R. and Schnitzer, M. (1963) Metallo-organic interaction associated with podzolization; Proc. Soil Sci. Soc. Am., v. 27, p. 171-176.

BIBLIOGRAPHY, CHAPTER V

Cramér, H. (1966) *Mathematical Methods of Statistics*; Princeton University Press: Princeton.

Matsui, E., Salati, E., Friedman, I. and Brinkmann, W.L.F. (1976) *Isotopic hydrology in the Amazonia: 2. Relative discharges of the Negro and Solimoes rivers through ^{18}O concentrations*; *Water Resour. Res.* v. 12, p. 781-785.

Meade, R.H., Nordin, C.F., Jr., Curtis, W.F., Mahoney, H.A. and Delaney, B.M. (1979) *Suspended-sediment and velocity data, Amazon River and its tributaries, June-July, 1976 and May-June, 1977*; U.S. Geological Survey Open-File Report 79-515, 42 p.

Oltman, R.E. (1968) *Reconnaissance Investigations of the Discharge and Water Quality of the Amazon River*; U.S.G.S. Circ. 552, 16 p.

Oltman, R.E., Sternberg, H.O'R., Ames, F.C., and Davis, L.C., Jr. (1964) *Amazon River investigations, Reconnaissance measurements of July, 1963*; U.S. Geological Survey Circ. 486, 15 p.

Raimondi, A. (1879) *Resolución del problema: Cuál de los ríos que forman el Amazonas, se puede reputar como el río madre?*; *El Perú, Impreta del Estado*: Lima, t. III, p. 577-584.

Tastevin, C. (1929) *Le delta du Japurá et le Piuriny*; *Géographie*; Paris, v. 51, p. 280-298.

Tastevin, C. (1920) *Le fleuve Japurá (Amazonie)*; *Geographie*: Paris, v. 33, p. 1-36.

BIBLIOGRAPHY, CHAPTER VI

Emerson, S. (1975) Chemically enhanced CO₂ gas exchange in a eutrophic lake: A general model; Limnology and Oceanography, v.20, p.743-753

Oltman, R.E. (1968) Reconnaissance Investigations of the Discharge and Water Quality of the Amazon River; U.S.G.S. Cir. 552, 16p.

BIBLIOGRAPHY, APPENDIX III

- Archer, A.W. (1975) The Indirect Colorimetric Determination of Sulfate with 2-Aminoperimidine; *Analyst*, v. 100, p. 755-757.
- Boyle, E.A., Edmond, J.M. and Sholkovitz, E.R. (1977) The mechanism of iron removal in estuaries; *Geochim. Cosmochim. Acta*, v. 41, p. 1313-1324.
- Dougan, W.K. and Wilson, A.L. (1974) The Absorptiometric Determination of Aluminum in Water. A Comparison of Some Chromogenic Reagents and the Development of an Improved Method; *Analyst*, v. 99, p. 413-430.
- Edmond, J.M. (1970) High precision determination of titration alkalinity and total carbon dioxide content of seawater by potentiometric titration; *Deep-Sea Res.*, v. 17, p. 737-750.
- Fishman, M.J. and Downs, S.C. (1966) Methods for Analysis of Selected Metals in Water by Atomic Absorption; U.S. Geological Survey Water-Supply Paper 1540-C, 45 p.
- Gardner, W.S., Wynne, D.S., and Dunstan, W.M. (1976) Simplified Procedure for the Manual Analysis of Nitrate in Seawater; *Marine Chemistry*, v. 4, p. 393-396.
- Klinge, H. and Olhe, W. (1964) Chemical properties of rivers in the Amazonian area in relation to soil conditions; *Verh. Internat. Verein. Limnol.*, v. 15, p. 1067-1076.
- Menzel, D.W. and Corwin, N. (1965) The Measurement of Total Phosphorous in Seawater Based on the Liberation of Organically Bound Fractions by Persulfate Oxidation; *Limnol. Oceanogr.*, v. 10, p. 280-282.
- Menzel, D.W. and Vaccaro, R.F. (1964) The measurement of dissolved organic and particulate carbon in seawater; *Limnol. Oceanogr.*, v. 9, p. 138-142.
- Santos, U. de M. and Santos, A dos (1970) Método para investigações comparativas sobre materiais húmicos nas águas naturais da região amazônica; *Boletim do INPA*, n. 7, 4 p.
- Scheiner, D. (1976) Determination of Ammonia and Kjeldahl Nitrogen by Indophenol Method, *Water Res.*, v. 10, p. 31-36.
- Solorzano, L. (1969) Determination of Ammonia in Natural Waters by the Phenolhypochlorite Method; *Limnol. Oceanogr.*, v. 14, p. 799-801.

Strickland, J.D.H. and Parsons, T.R. (1968) A Practical Handbook of Seawater Analysis; Fisheries Res. Board of Canada, Bull. 167, 311 p.

Stookey, L.L. (1970) Ferrozine-A New Spectrophotometric Reagent for Iron; Analytical Chemistry, v. 42, p. 779-781.

BIOGRAPHIC SKETCH

The author was born on 3 September 1952 in Summit, New Jersey, and at the age of 4 moved to North Andover, Massachusetts, where he went to school. His interests in natural sciences were instilled through visits, undertaken by his family, to natural features of North America such as bogs, tidepools, volcanos, glaciers, and rain forests. In September 1970, he entered M.I.T. where he received a B.S. in Earth and Planetary Sciences. Here, field work in geochemistry, geology, and astronomy proved most inspiring. In September 1974 he entered the M.I.T.-W.H.O.I. Joint Program in Oceanography. In addition to his thesis he also worked on advection-diffusion modelling, rain and atmospheric chemistry, and Precambrian geology. On 9 August 1975 he married Isabel Morales.

Professional Societies

American Geophysical Union
Sigma Xi

Publications

Boyle, E., R.A. Collier, A.T. Dengler, J.M. Edmond, A.C. Ng, and R.F. - Stallard (1974) On the chemical mass-balance in estuaries: *Geochimica et Cosmochimica Acta*, v.38, p.1719-1728

Caesar, J., R. Collier, J. Edmond, F. Frey, G. Matisoff, A. Ng, and R. - Stallard (1976) Chemical dynamics of a polluted watershed, the Merrimack River in Northern New England: *Environmental Science and Technology*, v.10, p.697-704

Stallard, R.F., J.M. Edmond, and R.E. Newell (1975) Surface Ozone in the South East Atlantic between Dakar and Walvis Bay: *Geophysical Research Letters*, v.2, p.289-292

Chan, L.H., J.M. Edmond, R.F. Stallard, W.S. Broeker, Y.C. Chung, R.F. - Weiss, and T.L. Ku (1976) Radium and Barium at Geosecs Stations in the Atlantic and Pacific: *Earth and Planetary Science Letters*, v.32, p.258-267